Vol. 132, December 1, 1981
Complete in one issue

ISSN 0003-2670

ANALYTICA CHIMICA ACTA

International journal devoted to all branches of analytical chemistry

ELSEVIER SCIENTIFIC PUBLISHING COMPANY

ANALYTICA CHIMICA ACTA

International journal devoted to all branches of analytical chemistry
Revue internationale consacrée à tous les domaines de la chimie analytique
Internationale Zeitschrift für alle Gebiete der analytischen Chemie

PUBLICATION SCHEDULE FOR 1981 (incorporating the section on Computer Techniques and Optimization).

	J	F	M	A	M	J	J	A	S	O	N	D
Analytica Chimica Acta	123	124/1	124/2	125	126	127	128	129	130/1	130/2	131	132
Section on Computer Techniques and Optimization		133/1			133/2			133/3			133/4	

Scope. *Analytica Chimica Acta* publishes original papers, short communications, and reviews dealing with every aspect of modern chemical analysis, both fundamental and applied. The section on *Computer Techniques and Optimization* is devoted to new developments in chemical analysis by the application of computer techniques and by interdisciplinary approaches, including statistics, systems theory and operation research. The section deals with the following topics: Computerized acquisition, processing and evaluation of data. Computerized methods for the interpretation of analytical data including chemometrics, cluster analysis, and pattern recognition. Storage and retrieval systems. Optimization procedures and their application. Automated analysis for industrial processes and quality control. Organizational problems.

Submission of Papers. Manuscripts (three copies) should be submitted as designated below for rapid and efficient handling:

Papers from the Americas to: Professor Harry L. Pardue, Department of Chemistry, Purdue University, West Lafayette, IN 47907, U.S.A.

Papers from all other countries to: Dr. A. M. G. Macdonald, Department of Chemistry, The University, P.O. Box 363, Birmingham B15 2TT, England.

For the section on *Computer Techniques and Optimization:* Dr. J. T. Clerc, Universität Bern, Pharmazeutisches Institut, Sahlistrasse 10, CH-3012 Bern, Switzerland.

American authors are recommended to send manuscripts and proofs by INTERNATIONAL AIRMAIL.

Submission of an article is understood to imply that the article is original and unpublished and is not being considered for publication elsewhere. Upon acceptance of an article by the journal, the author(s) resident in the U.S.A. will be asked to transfer the copyright of the article to the publisher. This transfer will ensure the widest dissemination of information under the U.S. Copyright Law.

Information for Authors. Papers in English, French and German are published. There are no page charges. Manuscripts should conform in layout and style to the papers published in this Volume. Authors should consult Vol. 121, p. 353 for detailed information. Reprints of this information are available from the Editors or from: Elsevier Editorial Services Ltd., Mayfield House, 256 Banbury Road, Oxford OX2 7DE (Great Britain).

Reprints. Fifty reprints will be supplied free of charge. Additional reprints (minimum 100) can be ordered. An order form containing price quotations will be sent to the authors together with the proofs of their article.

Advertisements. Advertisement rates are available from the publisher.

Subscriptions. Subscriptions should be sent to: Elsevier Scientific Publishing Company, P.O. Box 211, 1000 AE Amsterdam, The Netherlands. The section on *Computer Techniques and Optimization* can be subscribed to separately.

Publication. *Analytica Chimica Acta* (including the section on *Computer Techniques and Optimization*) appears in 11 volumes in 1981. The subscription for 1981 (Vols. 123-133) is Dfl. 1639.00 plus Dfl. 198.000 (postage) (total approx. U.S. $735.00). The subscription for the *Computer Techniques and Optimization* section only (Vol. 133) is Dfl. 149.00 plus Dfl. 18.00 (postage) (total approx. U.S. $67.00). Journals are sent automatically by airmail to the U.S.A. and Canada at no extra cost and to Japan, Australia and New Zealand for a small additional postal charge. All earlier volumes (Vols. 1-121) except Vols. 23 and 28 are available at Dfl. 164.00 (U.S. $66.00), plus Dfl. 13.00 (U.S. $5.20) postage and handling, per volume.

Claims for issues not received should be made within three months of publication of the issue, otherwise they cannot be honoured free of charge.

Customers in the U.S.A. and Canada who wish to obtain additional bibliographic information on this and other Elsevier journals should contact Elsevier/North Holland Inc., Journal Information Center, 52 Vanderbilt Avenue, New York, NY 10017. Tel: (212) 867-9040.

ANALYTICA CHIMICA ACTA
VOL. 132 (1981)

ANALYTICA CHIMICA ACTA

International journal devoted to all branches of analytical chemistry

ELSEVIER SCIENTIFIC PUBLISHING COMPANY

Anal. Chim. Acta, Vol. 132 (1981)

Analytica Chimica Acta, 132 (1981) 1—10
Elsevier Scientific Publishing Company, Amsterdam — Printed in The Netherlands

AMPEROMETRIC DETECTION OF SIMPLE ALCOHOLS IN AQUEOUS SOLUTIONS BY APPLICATION OF A TRIPLE-PULSE POTENTIAL WAVEFORM AT PLATINUM ELECTRODES

SCOTT HUGHES, P. LAWRENCE MESCHI[a] and DENNIS C. JOHNSON*
Department of Chemistry, Iowa State University, Ames, IA 50011 (U.S.A.)
(Received 15th June 1981)

SUMMARY

Application of a triple-pulse waveform is described for the anodic detection of methanol, ethanol, and ethylene glycol. The execution of the waveform incorporates the cleaning and reactivation of the platinum electrode, by alternate anodic and cathodic polarization, with measurement of the faradaic signal for the analyte at the reduced electrode surface. Some results for formic acid are also presented. The waveform is completed within approximately 2 s and the faradaic signal exhibits no decay with time as would be the case for amperometric detection at a constant applied potential. Calibration curves made by plotting $-1/I$ vs. $1/C$ are linear. This is consistent with a reaction mechanism in which the analyte is adsorbed prior to anodic detection. The technique is applicable for detection in chromatographic and flow-injection systems.

The oxidation of the lower-molecular-weight alcohols and formic acid on platinum electrodes has been extensively studied during the past two decades for their possible use in fuel cells [1—3]. The literature from this research is extensive and only representative references will be cited. The oxidation is characterized by a large initial current which decays rapidly during the first several seconds, dropping to a negligible value within a few minutes [4, 5]. The anodic current is believed to arise from the oxidation of hydrogen atoms produced by the heterogeneous dehydrogenation of the adsorbed organic molecules [6, 7]. The organic residue of the dehydrogenation reaction, possibly including carbon monoxide, remains strongly adsorbed to the electrode surface and severely hinders further adsorption of molecules from the bulk of the solution. The application of these surface-catalyzed oxidations of organic compounds in chemical analysis has not gained much attention because of the concomitant loss of electrode activity.

The loss of activity for noble-metal electrodes, from adsorbed organic compounds in particular, has plagued electroanalytical chemists since the inception of solid-electrode voltammetry [8]. This has been true even for inorganic species in solutions free of organic compounds except at the trace

[a]Present address: EXXON Research and Engineering Co., Linden, NJ 07036, U.S.A.

level. The associated literature usually describes some type of pretreatment routine found by the trial-and-error method to maintain a reproducible electrode activity. In addition to occasional resurfacing of the electrode by grinding or polishing, the pretreatment usually involves repeated anodic and cathodic polarization of the electrode surface. Whereas anodic oxidations of organic compounds from solution seldom occur at rates approaching the mass-transport limitation at oxide-covered platinum electrodes, adsorbed organic material is oxidatively degraded quite efficiently to carbon dioxide simultaneously with the process of formation of the oxide layer [5]. The subsequent cathodic polarization is necessary to reduce the PtO and regenerate the active platinum surface.

This paper describes the use of a triple-step pulsed-potential waveform to achieve the maintenance of uniform electrode activity with "simultaneous" amperometric detection of simple alcohols in aqueous solutions; the detection of formic acid is also described. The faradaic signal is determined at a potential, E_1, for oxidation of the adsorbed compounds without formation of PtO. The charging current associated with a potential step to E_1 decreases rapidly ($\ll$100 ms) and the faradaic signal is measured before significant loss of electrode activity has occurred. The faradaic signal is retained in the potentiostat by a sample-hold circuit until updated following successive repetitions of the waveform. The surface of the platinum electrode is then cleaned of the adsorbed organic residue by stepping the applied potential to the positive limit E_2 accessible for the solvent, at which value the adsorbed organic material is believed to be oxidatively desorbed as CO_2 simultaneously with formation of PtO. The potential is then stepped to a value E_3 near the negative limit for the solvent where PtO is reduced and adsorption of the organic analyte can occur. The time period for execution of the waveform is typically 1—2 s and no decay of the faradaic signal is observed for hydrodynamic electrodes over long periods of time (hours). The cycle time for the waveform is sufficiently short to permit application of the detection scheme for liquid chromatography and flow-injection systems with satisfactory definition of peak shape.

The realization of greater stability in the electrochemical response of solid electrodes by application of a two-step pulsed-potential waveform has been reported. MacDonald and Duke [9] observed an improvement in stability for the anodic detection of *p*-aminophenol at a platinum flow-through electrode when normal pulse (n.p.) amperometry was used instead of constant potential (d.c.) amperometry. Stulik and Hora [10] applied periodic potential pulses during cathodic detection of Fe^{3+} and Cu^{2+} at a platinum electrode. Improved stability of the cathodic signal was achieved when the pulse amplitude was sufficiently large to result in formation and subsequent dissolution of PtO on the electrode surface during the pulse cycle. The faradaic signal was measured at the negative potential after reduction of the oxide film. For both examples cited above, the loss of sensitivity observed in the absence of the pulsed waveform was not nearly

so precipitous as for the case of the compounds tested in the research reported here.

EXPERIMENTAL

Instrumentation

Current—potential curves (I—E) were obtained by cyclic voltammetry at a platinum rotated-disc electrode (RDE, 0.460 cm^2; Pine Instrument Co., Grove City, PA). The rotator was model PIR, Pine Instrument Co. A platinum-disc flow-through detector (0.076 cm^2) was constructed in the chemistry shop at Iowa State University after a design by Lindstrom [11] which is similar to the so-called "wall-jet" detector [12, 13]. The detector body was machined from glass-filled (25%) teflon (Crown Plastic Inc., St. Paul, MN).

The flow-injection system was constructed according to the conventional design. Flow of the electrolytic solution was maintained by a Milton Roy Model CK miniPump (Laboratory Data Control, Riviera Beach, FL) with dual pistons operating 180° out of phase. A model 709 Pulse Dampener (Laboratory Data Control) connected to a 40-ft. stainless-steel tube (0.016 in. i.d. × 1/6 in. o.d.), provided sufficient back-pressure to eliminate pulsations in the fluid flow. The stainless-steel tubing connecting the electrolyte reservoir and the pump was 0.11 in. i.d. × 1/8 in. o.d., and all other tubing was stainless steel with dimensions 0.05 in. i.d. × 1/16 in. o.d. Swagelok fittings were used for all connections. The sample injection valve was a Rheodyne Model 7125 (Larry Bell and Associates, Minneapolis, MN) with a sample volume (V_s) of 250 μl. Flow rate was calibrated by measurement of the volume delivered to a 10-ml buret during a known period of time, and a flow rate (v_f) of 0.500 ml min^{-1} was used.

Potentiostatic control was achieved with a three-electrode potentiostat assembled in this laboratory from operational amplifiers according to the conventional design. The reference electrode was a miniature saturated calomel electrode (SCE) filled with a saturated solution of KCl. All potentials are reported in V vs. SCE.

A block diagram of the instrument for generating the potential waveform is shown in Fig. 1. Three adjustable voltage signals (E_1, E_2, and E_3 identified above) were connected to the input of the potentiostat through AD 7513 analog switches (Analog Devices Inc., Norwood, MA). The switches were opened and closed at precisely controlled intervals by digital pulses produced by a timing circuit constructed from five National Semiconductor 555 timing modules in their monostable configurations as shown in Fig. 2. Variable resistors and capacitors connected to each monostable (MS) circuit enabled the pulse times to be varied continuously from 0.1 ms to 12 s. The monostables were arranged in two interacting sequences (see Fig. 2). The main sequence (MS 1—3) was responsible for controlling the potential waveform. Within the sequence, the trigger terminal of each MS was connected to the output of the preceding MS, with MS1 connected to the output of MS3, and

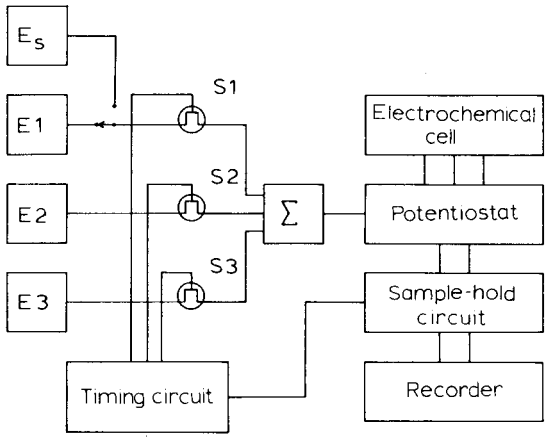

Fig. 1. Block diagram of instrumentation. S1—3, Analog Devices 7513 analog switches; E1—3, adjustable sources of voltage; E_s, linear voltage ramp.

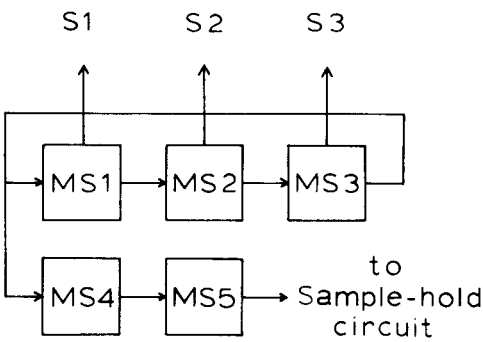

Fig. 2. Block diagram of timing circuit. MS1—5, National Semiconductor 555 timing modules.

triggering occurred with HI-to-LO transition at the end of a pulse period. The second sequence of monostables (MS 4,5) controlled the analog sample—hold circuit of the potentiostat for measurement of the faradaic signal during application of the potential E_1. Monostable 4 was triggered simultaneously with MS1 and was used to produce a time-delay between the application of E_1 and the activation of the sample-hold circuit. The time period for sampling the faradaic current was controlled by MS 5. Further details of the circuitry are reported elsewhere [14].

Chemicals

All chemicals were reagent grade. Solutions contained 0.10 M H_2SO_4 as the supporting electrolyte. All water had been distilled, demineralized and passed through a 12 in. × 1.5 in. i.d. column of activated carbon. Dissolved oxygen was removed from all solutions by saturation with nitrogen.

RESULTS AND DISCUSSION

Cyclic voltammetry

Linear scan cyclic voltammetry at the platinum RDE was used for preliminary characterization of the anodic response of methanol, ethanol, ethylene glycol, and formic acid in 0.1 M H_2SO_4. Representative I—E curves (Fig. 3) are consistent with published results of similar studies. Mechanisms for the reactions have been presented [1—7] and will not be reviewed in detail. The organic compounds are partially oxidized by the surface-catalyzed anodic dehydrogenation on the platinum electrode free of PtO. The products of the oxidation are strongly adsorbed at the electrode and the accumulation of these products leads to loss of electrode activity and, hence, the peaked response of the signal on the positive sweep of potential at approximately 0.4 V. The adsorbed species are oxidized, probably to carbon dioxide, simultaneously with the formation of PtO on the positive sweep for $E >$ 0.9 V. There is negligible oxidation of the organic compounds in the diffusion layer at the surface of an electrode covered by PtO during the negative sweep of potential for $1.2 > E > 0.6$. The reduction of PtO commences on the negative sweep for $E < 0.6$ V producing a cathodic peak. The production of platinum sites free of oxide and adsorbed organic residue permits the onset of oxidation of organic compounds from the solution and the net current shifts to an anodic value on the negative sweep at $E \simeq 0.4$ V. The half-wave potential for the anodic processes is approximately 0.2 V and no oxidation occurs for $E < 0.1$ V.

The cathodic and anodic peaks observed in the vicinity of 0.0 V in the absence of organic compounds correspond to the reversible formation and

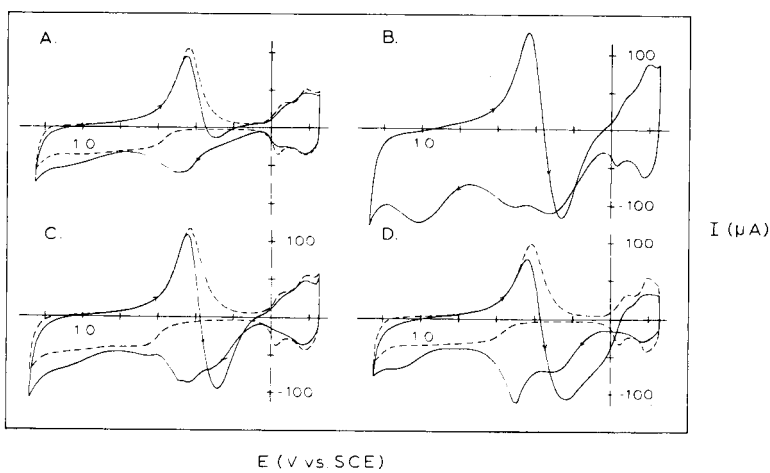

Fig. 3. Current—potential curves obtained by cyclic voltammetry at the platinum RDE. Conditions: ω = 41.9 rad s^{-1}; ϕ = 3.0 V min^{-1}. Curves: A, 6.5 mM methanol; B, 6.0 mM ethanol; C, 4.0 mM ethylene glycol; D, 2.6 mM formic acid; (----) residual curve.

dissolution of adsorbed hydrogen atoms at the platinum surface. The sizes of these peaks are diminished slightly with the addition of the organic materials to the solution as the result of adsorption of the compounds. This suppression has been used for estimation of the adsorption isotherms for organic compounds [15].

The heights of the anodic peaks observed on the positive sweep of potential, for the compounds tested, vary in proportion to the rate of potential scan (ϕ). Hence, these processes are surface-controlled and the overall anodic processes are designated as being surface-catalyzed because there is no evidence that the reaction could occur in the absence of the adsorption step. Additions of small quantities of the sodium salts of chloride, bromide and iodide, known for adsorbing at platinum surfaces, completely eliminates the response to the organic compounds. Therefore, the affinity of the platinum surface for adsorption is essential in promoting the oxidation of the organic compounds.

Calibration curves for ethanol

The faradaic signal for the compounds studied was observed to increase nonlinearly with bulk concentration (C^b) and the response for ethanol was studied in detail. The peak current (I_p) measured at 0.35 V on the positive sweep was observed to be a linear function of C^b only for $C^b < 1$ mM. A linear plot was produced for $1/I_p$ vs. $1/C^b$. Such behavior is concluded to be consistent with a mechanism whereby the faradaic signal is proportional to the fractional surface coverage by the adsorbed organic compound, θ_{RH}. In this discussion RH is used to represent the organic compound to be detected anodically and the underline designates the adsorbed state of the molecule. The fractional surface coverage $\theta_{\underline{RH}}$ is related to the molar coverage of the surface by $\theta_{\underline{RH}} = \Gamma_{\underline{RH}}/\Gamma_{\underline{RH},max}$, where $\Gamma_{\underline{RH},max}$ is the coverage (mol cm^{-2}) at an infinite value of C^b_{RH}. At equilibrium in the adsorption reaction described by

$$RH + \underline{H_2O} \underset{k_{-1}}{\overset{k_1}{\rightleftharpoons}} \underline{RH} + H_2O \tag{1}$$

the Langmuir isotherm can be derived assuming $\theta_{\underline{RH}} + \theta_{\underline{H_2O}} = 1$ and is given by

$$\theta_{\underline{RH}} = KC^b_{RH}/(1 + KC^b_{RH}) \tag{2}$$

where $K = k_1/k_{-1}$.

The anodic reaction is irreversible

$$\underline{RH} \overset{k_2}{\rightarrow} \underline{R} + H^+ + e \tag{3}$$

and I_p is given by

$$I_p = -nFA(d\Gamma_{\underline{RH}}/dt) = -nFAk_2\Gamma_{\underline{RH},max}\theta_{\underline{RH}} \tag{4}$$

The combination of Eqns. (2) and (4) yields

$$I_p = -K'C^b_{RH}/(1 + KC^b_{RH}) \quad (5)$$

where $K' = nFA\Gamma_{RH,max}k_2K$. The plot of $-1/I_p$ vs. $1/C^b_{RH}$ is expected to be linear. Also, for $KC^b_{RH} \ll 1$, i.e. low C^b_{RH}, the plot of $-I_p$ vs. C^b_{RH} is predicted to be linear.

Effect of rotational velocity

The derivation of Eqn. (5) was based on the assumption that θ_{RH} has reached its equilibrium value and that this equilibrium is not disturbed by the fact of the anodic detection at E_1. At equilibrium, the concentration of RH at the electrode surface in the diffusion layer, C^s_{RH}, would be at the value C^b_{RH} and variation of rotational velocity ω of the electrode would not be predicted to influence I_p. The value of I_p was in fact observed to decrease with increases in ω. A similar negative dependence has been reported by Breiter and Gilman for methanol at a platinum electrode in 1 M $HClO_4$ [15]. The explanation for this phenomenon as suggested by these workers is that reaction intermediates formed by the initial charge-transfer step can either undergo further anodic reaction or they can be lost from the surface by desorption followed by mass transport. Increased rates of stirring would decrease the likelihood of subsequent oxidation steps. Plots of I_p vs. $\omega^{1/2}$ for ethanol were linear with a slope of -1. This result is consistent with a process in which a reaction intermediate is lost at a mass-transport limited rate [16].

Triple-pulse voltammetry

The selection of the appropriate value of E_1 which would produce maximum sensitivity for triple-pulse amperometric detection of organic compounds in a flowing stream was made on the basis of triple-pulse voltammetry, as illustrated in Fig. 4 for ethanol at the platinum RDE. Also shown is the I—E curve obtained by the conventional (i.e., d.c.) linear scan voltammetry in the absence of ethanol. Values of E_2 and E_3 were 1.25 and 0.00 V, respectively. The time periods for application of E_2 and E_3 in the waveform were 0.4 and 0.8 s, respectively. These time periods were found empirically to be sufficiently long for the corresponding currents to decay to negligible values. In place of the constant voltage applied as E_1, a linear voltage scan was substituted, E_s (5 mV s^{-1}). The delay time for measurement of the pulse current at $E_1 = E_s$ was 45 ms, which was sufficient for the charging current to decay to a negligible value; the sample-hold circuit was in the "sample" state for 8.0 ms. The total time at $E_1 = E_s$ was 0.2 s. Hence, the total period for completion of the waveform was 1.4 s. From Fig. 4, a value of $E_1 = 0.26$ V is concluded to be optimum for the triple-pulse amperometric detection of ethanol in a fluid stream.

Triple-pulse amperometric detection with a constant value of $E_1 = 0.26$ V is compared to d.c. detection at the RDE in Fig. 5 for ethanol. For d.c.

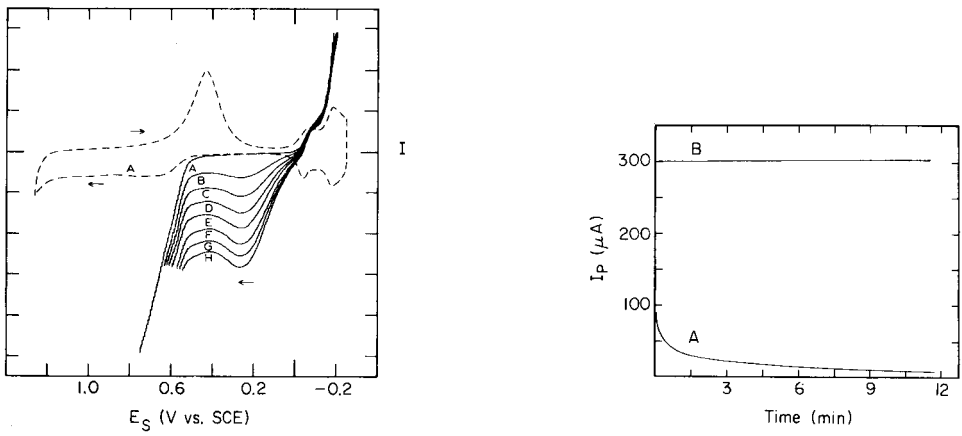

Fig. 4. Current—potential curves for ethanol obtained by triple-pulse voltammetry at the platinum RDE. Conditions: ω = 41.9 rad s^{-1}. (—) Triple-pulse voltammetry, 100 μA div^{-1}, $E_1 = E_S$ (0.2 s), E_2 = 1.25 V (0.8 s), E_3 = 0.00 V (0.4 s), ϕ = 0.30 V min^{-1}. (---) Background I—E curve by linear sweep voltammetry, 50 μA div^{-1}, ϕ = 3.0 V min^{-1}. [Ethanol] (mM): A, 0.00; B, 1.14; C, 2.28; D, 3.41; E, 4.56; F, 5.66; G, 6.78; H, 7.89.

Fig. 5. Comparison of long-term stability of response for ethanol at the platinum RDE by triple-pulse and d.c. detection. Conditions: ω = 41.9 rad s^{-1}, [ethanol] = 7.89 mM. Curves: A, d.c. detection, E = 0.26 V; B, triple pulse detection, E_1 = 0.26 V (0.2 s), E_2 = 1.25 V (0.8 s), E_3 = 0.00 V (0.4 s).

detection, the potential of the platinum electrode was repeatedly switched between 1.25 V and 0.00 V to insure a clean electrode surface prior to recording the I—T curve at the constant potential 0.26 V. The signal for the triple-pulse detection was observed to remain constant for 0.5 h at which time the experiment was discontinued.

Flow-injection detection

The successful maintenance of electrode activity by application of the triple-pulse waveform is illustrated in Fig. 6 for flow-injection determination of ethanol using the platinum-disc flow-through detector. Peaks for twelve successive injections of 250 μl each containing 52 μg ethanol are shown for v_f = 0.50 ml min^{-1}. The relative standard deviation in I_p is 0.8%. Similar studies for methanol and formic acid yielded comparable results. Direct-current detection is useless with no response observed after the second injection.

Calibration studies were made for ethanol by the flow-injection method. Concentrations were is the range 0.17--2.4 mM (0.78--11 μg per 100-μl sample) and the results are plotted in Fig. 7. The plot of $1/I_p$ vs. $1/C^b$ is linear with slope = 0.0866 ± 0.0018, intercept = 0.023 ± 0.004, standard error = 5.0 × 10^{-3} μA^{-1}, and r^2 = 0.9989. The uncertainties in slope and intercept represent the 90% confidence intervals. These results are consistent with the mechanism proposed above (Eqn. 5).

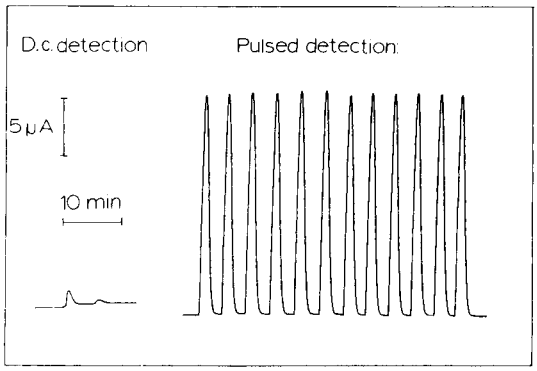

Fig. 6. Comparison of detection peaks for ethanol in flow-injection detection with d.c. and triple-pulse detection. Conditions: V_S = 250 μl, v_f = 0.50 ml min^{-1}, [ethanol] = 5.2 mM. D.c. detection at E = 0.26 V. Triple-pulse detection at E_1 = 0.26 V (0.50 s), E_2 = 1.25 V (1.18 s), E_3 = 0.00 V (0.85 s).

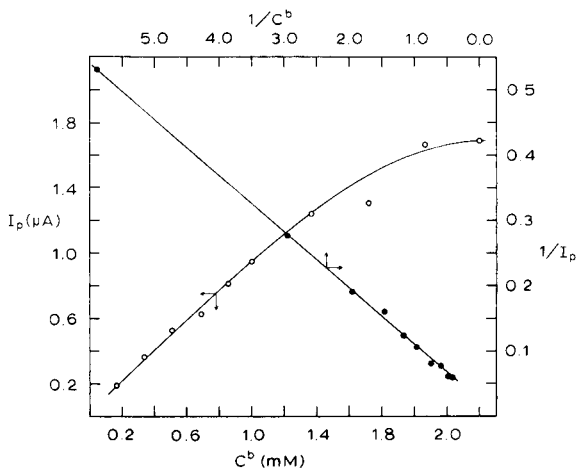

Fig. 7. Calibration curves for ethanol by flow-injection with triple-pulse detection. Conditions: V_S = 100 μl, v_f = 0.375 ml min^{-1}, E_1 = 0.26 V (0.2 s), E_2 = 1.25 V (0.7 s), E_3 = 0.00 V (0.4 s).

Conclusions

The triple-pulse amperometric technique described has been illustrated to maintain a uniform level of electrode activity during the anodic detection of several simple organic molecules including methanol, ethanol, ethylene glycol and formic acid. The matter of the choice of time for application of potentials E_2 and E_3 was not observed to be critical. At E_1, where the faradaic signal is measured, the sampling of current was started at 45 ms and terminated in less than 10 ms. A prerequisite of reactivity is concluded to be adsorption of the compound, and the presence of other surfactants interferes with the detection. There is virtually no possibility of the selective measure-

ments of mixtures without prior separation and future applications are viewed strictly in terms of amperometric detection in liquid chromatography. The study is being extended to more complex polyalcohols than ethylene glycol and to carbohydrates.

The authors are grateful to the National Science Foundation for support of a portion of this work through grant CHE 76-17826.

REFERENCES

1 N. L. Weinberg and H. R. Weinberg, Chem. Rev., 68 (1968) 449.
2 B. E. Conway, Rev. Pure Appl. Chem., 18 (1968) 105.
3 S. D. Ross, M. Finkelstein and E. J. Rudd, in A. T. Blomquist and H. H. Wasserman (Eds.), Anodic Oxidation, Vol. 32 of Organic Chemistry, Academic Press, New York, 1975.
4 M. W. Breiter, Electrochim. Acta, 8 (1963) 973.
5 J. Giner, Electrochim. Acta, 9 (1964) 63.
6 A. N. Frumkin and B. I. Pollovchenko, Dokl. Akad. Nauk. SSR, 150 (1953) 349.
7 A. P. Tomilov, S. G. Mairanovskii, M. Ya Fioshin and V. A. Smironov, Electrochemistry of Organic Compounds, Halsted, New York, 1972, p. 314.
8 R. Adams, Electrochemistry at Solid Electrodes, M. Dekker, New York, 1969.
9 A. MacDonald and P. D. Duke, J. Chromatogr., 83 (1973) 331.
10 K. Stulik and V. Hora, J. Electroanal. Chem., 70 (1976) 253.
11 T. R. Lindstrom, Ph.D. Thesis, Iowa State University, Ames, IA, 1980.
12 J. Yamada and H. Matsuda, J. Electroanal. Chem. Interfacial Electrochem., 44 (1973) 189.
13 B. Fleet and C. F. Little, J. Chromatogr. Sci., 12 (1974) 747.
14 P. L. Meschi, Ph.D. Thesis, Iowa State University, Ames, IA, 1981.
15 M. W. Breiter and S. Gilman, J. Electrochem. Soc., 109 (1962) 622, 1099.
16 W. J. Albery and M. L. Hitchman, Ring-disc Electrodes, Clarendon Press, Oxford, 1971.

Analytica Chimica Acta, 132 (1981) 11—22
Elsevier Scientific Publishing Company, Amsterdam — Printed in The Netherlands

AMPEROMETRIC DETECTION OF SIMPLE CARBOHYDRATES AT PLATINUM ELECTRODES IN ALKALINE SOLUTIONS BY APPLICATION OF A TRIPLE-PULSE POTENTIAL WAVEFORM

SCOTT HUGHES and DENNIS C. JOHNSON*
Department of Chemistry, Iowa State University, Ames, IA 50011 (U.S.A.)
(Received 20th July 1981)

SUMMARY

The response of ten simple carbohydrates was investigated voltammetrically at platinum electrodes in 0.10 M sodium hydroxide by application of a conventional linear sweep waveform and a triple-pulse waveform. Linear-sweep data were interpreted to suggest that electrochemical reactions of the carbohydrates involve oxidation of adsorbed hydrogen atoms produced by surface-catalyzed dehydrogenation of the adsorbed carbohydrate. The triple-pulse measurement technique was evaluated for a flow-injection system by introducing 100-μl samples into a stream of 0.1 M NaOH with a flow rate of 0.375 ml min^{-1}, and measuring the peak current. Peak currents for ten carbohydrates at 0.5 mM ranged from 17 to 42 μA and a detection limit of 0.01 mM was evaluated for dextrose. Calibration plots of reciprocal peak current (I_p^{-1}) vs. reciprocal of concentration (C^{-1}) were linear for dextrose and sorbitol concentrations between 0.1 and 1.0 mM.

The need to quantify carbohydrates has been an important problem for many years in studies of plant, animal, and human nutrition. Recent advances in the area of human health, for example, have led to greater recognition of a probable correlation between the presence of individual carbohydrates in the human diet and the occurrence of undesirable physiological conditions including cardiovascular disease and diabetes, as well as dental decay [1, 2].

High-performance liquid chromatography (h.p.l.c.) has become the accepted instrumental technique for separation of carbohydrates in their complex mixtures. Separations have been reported on nonpolar stationary phase columns, with acetonitrile—water as eluent, and on cation-exchange columns with water as the eluent [1—3]. Carbohydrates exhibit only weak absorbance in the u.v.-visible region of the electromagnetic spectrum and measurement of refractive index is the present method of detection for carbohydrates in h.p.l.c. Refractive index detectors have sensitivities less than desired and a definite need persists for more sensitive methods of detection.

Recent interest in the electrochemical oxidation of carbohydrates, especially glucose, on platinum electrodes in neutral aqueous solutions has largely been motivated by the possible utilization of in vivo fuel cells to provide

0003—2670/81/0000—0000/$02.50

electrical power for heart pacers or perhaps even artificial hearts [4]. The oxidation of glucose at platinum electrodes in phosphate solutions buffered at pH 7.5 is characterized by a large initial current which decays rapidly during the first several seconds, finally reaching a negligible value within a few minutes. The anodic current is believed to result from oxidation of hydrogen atoms produced when the glucose, adsorbed in the hemiacetal form, undergoes surface-catalyzed dehydrogenation of the C_1-atom adjacent to the hemiacetal hydroxyl group [4—6]. Gluconolactone is the primary product of the oxidation ($n = 2$) and undergoes hydrolysis following desorption to produce gluconic acid. The desorption of the primary product is very slow, however, leading to the observed rapid loss of activity for the platinum electrode.

Colton et al. [7] investigated the use of the oxidation of glucose at an implantable platinum electrode for in vivo determinations of glucose. They obtained reproducible results only by application of successive anodic and cathodic polarizations prior to recording the current—voltage (I—E) curve for a positive sweep of electrode potential. The time required for each determination was approximately 6 min. This technique is too slow to be applied for detection in h.p.l.c.

This report describes the applicability of triple-pulse amperometry [8] for detection of several carbohydrates including aldoses, ketoses and sugar alcohols. The waveform of the applied potential [8] was designed to incorporate amperometric measurement together with the potentiostatic cleaning and reactivation of the electrode surface within a single waveform. The waveform consists of an intermediate potential E_1 to permit measurement of current resulting from oxidation of an adsorbed species, a more anodic potential E_2 to desorb species from the electrode surface, and a more cathodic potential E_3 to reduce PtO on the surface and enhance adsorption of the species to be oxidized at E_1. The result is a reproducible state of electrode activity for each measurement which makes possible precise amperometric measurement of many organic compounds. The time period for completion of the waveform is 0.5—1 s which is sufficiently short to permit virtually continuous monitoring of the effluent stream for flow-injection and h.p.l.c. systems.

EXPERIMENTAL

Instrumentation

Current—potential curves were obtained by cyclic and triple-pulse [8] voltammetry at a platinum rotated-disc electrode (RDE, 0.460 cm^2; Pine Instrument Co., Grove City, PA). The rotator was Model PIR (Pine Instrument Co.). A platinum-disc flow-through detector (0.076 cm^2) was constructed as described previously [8, 9].

The flow-injection apparatus was assembled according to conventional design. Flow of the electrolyte solution was maintained by a Milton Roy

Model CK miniPump (Laboratory Data Control, Riviera Beach, FL) with dual pistons operating 180° out of phase. A Model 709 Pulse Dampener (Laboratory Data Control) connected to a 40-ft stainless-steel tube provided sufficient back-pressure to eliminate pulsations in the flow rate. The stainless-steel tubing connecting the electrolyte reservoir and the pump was 0.11 in. i.d. × 1/8 in. o.d., and all other tubing was stainless steel with dimensions 0.016 in. i.d. × 1/16 in. o.d.; Swagelok fittings were used for all connections. The sample injection valve was a Rheodyne Model 2125 (Larry Bell and Associates, Minneapolis, MN) with a sample volume (V_s) of 100 μl. An adjustable needle valve constructed from Kel-F was connected in the flow system after the detector to generate sufficient back-pressure (<10 psi) to eliminate bubble formation in the detector. Flow rates were calibrated by measurement of the volume delivered to a 10-ml buret during a known period of time, and a flow rate of 0.375 ml min^{-1} was used.

Potentiostatic control was achieved with a Model 173 potentiostat equipped with a Model 176 current-to-voltage converter (Princeton Applied Research, Princeton, NJ). Compensation for *IR* loss was used with the flow-through detector. The reference electrode was a miniature saturated calomel electrode (SCE) filled with a saturated solution of KCl. All potentials are reported as V vs. SCE. The instrument for generating the triple-pulse potential waveform was described previously [8].

Chemicals

All chemicals were reagent grade. All solutions contained 0.10 M NaOH as the supporting electrolyte. All water had been distilled, demineralized, and passed through a 12-in. long × 1.5-in. i.d. column of activated carbon. All solutions of carbohydrates were prepared in 0.10 M NaOH just prior to use to minimize decomposition under the alkaline conditions. Dissolved oxygen was removed from all solutions by saturation with nitrogen.

RESULTS AND DISCUSSION

Cyclic voltammetry

The compounds studied, listed in Table 1, included a ketose, aldoses, and several of the sugar alcohols. The choice of 0.10 M NaOH as the supporting electrolyte was made because the anodic sensitivity for the carbohydrates improves at higher pH.

Preliminary characterization of the anodic response of the compounds tested was based on *I—E* curves obtained by cyclic voltammetry at the platinum RDE. Representative curves are shown in Fig. 1 for dextrose and sorbitol. For the purpose of discussion, the potential axis is divided into three segments and identified on the basis of characterization processes occurring at the platinum RDE in the absence of the carbohydrates. In the hydrogen region (—0.6 to —0.9 V), cathodic and anodic peaks are observed for the supporting electrolyte corresponding to the formation (negative scan)

TABLE 1

Comparison of peak currents for compounds tested by the flow-injection procedure[a]

Compound	Formula	$-I_p(\mu A)$	Compound	Formula	$-I_p(\mu A)$
Dextrose[b]	$C_6H_{12}O_6$	39.1	Xylose[b]	$C_5H_{10}O_5$	33.8
Galactose[b]	$C_6H_{12}O_6$	33.6	Fructose[d]	$C_6H_{12}O_6$	16.9
Mannose[b]	$C_6H_{12}O_6$	29.4	Perseitol[e]	$C_7H_{16}O_7$	38.0
Rhamnose[c]	$C_6H_{12}O_5$	18.3	Mannitol[e]	$C_6H_{14}O_6$	39.2
Arabinose[b]	$C_5H_{10}O_5$	34.4	Sorbitol[e]	$C_6H_{14}O_6$	41.7

[a]Sample: 100 μl of 0.5 mM carbohydrate in 0.1 M NaOH injected into a stream of 0.1 M NaOH. Conditions: v_f = 0.375 ml min^{-1}; E_1 = −0.40 V (155 ms), E_2 = +0.80 V (185 ms) and E_3 = −1.0 V (223 ms). [b]Aldohexose. [c]Methyl pentose. [d]Ketohexose. [e]Sugar alcohol.

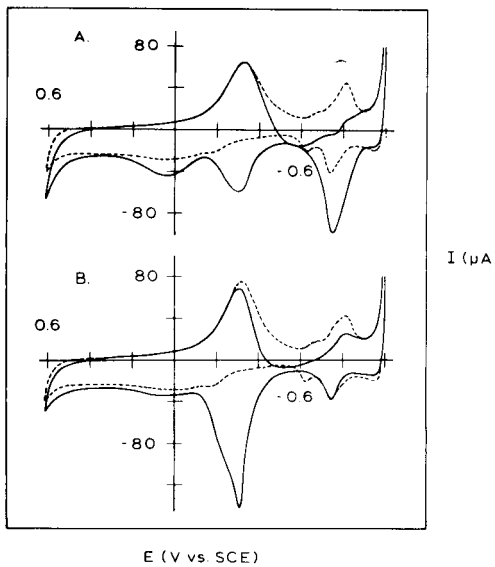

Fig. 1. Current—voltage curves at a platinum RDE by cyclic voltammetry. Conditions: ω = 400 rev min^{-1}, ϕ = 3.0 V min^{-1}. (----) Residual curve for 0.10 M NaOH. (—) Carbohydrate present: A, 0.40 mM dextrose; B, 0.40 mM sorbitol.

and dissolution (positive scan) of adsorbed hydrogen atoms. Virtually no faradaic reactions of the electrode surface occur in the double-layer region (−0.2 to −0.5 V), and in the absence of electroactive solute, the small observed currents correspond to charging of the electrical double layer at the electrode–solution interface. The oxide region (+0.6 to −0.1 V) corresponds to the range of potentials for which a layer of platinum oxide is formed on the electrode surface. The cathodic peak observed on the negative scan at −0.3 V corresponds to reduction of the oxide.

Dextrose and the other aldoses produced anodic peaks on the positive scan in the hydrogen region as well as in the double-layer region. The ketose and

sugar alcohols produced anodic peaks in the double-layer region but produced virtually no increase in the peak for anodic dissolution of adsorbed hydrogen atoms in the hydrogen region. The heights of all anodic peaks obtained on the positive scan for the carbohydrates tested, varied in a linear fashion with changes in the rate of potential scan (ϕ) and these reactions are concluded to be surface-controlled. Furthermore, a linear relationship was obtained for the reciprocal of peak current and the reciprocal of the concentration of the carbohydrates, an observation consistent with a mechanism whereby the faradaic signal is proportional to the fractional surface coverage by the adsorbed organic compounds with adsorption according to the Langmuir isotherm [8, 10].

Ernst et al. [6], working with phosphate buffer at pH 7.5, observed an identical potential dependence for the adsorption of hydrogen atoms and the adsorption of glucose at platinum in the hydrogen region. They proposed a reaction mechanism whereby adsorbed hydrogen atoms promote adsorption of glucose by hydrogen bonding to the hydroxyl group on the C_1 atom for the hemiacetal form of the glucose molecule. Although hydrogen bonding should also promote the adsorption of the sugar alcohols, the absence of an anodic peak for sorbitol at pH 7.5 was attributed, by Ernst et al., to the absence of the easily oxidized hemiacetal form of that compound. A similar benefit from hydrogen atoms was observed for the compounds tested in this study as illustrated for dextrose and sorbitol in Fig. 2. When the negative limit of the cyclic potential scan was shifted from —1.0 to —0.6 V, a pro-

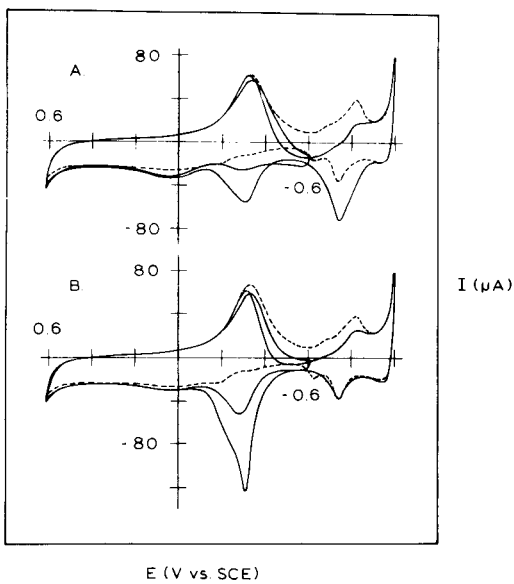

Fig. 2. Effect on *I—E* curves of decreased limit of negative scan. Conditions: ω = 400 rev min^{-1}, ϕ = 3.0 V min^{-1}. (----) Residual curve for 0.10 M NaOH. (—) Carbohydrate present: A, 0.22 mM dextrose; B, 0.22 mM sorbitol.

nounced decrease was observed for the anodic peaks in the double-layer region.

Cyclic voltammetry with interrupted scan

The absence of any significant change in the anodic peak for adsorbed hydrogen atoms in the *I—E* curves obtained by cyclic voltammetry (Fig. 1) upon addition of sorbitol might be concluded as evidence that oxidation of sorbitol by a mechanism involving surface-catalyzed hydrogenation cannot occur. That such a conclusion is tentative is apparent from the recognition that sorbitol is oxidized in the double-layer region during the negative scan of potential (see Fig. 1). Because the product of that reaction is believed to be strongly adsorbed, there is probably an insufficient quantity of unoxidized sorbitol present on the electrode surface at the start of the subsequent positive scan to produce a significant anodic peak in the hydrogen region. To test this possibility, the potential of the platinum RDE was stepped rather than scanned from 0.60 V to −0.94 V following completion of the positive scan. The value of electrode potential was maintained at −0.94 V for 4 s and the *I—E* curve was recorded for the positive scan of potential. The curves are shown in Fig. 3 for sorbitol and dextrose along with *I—E* curves for the background processes obtained under the same conditions but without carbohydrates. A substantial peak was obtained for sorbitol, as well as dextrose, in the hydrogen region. It is concluded that sorbitol, as well as dextrose, undergoes substantial dehydrogenation on the platinum electrode surface. Three possible reasons why the peak for sorbitol in the hydrogen region is smaller than the peak for dextrose are that the surface coverage by sorbitol at equilibrium is less than for dextrose at the same concentration, the rate of desorption of the primary oxidation product is faster for dextrose than for sorbitol, and/or the rate of catalytic dehydrogenation is less for sorbitol.

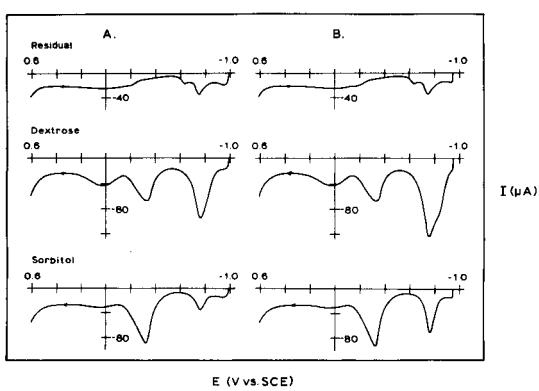

Fig. 3. Current—voltage curves at platinum RDE by cyclic voltammetry with interrupted scan. Conditions: as in Fig. 1, positive scan only is shown. A, Cyclic voltammetry without interruption; B, with interruption of scan at −0.94 V for 4 s.

Flow-injection voltammetry

It is expected that significant new information about the voltammetric response of surface-controlled reactions might be obtained if that response could be measured in the absence of the compound from the bulk solution. This would be particularly useful for differentiating surface-controlled processes resulting from the reaction of adsorbed solute, from those for dissolved solute undergoing reaction controlled by surface transformations. The use of the RDE under conditions of media exchange is cumbersome and accomplishment of this goal by flow-injection voltammetry was investigated. In these experiments, a specified volume of sample was injected into the stream of supporting electrolyte for a constant electrode potential and the resulting *I—t* curve was recorded. When all the dissolved sample had been flushed from the detector by the continuous flow of supporting electrolyte, the *I—E* curve was recorded for a positive, linear sweep of potential. Data obtained in this manner are shown for sorbitol and dextrose in Fig. 4. Note that the direction of the potential axis has been reversed in the figure to be consistent with the time axis of *I—t* curves. Clearly, oxidation of both sorbitol and dextrose occurs for injection at $E = -0.80$ V. The *I—E* curves obtained 45 s after injection, when all carbohydrate had been washed from the detector cell, clearly show anodic peaks in the hydrogen and double-layer regions for both sorbitol and dextrose. These peaks can originate only from the adsorbed carbohydrates. When a period greater than 45 s was allowed to transpire before recording the *I—E* curves, the anodic peaks in the double-layer region were smaller than for 45 s, undoubtedly because of the slow desorption of the reaction products of the oxidation in the hydrogen region.

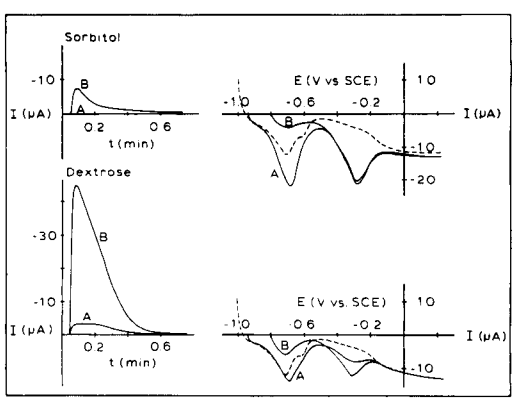

Fig. 4. Current—time and *I—E* curves for the platinum flow-through electrode following injections of sorbitol or dextrose into 0.10 M NaOH. *I—t* curves: A, —0.94 V; B, —0.80 V. *I—E* curves: (----) residual in absence of carbohydrate; *E* during injections: A, —0.94 V; B, —0.80 V; $\phi = 3.0$ V min^{-1}. Other parameters: $V_s = 100$ μl, $v_f = 0.375$ ml min^{-1}, $C^b = 2.5$ mM.

Effect of rotational velocity

For an increase in rotational velocity (ω) of the platinum RDE, the anodic peak for dextrose in the hydrogen region of *I—E* curves obtained by cyclic voltammetry increased whereas the peak in the double-layer region decreased. The anodic peak for sorbitol in the double-layer region also decreased with increases of ω. The values of peak currents are plotted in Fig. 5 as a function of $\omega^{1/2}$ for typical conditions of concentration. Linearity of plots of faradaic signal vs. $\omega^{1/2}$ are traditionally regarded as diagnostic evidence of mass-transport control in the reaction mechanism at a RDE [11]. Although the best linear fits of data are shown in Fig. 5, it is apparent that the data would conform better to a curvilinear model. A negative dependence of the anodic peak for dextrose in the double-layer region for 1 M H_2SO_4 has been reported by Skou [10]. This was explained by a mechanism involving desorption and diffusional loss of the enediol form of dextrose reportedly produced on the electrode surface prior to oxidation. Alternatively, similar results would be expected for a mechanism in which intermediate products of a multi-electron oxidation involving sequential charge-transfer steps are lost from the electrode surface by desorption and convective-diffusional mass transport.

The positive dependence of the anodic peak for dextrose on rotational velocity in the hydrogen region is expected if the product of that oxidation is lost by desorption and mass transport to regenerate active surface sites. It is concluded, then, that for carbohydrates the anodic process in the double-layer region corresponds to sequential oxidation steps for the adsorbed product of the primary oxidation occurring in the hydrogen region. A simplified sequence is proposed which accounts qualitatively for the anodic response of the carbohydrates. The proposed sequence is

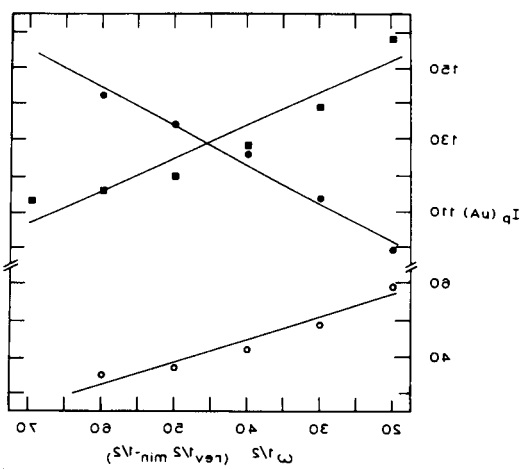

Fig. 5. Effect of rotational velocity on anodic peaks from cyclic voltammetry at the platinum RDE. Conditions: ϕ = 3.0 V min^{-1}. (•) Peak in hydrogen region for 0.40 mM dextrose in 0.10 M NaOH; (○) peak in double-layer region for 0.40 mM dextrose; (▪) peak in double-layer region for 4.94 mM sorbitol.

$$S + R \rightleftharpoons S\text{—}\underline{R} \quad \text{(adsorption)} \quad (1)$$

$$S\text{—}R \rightarrow S\text{—}\underline{R}' + ne \quad \text{(primary anodic reaction in hydrogen region)} \quad (2)$$

$$S\text{—}\underline{R}' \rightarrow S + R' \quad \text{(slow desorption to regenerate active surface site)} \quad (3)$$

$$S\text{—}\underline{R}' \rightarrow S\text{—}\underline{R}'' + n'e \quad \text{(secondary anodic reactions and desorption in the double-layer region)} \quad (4)$$

$$\rightarrow S + R''$$

where S represents an active surface site, R is the reactant dissolved in the bulk solution of supporting electrolyte, R′ and R″ represent successively higher oxidation states of R, and the underline denotes that the indicated species is in the adsorbed state.

The anodic signal in the hydrogen region is enhanced for an increased rate of desorption by Eqn. (3). Because the anodic current in the double-layer region results from oxidation of adsorbed species by Eqn. (4), the signal is decreased if desorption of R′ and R″ is increased.

Triple-pulse voltammetry

The selection of the appropriate value of the potential E_1 for triple-pulse amperometry in a fluid stream [8] was made on the basis of triple-pulse voltammetry at the platinum RDE wherein a linear voltage sweep (E_s, 5 mV s^{-1}) was substituted for a constant value of E_1. Representative I—E curves obtained by this method are shown in Figs. 6 and 7 for dextrose and sorbitol, respectively. Values of potentials E_2 and E_3 (and their duration)

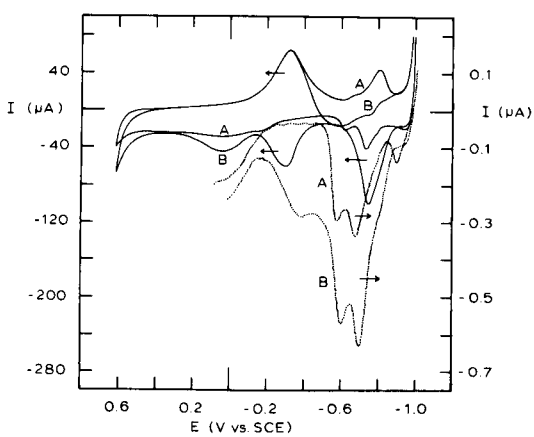

Fig. 6. Current—voltage curves for dextrose at a platinum RDE by cyclic voltammetry and triple-pulse voltammetry. Cyclic voltammetry (—): ϕ = 3.0 V min^{-1}; A, residual; B, 0.50 mM dextrose. Triple-pulse voltammetry (---): $E_1 = E_s$ (125 ms), E_2 = 0.70 V (500 ms) and E_3 = —1.00 V (250 ms), ϕ = 0.30 V min^{-1}; A, residual; B, 2.5 mM dextrose.

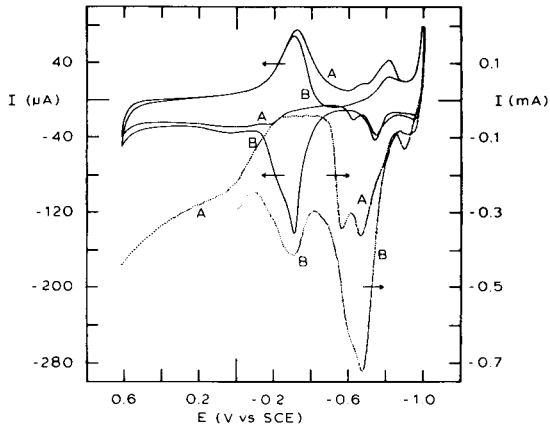

Fig. 7. Current—voltage curves for sorbitol at a platinum RDE by cyclic voltammetry and triple-pulse voltammetry. Conditions identical to Fig. 6 except that sorbitol was substituted for dextrose.

for oxidative cleaning and reduction of the electrode surface were +0.70 V (500 ms) and −1.00 V (250 ms), respectively. The potential $E_1 = E_s$ was applied for a total time of 125 ms with the measurement of current (1 ms) done after 100 ms. Curves are also shown which were obtained for the supporting electrolyte alone. A substantial increase of the anodic peaks in the hydrogen region was obtained with addition of sorbitol and dextrose. The enhanced peaks have shapes and positions identical to the peaks observed in the absence of the organic compounds and the conclusion is reaffirmed that the enhanced signal is from adsorbed hydrogen atoms produced by surface-catalyzed dehydrogenation of the carbohydrates.

Anodic peaks were also obtained for both sorbitol and dextrose in the double-layer region with peak potentials of −0.30 V for sorbitol and −0.38 V for dextrose. The background currents for these faradaic peaks are minimal. The electrochemical behavior of all sugar alcohols tested was similar to that of sorbitol and the behavior of the aldoses and ketoses tested was similar to that of dextrose. An optimum value of E_1 for detection of aldoses in 0.1 M NaOH was concluded to be −0.40 V and the value for the alcohols and ketoses was concluded to be −0.30 V. The value of −0.40 V was chosen as the best single potential applicable for all three classes of compounds. At that potential, little change in the analytical signal was observed for small changes of potential and, furthermore, the background was minimal.

Flow-injection detection

The triple-pulse amperometric technique with the platinum-disc flow-through detector was evaluated for flow-injection applications. The response was maximized for dextrose by variation of the time periods for application of each of the three potentials in the waveform. The faradaic response for

E_1 = −0.40 V was observed to increase in a nearly linear fashion when the time for E_3 = −1.0 V was increased from 100 to 223 ms. This probably happens because increased time at the cathodic potential results in the accumulation of a greater quantity of adsorbed compound. Beyond 223 ms, the faradaic signal decreased probably because electrode fouling was more appreciable resulting from the more extensive dehydrogenation at E_1. The value of E_2 was increased to +0.80 V and the time of oxidative cleaning was decreased to 185 ms. These values of potential and time were sufficient for complete cleaning of the electrode surface as indicated by the reproducibility of the faradaic signals at E_1. The value of E_3 was set at −0.40 V, as discussed previously, for a total time of 155 ms. Current measurement was achieved in a period of 1 ms initiated 118 ms after application of E_1. The total cycle time for this waveform was 563 ms.

Values of peak heights (I_p) obtained under these conditions are given in Table 1 for injections of 100-μl aliquots of 0.50 mM solutions of each compound. It should be noted that, because of dispersion of the sample plug in the fluid stream, I_p is less than the steady-state signal which would be observed for continual flow of a solution 0.50 mM in analyte [12]. However, dispersion affects each sample in an identical manner so that intercomparison of values for I_p leads to correct conclusions regarding relative sensitivities of the triple-pulse technique for these compounds.

Calibration studies were conducted for dextrose and sorbitol by the flow-injection method. Concentrations were in the range 0.10—1.00 mM (1.8—18 μg per 100 μl for dextrose). Three injections were made for each concentration. The peaks obtained for dextrose are shown in Fig. 8. As expected for detection of an adsorbed analyte [8], plots of $-1/I_p$ vs. $1/C$ were linear for both dextrose and sorbitol. Least-squares statistics describing the plots are given in Table 2. In comparison, peaks recorded (not shown) for a constant applied potential were negligibly small after two injections and were useless for detection of carbohydrates.

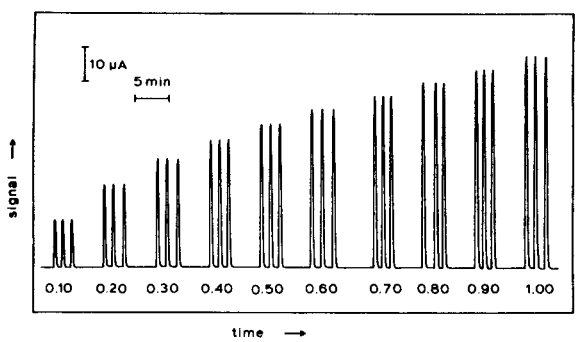

Fig. 8. Peaks obtained with the flow-injection system for dextrose in 0.10 M NaOH. Conditions: E_1 = −0.40 V (155 ms), E_2 = +0.80 V (185 ms), E_3 = −1.0 V (223 ms); v_f = 0.375 ml min^{-1}; V_s = 100 μl; concentration given below peaks as mM.

TABLE 2

Least-squares statistics for plots of $1/I_p$ vs. $1/C$[a]

Parameter	Dextrose	Sorbitol
Slope (mM μA^{-1})	$(5.9 \pm 0.2) \times 10^{-3}$	$(4.4 \pm 0.1) \times 10^{-3}$
Intercept (μA^{-1})	$(11.0 \pm 0.9) \times 10^{-3}$	$(14.5 \pm 0.2) \times 10^{-3}$
Standard error (μA^{-1})	1.1×10^{-3}	2.8×10^{-4}
r^2	0.9963	0.9995

[a]Data obtained by flow injection for three runs on each of ten concentrations between 0.1 and 1.0 mM. Conditions given in Table 1. Uncertainties represent 90% confidence limits.

The detection limits for dextrose and sorbitol by triple-pulse detection (50% uncertainty in I_p) are approximately 0.01 mM (0.2 μg per 100 μl for dextrose). The detection limit for dextrose by refractive index has been reported as 50 μg per 100 μl, although this value was determined for h.p.l.c. under dispersive conditions somewhat different than for this work.

These results strongly suggest that triple-pulse amperometry at a platinum flow-through electrode under a waveform executed with a frequency of 1—2 Hz should be satisfactory for detection in h.p.l.c. Actual applicability must be verified for the eluent specified for any desired separation.

REFERENCES

1 P. E. Shaw, C. W. Wilson, III and R. J. Knight, Jr., J. Agric. Food Chem., 28 (1980) 379.
2 J. K. Palmer and W. B. Brandes, J. Agric. Food Chem., 22 (1974) 709.
3 H. D. Scobell, K. M. Brobst and E. M. Stelle, Cereal Chem., 54 (1977) 905.
4 M. L. B. Rao and R. F. Drake, J. Electrochem. Soc., 116 (1969) 334.
5 S. Ernst, J. Heitbaum and C. H. Hamann, J. Electroanal. Chem., 100 (1979) 173.
6 S. Ernst, J. Heitbaum and C. H. Hamann, Ber. Bunsenges. Phys. Chem., 84 (1980) 50.
7 C. K. Colton, J. Giner and S. Morris, J. Electrochem. Soc., 126 (1979) 43.
8 S. Hughes, P. L. Meschi and D. C. Johnson, Anal. Chim. Acta, 132 (1981) 1.
9 T. R. Lindstrom, Ph.D. Thesis, Iowa State University, Ames, IA, 1980.
10 E. Skou, Electrochim. Acta, 22 (1977) 313.
11 W. J. Albery and M. L. Hitchman, Ring-Disc Electrodes, Clarendon Press, Oxford, 1971.
12 P. L. Meschi and D. C. Johnson, Anal. Chim. Acta, 124 (1981) 303.

Analytica Chimica Acta, 132 (1981) 23—33
Elsevier Scientific Publishing Company, Amsterdam — Printed in The Netherlands

POTENTIOMETRIC STRIPPING ANALYSIS AT A STATIONARY ELECTRODE

CHRISTIAN LABAR and LUC LAMBERTS*

Laboratoire de Chimie Analytique et de Spectrométrie de Masse, Facultés Universitaires Notre-Dame de la Paix, 61, rue de Bruxelles, B 5000 Namur (Belgium)

(Received 13th March 1981)

SUMMARY

The feasibility of controlling the transport mechanism of the oxidizing species at the working electrode during the stripping step of potentiometric stripping analysis is demonstrated. When linear diffusion of the oxidizing species is the rate-determining mechanism at the working electrode/solution interface and when the physical properties of the medium are considered to lower the diffusion coefficient of the oxidizing species, the relative sensitivity of the technique is enhanced by a factor of 50 for all the common ions studied by potentiometric stripping analysis. Examples and comparison with the normal procedure are given for Cu, Cd, Zn, Pb, Bi, Tl and Ga. The "stationary electrode" procedure is compatible with the normal instrumentation without great modification; it is self-optimizing with respect to time and resolution and preserves all the inherent advantages of potentiometric stripping analysis compared to other electrochemical techniques of trace analysis. The enhancement of the relative sensitivity by this modification permits measurements in the 0.01—0.1 ppb range for metal ions; the total time required is 2—4 min for a single determination and the relative standard deviations are about 3%.

Anodic stripping voltammetry is now a well established technique for trace metal determinations. During pre-electrolysis, metal ions are reduced and amalgamated at a working electrode (mercury drop, mercury or gold film electrode); the reduced metals are then re-oxidized by means of a linear potential ramp imposed between the working electrode and a suitable reference electrode, the current between the working electrode and a platinum counter electrode being measured. Several techniques have been applied for obtaining the analytically valuable faradaic current, eliminating the background capacitance current [1—3].

Until 1976 [4], little attention was paid to studies of the time—potential behaviour of the working electrode as it undergoes chemical oxidation after completion of the pre-electrolysis step. Provided that a suitable oxidizing agent is present, all metals amalgamated at the working electrode will be re-oxidized at a rate dependent on the transport of the oxidizing agent to the working electrode. This will result in a stepwise increase in the potential of the working electrode; the time elapsed in each step is proportional to the amount of given metal deposited at the electrode and, analogously to

anodic stripping voltammetry, to the activities of the given metal ions in the solution.

The analytical possibilities inherent in the potential variations of a working electrode caused by controlled chemical oxidation of amalgamated metals provided the starting point for a new technique referred to as potentiometric stripping analysis (p.s.a.).

Principle of normal potentiometric stripping analysis

If a working electrode, consisting of material insoluble in mercury and with a high hydrogen overvoltage, is held potentiostatically at a sufficiently cathodic potential in a deaerated medium containing mercury(II) ions and mercury-soluble metal ions Me^{n+}, then the reactions $Hg^{2+} + 2e^- \rightarrow Hg$ and $Me^{n+} + ne^- \rightarrow Me(Hg)$ will occur simultaneously at a rate proportional to the activities of mercury(II) and the metal ion in the sample. If the hydrodynamic conditions at the working electrode surface are kept constant (by rotating the electrode or by stirring the solution), the rate of reduction of Me^{n+} ions will be constant until a significant fraction of metal ion activity has been reduced; for small electrode surfaces, the metal ion activity will decrease only very slowly.

If with unchanged hydrodynamic conditions, the potentiostatic circuitry is disconnected while the working electrode and a suitable reference electrode remain connected to a high input impedance voltmeter, the potential changes caused by the reactions $Me(Hg) + n/2\ Hg^{2+} \rightarrow Me(n+) + n/2\ Hg$, will be observed on the potential vs. time recording. The curve obtained consists of a normal redox titration curve superimposed on a capacitance background [4]. After correction for the background, the time elapsed between two consecutive equivalence points will be proportional to the amount of particular metal in the mercury phase. Analogously to anodic stripping voltammetry, the amount of amalgamated metal is proportional to the Me^{n+} activity ($a_{Me^{n+}}$) in the sample and to the time of pre-electrolysis (plating)

$$t = i_{Me^{n+}}\, t_p / i_{Hg^{2+}} = n_{Me^{n+}}\, D_{Me^{n+}}\, a_{Me^{n+}_{(d)}}\, t_p / 2\, D_{Hg^{2+}}\, a_{Hg^{2+}_{(d)}} \qquad (1)$$

where t is the time elapsed between two consecutive equivalence points; $i_{Me^{n+}}$ is the pre-electrolysis current for Me^{n+} ions; t_p is plating time; $i_{Hg^{2+}}$ is the pre-electrolysis current from Hg^{2+} ions; $D_{Hg^{2+}}$ and $D_{Me^{n+}}$ are the diffusion coefficients of Me^{n+} and Hg^{2+} ions, respectively ($cm^2\ s^{-1}$); a is the activity of the relevant ion and suffix (d) indicates a distance d from the electrode/solution interface.

The potential—time curve can form the basis for qualitative as well as quantitative analysis, with use of calibration plots, internal standards or standard additions [5—15]. It must be emphasized that, during the plating and measuring steps, the hydrodynamic conditions at the working electrode surface are kept constant.

Principle of potentiometric stripping analysis at a stationary electrode

The main practical difference between normal p.s.a. and p.s.a. in stationary solution is that, in the latter technique, the hydrodynamic conditions at the working electrode surface are drastically changed between the plating and measuring steps. A few seconds before the end of the pre-electrolysis step, stirring is interrupted and the sample is allowed to settle completely, so that the measuring step is done in a medium where the rate of diffusion of Hg^{2+} ions controls the transport of oxidizing agent at the working electrode/solution interface. In the case of a planar working electrode, and considering the velocity in the direction perpendicular to the electrode surface, the flux J of electroactive species Hg^{2+} during the measuring step is given [16] by

$$J = -a_{Hg^{2+}} [(D_{Hg^{2+}}/RT) (\delta\mu/\delta x) + (D_{Hg^{2+}} 2F/RT) (\delta\phi/\delta x) - \sigma] \quad (2)$$

where μ is the chemical potential; ϕ is the electrode inner potential; x is the distance from the electrode area in the solution; σ is the velocity in the direction perpendicular to the planar working electrode; R, T, F have their usual meanings and other terms are as defined above; in the second term in square brackets, 2 relates to the charge on Hg^{2+} ions.

In p.s.a. in stationary solution, the parameters affecting the value of flux J are considered so that the diffusion process effectively controls the transport of oxidizing species, and the medium is kept (or modified to) pre-determined conditions which enable the diffusion rate to be minimized. This enhances the relative sensitivity and detection limit of the technique for a given pre-electrolysis time [7].

EXPERIMENTAL

Instrumentation

The basic unit consists of the Radiometer ISS-820 Ion Scanning System [17]; this system comprises a REA 120 Ion Scanning Module plugged into a REC-80 Servograph (with REA-260 derivative unit) and a TTA-80 titration cell assembly. The ion-scanning module serves as the control unit for the system; it contains facilities for selection of electrolysis voltage (−2.99 to 0 V vs. SCE) and electrolysis time (1—64 min, with a manual position for other selected plating times), allowing for a wide range of activity measurements. The high-performance servo-recorder registers the potential vs. time curves during the scanning period. The ion-scanning assembly is furnished with three electrodes (glassy carbon F3500, SCE K4040 and Pt P-1312) and a constant-rate stirrer; the sample vessel is designed to ensure anaerobic conditions for the sample. Analytical procedures for cleaning electrodes, testing the SCE for Hg(II) leakage, conservation and cleaning of the glassy carbon electrode and vessels have already been described [6—9].

Two seconds before stripping is initiated, the potentiostatic circuitry is disconnected, and the paper feed of the servograph is automatically started and stopped after a given fraction (1/16) of the selected plating time. The

unit can be operated in a repetitive mode eliminating the reaction between Hg(I) and Hg(II) ions, $Hg(I) + Hg(II) + 2\ Cl^- \rightarrow Hg_2Cl_2$, which forms a film of Hg_2Cl_2 on the working electrode [6—9, 17]. A period of 8 s is allowed for the operator to modify the sample composition according to the analytical procedure (calibration plot, standard addition, internal standard, etc.) compatible with the nature of the sample.

Chemicals

All chemicals used were of analytical reagent (pro analysi) grade; triple-distilled water was always employed and the usual cleaning procedures for trace element analysis were followed [18]. In order to keep within routine perspectives, no special pre-purification of chemicals was done. Background subtraction of experimental signals observed on the recorder was calculated in the normal way for p.s.a. All preparations and dilutions from stock solutions were done with special care, to minimize relative errors [19]. All experiments were done at 20 ± 1°C.

Procedures

Except for the change of hydrodynamic conditions at the working glassy carbon electrode and modifications of the physicochemical properties of solutions, p.s.a. in stationary solutions is essentially identical to normal p.s.a., the procedures for which have been discussed previously in some detail [6, 9, 10, 15, 17, 20].

The glassy carbon electrode, after polishing, is pre-plated in a 2.50×10^{-2} M $HgCl_2$—0.5 M NaCl solution. Dissolved oxygen is previously removed by prolonged bubbling with nitrogen (N48) purified by Oxy-trap 0.42 (Chem. Lab. Ind., Alltech Assoc.). Usually, 4—6 pre-coating—stripping cycles of 4 min each were necessary to obtain reproducible signals. After completion of the last cycle, Me^{n+} ions are introduced by injection of 1.0 ml of stock solution in the activity range 10^{3^-}—10^{6^-}. The deaeration of the medium is completed during the total cycle.

An outline of the automatic procedure, with indication of the differences from p.s.a., is given in Table 1. Times depend on the instrumental conditions selected.

RESULTS AND DISCUSSION

Diffusion of oxidizing species as the rate-controlling transport mechanism

In order to be sure that diffusion of the oxidizing species controls the rate of transport at the mercury—glassy carbon electrode/solution interface during the stripping step, various solution settling times before the end of the plating step were imposed for a constant total plating time. Figure 1 illustrates the variation of the rate of transport (simply taken as the inverse of the "stripping plateau" (see below)) with the settling time of the solution. It can be seen that the rate of oxidation by mercury(II) ions diminishes

TABLE 1

Outline of the procedure for p.s.a. under stationary conditions (p.s.a.s.)

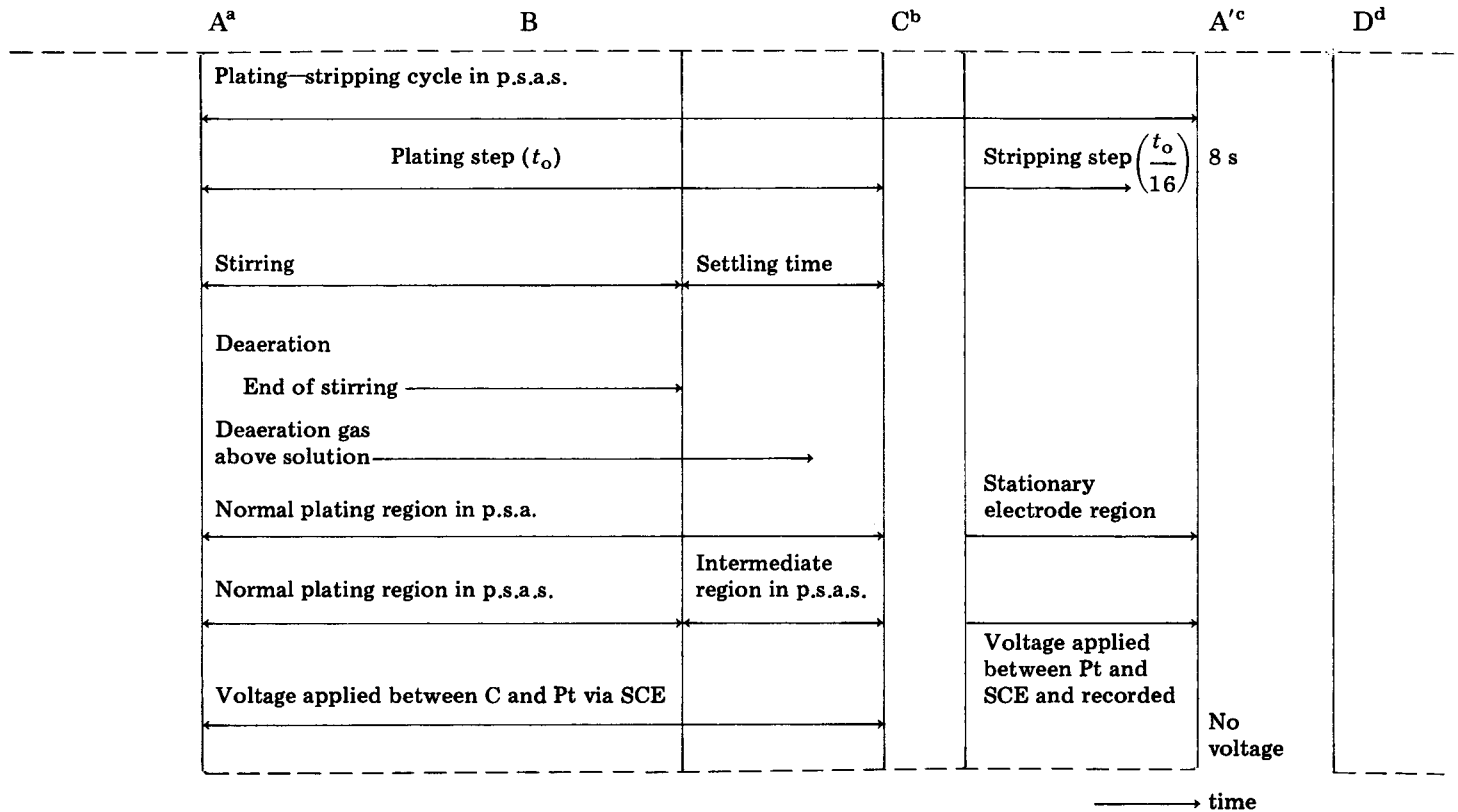

[a]Modification of the medium to obtain lower diffusion rate (see Detection limits). [b]Electronically imposed disruption of voltage between plating and stripping steps. [c]Standard addition, calibration plot; modification of the solution or automatic new plating—stripping cycle in the same medium by p.s.a. at a stationary electrode. [d]Following plating—stripping cycle in the modified procedure.

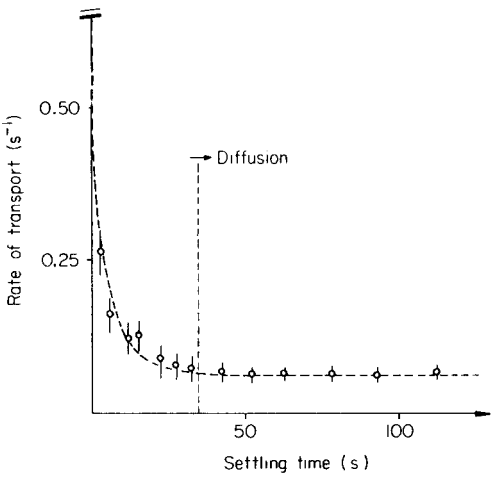

Fig. 1. Effect of variations of settling period on the rate of the transport mechanism of Hg^{2+} ions. Solution conditions: 7.36×10^{-7} M $ZnCl_2$, 2.50×10^{-3} M $HgCl_2$, 0.50 M NaCl. Instrumental conditions: continuous N_2 flow, plating at −1.2 V vs. SCE for 8 min, 0.2 cm s^{-1} chart speed, 2 V full scale, 6 cyclic scans. $\sigma = \pm 2.03\%$ in the "diffusion" region.

rapidly for settling periods in the range 2—10 s, during which the stripping signals were very irreproducible (relative standard deviation for 6 cycles, 8%). The rate reaches a constant value of 6.5×10^{-2} s^{-1} for all settling periods exceeding 30 s. In this range, the rate of oxidation is lower than the corresponding rate of normal p.s.a. (without a settling period) by a factor of 1.30/0.065 = 20; the rate is also reproducible (for 6 cycles, $\sigma = \pm 2.03\%$).

These facts indicate that the transport mechanism of the oxidizing species at the electrode/solution interface is mainly governed by linear diffusion of mercury(II) ions in the layers of solution in contact with the interface; the working electrode is thus in "stationary conditions". Under these conditions, the oxidation process is slowed down by a factor of 20 compared to normal p.s.a. and the relative sensitivity of the method, previously defined [10, 13, 15] as the time signal obtained with a given set of experimental conditions, is enhanced proportionally. It must be remembered that any effect of transport by conduction is eliminated from the observed signals by background subtraction.

These results agree closely with theoretical models and calculations obtained by various studies in anodic stripping voltammetry at a mercury film electrode [21—23].

Determination of metal ions

As already demonstrated [5, 7, 10—15], all metal ions which can be determined by anodic stripping voltammetry can also be measured by potentiometric stripping analysis. The fact that different rates of diffusion are utilized in the proposed method does not affect the breadth of application.

As expected theoretically, the potentials at the half-titration points on the stripping curves obtained in p.s.a. at a stationary electrode correspond closely to the potentials at the stripping peaks in anodic stripping voltammetry [14, 15]. Practically, all the qualitative information available from normal p.s.a., and all the recommendations for the best composition of electrolytes can be extrapolated from previous p.s.a. studies to the proposed modification. Particularly, the two modes of operation are self-optimizing for potential resolution of metal ion mixtures.

Figure 2 illustrates these conclusions for mixtures of the commonest metal ions measured by anodic stripping voltammetry and normal p.s.a.

Detection limits

The detection limits in potentiometric stripping techniques depend on the plating time, the Hg^{2+} activity, the glassy carbon surface, and the extent of computerization of the instrumentation [17, 20, 24, 25], as well as on the rate of transport of the oxidizing species at the working electrode/solution interface. The main difference between normal p.s.a. and p.s.a. in stationary solutions is the difference in this rate of transport. All parameters

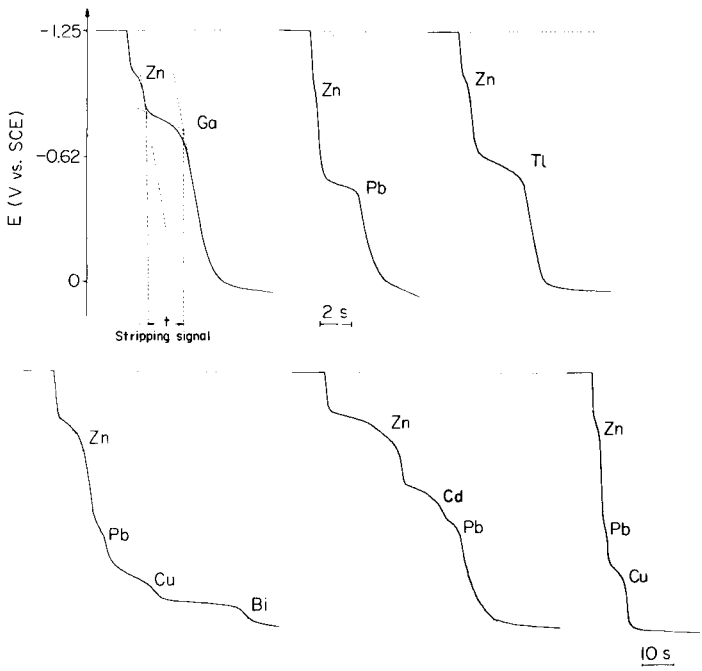

Fig. 2. Stripping curves for common metal ion mixtures under stationary conditions. Solution conditions: 10^{-7}—10^{-8} M Me^{n+} (as chloride), 2.50×10^{-3} M $HgCl_2$, 0.01—0.1 M HCl, 0.5 M NaCl. Instrumental conditions: continuous N_2 flow, plating at —1.25 V vs. SCE for 4 min, 1—0.2 cm s^{-1} chart speed, 2 V full scale, 6 cyclic scans, 35-s settling period. The 2-s scale shown is relevant for all except the last curve.

lowering the rate of solution diffusion of (Hg^{2+}) ions (Eqns. 1 and 2) influence the detection limit. Figure 3 illustrates the effect of increasing viscosity of the medium (thus lowering the diffusion coefficient) by addition of a viscous substance without tensio-active contribution; the addition of up to 5% 1,2,3-propanetriol would therefore improve detection limits further.

The detection limit depends on the Hg^{2+} activity in the medium or, more exactly, on the ratio of the activities of Hg^{2+} to Me^{n+} in the electrochemical cell solution. Analytical considerations of p.s.a. techniques [9—15] indicate a linear dependence of the oxidation rate on this ratio over a large range of values. The signal dependence on this ratio is illustrated, for p.s.a. in stationary solutions, in Fig. 4 for ratios ranging from 10 to 10 000 with a zinc ion activity of 10^{-8} M. This figure requires some comment. As in conventional p.s.a., the relationship is approximately linear; at low ratios (below 5 mg Hg^{2+} l^{-1}), traces of oxygen can contribute to the overall process, causing deviations from linearity [6—8]. The effect is less under the present conditions, possibly because of better nitrogen purification and flushing arrangements. It should be mentioned that, for $Hg^{2+}/Zn^{2+} < 100$, the stripping signals observed were irreproducible (σ = 10% for 6 cycles), which was not the case for higher ratios (σ = 3% for 6 cycles).

The question of detection limit in potentiometric stripping analysis is largely an instrumental problem. In normal p.s.a., low metal ion activities can only be determined (on commercially available instrumentation) by time-consuming cycles, with long plating steps. In computerized p.s.a. [12, 15, 24, 25] such problems can be partly circumvented, but it is very difficult to claim numerical values for detection limits, not only because of interference problems, types of media studied and instrumental possibilities,

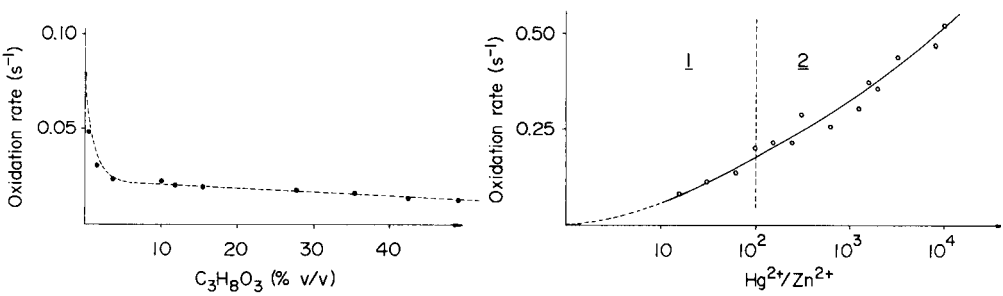

Fig. 3. Effect of addition of 1,2,3-propanetriol on the rate of transport of Hg^{2+} ions. Solution conditions: 7.36 × 10^{-7} M $ZnCl_2$ (19.2 ppb), 2.5 × 10^{-3} M $HgCl_2$, 0.5 M NaCl. Instrumental conditions: as for Fig. 2. σ = 3.0% (n = 6).

Fig. 4. Variation of the oxidation rate with the ratio $a_{Hg^{2+}}/a_{Me^{n+}}$ in solution. Solution conditions: 10^{-9} M $ZnCl_2$, 0.5 M NaCl, variable $HgCl_2$ concentration, 16% (v/v) 1,2,3-propanetriol. Instrumental conditions: continuous N_2 flow, plating at —1.25 V vs. SCE for 2—8 min, 1—0.1 cm s^{-1} chart speed, 2 V full scale, 6 cyclic scans, 35-s settling period. Reproducibility (n = 6): 3.0% for region 2 and 8—10% for region 1.

but because general considerations indicate that detection of 100 ppb "heavy metal" requires practical plating steps of 20 min to be considered in normal p.s.a. Further, 3--4 plating—stripping cycles are frequently necessary in quantitative p.s.a. to achieve the required accuracy and reproducibility, so that normal p.s.a. for a sample containing 100 ppb "heavy metals" may take 90—180 min [6, 12, 14].

The use of p.s.a. under stationary conditions largely eliminates this disadvantage of the normal p.s.a. technique for routine analysis without instrument modification. Figure 5 illustrates this practical point of view for

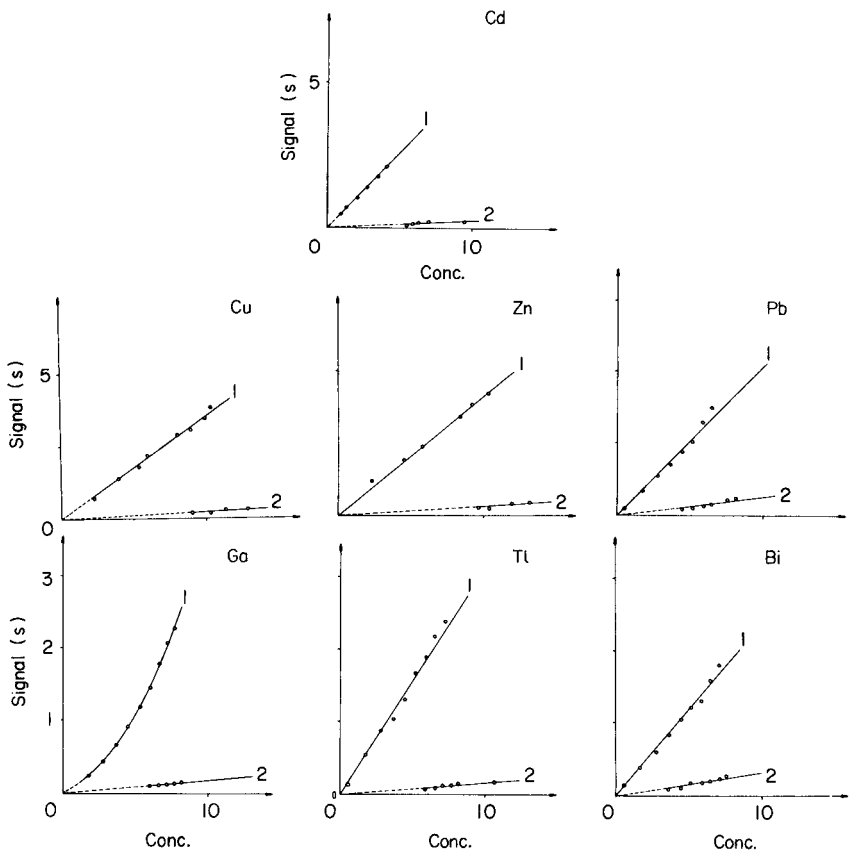

Fig. 5. Comparison between calibration plots obtained by p.s.a. under stationary conditions (curves 1) and by normal p.s.a. (curves 2) for the same solution conditions for common metal ions. The concentration axes relate to 1—10 × 10^{-8} M solutions of the metal ion in all cases. Solution conditions: 10^{-7}—10^{-8} M Me^{n+}, 2.50 × 10^{-4} M $HgCl_2$, 0.50 M NaCl, 0.10 M HCl. Instrumental conditions: continuous N_2 flow, plating at —1.25 V vs. SCE for 4 min, 0.5—0.015 cm s^{-1} chart speed, 2 V full scale, 6 cyclic scans. For p.s.a. under stationary conditions, 10% (w/v) 1,2,3-propanetriol was added and the settling time was 35 s; 1,2,3-propanetriol was not added for normal p.s.a. The reproducibility (n = 6) was about 30% for normal p.s.a. and ⩽3.5% for the modified method.

the most common metal ions studied by p.s.a. techniques. Calibration plots for the normal and modified techniques were obtained with a pre-determined 4-min plating time compatible with routine analysis (one plating—stripping cycle terminated in 260 s). Figure 5 shows that normal mode does not provide quantitative results in the 10^{-8}—10^{-7} M Me^{n+} range; signals are lower than 1 s at the maximum recorder speed; that reproducibility is very poor, the instrumental uncertainty being ±0.1 s. In contrast the modified technique provides signals up to 3—5 s for the same range of concentrations at the same recorder speed with a reproducibility of about 3.5% which is qualitatively similar to anodic stripping voltammetry. The modified p.s.a. procedure is therefore useful for the ppb range of "heavy metal" ions with an experimental time suitable for routine analysis.

This practical point of view is emphasized by the fact that a new generation of commercially available instruments will be compatible with stationary electrode mode of operation [26].

Conclusions

Potentiometric stripping analysis at a stationary electrode can be done with the same simple instrumentation as for normal potentiometric stripping analysis and commercial instruments are now automatically provided with this mode of operation. Cell construction and electrode configuration must eventually be considered in optimizing the diffusion mechanism of the oxidizing species at the working electrode. Only simple modification of the physico-chemical properties of the medium is needed for the new technique and this can be included in the automatic plating—stripping cycles. All theoretical principles involved in normal p.s.a. are applicable.

The proposed method is particularly suited to measurements, without loss of resolution, in solutions in which the activities of the different metal ions vary considerably, e.g. by 4—6 orders of magnitude. Without loss of experimental time, normal p.s.a. can be applied for high metal activities ($\geqslant$1 ppm) and p.s.a. at a stationary electrode for lower metal activities (0.01—0.1 ppb). As in the normal mode, one metal ion is completely stripped before stripping of the next metal ion. Both procedures are self-optimizing with respect to time and resolution, in contrast to techniques based on anodic stripping voltammetry.

Advantages found in the normal mode of p.s.a. (e.g., calibration plots, standard addition, field experiments, samples containing only small activities of supporting electrolyte) [5—9] are retained in the modified procedure. The stationary electrode mode enhances the relative sensitivity by a factor of 20 (without modification of the viscosity of the medium) to 50 (with modification of this viscosity by a convenient substance) for all common metal ions studied compared to normal p.s.a. Activities of about 0.1 ppb can be measured with an experimental time of 2—4 min for a single measurement with a conventional recorder.

For very low metal activities, both potentiometric stripping techniques are

prone, like other analytical methods, to contamination and require background elimination or subtraction. Studies on this aspect [5, 15, 19] have given satisfying conclusions. With the stationary conditions, all parameters affecting the background contribution (capacitance signal) must be considered in attempts to enhance the analytically valuable signal. Automatic background subtraction is being studied to circumvent such difficulties.

Comparison between p.s.a. at a stationary electrode and computerized p.s.a. is of practical importance for routine work. Computerization of the proposed modification would allow very fast measurements of very low metal ion activities without loss of analytical precision, and is currently under study.

REFERENCES

1 E. Barendrecht, Stripping Voltammetry, in A. J. Bard (Ed.), Electroanalytical Chemistry, Vol. 2, M. Dekker, New York, 1967, p. 53.
2 E. Gileadi, E. Kirowa-Eisner and J. Penciner, Interfacial Electrochemistry, Addison-Wesley, Reading, MA, 1975.
3 T. R. Copeland, J. H. Christie, P. A. Osteryoung and R. K. Skogerboe, Anal. Chem., 45 (1973) 2171.
4 D. Jagner and A. Granéli, Anal. Chim. Acta, 83 (1976) 19.
5 D. Jagner and K. Årén, Anal. Chim. Acta, 100 (1978) 375.
6 D. Jagner, Anal. Chim. Acta, 105 (1979) 33.
7 D. Jagner and K. Årén, Anal. Chim. Acta, 107 (1979) 29.
8 D. Jagner, L. G. Danielsson and K. Årén, Anal. Chim. Acta, 106 (1979) 15.
9 D. Jagner and K. Årén, Anal. Chem. Symp. Ser. 2; Electroanal. Hyg. Environm. Clin. Pharm. Chem., Elsevier, Amsterdam, 1980, p. 175.
10 D. Jagner and K. Årén, Anal. Chim. Acta, 117 (1980) 165.
11 D. Jagner and S. Westerlund, Anal. Chim. Acta, 117 (1980) 159.
12 J. K. Christensen and L. Kryger, Anal. Chim. Acta, 118 (1980) 53.
13 D. Jagner, Anal. Chem., 50 (1978) 1924.
14 D. Jagner, Anal. Chem., 51 (1979) 342.
15 T. Anfält and M. Strandberg, Anal. Chim. Acta, 103 (1978) 379.
16 I. Fried, The Chemistry of Electrode Processes, Academic Press, London, 1973, p. 28.
17 A. M. Graabaek and D. J. Jensen, Ind. Res., 21 (1979) 124.
18 T. C. O'Haver, Chemical Aspects of Elemental Analysis, in J. D. Winefordner (Ed.), Trace Analysis, J. Wiley, New York, 1976.
19 R. B. Lamb and T. L. Isenhour, Anal. Chem., 52 (1980) 1158.
20 J. Mortensen, E. Ouziel, H. J. Skov and L. Kryger, Anal. Chim. Acta, 112 (1979) 297.
21 W. T. de Vries and E. van Dalen, J. Electroanal. Chem., 14 (1967) 315; 8 (1964) 366.
22 E. van Dalen, J. Electroanal. Chem., 12 (1966) 9; 9 (1965) 448.
23 T. M. Florence, J. Electroanal. Chem., 97 (1980) 219.
24 H. J. Skov and L. Kryger, Anal. Chim. Acta, 122 (1980) 179.
25 A. Granéli, D. Jagner and M. Josefson, Anal. Chem., 52 (1980) 2220.
26 J. Möller, in S. Eklund (Ed.), In Focus, No. 7, Tecator AB, Höganäs, Sweden, 1981, p. 7.

Analytica Chimica Acta, 132 (1981) 35—41
Elsevier Scientific Publishing Company, Amsterdam — Printed in The Netherlands

VOLTAMMETRIC DETERMINATION OF AGRICULTURALLY-SIGNIFICANT BENZENEARSONIC ACIDS

MARC ANDREWS and WILLIAM E. GEIGER, JR.*
Department of Chemistry, University of Vermont, Burlington, VT 05405 (U.S.A.)

(Received 28th May 1981)

SUMMARY

Direct current and differential pulse polarographic measurements are reported on a series of substituted benzenearsonic acid compounds that are important in agricultural applications. Compounds studied were *o*-aminobenzenearsonic acid, *p*-aminobenzenearsonic acid, *p*-nitrobenzenearsonic acid, *p*-ureidobenzenearsonic acid, and 3-nitro-4-hydroxybenzenearsonic acid. Polarographic reduction potentials varied with pH for all compounds, shifting to more negative values as the pH was increased. Although diffusion-controlled reduction waves were observed in all cases, some compounds exhibited a dependence of $E_{1/2}$ on concentration, especially at relatively high concentrations. Differential pulse polarographic peak currents were proportional to concentration from 10^{-4} M to 10^{-6} M.

Over the last several years, efforts have been made to develop methods for speciation of forms of arsenic that are present in the environment from natural, industrial, or other commercial sources. In some cases, methods have been developed to quantify particular chemical forms of arsenic under various environmental conditions. For example, inorganic arsenic(V) or arsenic(III), as well as methylarsonic acid and dimethylarsinic acid, can now be separated and quantified at trace levels by various chromatographic [1—6], spectroscopic [7—13], and electrochemical methods [6, 14—18]. An important class of organoarsenicals that has been much less widely studied is that of the substituted phenylarsonic acids. These acids are used extensively in agricultural applications, predominantly as animal growth promoters and feed stock additives [19]. This paper reports results of d.c. and differential pulse polarographic experiments on the 5 compounds (1)—(5) which show that it is feasible to quantify these compounds electrochemically down to con-

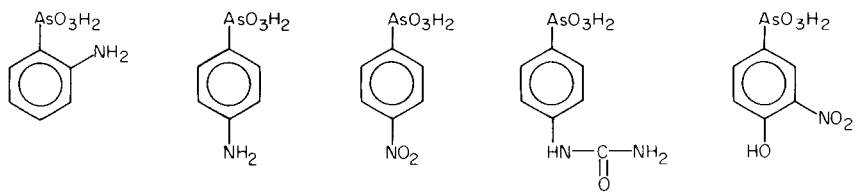

(1) (2) (3) (4) (5)

centrations slightly below 10^{-6} M. Comment is made on the effect of pH on the polarographic half-wave potentials and plateau currents for these compounds. Although the electrochemical waves themselves are quite reproducible, the reductions are generally highly irreversible and appear to be mechanistically complex.

EXPERIMENTAL

Reagents and apparatus

The arsenic compounds were obtained from commercial sources: *o*-aminobenzenearsonic acid (*o*-arsanilic acid) (1), and *p*-nitrobenzenearsonic acid (nitarsone) (3) from Aldrich; *p*-aminobenzenearsonic acid (*p*-arsanilic acid) (2) from Eastman; 4-ureidobenzenearsonic acid (carbarsone) (4), and 3-nitro-4-hydroxybenzenearsonic acid (roxarsone) (5) from Pfaltz and Bauer. Each acid was recrystallized from water (cooled to about 5°C) at least 6 times and subsequently dried in vacuo at 75°C. Supporting electrolytes were either Britton—Robinson buffers or HCl—NaCl solutions.

A Princeton Applied Research Model 174A Polarographic Analyzer was used with the routine measurement procedures described elsewhere [14]. Potentials are referred to the aqueous saturated calomel electrode (s.c.e.). A pulse height of 25 mV was used in differential pulse polarographic measurements. Scan rates of 5 mV s^{-1} and drop times of 1—2 s were employed. The dropping mercury electrode (Sargent) had typical flow rates of ca. 0.2 mg s^{-1}.

RESULTS AND DISCUSSION

General electrochemical behavior

Electroactivity of substituted phenylarsonic acids has been observed previously in the early work of Breyer [20] and later investigations by Maruyama and Furuya [21] and by Watson and Svehla [22—24]. The latter authors also did extensive mechanistic work on the unsubstituted compound, phenylarsonic acid, and were able to identify various oxidation states of arsenic in the final products. The present results on these substituted phenylarsonic acid compounds suggest very complex electrode mechanisms which may not only be pH-dependent, but also concentration-dependent, and may involve formation of films or adsorbed layers at the electrode surface.

In spite of these difficulties, under d.c. polarographic conditions, these compounds exhibited well-defined waves. In each case, a wave attributable to the arsonic acid group was observed close to the potential of electrolyte background and the nitro-substituted compounds (3) and (5) also showed waves arising from nitroreduction at much more positive potentials. Some pertinent polarographic data are collected in Table 1, in which $E_{1/2}$ potentials for the arsonic acid reduction are given for a representative pH. These waves are generally diffusion-controlled but highly irreversible. Inspection of the table shows that the polarographic slopes range from 95 to 200 mV/decade,

TABLE 1

Direct current polarographic data for benzenearsonic acid derivatives

Compound	pH	$E_{1/2}$(V)[a]	I[b]	Slope[c]
o-Aminobenzenearsonic acid	1.70	−1.01	6.41	95
	2.12	−1.02	6.62	200
p-Aminobenzenearsonic acid	1.49	−1.04	6.20	142
p-Nitrobenzenearsonic acid	1.11	−0.10[d]	—	—
	1.11	−1.05[e]	4.25	115
p-Ureidobenzenearsonic acid	3.02	−1.12	4.23	117
3-Nitro-4-hydroxybenzenearsonic acid	0.96	−0.10[d]	—	—
	0.96	−1.10[e]	9.45	130

[a]Versus aqueous saturated calomel electrode. [b]Diffusion current constant in units of μA mM^{-1} $mg^{-2/3}$ s^{-1}. [c]Slope of plot of log $[I/(I_d - I)]$ versus $-E$. Approximate error ±5 mV. [d]Reduction of nitro group. [e]Reduction of arsonic acid group.

far in excess of the $59/n$ mV/decade (n = number of electrons transferred) expected for a reversible process. Half-wave potentials were pH-dependent, which is to be expected for reductions in which protons are involved in the electron-transfer step.

The arsanilic acids

These compounds (1) and (2) were perhaps the best behaved among those studied. The *o*-isomer (1) exhibited a single wave between pH 0 and 3.2 with optimum resolution from the hydrogen discharge wave at about pH 1.6. The $E_{1/2}$ value became more negative as the pH increased (Fig. 1A) with a slope of about −140 mV/pH, until approximately pH 3, at which point there was a plateau in the plot. The inflection point at pH 3 should approximate that of the pK_a of (1), and is a bit higher than the reported value of $pK_a = 2.20$ [25]. The diffusion-limited current was independent of pH, but there was a definite dependence of $E_{1/2}$ on concentration, which was unexpected. Similar observations were made with several of the other compounds, and representative data are collected in Table 2. There was generally a small shift to more negative

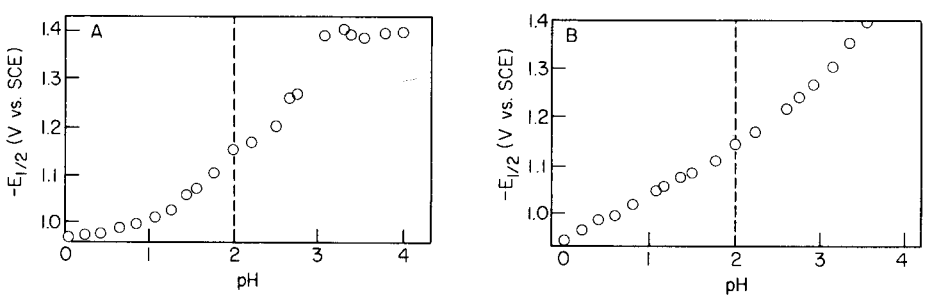

Fig. 1. Plot of $E_{1/2}$ vs. pH for the reduction of (A) *o*-aminobenzenearsonic acid and (B) *p*-aminobenzenearsonic acid. Left — HCl—NaCl medium; right — Britton—Robinson buffer.

TABLE 2

Dependence of $E_{1/2}$ on concentration for two of the compounds

o-Aminobenzenearsonic acid (pH 1.54)						
$-E_{1/2}$ (V)	1.02	1.04	1.09	1.11	1.12	1.13
Conc (mM)	0.15	0.28	0.46	0.70	1.12	1.35
p-Nitrobenzenearsonic acid (pH 1.12)						
$-E_{1/2}$ (V)[a]		0.14	0.14	0.15	0.15	0.16
Conc (mM)		0.29	0.54	0.91	1.07	1.45
$-E_{1/2}$ (V)[b]		1.05	1.06	1.08	1.10	1.14
Conc (mM)		0.29	0.54	0.91	1.07	1.45

[a]Nitro wave. [b]AsO_3H_2 wave.

values as the concentration was increased. This could mean that the reduction involves arsenic compounds that are somehow associated in solution prior to electron transfer. Fortunately, the reduction potentials are reasonably constant at concentrations below 10^{-4} M.

The reduction of (2) took place in a single diffusion-controlled, irreversible wave in the pH range 0—3.6. The dependence of $E_{1/2}$ on pH is shown in Fig. 1B; a linear dependence with a slope equal to about −140 mV/pH was observed in the pH range 0—2, and a somewhat steeper dependence was apparent in the range 2—3.6. Although this may signal a change in reduction mechanism as one proceeds from strongly- to mildly-acidic media, it is noted that the polarographic diffusion current does not change over this pH range. Controlled-potential electrolysis experiments on this compound at pH 1.5 or 2.5 did not yield tractable results. These attempts were complicated by partial background discharge and apparent regeneration of the starting material, making coulombic results meaningless. It is not possible to state definitively, therefore, how many electrons were involved in the reduction.

In spite of the mechanistic problems associated with the reduction of these compounds, both gave clean differential pulse polarographic (d.d.p.) peaks, which were useful for quantitative purposes. A typical d.p. polarogram is shown in Fig. 2, at two different concentrations. For the concentration range up to 10^{-4} M, the linearity and sensitivity for (1) are reflected in the slope and intercept at the regression equation, $\log I_p = (0.91 \pm 0.02) \log C - 4.2 \pm 0.02$ where I_p is in μA and C in μM. The detection limit was slightly below 10^{-6} M. It seems clear that d.p.p. methods are suitable for quantification of these arsenicals in moderately dilute solutions. The optimum pH for the measurements (i.e., the pH at which the wave was best separated from electrolyte breakdown) and other conditions are given in Table 3 for all 5 compounds studied.

The nitro arsenicals

Each of these compounds (3) and (5) exhibited 2 waves, one arising from reduction of the nitro group (at −0.09 V in pH 1.0 media) and one at more

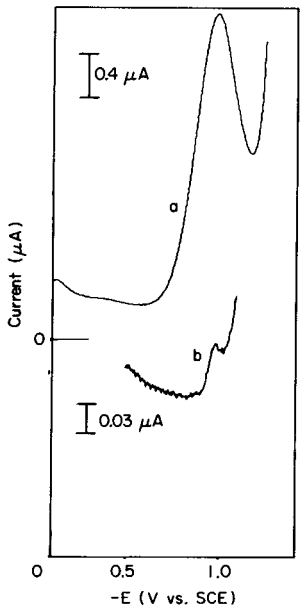

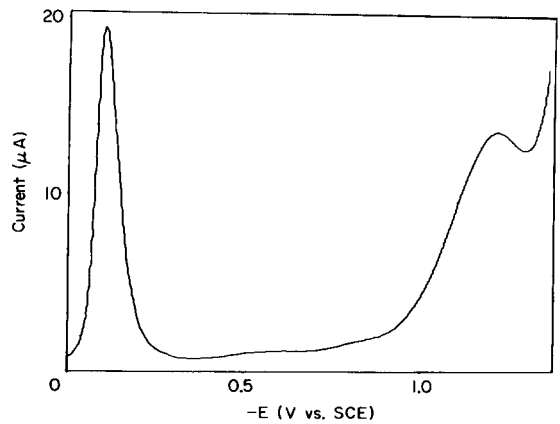

Fig. 2. Differential pulse polarograms of *o*-aminobenzenearsonic acid: pH 1.60 in HCl—NaCl; pulse width 25 mV; drop time 0.5 s; scan rate mV s^{-1}. a: 1 × 10^{-4} M; b: 1 × 10^{-6} M.

Fig. 3. Differential pulse polarogram of *p*-nitrobenzenearsonic acid in HCl—NaCl: pH 1.00; 4.5 × 10^{-4} M; pulse width 50 mV; drop time 0.5 s.

negative potentials, having the characteristics of an arsonic acid group reduction. Figure 3 displays a pulse polarogram of *p*-nitrophenylarsonic acid showing the broad peak near electrolyte background arising from reduction of the AsO_3H_2 group. Because reduction on nitro compounds has received much attention [26], measurements were largely restricted to the arsenic

TABLE 3

Recommended conditions[a] for quantification of organoarsenicals by differential pulse polarography

Compound	$-E_{1/2}$ (V)[b]	pH
o-Aminobenzenearsonic acid	1.04	1.60
p-Aminobenzenearsonic acid	1.00	1.81
p-Nitrobenzenearsonic acid	1.02	1.00
p-Ureidobenzenearsonic acid	0.72	0.50
3-Nitro-4-hydroxybenzenearsonic acid	0.90	0.92

[a]Pulse width 25 mV, drop time 0.5—2s. Criterion for choice was maximum resolution from background discharge current. [b]Peak potential of d.p.p. wave.

wave, and some of the data are presented in Tables 1—3.

Again, highly irreversible, diffusion-controlled waves were observed. Solution pH had the expected effect on the $E_{1/2}$ values; as shown in Fig. 4, both waves shifted to more negative values as the pH was increased. The slope for the arsonic acid wave of (3) was —152 mV/pH from pH 0 to 2.

These nitro arsenicals also exhibited the property of $E_{1/2}$ dependence on concentration, at least for the arsonic acid wave. Data of Table 2 over the concentration range 0.3—1.45 mM show that there is little dependence of $E_{1/2}$ of the first (nitro) wave on concentration, but that there are shifts of about —80 mV per mM concentration-change for the second (arsenic) wave.

Working curves of concentration versus peak height were linear over the range 10^{-4}—10^{-6} M for the arsenic wave, for both (3) and (5). The regression equations for these compounds were $\log I_p = (0.99 \pm 0.06) \log C - 4.0 \pm 0.06$ for (3) and $I_p = (0.97 \pm 0.05) \log C - 4.2 \pm 0.04$ for (5) where I_p is in μA and C is in μM.

4-Ureidobenzenearsonic acid

This compound (4) exhibited complex electrode behavior. At pH > 2, a single reduction wave was observed, having the same general characteristics seen previously for the other arsenicals (Table 1). But at lower pH values, a second wave appeared at more positive potentials. Studies on this compound were brief, and restricted to d.p.p. measurements on the wave at pH > 2. This wave would seem to be suitable for quantitative purposes because linear

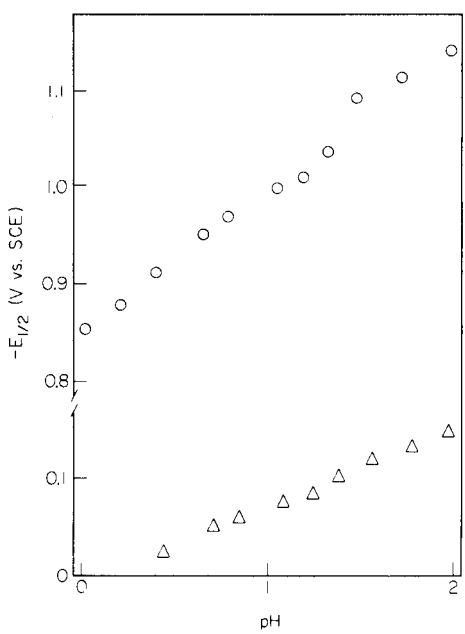

Fig. 4. Plot of $E_{1/2}$ vs. pH for *p*-nitrobenzenearsonic acid in HCl—NaCl.

working curves in the 10^{-4}—10^{-6} M range were obtained with a regression equation of $\log I_p = (0.95 \pm 0.04) \log C - 4.3 \pm 0.04$.

Conclusions

In principle, differential pulse polarography may be used to quantify these species, individually, down to levels of about 10^{-6} M, but the similarities of their $E_{1/2}$ potentials will make it difficult to distinguish components in a mixture without a separation step. All of the reductions are highly irreversible, an observation made from polarographic wave shapes and confirmed by cyclic voltammetry measurements. The latter yielded very drawn-out, irreversible waves for all the compounds. Certain aspects of the electrochemical behavior, such as the negative shift of $E_{1/2}$ as pH is increased, are easily understood, but others, such as a negative dependence of $E_{1/2}$ on concentration, are not. Although the polarographic waves are reproducible, the reduction mechanisms appear to be rather complex.

The authors are grateful to the National Science Foundation for providing partial support for this investigation. They also thank Prof. Kurt Irgolic of Texas A & M University for communication of some data prior to publication.

REFERENCES

1 C. J. Soderquist, D. G. Crosby and J. B. Bowers, Anal. Chem., 46 (1974) 155.
2 A. W. Fickett, E. H. Daughtrey and P. Mushak, Anal. Chim. Acta, 79 (1975) 93.
3 J. D. Lodmell, Ph.D. Thesis, University of Tennessee, 1973.
4 G. R. Rice, L. S. Shepard, G. Colonas and N. E. Hester, Anal. Chem., 53 (1981) 610.
5 L. D. Johnson, K. L. Gerhardt and W. A. Ave, Sci. Total Environ., 1 (1972) 108.
6 F. T. Henry and T. M. Thorpe, Anal Chem., 52 (1980) 80.
7 S. A. Peoples, P. C. Kearny and D. D. Kaufman, Proc. West. Pharmacol. Soc., 14 (1971) 178.
8 M. G. Haywood and J. P. Riley, Anal. Chim. Acta, 85 (1976) 219.
9 T. Kamada, Talanta, 23 (1976) 835.
10 R. S. Braman and C. C. Foreback, Science, 182 (1973) 1247.
11 R. S. Braman, L. L. Justin and C. C. Foreback, Anal. Chem., 44 (1972) 2195.
12 Y. Talmi and D. T. Bostik, Anal. Chem., 47 (1975) 2145.
13 M. B. Casvalho and D. M. Hercules, Anal. Chem., 50 (1978) 2030.
14 R. K. Elton and W. E. Geiger, Jr., Anal. Chem., 50 (1978) 712.
15 R. K. Elton and W. E. Geiger, Jr., Anal. Lett., 9 (1976) 665.
16 R. C. Bess, K. J. Irgolic, J. E. Flannery and T. H. Ridgway, Anal. Lett., 9 (1976) 1091; 10 (1977) 415.
17 D. J. Myers and J. G. Osteryoung, Anal. Chem., 45 (1973) 267.
18 F. T. Henry, T. O. Kirch and T. M. Thorpe, Anal. Chem., 51 (1979) 215.
19 C. C. Calvert, in E. A. Woolsen (Ed.), Arsenical Pesticides, Am. Chem. Soc., Washington, DC, 1975, Ch. 5.
20 B. Breyer, Chem. Ber., 71 (1938) 163.
21 M. Maruyama and T. Furuya, Bull. Chem. Soc. Jpn., 30 (1957) 650.
22 A. Watson, W. F. Smyth, G. Svehla and K. Vadasi, Z. Anal. Chem., 253 (1971) 106.
23 A. Watson and G. Svehla, Proc. Soc. for Anal. Chem., London, 1974, p. 163.
24 A. Watson and G. Svehla, Analyst, 100 (1975) 489.
25 D. Pressman and D. H. Brown, J. Am. Chem. Soc., 65 (1943) 540.
26 See, e.g., H. Lund, in M. M. Baizer (Ed.), Organic Electrochemistry, M. Dekker, New York, 1973, Ch. 7.

Analytica Chimica Acta, 132 (1981) 43—50
Elsevier Scientific Publishing Company, Amsterdam — Printed in The Netherlands

RESPONSE AND SELECTIVITY CHARACTERISTICS OF ALKYLAMMONIUM ION-SELECTIVE ELECTRODES

LARRY CUNNINGHAM and HENRY FREISER*
Department of Chemistry, University of Arizona, Tucson, AZ 85721 (U.S.A.)
(Received 26th May 1981)

SUMMARY

A series of poly(vinyl chloride) matrix coated-wire electrodes based on dinonylnaphthalene sulfonic acid (DNNS) selective to various alkylammonium ions was prepared and selectivity characteristics were evaluated. A set of tributylammonium electrodes was used to study the interference by a homologous series of alkylammonium ions. Selectivity coefficient ($k_{i,j}^{pot}$) values for alkylammonium ions at a given carbon number decreased in the order primary, secondary, tertiary, quaternary. A linear increase in log $k_{i,j}^{pot}$ with carbon number was observed in each series. Two additional sets of electrodes selective to dodecylammonium ion and to di-*n*-hexylammonium ion were evaluated for response to other C-12 amines. Electrodes for primary amines showed little or no response to secondary and tertiary amines, while electrodes for tertiary amines responded strongly to primary amines and less strongly to secondary amines. The effect of structural modifications was evaluated in a study of N-substituted cyclohexylamines. The dependence of the magnitude of $k_{i,j}^{pot}$ on the concentration of the interference was determined for both strongly and weakly interfering species. For strong interferences, $k_{i,j}^{pot}$ was observed to increase to a maximum value of characteristic concentration. For weak interferences, the $k_{i,j}^{pot}$ variation with concentration was markedly less. Guides for estimating the response to an interfering species based on its structure and molecular weight were obtained. The results are compared to analogous solvent-extraction systems. The significance of these results is discussed in terms of quantifying different components in binary mixtures using several electrodes simultaneously.

Previous work in this laboratory has demonstrated that poly(vinyl chloride) membrane electrodes incorporating dinonylnaphthalene sulfonic acid (DNNS) are selective for large organic cations such as dodecyltrimethylammonium [1], phencyclidine [2] and propranolol [3]. Because interference from compounds of structure similar to that of the primary ion is encountered when these electrodes are applied, a thorough understanding of their response characteristics in complex mixtures is necessary. Such characteristics include not only values of $k_{i,j}^{pot}$ for different ionic species, but also the long- and short-term effects on electrode response to samples containing high levels of interferences. Some puzzles that still remain unanswered include the way in which $k_{i,j}^{pot}$ varies with the activity of the interfering ions.

Earlier studies were conducted to examine the selectivity of DNNS electrodes with respect to a variety of singly charged cations. It was found that

0003—2670/81/0000—0000/$02.50

alkali and alkaline earth metal ions and organic ions much smaller than the primary ion showed no appreciable interference. In this work, a systematic approach to the interference problem was undertaken in which electrodes selective to tertiary, secondary, and primary ammonium ions were used. A complete study of the response of tributylammonium (TBA^+) electrodes to homologous series of amines established a relationship between selectivity and structure. Tributylammonium (TBA^+) was chosen as the primary ion because its molecular weight (185.4) was nearest the average molecular weight (181.7) in the range of ions considered. In this way, interference from both smaller and larger ions was observed.

Because selectivity is not only a function of molecular weight but also of the types of substituents in a molecule, responses of the TBA^+-sensitive electrodes to solutions of TBA^+Cl^- containing N-ethyl-, N-(2-cyanoethyl)-, N-(2-hydroxyethyl)-, and N-(3-aminopropyl)-cyclohexylammonium chlorides were measured. With these compounds, the carbon number and the degree of nitrogen substitution were constant in order to isolate the substituent effect.

Variations in the nature of the primary ion were also of interest. In addition to tributylammonium electrodes, others selective for dodecylammonium (DDA^+), di-*n*-hexylammonium (DHA^+) and tripropylammonium (TPA^+) were prepared as described below. Response of these electrodes to the other C-12 ions was then evaluated.

EXPERIMENTAL

Reagents

Amines obtained from Eastman (Rochester, NY) were further purified by vacuum distillation. Amines obtained as hydrochlorides were dried over calcium chloride, while others were converted to hydrochlorides by dissolving in a minimum of 0.1 M HCl. Acetate (10^{-2} M) buffer pH 4.00 was the main diluent for all solutions. Dioctylphthalate (Eastman) and chromatographic-grade poly(vinyl chloride) (Polysciences, Warrington, PA) were used as obtained.

Potentiometric measurement system and electrode preparation and handling

A double-junction Ag/AgCl reference electrode containing 0.1 M NH_4NO_3 in the external junction was used for all experiments. Potentiometric measurements were done with a microcomputer-controlled system described earlier [4] as well as a Nova 2/10-based system.

Both conventional polymeric membrane and coated-wire electrodes were evaluated for their response to TBA^+. Coated-wire electrodes were used for all remaining studies, having proved equal to, and in most cases better than, the conventional electrodes employing a Ag/AgCl internal reference.

The solution used to cast membranes was made as described previously [5]. To this solution, pure amine was added in stoichiometric relation to DNNS. It was then possible to cast membranes [6] or coat copper wires [7].

Both types of electrodes were then soaked in a 10^{-3} M alkylammonium ion solution for several days in order to stabilize, during which time the membranes became opaque (probably owing to hydration). Electrodes were then repeatedly calibrated during the course of the selectivity studies.

Selectivity coefficients

Values of $k_{i,j}^{pot}$ were calculated by using the mixed-solution method [8]. In a typical selectivity determination, a set of five electrodes was calibrated by using the NOVA 2/10 system. Immediately after the calibration, a standard solution of an interfering ion was added to the calibration vessel containing the final concentration of primary ion. In this fashion, the value of $k_{i,j}^{pot}$ at specified levels of interferences was calculated from the responses of electrodes in each solution tested. The accuracy of this approach was also increased by using the slope of the electrode response calculated by the computer immediately after the calibration run. An entire calibration and selectivity determination of five electrodes required 30—45 min, depending on the number of solutions desired.

RESULTS

Shown in Table 1 are response characteristics for both conventional and coated-wire ion-selective electrodes. Nearly Nernstian responses were obtained for both types. Detection limits were also virtually identical. Electrodes in use over five months are still functional.

Selectivity coefficients for TBA^+ coated-wire electrodes are plotted against the number of carbon atoms in the ion in Fig. 1. The linear increase on log $k_{i,j}^{pot}$ with carbon number for each series, expected from the corresponding increase of lipophilicity of the ion, facilitates estimation of $k_{i,j}^{pot}$ values for amines of known molecular weight and degree of nitrogen substitution. The plot of log $k_{i,j}^{pot}$ vs. carbon number for the tributylammonium electrode shows that the selectivity order is primary > secondary > tertiary > quaternary. At low carbon numbers, secondary alkylammonium ions and tertiary alkylammonium ions have approximately equal $k_{i,j}^{pot}$ values.

TABLE 1

Response characteristics of DNNS-based ion-selective electrodes at 25°C

	Conventional TBA^+	Coated-wire TBA^+
Slope (mV/log[TBA^+])	58.59 ± 0.50[a]	59.53 ± 0.67[a]
Std. deviation (mV)	0.30[b]	1.10[b]
Intercept (mV)	306 ± 10[a]	333 ± 12[a]
Std. deviation	8.7[b]	8.3[b]
Detection limit	4.0×10^{-6} M	4.0×10^{-6} M
Logarithmic range	−2.0 to −5.0	−2.0 to −5.0

[a]Standard deviation for individual electrodes. [b]Standard deviation among several (15) electrodes.

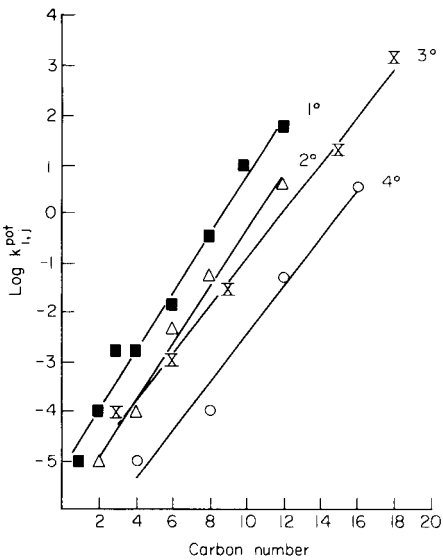

Fig. 1. Dependence of log $k^{pot}_{i,j}$ on the carbon number of interfering ammonium ions for tributylammonium coated-wire electrodes: (■) primary; (△) secondary; (×) tertiary; (○) quaternary.

In Table 2, log $k^{pot}_{i,j}$ values are given for substituted cyclohexylamines. It is interesting to note that the compounds gave lower $k^{pot}_{i,j}$ values than dibutylamine, an aliphatic amine of the same carbon number. As expected, the most hydrophilic compound was the least interfering (log $k^{pot}_{i,j}$ = −2.35 for N-(2-hydroxyethyl)cyclohexylamine).

The dependence of selectivity behavior on degree of N-substitution of the primary ion was evaluated by using coated-wire electrodes for three isomeric ions, namely, dodecylamine, di-*n*-hexylamine, and tributylamine. Responses of each electrode to the other C-12 amines resulted in the $k^{pot}_{i,j}$ values shown in Table 3. It is clear that electrodes selective to primary amines showed greatest selectivity while tertiary amine electrodes were least selective.

TABLE 2

Log $k^{pot}_{i,j}$ and log P values for substituted cyclohexylamines at 25°C

Compound	Log $k^{pot}_{i,j}$ [a]	Log P (Hansch)
N-Ethylcyclohexylamine	−1.97	−1.36
N-2-Hydroxyethylcyclohexylamine	−2.35	−3.98
N-2-Cyanoethylcyclohexylamine	−2.12	−2.16
N-3-Aminopropylcyclohexylamine	−2.22	−3.52

[a] TBA^+ coated-wire electrode. The concentration of interfering ion was 10^{-2} M with a background level of 10^{-4} M TBA^+.

TABLE 3

Values of $k_{i,j}^{pot}$ for three coated-wire electrodes containing C-12 amines[a]

Interfering ion	$k_{i,j}^{pot}$ with primary ion		
	DDA^+	DHA^+	TBA^+
DDA^+	—	2.36 ± 0.6[b]	50.1 ± 3.0
DHA^+	0.4 ± 0.2	—	3.8 ± 0.4
TBA^+	Not measurable	0.6 ± 0.5	—

[a]Average values for 35 electrodes. [b]Standard deviation of $k_{i,j}^{pot}$ values among 35 electrodes.

Memory effects are ascribed to changes in electrode response after exposure to strong interferences. It was observed that the calibration curve for the TBA^+ coated-wire electrode would shift by as much as +20 mV after exposure to interferences having six carbon atoms or less, and by +100 mV after exposure to very strong interferences such as trihexylammonium ion. The magnitude and duration of this temporary shift increased with the magnitude of $k_{i,j}^{pot}$ for the interfering substance which caused it. It also depended on the concentration and time of exposure to the interference. For this reason, exposure times were usually kept below 15 min. To restore electrode response, soaking in 10^{-3} M TBA for 15 min was necessary after exposure to the more weakly interfering species. In extreme cases, such as overnight soaking in 10^{-3} M trihexylammonium ion (THA^+), the TBA^+ coated-wire electrode required soaking for 3 h in the TBA^+ bathing solution before the TBA^+ response returned. In this latter case, absolutely no TBA^+ response was attainable prior to the soaking period.

It is important to note that the change in $k_{i,j}^{pot}$ observed was not due to hysteresis. This was proven by observing the electrode response at 5-min intervals while soaking in 10^{-4} M TBA^+ which was 10^{-4} M in THA^+, during which time ($\approx$1 h) it did not fluctuate by more than 2 mV. The presence of primary ion helped to prevent temporary loss of electrode response, which occurred when the electrodes were soaked overnight in 10^{-3} M THA^+.

The dependence of $k_{i,j}^{pot}$ on concentration is shown in Fig. 2A (DDA = j) and 2B (THA = j). The range in which there was a Nernstian response to the primary ion (TPA^+) was chosen as the region of interest. Above a 10^{-4} M concentration of DDA^+ or THA^+, $k_{i,j}^{pot}$ is seen to increase only gradually, whereas below this level, it is a very sensitive function of the concentration of DDA^+ or THA^+. At low concentrations of the interference, the effect on the potential was small, however, reducing the reliability of the calculation of $k_{i,j}^{pot}$.

DISCUSSION

It is apparent that poly(vinyl chloride) matrix membrane electrodes can be made selective to a wide variety of organic cations. The coated-wire type

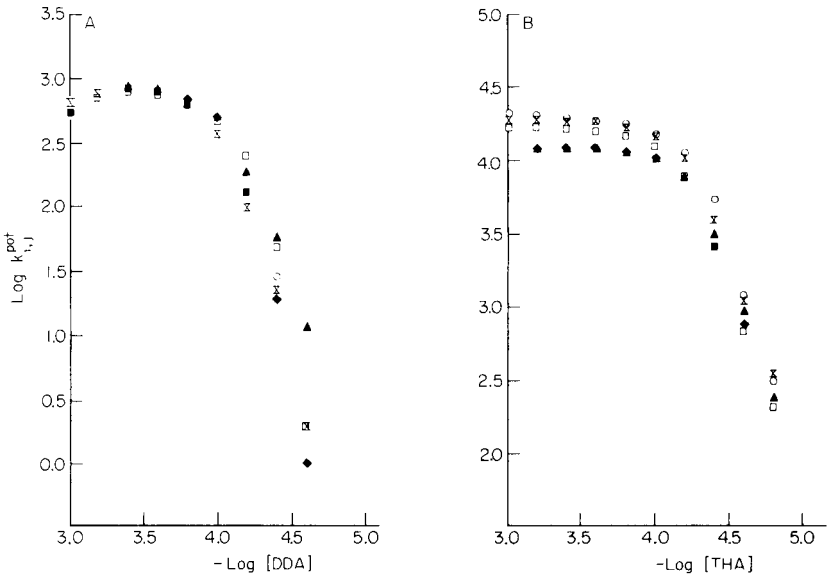

Fig. 2. Dependence of log $k^{pot}_{i,j}$ on the concentration of (A) dodecylammonium ion, and (B) trihexylammonium ion for tripropylammonium coated-wire electrodes where [TPA^+] = 1×10^{-3} M. The points indicate results obtained with individual electrodes.

of electrode is sufficiently well behaved to continue to provide an extremely convenient method for studying membrane processes. The small size of such electrodes enables multiple calibrations to be done in a relatively small solution volume.

The selectivity characteristics of the TBA^+ electrodes towards the other amines studied show that $k^{pot}_{i,j}$ is closely related to carbon number. The importance of the degree of nitrogen substitution is indicated by the tenfold decrease in $k^{pot}_{i,j}$ values at a given carbon number as additional alkyl groups are added. This effect is possibly due to the greater degree of hydrogen bonding in the membrane for compounds having a less sterically hindered nitrogen. The overlap of the plots for secondary and tertiary alkylammonium ions at low carbon numbers indicates that these compounds have about the same degree of hydrogen bonding. As the carbon number increases in these series, the steric effect of the tertiary alkylammonium ions becomes much greater than for secondary alkylammonium ions. Quaternary alkylammonium ions, having no hydrogen bonding, have the lowest $k^{pot}_{i,j}$ values, about 100-fold lower than those of the primary ammonium ions.

The significance of these results is best appreciated by comparison to solvent extraction systems. In a study of the ion-pair extraction of amines via picrate ion in various organic solvents, Gustavii [9] pointed out that the ion-pair formation constant (K_{IP}) as well as the distribution constant (K_D) determine the overall K_{ex}. When methylene chloride, a low dielectric solvent, was employed, the order of extraction was tertiary > secondary > primary

= quaternary. One reason given for this was the greater degree of hydrogen bonding experienced in aqueous media by the less substituted amines. In the electrode system, however, it would seem likely that hydrogen bonding occurs in the membrane as well as the aqueous phase. Otherwise, the selectivity order would be expected to be similar to that found in the extraction system.

For primary alkylammonium ion electrodes, a large degree of selectivity is observed over higher analogs. This also points out the importance of steric hindrance at the nitrogen. Apparently, the DNNS—dodecylamine ion pair is stronger than the DNNS—tributylamine ion pair; otherwise, it is expected that tributylamine would interfere with the dodecylammonium ion electrode response.

Though the exact value for $k_{i,j}^{pot}$ must be determined by experiment, the relative interference between two compounds can also be estimated from their distribution constants. Such values for amine hydrochlorides between octanol and water, as calculated by the correlation technique of Hansch [10], are plotted against carbon number in Fig. 3. Comparison to the log $k_{i,j}^{pot}$ vs. carbon number plots indicates that hydrogen bonding, though dominant in the aqueous phase, must also occur to an appreciable extent in the membrane phase. This behavior is expected for media of high dielectric constant, as is the case when sufficient amounts of dioctylphthalate are added to poly(vinyl chloride). This was also the case for picrate ion-pair extraction into methylene chloride [9] where it was shown that the partition coefficients of neutral amines decrease in the order $1° > 2° > 3° > 4°$. Since the slightly transparent polymer becomes opaque after soaking in aqueous solution and becomes clear again after drying in air, the concentration of water in the membrane is probably significant.

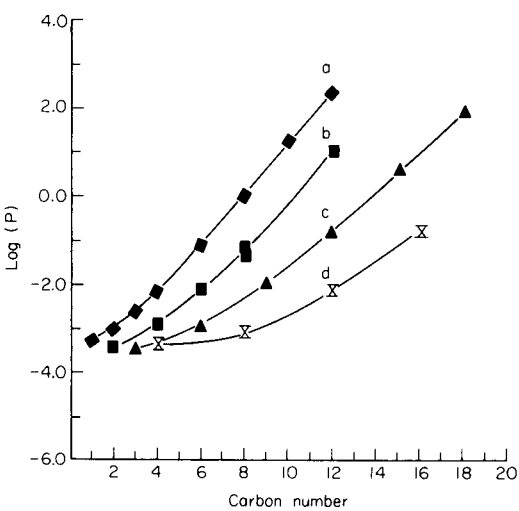

Fig. 3. Dependence of partition coefficient (P), as log P for the octanol/water system on the carbon number of various alkylammonium chlorides [10]: (a) primary; (b) secondary; (c) tertiary; (d) quaternary.

The importance of the partition coefficients is indicated by the relative magnitude of $k_{i,j}^{pot}$ values calculated for substituted N-ethylcyclohexylamines. The selectivity order corresponds to the relative solubility of the cyclohexylamines between octanol and water. In addition, the $k_{i,j}^{pot}$ value for di-isobutylamine ($\log k_{i,j}^{pot} = -1.56$) was less than that of dibutylamine ($\log k_{i,j}^{pot} = -1.27$) which is also expected from their distribution constants. It is apparent that the selectivity coefficient for a given compound can be reasonably estimated if a known value for a compound of the same family is available.

It has been shown that memory effects become significant when electrodes are exposed to powerful interferences for long periods of time. Even so, electrode response can be restored by soaking in sufficiently concentrated solutions of the primary ion. This behavior is consistent with an ion-exchange process occurring in the outer layer of the membrane exposed to the solution.

During the time scale of the selectivity coefficient measurement (15 min), the shifts in electrode response were slight, indicating that some interfering species were displacing the primary ion in the outer portion of the membrane. After long exposure times with strong, lipophilic interferences, this displacement was sufficient to nullify electrode response to the primary ion, probably resulting from more complete exchange of primary ion by interfering ion.

As demonstrated by this study, it is possible to measure binary mixtures using the coated-wire electrode. Of course, in the presence of strongly interfering species, significant and (in the time scale of the measurement technique) irreversible errors occur. Even so, provided their presence is suspected, it would be possible to minimize electrode contamination by measuring the concentration of the ions with their respective electrodes in the following sequence: 1°, 2°, 3°, 4°. For samples in which the interferences do not change drastically in their nature and/or concentrations, this approach could prove efficacious in that it involves minimum sample preparation, rapid equilibration of electrodes, and direct readout of concentrations.

This research was conducted with financial assistance from the Office of Naval Research.

REFERENCES

1 C. R. Martin and H. Freiser, Anal. Chem., 52 (1980) 562.
2 C. R. Martin and H. Freiser, Anal. Chem., 52 (1980) 1772.
3 T. Yamada and H. Freiser, Anal. Chim. Acta, 131 (1981) 233.
4 C. R. Martin and H. Freiser, Anal. Chem., 51 (1979) 803.
5 C. R. Martin and H. Freiser, J. Chem. Educ., 57 (1980) 512.
6 G. J. Moody and J. D. R. Thomas, in H. Freiser (Ed.), Ion-Selective Electrodes in Analytical Chemistry, Vol. I, Plenum, New York, 1978, p. 288.
7 H. Freiser, Ion-Selective Electrodes in Analytical Chemistry, Vol. II, Plenum, New York, 1980, p. 85.
8 K. Srinivasan and G. A. Rechnitz, Anal. Chem., 41 (1969) 1203.
9 K. Gustavii, Acta Pharm. Suecica, 4 (1967) 233.
10 C. Hansch and A. J. Leo, Substituent Constants for Correlation Analysis in Chemistry and Biology, J. Wiley, New York, 1979.

Analytica Chimica Acta, 132 (1981) 51—58
Elsevier Scientific Publishing Company, Amsterdam — Printed in The Netherlands

THE DETERMINATION OF FREE LONG-CHAIN QUATERNARY AMMONIUM SPECIES WITH AN ION-SELECTIVE ELECTRODE BASED ON A CETYLTRIMETHYLAMMONIUM ION PAIR

S. S. DAVIS* and O. OLEJNIK

Department of Pharmacy, University of Nottingham, University Park, Nottingham, NG7 2RD (Gt. Britain)

(Received 27th April 1981)

SUMMARY

The cetyltrimethylammonium ion-selective electrode described is based on a tetrazole ion-pair and silicone-rubber membranes. The electrode is almost Nernstian in response from 10^{-6} M to the critical micelle concentration. The electrode responds little to dodecyl- and decyltrimethylammonium ions and inorganic ions. Selectivity coefficients for numerous compounds are given. The uses of the ion-selective electrode are discussed in terms of the ability to monitor free quaternary ammonium ions in the presence of electrolyte and complexing additives. The electrode described can be useful in developing certain pharmaceutical formulations.

The nature and activity of ionic species in biological systems and formulated pharmaceutical products are of prime importance. For example, quaternary ammonium salts are present as antimicrobial preservatives in ophthalmic solutions. However, the total quantity of the quaternary additive in a formulation does not necessarily reflect the amount of the biologically active free species, because quaternary ammonium compounds with long alkyl chains may associate to form micelles. Various components of formulations can also affect the thermodynamic activity of the unassociated ionic species resulting in an enhanced state of micellisation or interactions, e.g., ion pairing [1, 2]. The activity of a preservative can be decreased further by surface adsorption onto plastic containers [3]. Many factors govern antimicrobial efficiency, and the increasing complexity of formulations often requires elaborate time-consuming assay procedures to isolate and determine a specific quaternary ammonium compound [4]. An assay procedure for unassociated quaternary ammonium species in situ is desirable, as this would allow the true free ion activity to be determined directly.

Sensitive analytical methods have become available for many ionic species by the development of ion-selective electrodes. Various electrodes that monitor quaternary ammonium ions have been constructed [5—7], and lipophilic ions have been incorporated into electrode membranes in order to produce a selective response for large lipophilic cations [7]. This indicates

the possibility of developing an electrode that would be highly selective for large organic ions frequently present in pharmaceutical formulations.

The construction and evaluation of a long-chain alkylammonium cation-selective electrode is presented. The electrode is based on a design given by Muratsugu et al. [5] and has been utilised to study the activity of cetyltrimethylammonium ions in solution together with the effects of electrolyte and complexing additives.

EXPERIMENTAL

Apparatus, reagents and solutions

An EIL model 7050 pH/mV meter, Farnell PR1 chart recorder module, and EIL calomel and Ag/AgCl reference electrodes were used in conjunction with the constructed cetyltrimethylammonium-selective electrode. Constant temperature conditions were maintained within a jacketed glass beaker using water circulated from a Churchill pump. A slow infusion apparatus (model 5200, Scientific and Research Instruments Ltd.) incorporating a 20-ml Everett glass syringe was used for addition of standard solutions in testing electrode response.

N-(3-Acetyl-5-ethyl-2-hydroxyphenyl)-5-carboxamido-1*H*-tetrazole (May and Baker) and cetyltrimethylammonium bromide (Fluka) were used to prepare the ion pair. Analytical-grade chemicals were used throughout. Solutions were prepared with deionised, double-distilled water with a conductance of less than 1.0×10^{-6} mho cm^{-1} at 25°C; this water was also used for rinsing the electrodes. Silastic silicone-rubber membrane (polymethylsiloxane) was obtained from Dow-Corning.

Construction of electrode

Assembly. The electrode (Fig. 1) was assembled by using two pyrex glass tubes having internal diameters of 22 mm and 10 mm, with lengths of 125 mm and 105 mm, respectively. A Silastic membrane square (0.125-mm thick; Dow-Corning), described below, was fixed to one end of the larger glass tube and held in position by an O-ring. This outer tube was filled with the ion-exchange liquid (see below) to a depth of 1 cm. A further Silastic square was positioned on the smaller glass tube and held securely with the aid of two Shuco plastic fasteners. This inner tube was filled with 1×10^{-3} M cetyltrimethylammonium bromide (C_{16}TAB) solution. The electrode was conditioned in 1×10^{-2} M C_{16}TAB solution for 1 h before use, and was stored in this solution when not in use.

Liquid sensor membrane. The organic solvent used had to be inert but compatible with the required ions present in the two aqueous solutions, i.e., the internal reference solution and the test solution. 1,2-Dichloroethane has been used as the sensor solvent containing the dibenzyldimethylammonium–tetraphenylborate ion-pair [6] and was selected for the preparation of the exchanger employed here.

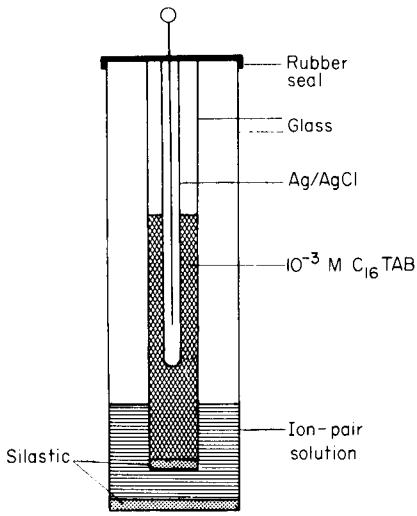

Fig. 1. Longitudinal section of the membrane electrode from two glass tubes and Silastic membranes.

The cetyltrimethylammonium cation ($C_{16}TA^+$) was paired with a series of large anions in tests designed to assess the optimal response of a possible electrode (Table 1). A tetrazole anion was finally selected although other large organic ions could also be used. To prepare the exchanger, 50 ml of 5×10^{-3} M tetrazole solution was buffered to pH 12.0 with a final ionic strength of 0.20, by adjustment with sodium chloride. The solution was transferred to a separating funnel to which was added 50 ml of 2×10^{-3} M C_{16}TAB solution at pH 12.0 and ionic strength 0.20. The resulting mixture with the precipitate was extracted with 100 ml of 1,2-dichloroethane by vigorous shaking and the contents were allowed to equilibrate for 48 h at ambient temperature. The organic ion-exchange liquid containing the quaternary ammonium—tetrazole ion pair was then separated from the aqueous phase and stored at 5°C for future use.

TABLE 1

The effect of different anions on the electrode response to cetyltrimethylammonium ions

Counter ions	Response (mV/dec. conc.) (n = 6)	Linear analytical range (M)
Tetraphenylborate	43.3 ± 2.4	5×10^{-5}—5×10^{-4}
Dodecylsulphate	44.8 ± 5.8	1×10^{-5}—5×10^{-4}
Tetrazole[a]	55.5 ± 2.0	1×10^{-6}—1×10^{-4}
Tetrazole[b]	54.1 ± 3.3	5×10^{-5}—1×10^{-4}

[a] *N*-(3-Acetyl-5-ethyl-2-hydroxyphenyl)-5-carboxamido-1*H*-tetrazole. [b] 5-Ethyl-2-hydroxy-3-propanoyl-*N*-(tetrazol-5-yl)benzamide.

Support membrane. The choice of a support membrane for the 1,2-dichloroethane ion pair system was critical. The ideal membrane needed to be robust but inert to the surrounding solvents; it had to provide negligible leaching of the membrane constituents and negligible leakage of solvent, and it had to be permeable to specific ions. Spectrapor cellulose and cuprophan membranes gave a non-Nernstian response when the electrode responses were recorded over a period of 24 h. Nylon-6 gave a near-Nernstian response initially but this decayed to 30.7 mV/decade during 24 h. The silicone-rubber membrane (Silastic) gave initial responses of more than 50 mV/decade which decayed only slowly over 24 h (see below).

The final system selected was a $C_{16}TA^+$—tetrazole$^-$ ion pair in 1,2-dichloroethane with a Silastic membrane. The useful life span of the electrode was approximately one week provided that no mechanical problems developed.

Procedures

Standard solutions were added automatically as described earlier [8] in tests of the efficiency of the electrode under various experimental conditions. The electrodes were first rinsed with water and then immersed in 100 ml of pure water at 25 ± 0.1°C. The solution was stirred at a constant rate maintained just below the speed which would cause the solution to form a vortex. After a stable potential reading had been achieved (±0.5 mV min^{-1}), the standard solution was added gradually and the millivolt response was recorded to obtain the calibration plots. Appropriate volume corrections were made in calculating the slopes.

In tests of the electrode lifetime, calibration plots were obtained as described above for standard solutions of $C_{16}TAB$ at specific time intervals over a period of 24 h.

For the determination of selectivity coefficients, a series of 1×10^{-3} M "interfering" ion solutions were prepared and standard $C_{16}TAB$ solution was added automatically. The millivolt responses at 1×10^{-4} M $C_{16}TA^+$ in these solutions were determined from a graphical presentation of the response data. Between analyses, the electrodes were rinsed thoroughly with water and blotted dry.

Conductimetric titrations were done as described by Mukhayer et al. [8] and adopted so as to compare results obtained by conductimetric titration with those determined by the ion-selective method.

RESULTS AND DISCUSSION

Calibration curve, detection limits, and electrode response

Potential measurements were recorded by calculating the change in the electrode response with respect to the initial potential at zero concentration of $C_{16}TA^+$. A typical electrode response to the change in the concentration of $C_{16}TA^+$ added is shown in Fig. 2. The linear region occurred over a 10^{-6}—10^{-4} M concentration range, the upper value being limited by the micellisation

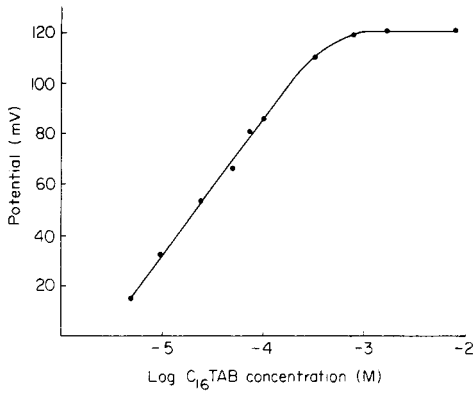

Fig. 2. Response of the electrode to cetyltrimethylammonium bromide prior to and after reaching the critical micelle concentration.

of C_{16}TAB. An electrode response of 53.0—55.5 mV/decade was determined over the 10^{-6}—10^{-4} M concentration range for freshly prepared electrodes. Calibration of an electrode at 4-h intervals over a period of 24 h showed that the response decreased gradually with time (Fig. 3) but the measurements at any particular time showed a high degree of stability and reproducibility (±0.2 mV). The electrode response was rapid, the response time being almost instantaneous with solutions at 10^{-4} M and less than 30 s for more dilute solutions down to 10^{-6} M.

Selectivity coefficients

The selectivity coefficient, k_{ij}, is the prime source of information concerning interferences on electrode response. In analytical applications, the selectivity for the analyte must be as high as possible, i.e., the selectivity coefficients must be small, so that the electrode will have a Nernstian dependence on the primary ion activity over a wide concentration range. From the conventional selectivity equations [9, 10], the k_{ij} coefficients were determined for various ions.

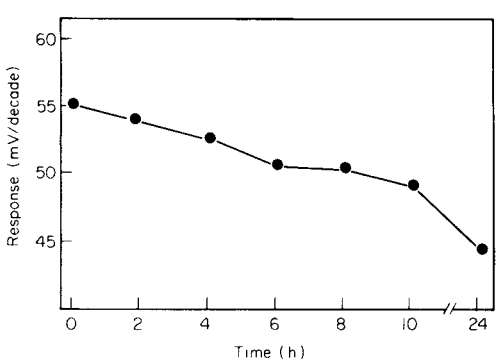

Fig. 3. Change in response of the electrode with time.

The electrode responded to quaternary ammonium ions of different chain lengths (Table 2) and marked interference occurred with C_{14}TAB. A decrease in selectivity coefficient with decreasing chain length was indicative of the expected relationship between the selectivity coefficient and the lipophilicity of the quaternary alkyl ammonium salts. In these selectivity tests, no attempt was made to control the pH of the solution. Interference from several compounds (e.g., sodium hydroxide and phosphoric acid) could be ascribed to a pH effect. For inorganic ions exhibiting no lipoidal behaviour or a change in pH, insignificant interference was evident as shown by their small k_{ij} values. The selectivity coefficients were comparable with values reported for sulphonates and inorganic anions [11].

Effect of electrolyte and complexing additives

The plateau effect in the potential response for the addition of C_{16}TAB at high concentrations represented constant thermodynamic activity and was the result of the formation of micelles (Fig. 2). The critical micelle concentration (c.m.c.) of 8.6×10^{-4} M at 25°C so derived, compared well with a literature value of 8.2×10^{-4} M obtained by conductivity measurements [12]. At the c.m.c. it was possible to add into the system various electrolytes or complexing agents that may be employed in a pharmaceutical formulation, e.g., sodium chloride, citrate buffers or non-ionic surfactants. For instance, the addition of sodium bromide will bring about a lowering of the c.m.c. because of increased micellisation of free ions [12] and this change in c.m.c. can be monitored directly by the electrode as shown in Fig. 4. In contrast, the conventional conductivity method for following changes in c.m.c. was inapplicable at ionic strengths greater than 5×10^{-2}. Thus the electrode could be used most successfully to optimise pharmaceutical formulations where one required a certain concentration of free unassociated quaternary species for antimicrobial activity (eye drops, contact lens solutions) as well as to investigate changes in concentration levels with storage.

TABLE 2

Selectivity coefficients of water-soluble compounds

Interfering compound	k_{ij}	Interfering compound	k_{ij}	Interfering compound	k_{ij}
C_{14}TAB	4.13	$C_6H_8O_6$[a]	7.85×10^{-2}	KCl	6.29×10^{-3}
C_{12}TAB	7.53×10^{-1}	KH_2PO_4	4.13×10^{-2}	NaCl	2.22×10^{-3}
C_{10}TAB	4.19×10^{-1}	$MgSO_4$	1.91×10^{-3}	$NaHCO_3$	1.46×10^{-1}
KBr	3.45×10^{-3}	H_3PO_4	1.11×10^{-1}	NaOH	4.66×10^{-1}
NH_2CONH_2	9.00×10^{-2}	$CaCl_2$	2.40×10^{-4}		

[a] Ascorbic acid.

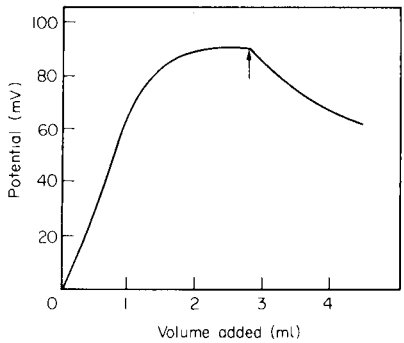

Fig. 4. Response of the electrode to addition of 2% (w/v) cetyltrimethylammonium bromide solution followed by 5% (w/v) sodium bromide solution. The arrow marks the point where the added solution was changed.

Another important application of the new ion-selective electrode was clearly illustrated by a study of complexation. Figure 5 shows the interaction of $C_{16}TAB$ with sodium citrate, the electrode potential response being compared with conductivity measurements. Changes in the specific conductivity were mirrored by the variation in the millivolt response. The advantage of the ion-selective technique was its ability to distinguish a true c.m.c. endpoint from an onset of complexation, because reliance on the conductivity data could lead to the erroneous conclusion that the first definite change in the gradient of the curve was due to a micellisation phenomenon. It was noted that in this region the millivolt response vs. added $C_{16}TAB$ relation altered in gradient but did not level off to a constant value. It was the invariate millivolt response that characterised micellisation (constant thermodynamic activity).

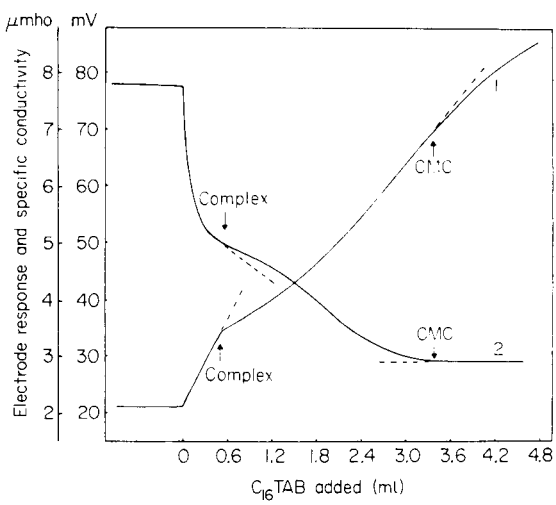

Fig. 5. Titration of sodium citrate (3×10^{-3}%) with cetyltrimethylammonium bromide (2.0%). (1) Conductivity measurements; (2) selective electrode measurements.

The authors thank the SRC for providing a CASE research studentship for one of us (O.O.). We are further grateful to May and Baker (Dagenham) for the tetrazole compounds.

REFERENCES

1 E. Tomlinson and S. S. Davis, J. Colloid Interface Sci., 74 (1980) 349.
2 S. S. Davis, E. Tomlinson and C. G. Wilson, Br. J. Pharmacol., 64 (1978) 444P.
3 N. E. Richardson, D. J. G. Davies, B. J. Meakin and D. A. Norton, Pharm. J., 223 (1980) 462.
4 N. E. Richardson, D. J. G. Davies, B. J. Meakin and D. A. Norton, J. Pharm. Pharmacol., 29 (1977) 717.
5 M. Muratsugu, N. Kamo, K. Kurihara and Y. Kobatake, Biochim. Biophys. Acta, 464 (1977) 613.
6 S. S. Davis and O. Olejnik, J. Pharm. Pharmacol., 31 (1979) 19P.
7 R. Scholer and W. Simon, Helv. Chim. Acta, 55 (1972) 1801.
8 G. I. Mukhayer, S. S. Davis and E. Tomlinson, J. Pharm. Sci., 14 (1975) 147.
9 G. E. Baiulescu and V. V. Cosofret, Applications for Ion-Selective Membrane Electrodes in Organic Analysis, Horwood, Chichester, 1977, p. 17.
10 R. P. Buck, Anal. Chem., 48 (1976) 23R.
11 S. H. Hoke, A. G. Collins and C. A. Reynolds, Anal. Chem., 51 (1979) 859.
12 B. W. Barry, J. C. Morrison and G. F. J. Russell, J. Colloid Interface Sci., 33 (1970) 554.

Analytica Chimica Acta, 132 (1981) 59—67
Elsevier Scientific Publishing Company, Amsterdam — Printed in The Netherlands

EFFECTS OF SOME SURFACE-ACTIVE SUBSTANCES ON POLAROGRAPHIC WAVES OF THALLIUM(I), LEAD(II), ANTIMONY(III) AND URANIUM(VI) IN ACETATE MEDIUM
Determination of Thallium with Electrochemical Masking by Dioctyl Sulphosuccinate

J. HERNÁNDEZ-MÉNDEZ*, R. CARABIAS-MARTÍNEZ and J. I. GARCÍA-GARCÍA
Department of Analytical Chemistry, Faculty of Chemistry, University of Salamanca (Spain)

(Received 10th March 1981)

SUMMARY

The effects of some surface-active substances on the polarographic waves of Tl(I), Pb(II), Sb(III) and U(VI) in an acetate medium are described. The shifts observed in half-wave potentials offer several possibilities for the selective polarographic determination of these species. A method for the determination of thallium(I) in the presence of large amounts of Sb(III) and U(VI) and commensurate amounts of Pb(II), with dioctyl sulphosuccinate, is proposed.

The principal use of surface-active substances in polarography has been the suppression of polarographic maxima, although other effects may be observed such as a decrease in the limiting current, a shift in the half-wave potential, wave doubling or even the elimination of waves, all of which may be used for analytical purposes. The influence of organic surface-active ions on the kinetics of electrode reactions is generally attributed to both steric hindrance and to an electrostatic effect [1].

Lingane [2] was the first to describe the effect of gelatin on a copper wave in a sulphuric acid medium. The effects of cationic, nonionic and anionic surfactants on the polarography of copper in a perchlorate medium were investigated by Kolthoff and Okinaka [3]; these effects were qualitatively explained by the theory of Frumkin [4]. Jacobsen and Kalland [5] suggested that polarograms were practically unaffected by the presence of surfactants, provided that the adsorbed layer had a charge opposite to that of the depolarizer. However, it has been shown experimentally that, apart from electrostatic effects, other factors should be taken into account because different electrode behaviour has been described for similar chemical species in the presence of the same surfactant [6]. The use of surface-active substances for electrochemical masking in order to carry out selective polarographic determinations has been reported by several authors. Thallium was determined in the presence of copper [7]. Subbaraman et al. [8, 9] studied

0003—2670/81/0000—0000/$02.50

the influence of camphor and gelatin on the polarographic behaviour of several di- and tri-phosphate complexes, the polarographic determination of thallium being possible in the presence of lead, copper, iron and bismuth. Mendalieva et al. [10] determined thallium in the presence of 25-fold amounts of lead and commensurate amounts of copper in perchloric acid, using the surface-active substance ANP-2. Lukaszewski [11] described a study of polyethylene glycols (m.w. 200—15 000) as electromasking agents; a method was proposed for the determination of lead and thallium in the presence of bismuth, antimony or indium. A systematic study of the effect of surfactants was reported by Jacobsen and Kalland [5]. According to Hoff and Jacobsen [12], the presence of an ionic surfactant may increase the height of a.c. polarographic peaks, which is useful for analytical purposes [13, 14]. Of interest is the transformation of $[In(C_2O_4)_2]^{2-}$, which is polarographically inactive, into a species reducible at a mercury drop electrode by the addition of decylamine or dodecylamine [15]. The influence of surface-active substances in anodic stripping voltammetric determinations has also been studied [16—19].

The use of surfactants obviously offers interesting possibilities. As is known [20], the polarographic waves of thallium(I), lead(II), antimony(III) and uranium(VI) cannot be distinguished in an acetic acid—ammonium acetate medium. It is shown in this paper that the half-wave potentials of these ions can be separated in the presence of different surfactants, which enables thallium to be determined in the presence of these other ions.

EXPERIMENTAL

Apparatus and chemicals

All polarograms were recorded with a Sargent model XVI d.c. polarograph. A conventional dropping mercury electrode and a saturated calomel electrode (SCE), were used. An N.B. Electronic Colora thermostat was employed. Dissolved oxygen was removed with nitrogen-free oxygen.

The supporting electrolyte in all experiments was 2.0 M acetic acid—2.0 M ammonium acetate (Panreac). The solutions of thallium, lead and uranium were prepared by dissolving thallium(I) carbonate (FEROSA), lead nitrate (Probus) and uranium(VI) acetate (Panreac); antimony(III) solutions were prepared by dissolving antimony trichloride in 0.5 M hydrochloric acid.

The solutions of surfactants were prepared by dissolving commercial products in distilled water. The substances used were: Triton X-100 (Merck), polyethylene glycols (PEG) of m.w. 300 and 400 (FEROSA), Aerosol 501 (Cyanamid), tetramethylammonium hydroxide (Eastman-Kodak), tetrabutylammonium chloride (Fluka), tetrabutylammonium iodide (BDH), alkylbenzyldimethylammonium chloride (Merck), cetyltrimethylammonium bromide (Merck), sodium dodecylsulphate (Eastman-Kodak), sodium dioctyl sulphosuccinate (Aerosol OT; Cyanamid), sodium bistridecyl sulphosuccinate (Aerosol TR; Cyanamid).

RESULTS AND DISCUSSION

Effect of non-ionic surfactants

Triton X-100. Parallel to the increase in concentration of Triton X-100, the reduction wave of lead shifted towards more negative potentials; the system appeared increasingly irreversible and the wave-height decreased. In the absence of surfactant, antimony(III) was reduced, giving two waves with half-wave potentials ($E_{1/2}$) of —0.45 and —0.55 V. The presence of Triton X-100 caused a decrease in the first wave, which could even disappear, while the second wave shifted to more negative potentials, such that at Triton X-100 concentrations of ca. 0.02% only one wave with $E_{1/2}$ of —0.93 V was observed.

The uranium(VI) wave was split into two new waves in the presence of small amounts of Triton X-100; the first disappeared on increasing the surfactant concentration, while the second appeared at more negative potentials.

Within the range of surfactant concentrations studied, the half-wave potential of thallium was unchanged. However, there was a slight decrease in wave-height on increasing the surfactant concentration. Table 1 shows that

TABLE 1

Effect of the non-ionic surfactants, Triton X-100 and Aerosol 501, on the wave-heights and half-wave potentials of Tl, Pb, Sb and U (all 1.0×10^{-3} M)

Surfactant conc. (%)	Tl(I)		Pb(II)		Sb(III)		U(VI)	
	$-E_{1/2}$(V)	I_l(μA)	$-E_{1/2}$(V)	I_l(μA)	$-E_{1/2}$(V)	I_l(μA)	$-E_{1/2}$(V)	I_l(μA)
Triton X-100								
0.000	0.51	4.24	0.51	4.90	0.45 0.55	2.75[a]	0.49	2.55
0.005	0.51	3.90	0.52	4.70	0.45 0.62	2.45[a]	0.50	2.01
0.01	0.51	3.90	0.57	4.40	0.80	2.45	0.50 0.80	1.97[a]
0.02	0.51	3.89	0.64	3.70	0.93	2.45	0.82	1.83
Aerosol 501								
0.000	0.50	4.22	0.52	4.90	0.45 0.56	2.73[a]	0.48	2.53
0.005	0.50	4.20	0.53	4.90	0.45 0.56	2.18[a]	0.48	2.49
0.01	0.50	4.18	0.54	4.90	0.45 0.56	2.12[a]	0.48	2.41
0.02	0.51	4.18	0.54	4.90	0.45 0.58	2.06[a]	0.48	2.39
0.04	0.51	4.18	0.54	4.90	0.45 0.62	2.00[a]	0.50	2.39
0.08	0.51	3.94	0.56	4.85	0.72	1.88	0.62	2.27
0.20	0.51	3.94	0.64	4.10	0.88	1.82	0.76	2.25

[a]Sum of the two waves.

lead, antimony and uranium should not interfere in the polarographic determination of thallium in the acetate medium when 0.02% Triton X-100 is present.

Polyethylene glycols (m.w. 300 and 400). The concentration range at which their influence was studied was 0.005—0.02%. The reduction waves of the four ions were not changed by the addition of PEG 300, except for a slight decrease in their wave-heights. Neither did the presence of PEG 400 affect the half-wave potentials of lead, thallium and uranium, but the first reduction wave of antimony(III) decreased in height, while the second shifted to more negative potentials. The results obtained in the presence of PEG 300 and 400 would not allow the selective polarographic determination of any of the species studied.

Aerosol 501. Among the ions studied, the only one whose behaviour was not modified by the presence of the surfactant was thallium. The other ions all underwent a shift in half-wave potential to more negative values (Table 1). This reagent, therefore, offers several possibilities as an electromasking agent. However, because of the irreversibility of the systems involved under the existing conditions, only that determination of thallium in the presence of antimony seems to be possible.

Effect of cationic surfactants

The concentration of quaternary ammonium ions was varied between 0.005 and 0.02%, but was extended for hexadecyltrimethylammonium bromide up to 0.20%. The half-wave potentials of lead, thallium and uranium hardly

TABLE 2

Effect of cetyltrimethylammonium bromide and alkylbenzyldimethylammonium chloride on the wave-heights and half-wave potentials of Tl, Pb, Sb and U (all 1.0×10^{-3} M)

Surfactant conc. (%)	Tl(I)		Pb(II)		Sb(III)		U(VI)	
	$-E_{1/2}$(V)	I_l(μA)	$-E_{1/2}$(V)	I_l(μA)	$-E_{1/2}$(V)	I_l(μA)	$-E_{1/2}$(V)	I_l(μA)
Cetyltrimethylammonium bromide								
0.00	0.51	4.26	0.52	4.90	0.45 0.55	2.70[a]	0.49	2.60
0.02	0.51	3.84	0.52	3.90	0.68	2.34	0.49	2.36
0.04	0.51	3.84	0.52	3.85	0.68	2.28	0.49	2.30
0.10	0.51	3.82	0.52	3.80	0.68	2.28	0.49	2.24
0.20	0.51	3.72	0.52	3.80	0.69	2.22	0.49	2.20
Alkylbenzyldimethylammonium chloride								
0.000	0.51	4.22	0.51	4.91	0.45 0.55	2.75[a]	0.49	2.55
0.005	0.51	4.10	0.54	4.31	0.70	2.63	0.49	2.37
0.01	0.51	4.16	0.56	4.11	0.78	2.63	0.49	2.19
0.02	0.52	4.16	0.57	4.01	0.79	2.57	0.49	2.16

[a]Sum of the two waves.

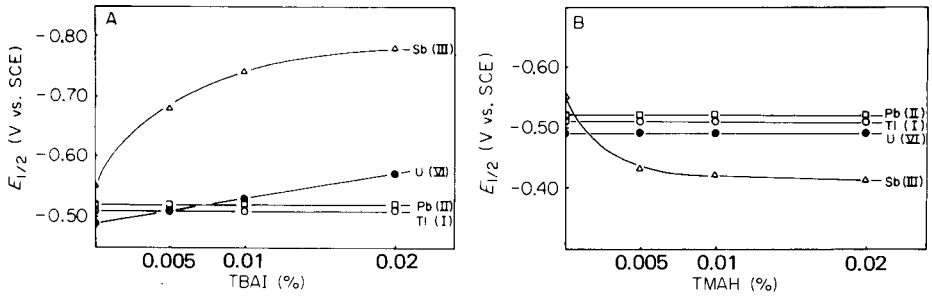

Fig. 1. Effects of (A) tetrabutylammonium iodide and (B) tetramethylammonium hydroxide on the half-wave potentials of Tl, Pb, Sb and U. In the absence of surfactant, the value for Sb(III) is that of the second wave.

changed in the presence of the cationic surfactants tested but their wave-heights decreased with increasing surfactant concentration (Table 2). Uranium was somewhat affected by the presence of tetrabutylammonium iodide because of the stronger adsorption of iodide on the mercury electrode (Fig. 1A).

The polarograms of antimony(III) were strongly influenced by the presence of cationic surfactants. There was an inhibition in the first reduction wave, which disappeared at higher surfactant concentrations and a simultaneous shift in the second wave to more negative potentials. Curiously in the presence of 0.005% tetramethylammonium hydroxide, antimony gave a single wave at −0.43 V, which was a shift to a more positive potential such as is infrequently observed (Fig. 1B). This fact might be explained by remembering that, because the antimony is present as anionic chloro complexes, the presence of the cationic surfactant facilitates the reduction process. The fact that when other cationic surfactants of greater molecular size than tetramethylammonium ions are used, the antimony wave shifts to more negative potentials, could be attributed to an increase in steric hindrance.

The above results clearly show the possibility of determining thallium, lead or uranium in the presence of antimony(III) by using any of the cationic surfactants studied except tetramethylammonium hydroxide.

Effect of anionic surfactants

The compounds studied were sodium dodecylsulphate and sodium dioctyl sulphosuccinate (0.005—0.20%) and sodium bistridecyl sulphosuccinate (0.005—0.10%), the highest concentration for the last being limited by its solubility in water.

Sodium dodecylsulphate. Thallium and lead behaved similarly. There was a slight decrease in the wave-height, but their half-wave potentials were hardly changed. The surfactant inhibited the first antimony(III) wave, shifting it to more negative potentials. The uranium wave also shifted to more negative values (Fig. 2A) which may permit the determination of thallium or lead in the presence of uranium or antimony by electromasking of the latter.

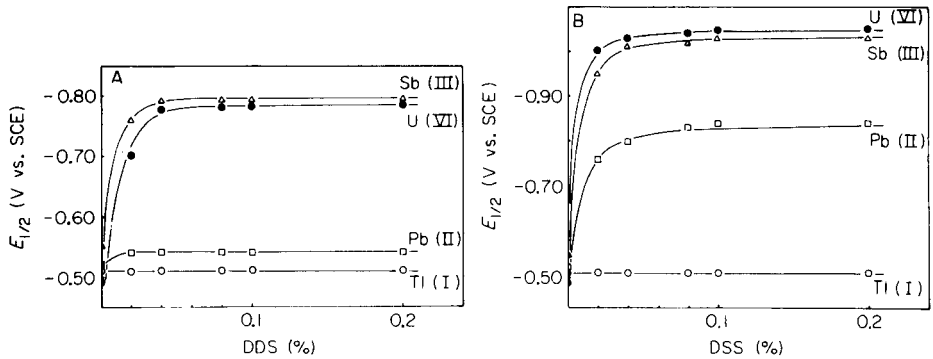

Fig. 2. Effects of (A) dodecylsulphate and (B) dioctyl sulphosuccinate on the half-wave potentials of Tl, Pb, Sb and U. In the absence of surfactant, the value for Sb(III) is that of the second wave.

Sodium bistridecyl sulphosuccinate. The behaviour of the electroactive species in the presence of this surfactant was very similar to that obtained with sodium dodecylsulphate. The half-wave potentials of thallium and lead were unchanged whereas those of uranium and antimony shifted to more negative values, though this was less pronounced as in the previous case. Thus, in the presence of 0.08% of surfactant the half-wave potentials of uranium and antimony were —0.54 and —0.66 V, respectively. It can be concluded that the slight differences between the half-wave potentials of the species studied do not allow the polarographic differentiation of these species.

Sodium dioctyl sulphosuccinate. The reduction wave of thallium was not modified by the presence of this compound in the concentration range studied. The polarographic waves of lead, antimony and uranium were distorted in the presence of the surfactant, and a shift was observed to more negative potentials. In the 0.005—0.08% range of surfactant the shift was a function of surfactant concentration; for a 0.10% solution, the half-wave potentials reached values of —0.84, —1.03 and —1.05 V, respectively, these values remaining constant at greater concentrations of surfactant (Fig. 2B). The presence of surfactant also caused a decrease in the wave-heights. The changes observed in the shapes of the waves indicated that the systems became irreversible.

From theoretical considerations, the predominant species in the solution were: TlAc, $[PbAc_3]^-$, $[SbCl_4]^-$ and $[UO_2Ac_3]^-$ (Ac = acetate). Thus, it seems that electrode reactions of negatively-charged complexes are inhibited by the presence of anionic surfactants, in agreement with the work of Jacobsen and Kalland [5].

The difference between the half-wave potentials of thallium and lead is greater than 200 mV, so that it would seem feasible to carry out the polarographic determination of thallium in the presence of the other ions studied by using dioctyl sulphosuccinate as the electromasking agent.

DETERMINATION OF THALLIUM IN THE PRESENCE OF LEAD, ANTIMONY AND URANIUM

The above results encouraged a more detailed study on the polarographic behaviour of thallium in acetic acid—ammonium acetate medium in the presence of the dioctyl sulphosuccinate, in order to determine the nature of the polarographic wave. For this purpose, classical criteria were employed. The influence of the height of the mercury column on the wave-height of thallium is summarized in Table 3. The high correlation coefficients (r) obtained indicate that the wave is not controlled by a kinetic process. The correlation coefficient for the $h_c^{1/2}$ dependence is greater than that for the h_c dependence, showing that the process is likely to be diffusion-controlled.

The temperature of the solution was varied between 25 and 55°C. The temperature coefficient obtained was 1.54% and the relationship between log (current) and temperature was linear. This is typical of diffusion-controlled processes [21].

Thallium concentrations were varied between 4.0×10^{-5} and 1.0×10^{-3} M. The temperature was maintained at 25 ± 0.5°C, the height of the mercury column was 60.5 cm and the dioctyl sulphosuccinate concentration was 0.04%. Linear relationships between current and the thallium concentration were obtained, both in the presence of the surfactant and in its absence, again indicating that the electrode process is diffusion-controlled.

Determination of thallium

Figure 3 shows the polarographic curves of thallium, lead, uranium and antimony in the presence of 0.04% dioctyl sulphosuccinate as well as in its absence. It is clear that thallium can be determined without the preliminary removal of the other ions. Table 4 shows the results obtained from this determination. The precision of the proposed method was estimated from

TABLE 3

Effect of corrected mercury height (h_c) on the wave-height (I_l) for 2.0×10^{-4} M thallium in 2.0 M acetic acid—2.0 M ammonium acetate with addition of 0.04% dioctyl sulphosuccinate

h_c (cm)	I_l (μA)	I_l/h_c[a] (μA cm^{-1})	$I_l/h_c^{1/2}$[b] (μA cm$^{-1/2}$)	h_c (cm)	I_l (μA)	I_l/h_c[a] (μA cm^{-1})	$I_l/h_c^{1/2}$[b] (μA cm$^{-1/2}$)
41.26	0.76	0.018	0.118	51.26	0.85	0.016	0.119
43.26	0.78	0.018	0.119	53.26	0.87	0.016	0.119
45.26	0.80	0.018	0.119	55.26	0.89	0.016	0.120
47.26	0.81	0.017	0.118	57.26	0.91	0.016	0.120
49.26	0.84	0.017	0.119	59.26	0.92	0.015	0.119

[a] $r = 0.9956$. [b] $r = 0.9968$.

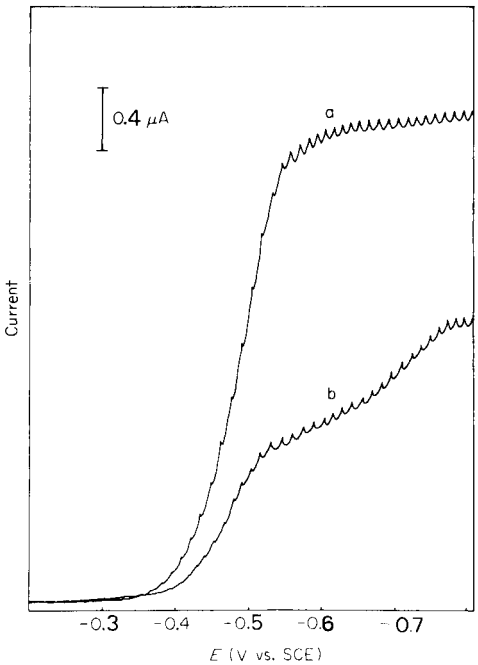

Fig. 3. Polarographic curves of Tl, Pb, Sb and U at equimolar concentrations (2.0×10^{-4} M) in an acetic acid—acetate medium (a) before, (b) after addition of 0.04% dioctyl sulphosuccinate.

ten replicates containing the four ions in equimolar concentrations (2.0×10^{-4} M). The relative standard deviation was 2.6%.

In order to establish the limiting proportion for which it is possible to carry out this determination, thallium was determined in the presence of various amounts of the other ions by a standard addition method. Table 5 shows the results obtained. The determination of thallium is clearly possible in the presence of large amounts of uranium and antimony and commensurate amounts of lead. For proportions greater than those studied, differentiation between the waves of thallium and the other ions is not clear and the results are not reproducible.

TABLE 4

Determination of thallium in the presence of 2×10^{-4} M concentrations of lead, uranium and antimony, and 0.04% dioctyl sulphosuccinate

Tl taken (10^{-4} M)	10.00	6.00	4.00	2.00	1.00	0.80	0.60
Tl found (10^{-4} M)	9.92	6.13	4.02	2.02	0.98	0.78	0.59
Difference (%)	−0.8	+2.2	+0.5	+1.0	−2.0	−2.5	−1.6

TABLE 5

Determination of thallium (2.0×10^{-4} M) in the presence of various molar ratios of lead, uranium and antimony. Conditions as Table 4

Tl:Pb	Tl found (10^{-4} M)	Tl:U	Tl found (10^{-4} M)	Tl:Sb	Tl found (10^{-4} M)
1:0.3	1.97	1:1	1.96	1:1	1.99
1:0.4	1.96	1:2	2.02	1:2	2.03
1:0.5	1.98	1:5	1.96	1:5	2.03
1:1	2.03	1:10	2.04	1:10	1.96
1:2	2.07	1:15	2.06	1:15	1.95
1:4	2.05	1:20	1.96	1:20	1.94
1:5	2.10	1:25	1.90	1:25	1.92

REFERENCES

1 J. Heyrovsky and J. Kuta, Principles of Polarography, Academic Press, New York, 1966.
2 J. J. Lingane, Ind. Eng. Chem. Anal. Educ., 15 (1943) 584.
3 I. M. Kolthoff and Y. Okinaka, J. Am. Chem. Soc., 81 (1959) 2296.
4 A. N. Frumkin, Zh. Fiz. Khim., 24 (1950) 244.
5 E. Jacobsen and G. Kalland, Anal. Chim. Acta, 30 (1964) 240.
6 R. W. Schmid and C. N. Reilley, J. Am. Chem. Soc., 80 (1958) 2087.
7 T. Fujinaga and K. Isutsu, Bunseki Kagaku, 10 (1961) 63.
8 P. R. Subbaraman, P. S. Schetty and J. Gupta, Anal. Chim. Acta, 26 (1962) 179.
9 P. S. Shetty, P. R. Subbaraman and J. Gupta, Anal. Chim. Acta, 27 (1962) 429.
10 D. K. Mendalieva, M. K. Nauryzbaev and V. P. Gladyshev, J. Anal. Chem. USSR, 32 (1977) 123.
11 Z. Lukaszewski, Talanta, 24 (1977) 603.
12 H. K. Hoff and E. Jacobsen, Anal. Chim. Acta, 54 (1971) 511.
13 N. Gundersen and E. Jacobsen, J. Electroanal. Chem., 20 (1969) 13.
14 E. Jacobsen and G. Tandberg, Anal. Chim. Acta, 47 (1969) 285.
15 E. Jacobsen and G. Tandberg, J. Electroanal. Chem., 30 (1971) 161.
16 W. Kemula and S. Glodwski, Rocz. Chem., 36 (1962) 1203.
17 G. E. Batley and T. M. Florence, J. Electroanal. Chem., 72 (1976) 121.
18 Z. Lukaszewski, M. K. Pawlak and A. Ciszewsky, J. Electroanal. Chem., 103 (1979) 217.
19 L. G. Petrova, V. I. Ignatov and E. Ya. Neiman, J. Anal. Chem. USSR, 33 (1978) 1498.
20 M. A. Desesa, D. N. Hume, A. C. Glamm and D. D. DeFord, Anal. Chem., 25 (1953) 983.
21 L. Meites, Polarographic Techniques, Interscience, New York, 1965.

Analytica Chimica Acta, 132 (1981) 69—74
Elsevier Scientific Publishing Company, Amsterdam — Printed in The Netherlands

POTENTIAL METHODS IN PATTERN RECOGNITION
Part 4. A combination of ALLOC and Statistical Linear Discriminant Analysis

D. COOMANS and D. L. MASSART*

Farmaceutisch Instituut, Vrije Universiteit Brussel, Laarbeeklaan 103, B-1090 Brussel (Belgium)

I. BROECKAERT

Dienst Gastro-Enterologie, Sint Pieter Hospitaal, Hoogstraat 322, B-1000 Brussel (Belgium)

(Received 1st June 1981)

SUMMARY

It is shown that ALLOC when associated with descriptive statistical linear discriminant analysis ("display" SLDA) is in some situations a better alternative than ALLOC and SLDA for classification purposes ("classification" SLDA). It is possible with a combination of "display" SLDA and ALLOC to adjust the suboptimal decision boundaries of "classification" SLDA when the underlying assumptions about the data in "classification" SLDA are not fulfilled, whereas the combination of "display" SLDA with ALLOC permits classification of new objects without computer assistance which is not possible with ALLOC alone. The performance of "display" SLDA—ALLOC is discussed on the basis of the differentiations between THYROID functional states.

In Parts 1 and 3 of this series [1, 2] the supervised classification and feature selection method ALLOC of Hermans and Habbema [3, 4] was discussed. The classification of ALLOC may be called "direct", i.e., although a rudimentary learning step is present in which the smoothing parameters are determined, all objects of the learning set are required whenever a test object has to be classified. Therefore, test objects can only be classified with computer assistance. In some situations this can be a disadvantage. With an "indirect" classification technique such as statistical linear discriminant analysis (SLDA), the computer is used to extract the information from the learning set and to translate it into one or more functional relationships of the features [5—7]; this need be done only once. The functional relations obtained can be used for further classification of test objects. Only a desk calculator or a diagram is needed for this purpose. In order to be able to use ALLOC in the same way, an attempt was made to preprocess the learning set by means of SLDA.

In fact, SLDA is normally used for two different purposes, description and classification. In the former, the aim is to derive linear discriminant functions (canonical variables) which are linear combinations of the original variables of a learning set. The linear discriminant functions are considered as new

0003—2670/81/0000—0000/$02.50

variables and transform the pattern space (original variables) in a discriminant space with a reduced number of dimensions and with minimum loss of separability between the learning classes. In this way, it is often possible to reduce the pattern space to a 1- or 2-dimensional discriminant space without significant loss of information. In this situation, the discriminant space can be used as a display method for the objects of the pattern space. When the purpose is classification, linear classification functions are derived which describe in a statistical way linear boundaries between the learning classes in the pattern space. On the basis of these classification functions, a classification rule for the test objects can be formulated. Thus, SLDA can be either a preprocessing or display technique or a supervised pattern recognition technique. Both techniques are often combined in one application. The classification boundaries are then indicated on a display map [8]. From the statistical point of view, the most important difference between the two kinds of SLDA is that when the technique is used for display purposes, no assumptions are made about the data. For classification purposes however, the learning classes must have a multivariate normal distribution with equal variance—covariance matrices in order to obtain optimal decision boundaries. Because "display" SLDA does not require assumptions about the data, it may be a suitable preprocessing technique for combination with ALLOC.

This paper shows that the "display" SLDA—ALLOC combination permits adjustment of the suboptimal decision boundaries which are often obtained by "classification" SLDA. These suboptimal boundaries occur when the assumptions about the data made in "classification" SLDA are not fulfilled. The performance of the "display" SLDA—ALLOC combination is illustrated on the basis of the THYROID example used in previous papers [1, 2, 5, 9].

METHOD

The procedure consists of the following steps: (1) preprocessing of the original data by linear combination of the features with discriminant weights [6] ("Display" SLDA procedure) and plotting of the objects on a SLDA diagram; and (2) calculation of the *a posteriori* probabilities of class membership for the objects represented in the SLDA diagram. This is done by ALLOC classification on the discriminant scores of the objects.

In step 1 canonical variates which are linear functions of the features, are calculated [3, 5] by means of SLDA. The canonical variates describe the discrimination between learning classes in a statistical sense of maximization of the ratio of between-class variation to within-class variation. In order to use SLDA as a display technique, the original measurements of the objects of the learning classes are transformed to discriminant scores, i.e., by substitution of the measurements of an object in the canonical variate one discriminant score is obtained for each canonical variate. For the display, one or two canonical variates may be used as axes of a diagram on which the objects of

the learning set are plotted (SLDA plot). The number of axes used depends on specific circumstances (see Results and Discussion).

In the second step, ALLOC classification is applied to the discriminant scores of the learning objects. From the ALLOC classification, the *a posteriori* probabilities [1, 3, 4] of class membership are obtained. These probabilities are used to define new and better classification boundaries in the SLDA diagram between the different classes of the learning set.

Calculation of these probabilities for supplementary positions in the SLDA diagram (called artificial test objects) may be necessary when the learning set is inadequate for determining the classification boundaries in a sufficiently accurate way. The artificial test objects are located on the SLDA diagram in the neighbourhood where the boundary is expected but where too few learning objects are present. With the discriminant scores of these artificial objects, the *a posteriori* probabilities are computed by using ALLOC.

Data set and programs

The THYROID data set comprises 215 patients divided into three classes, namely EUthyroid (150 normal cases), HYPERthyroid (35 cases) and HYPOthyroid (30 cases). For each patient, the results of 5 laboratory tests are available (RT3U, T4, T3, TSH and ΔTSH). This data set was used in earlier work [1, 2, 5, 9]. The following computer programs or packages were used in this study: ALLOC [1] for classification on the basis of potential functions, SPSS [8] for the application of SLDA, and the BAYES routine of the ARTHUR package [10, 11, 12] for the Bayes classification on the basis of frequency histograms.

RESULTS AND DISCUSSION

In Fig. 1 the SLDA diagram (2 canonical variables cv_1 and cv_2) of the members of the three THYROID classes, HYPO, EU and HYPER, is shown with the boundaries between these three classes as defined by SLDA (full lines). SLDA used as a classification technique separates the classes by lines corresponding to boundaries indicating equal *a posteriori* probabilities for each pair of related classes; for instance, for EU/HYPO, $P(EU/cv_1, cv_2) = P(HYPO/cv_1, cv_2) = 0.5$. It can be seen that the position of these boundaries is not optimal, especially for the EU/HYPO differentiation. The EU/HYPO boundary is clearly not close enough to the EU class. This happens because the assumptions of multivariate normal distributions with equal variance–covariance matrix for the three classes is not fulfilled. An improvement can be obtained by better estimation of the probabilities. This is done by means of recalculation of the *a posteriori* probabilities from the discriminant scores with ALLOC. If ALLOC must be used for each calculation of a new test object, there is no important practical advantage in the use of "display" SLDA–ALLOC instead of ALLOC on the original data (except maybe that the number of features to be handled by ALLOC is reduced in an important

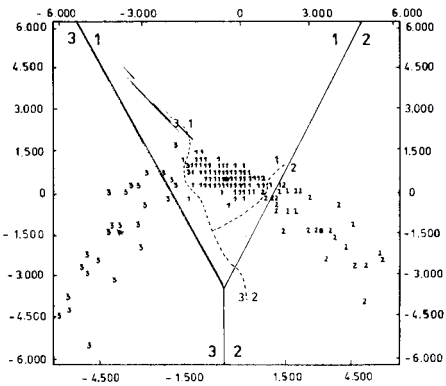

Fig. 1. SLDA plot. The horizontal is the 1st canonical variate (cv_1) and the vertical is the 2nd canonical variate (cv_2) of the HYPO (3), EU (1) and HYPER (2) classes of the THYROID example. The full lines indicate the SLDA boundaries between the classes and the dotted curves indicate the ALLOC boundaries. The numbers indicate the positions where one or more members of the learning classes are situated.

way when the data are preprocessed by "display" SLDA). Therefore, it is preferable to draw the ALLOC boundaries once and for all on the SLDA plot. In this way, ALLOC must not be used for the classification of test objects. The position of these boundaries can be determined approximately on the basis of the recalculated *a posteriori* probabilities of the learning objects in the SLDA diagram. In order to obtain a relatively reliable boundary, some supplementary points may be required. Approximate ALLOC boundaries for the EU/HYPER and EU/HYPO differentiation are shown in Fig. 2 A and B respectively. In order to simplify comparison, the approximate ALLOC boundaries are drawn in Fig. 1. The approximate ALLOC boundary is drawn in such a way that it approximately corresponds to a curve indicating an *a posteriori* probability of 0.5. Beside the learning objects, artificial test objects (see Method) were plotted in order to make a better approximation of the position of the ALLOC boundary (see Fig. 2). Figure 2 reveals clearly that the ALLOC boundaries are much closer to the EU-class than are the "classification" SLDA boundaries.

This means that ALLOC is indeed able to recognise that the EU class is a very dense class in contrast to the HYPO and HYPER classes. As mentioned above, however, SLDA assumes the same variation in the three classes which is represented by the pooled variance—covariance matrix so that the variations in the HYPER and HYPO classes are underestimated and the variation in the EU overestimated.

In probabilistic classifications, more than one probability level is often of interest. For instance, in order to have an idea about the overlap between classes and with the intention of defining regions where some doubt exists about the classifications, other *a posteriori* probability levels than 0.5 may be asked for. For this purpose, diagrams with one canonical variate may be more attractive than the two-dimensional SLDA diagrams. In order to describe the discrimi-

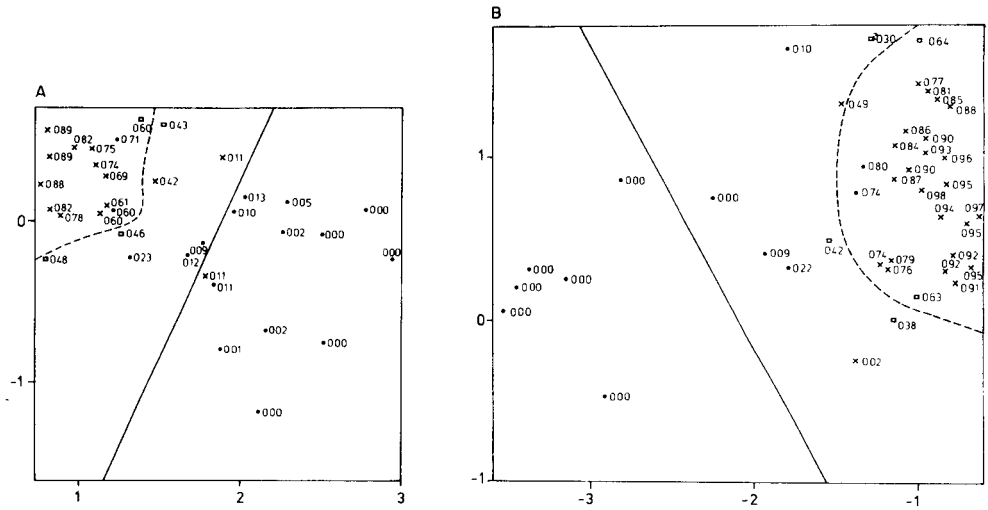

Fig. 2. Parts of the SLDA plot of Fig. 1 showing in more detail the overlapping region between (A) EU and HYPER and (B) EU and HYPO. The dotted line indicates the approximate ALLOC boundary and the full line the classification SLDA boundary. The values are the ALLOC *a posteriori* probabilities of EU class membership for (×) EU cases, (○) HYPER cases, and (□) artificial test cases.

nation between the three classes of the THYROID example without important loss of information, two canonical variates are necessary [5]. Therefore, the THYROID problem is better divided into three binary differentiations: EU/HYPO, EU/HYPER and HYPO/HYPER. The last, however, is not of interest from the clinical point of view [8]. When one canonical variate is used, the relationship between the *a posteriori* probabilities and the corresponding discriminant scores DS can be visualized in a diagram. As an example, Fig. 3

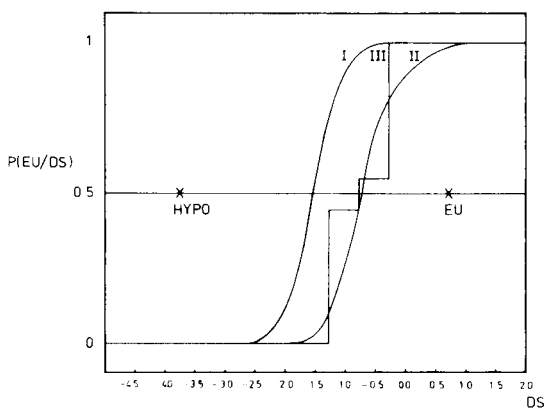

Fig. 3. Relationship between the *a posteriori* probability of EU class membership P(EU/DS) and the values for the canonical variate (discriminant scores DS) for the differentiation EU/HYPO. (I) SLDA probabilities; (II) ALLOC probabilities; (III) probabilities of the BAYES histogram method.

shows this relationship for the differentiation EU/HYPO. The *a posteriori* probabilities were calculated on the basis of "classification" SLDA (curve I), and by the ALLOC classification applied to the discriminant scores of the learning objects (curve II), and then compared with the true distribution estimated with the BAYES method (histogram III).

The three lines I, II and III show the relationship between the discriminant scores DS and the probability referred to the EU class, i.e. P (EU/DS). For the three lines, it can be observed that in the center of the EU class, P (EU/DS) = 1, which means that the EU functional state of the thyroid is completely certain in that region. The certainty about this state decreases with decreasing value of the discriminant scores; in the center of the HYPO class, P (EU/DS) becomes zero, which means that the HYPO state is certain. The boundaries corresponding to the minimum probability of error classification (i.e., the DS value corresponding to P (EU/DS) = 0.5) for ALLOC and the BAYES method (true distribution) are very close to each other. They differ, however, from the SLDA boundary which is situated halfway between the two class centroids. The boundaries for ALLOC and the true distribution are situated more closely to the EU class which corresponds to the diagram in Fig. 2B.

In conclusion, it can be stated that the association of "display by SLDA" and ALLOC is an attractive alternative for both "classification by SLDA" and ALLOC, because certain disadvantages associated with these techniques may be avoided.

REFERENCES

1 D. Coomans, I. Broeckaert and D. L. Massart, Anal. Chim. Acta, 133 (1981) 215.
2 D. Coomans, M. P. Derde, I. Broeckaert and D. L. Massart, Anal. Chim. Acta, 133 (1981) 241.
3 J. Hermans and J. D. F. Habbema, Manual for the ALLOC-discriminant analysis program, Department of Medical Statistics, University of Leiden, P.O. Box 2060, Leiden, Netherlands, 1976.
4 J. D. F. Habbema and J. Hermans, Technometrics, 19 (1977) 487.
5 D. Coomans, L. Kaufman and D. L. Massart, Anal. Chim. Acta, 112 (1979) 97.
6 D. L. Massart, A. Dijkstra and L. Kaufman, Evaluation and Optimization of Laboratory Methods and Analytical Procedures, Elsevier, Amsterdam,
7 H. E. Solberg, CRC Crit. Rev. Clin. Lab. Sci., (1978) 209.
8 N. N. Nie, C. H. Hull, J. G. Jenkins, K. Steinbrenner and D. Bent, Statistical Package for the Social Sciences (SPSS), McGraw-Hill, New York, 1975.
9 D. Coomans, D. L. Massart, I. Broeckaert, M. Jonckheer and P. Blockx, Anal. Chim. Acta, 103 (1978) 409.
10 S. Kullback, Information Theory and Statistics, J. Wiley, New York, 1959.
11 D. L. Duewer, J. R. Koskinen and B. R. Kowalski, ARTHUR, (available from B. R. Kowalski, University of Washington, Seattle).
12 A. M. Harper, D. L. Duewer and B. R. Kowalski, in B. R. Kowalski (Ed.), Chemometrics, Theory and Practice, Am. Chem. Soc. Symp. Ser., No. 52, 1977.

Analytica Chimica Acta, 132 (1981) 75—88
Elsevier Scientific Publishing Company, Amsterdam — Printed in The Netherlands

SIMULATION OF MASS SPECTRAL INTENSITIES BY REGRESSION ANALYSIS OF CALCULATED STRUCTURAL CHARACTERISTICS

HAYDEN A. CLARK[a] and PETER C. JURS*

Department of Chemistry, 152 Davey Laboratory, The Pennsylvania State University, University Park, PA 16802 (U.S.A.)

(Received 12th November 1980)

SUMMARY

Intensities of low-resolution, electron-impact mass spectral peaks were modelled with equations found by multiple linear regression analysis of experimental spectra and molecular descriptors derived from connection tables. Spectra of 246 hydrocarbons, including acyclic alkanes and alkenes, and cyclic alkanes and alkenes, were used. A randomly selected sample of twenty compounds was reserved for later evaluation of predictive capability. Molecular structure descriptors including molecular connectivity indices, substructure counts and molecular connectivity environments, numbers of double bonds, numbers of rings plus double bonds (unsaturations), path counts, and molecular weights were used as potential independent variables in a stepwise multiple linear regression analysis program to simulate logarithmically transformed peak intensities. Simulated spectra were compared to observed spectra by using correlation coefficient and Euclidean distance criteria. Simulated spectra were treated as unknowns in a file-searching experiment. The simulated spectra produced by the model equations were very similar to the actual observed spectra for both the training set of compounds and the set of unknown compounds.

Ideally, the prediction of a physical property of a chemical compound would be based on a fundamental theory. In principle, it is possible to calculate the intensities of mass spectral peaks using quantum mechanics. In practice, this has been done only by using the reasonable simplifications of molecular orbital theory, and also for small molecules, e.g., propane [1]. Given the vast amount of mass spectral data and the impracticability of fundamental theoretical calculations, the development of empirical interpretation and prediction rules has received much attention. General rules for interpretation of organic mass spectra have been known for many years [2, 3]. As these rules can be stated as algorithms, they have naturally been coded as computer programs [4].

Several kinds of transformations have been used to interpret mass spectra. The linear learning machine approach has been used to predict the presence or absence of functional groups [5, 6]. Explicit coding of empirical rules has been combined with a search of large files of known spectra to yield general

[a]Present address: Systems Research, The Dow Chemical Company, Midland, Michigan 48640, U.S.A.

0003—2670/81/0000—0000/$02.50

structural information about unknown compounds for later rationalization into complete structures [7].

The heuristic program system DENDRAL has been applied to mass spectra of many classes of compounds [8]. The programs were used to develop fragmentation rules from observed spectra and thus predict spectra of other compounds. A simple fragmentation theory based on bond type, or optionally a substructure match, has been added to the rule-based predictor [9].

The linear learning machine has been used to predict as well as interpret spectra [10—12]. A major disadvantage of this approach is poor determination of peak intensity. The nature of this technique is to find a partition which divides a data set into two classes. For prediction of mass spectral peak intensities, an intensity threshold must be chosen. An attempt would be made to divide the structures into two groups which have intensities at the mass spectral peak in question above or below the chosen value, say 50% of the base peak. To predict whether a compound would exhibit a peak with intensity above or below, say 10%, another partition would have to be found. The existence of such a partition is never guaranteed, and finding a group of structural characteristics upon which to base the partition can consume large amounts of time both of the analyst and the computer programs.

The work reported here involves the development of linear model equations for the prediction of peak intensities at integral mass positions in low-resolution mass spectra. The independent variables used are calculated molecular structure descriptors. The linear equations are of the following form

$$I_{jm} = C_m + \sum_{k=1}^{n} a_k x_{kj} \qquad (1)$$

where I_{jm} is the peak intensity at nominal m/z for compound j; C_m is a constant derived from regression analysis; a_k is the kth of n coefficients in the equation derived from regression analysis; and x_{kj} is the value of the kth molecular structure descriptor for compound j. To predict the entire mass spectrum of a compound, many individual predictions using equations of this form are made. The objective of this work is to show that regression equations of the form of Eqn. (1) can be developed to predict the intensities of low-resolution mass spectral peaks based on calculated molecular structure descriptors. The set of compounds and corresponding spectra used are of limited structural diversity in order to provide a test case for the methodology.

THE DATA SET

Structures

A set of 246 hydrocarbons ranging from C_5 to C_{10} was selected. The structures contained at most two unsaturations — only structures for which the sum of rings plus double bonds was zero, one, or two were used. No compounds with triple bonds were in the set. This set was selected to demonstrate that a model could be developed using a set of compounds with some limited

structural diversity in a controlled test situation. Within the data set were 164 acyclic compounds, 85 with no double bonds and 79 with one or two double bonds. There were 82 cyclic compounds, 57 with only single bonds, and 25 with one double bond. Rings contained three to eight atoms. A set of twenty compounds was selected at random to be used later as "unknowns" for evaluation of the performance of the system. This left 226 compounds to be used in development of the model equations.

The structure of each compound was entered into the computer system by sketching on a CRT screen under control of an interactive program. All the internal storage format (connection tables and associated information regarding rings, etc.) was developed by the program. These internal representations were used to develop the structural descriptors at a later stage of the project.

Spectra

The low-resolution mass spectra used were taken from a file purchased from the Mass Spectrometry Data Center, Atomic Weapons Research Establishment, United Kingdom Atomic Energy Authority, Aldermaston. The magnetic tape contained 6628 mass spectra taken from the ASTM E-14, DOW, API, and TRC collections. The spectrum for each compound in the data set was taken from the tape. Out of the total of 246 spectra, 240 were collected on CEC 21-101, 102, 103, and 103C mass spectrometers, and six were taken on other machines. The source temperatures (°C) reported were as follows: 275 (14); 267 (1); 265 (1); 250 (67); 245 (146); 237 (1); 230 (10); 180 (2); none reported (4). Thus, the majority of the spectra (213 or 87%) were taken with source temperatures of 245° C or 250° C and very few spectra were taken with substantially different source temperatures. The energy of the ionizing electrons was reported to be 70 eV for all spectra save seven for which these data were missing from the tape. Thus, the spectral data were generally collected under close to standardized conditions, and the data set was an appropriate collection for study by regression techniques.

The spectra were encoded on the tape with the base peak intensity for each spectrum scaled to the value 9999. Transformed intensities (I_t) were derived from the reported intensities (I) with the following logarithmic operation: $I_t = 64 \ln (I)/\ln (9999)$. After this transformation the base peak has an intensity of 64; 10% of base peak intensity is transformed to 48; 1% to 32; 0.1% to 16. Thus the perception of strong, medium, weak, and very weak is transformed into a linear scale for the regression studies. This transformation should have the added effect of making instrumental variations in spectral data collection less important than they otherwise would be because much of the detailed intensity information is lost through this transformation.

Spectrum data collation

The mass spectral data were collated into lists of dependent variables, suitable for regression analysis. Two kinds of lists were formed, fragments and losses. A fragment list of intensities comprised all peaks observed for

a particular m/z. For example, all of the intensities at m/z 55 were collated into one list. A loss list was the list of intensities corresponding to the loss of a specific neutral fragment. The loss of zero (molecular ion) was included in the analysis.

In selecting compounds to include in the intensity lists, two restrictions were imposed. First, only compounds with molecular weight greater than or equal to the relevant mass value were chosen. The structural characteristics of a pentane clearly have nothing to do with intensities of peaks above m/z 72 (except for their own M + 1 ions at m/z 73). Thus, the number of compounds used to develop each model for each m/z depended on the number of compounds with molecular weights equal to or exceeding the m/z of interest. The equations for m/z values between 40 and 60 were based on all 226 compounds. For higher m/z values, the number of compounds in the models decreased. There were 138 compounds in the model for m/z 100 and only 59 compounds in the model for the largest fragment peak considered, m/z 128. Second, if the m/z being collated was less than the lowest mass peak reported in a spectrum, the compound was left out of the model. For example, if the lowest mass peak reported in a particular spectrum was m/z 41, then zero was not presumed to be the intensity observed for lower masses although it was for peaks at m/z above the lowest reported. Inclusion of arbitrary values of zero intensity for such cases would have led to distortions in the simulation equations. The number of compounds in the model for m/z 15 was only 155 out of the potential 226 compounds.

The sets of compounds used in development of the loss peak equations were also selected. A compound was included in a model only if the resulting fragment mass was more than half of the molecular weight. All of the compounds were used to form a model for the molecular ion intensity and for small losses, such as 15 and 29. Five-carbon compounds were not used in the development of the model equation for the 43 loss peak.

The peaks and losses simulated are listed in Table 1. Part A is the list of the 12 loss peaks simulated; part B is the list of the 58 fragment peaks simulated. These 70 peaks account for 96.2% of the reported total ion current.

STRUCTURAL DESCRIPTORS

The overall goal of this work was to find model equations correlating the experimentally observed mass spectral peak intensities with structural char-

TABLE 1

Mass spectral peaks and neutral losses simulated

A. Losses	0, −1, −14, −15, −26, −27, −28, −29, −40, −41, −42, −43
B. Fragments	13, 14, 15, 16, 25, 26, 27, 29, 30, 37, 38, 38, 40, 41, 42, 43, 44, 52, 53 54, 55, 56, 57, 58, 66, 67, 68, 69, 70, 71, 72, 80, 81, 82, 83, 84, 85, 86 94, 95, 96, 97, 98, 99, 100, 108, 109, 110, 111, 112, 113, 114, 123, 124, 125, 126, 127, 128

acteristics. The independent variables in the regression analyses were computed structural characteristics. Over a period of years, a group of related computer programs to characterize chemical structures and to classify them according to some property has come to be known as ADAPT, an acronym for automated data analysis using pattern recognition techniques [13, 14]. The classification programs were designed for discrete, category problems such as biological activity/inactivity rather than prediction of values of a continuous variable. The structure characterization, or descriptor generation, programs of ADAPT were used extensively in this work.

The 28 descriptors used to characterize the 246 structures are shown in Table 2, together with actual values for three example compounds, *n*-decane, methylcyclohexane, and 2-methyl-2-heptene. The following paragraphs explain each descriptor in detail.

Structures of molecules are represented in all of these programs as molecular graphs. A graph is defined as a set of nodes, or atoms, and edges, or

TABLE 2

Descriptors used to characterize structures

Descriptor	Average	S.d.	*n*-Decane	Methyl-cyclohexane	2-Methyl-2-heptene
1 substr. count 1	2.780	1.509	2	1	3
2 substr. count 2	0.797	0.871	2	0	1
3 substr. count 3	0.211	0.465	0	0	0
4 substr. count 4	0.167	0.479	0	0	0
5 substr. count 5	1.240	1.955	0	5	0
6 substr. count 6	0.337	0.685	0	1	0
7 substr. connectivity 7	1.488	0.471	1.414	1.732	1.374
8 substr. connectivity 8	1.132	1.047	1.914	0	1.914
9 substr. connectivity 9	0.703	1.148	2.414	0	2.414
10 substr. connectivity 10	0.596	1.049	0	0	0
11 substr. connectivity 11	0.802	1.342	0	0	0
12 substr. connectivity 12	0.362	0.926	0	0	0
13 substr. connectivity 13	0.424	0.916	0	0	1.866
14 substr. connectivity 14	0.229	0.783	0	0	2.404
15 substr. connectivity 15	2.117	0.860	2.289	2.557	2.117
16 substr. connectivity 16	1.650	1.445	0	2.808	0
17 substr. connectivity 17	0.647	0.957	0	0	2.404
18 substr. connectivity 18	0.210	0.446	0	0	0
19 substr. connectivity 19	0.349	0.897	0	0	0
20 number of double bonds	0.467	0.583	0	0	1
21 molecular weight	108.268	21.358	142	98	112
22 total number of paths	42.874	20.472	55	48	36
23 number paths, length 5	3.882	4.434	5	8	3
24 number paths, length 6	1.780	2.949	4	2	2
25 path one connectivity	1.655	0.726	1.957	1.894	1.110
26 number of rings plus number of double bonds	0.817	0.690	0	1	1
27 cluster three connectivity	0.666	0.641	0	0.289	0.289
28 path—cluster four connectivity	0.828	0.809	0	0.408	0.204

bonds. When different types of atoms or bonds are identified, the resulting set is called a labeled graph. This representation is inherently planar, or two-dimensional. Spatial information may be appended to complete the molecular graph. Some of the programs in ADAPT supply information based on the entire molecule, such as the total number of paths, molecular connectivity indices, and molecular weight.

Molecular connectivity indices

Molecular connectivity indices have been widely applied in quantitative structural analysis. These indices have been correlated to molecular properties such as boiling points and enthalpies of formation of alkanes [15], water solubility and boiling point of alkanes and alcohols [16], octanol—water partition coefficients [17], and several biological activities of various kinds of compounds [18].

As originally proposed by Randić, molecular connectivity is very simple to calculate. A molecule is considered as a graph, with each atom a vertex and each bond an edge, ignoring protons. The connectivity index is a sum of values associated with each bond in the molecule. This value is $1/(c_i c_j)^{1/2}$ where c is the connectivity of an atom, or the number of non-hydrogen atoms to which it is bound, and i and j are atom indices defining the bond. While the results for these simple examples are impressive, several limitations are evident. Heteroatoms, multiple bonds, and rings are not accounted for.

This concept has been expanded into a series of connectivity indices, ${}^{m}\chi_{t}$ [18], where m is defined as the number of bonds in a subgraph, and t is the type of subgraph. Further, a valence weight is used in place of connectivity, allowing differentiation among heteroatoms and bond types. This valence weight is defined as $d = Z - h$ where Z is the number of valence electrons on an atom, and h is the number of protons. For a subgraph with one or two edges, no branching within the subgraph is possible, i.e., only path subgraphs are possible.

The molecular connectivity indices used here were descriptor 25, m = 1, t = path; descriptor 27, m = 3, t = cluster; descriptor 28, m = 4, t = path—cluster.

Substructures

It has long been recognised that structural features relate qualitatively and quantitatively to physical properties. A compound with a carbonyl group will display a characteristic absorption in the infrared region, and will display characteristic cleavages in a mass spectrometer. In the ADAPT system, there are two ways to represent the presence of a substructure.

The first representation is the number of occurrences of the substructure in a structure. For example, the methyl substructure, CH_3—, is found three times in 2-methylpentane and 3-methylpentane, and four times in 2,2-dimethylbutane and 3,3-dimethylbutane.

Descriptors 1 through 6 in Table 2 are substructure count descriptors. These substructures are shown in Table 3. Substructures 5 and 6 are "ring" substructures. They are constrained to match only ring atoms in a molecule. Substructure 5 would be found five times in methylcyclohexane; substructure 6 once. Neither would be found in *n*-decane or 2-methyl-2-heptene.

In the second representation of substructures, the atoms in the structure which match the substructure atoms are considered as a pseudomolecule, and a molecular quantity is calculated as if the matching atoms in the structure were in fact a molecule. When more than one match is found, the average is taken. The molecular quantity used in this work was path one molecular connectivity. Using the methyl substructure the value for 2-methylpentane is 1.626, for 3-methylpentane 1.520, for 2,2-dimethylbutane 1.854, and for 2,3-dimethylbutane 1.732. The absolute values of these descriptors are not as important as the fact that they are different from one another, thereby coding the different ways in which the methyl substructure is imbedded within the structures. These descriptors have been called environment descriptors for this reason. This representation introduces a sort of "fine tuning" of substructure match, as well as increasing the potential variation in the data set. The substructures for descriptors 7 through 19 are shown in Table 4.

Four of the substructure connectivity descriptors are based, in a sense, on the same match. Descriptors 7, 8, 18, and 19 correspond to descriptors 1 through 4, respectively. The match used for substructure connectivity, however, contains the atoms adjacent to the explicitly named atoms in the substructure. For example, the substructure count for descriptor one in methylcyclohexane contains information relating to one atom in the structures; the substructure connectivity descriptor, information relating to two atoms.

Paths and other descriptors

A path, in graph theoretic terms, is a sequence of atoms (connected by bonds) in which no atoms are repeated (no rings, no branching). A molecular graph contains as subgraphs paths of differing length, where length is the number of bonds in the path. Descriptor 22 is the total number of paths in a molecule; descriptor 23 the number of paths of length 5; descriptor 24 the number of paths of length 6.

Three additional quantities were used to characterize structures; molecular weight, descriptor 21; number of double bonds, descriptor 20; and number

TABLE 3

Substructures used for substructure count descriptors

1. CH_3—	2. CH_3—CH_2—	3. CH_2=
4. $(CH_3)_3C$—	5. —CH_2—(ring)	6. —CH < (ring)

TABLE 4

Substructures used for molecular connectivity environment descriptors

7. CH_3—	8. CH_3—CH_2—	9. CH_3—CH_2—CH_2—	10. $(CH_3)_2CH$—	
11. > C <	12. —CH=CH—	13. =C <	14. > C=CH—	
15. —CH_2—	16. > CH—	17. =CH—	18. CH_2=	19. $(CH_3)_2C$—

of unsaturations (number of rings + double bonds for this set of structures), descriptor 26.

Before the regression analyses, the descriptors were transformed to have a mean zero and a constant standard deviation. Scaling the descriptors so that each has the same approximate range of values, reduced the chance that a term would be entered into a prediction equation due to computational artifacts. This preprocessing is often called standardizing the variables or autoscaling and is a common procedure in statistical analyses.

CONSTRUCTION OF SIMULATIONS

The next step was to construct the linear model equations for each fragment peak and for each loss peak. The form of each model equation was that of Eqn. (1). For the construction of each equation, there was a pool of 28 independent variables, i.e., the 28 molecular structure descriptors. The individual models were found by stepwise multiple linear regression analysis. The programs to perform these anlyses were taken from the IBM Scientific Subroutine Package, and modified.

This method calculates coefficients for a linear equation one term at a time, selecting from the pool of independent variables the one variable which best explains the remaining variation in the dependent variable. The algorithm, as modified, recognizes three types of independent variables: (1) those currently in the equation; and of those not in the equation, (2) free, or available to the model, and (3) deleted, or not available. Initially all descriptors were considered as free independent variables for each simulation.

In starting the construction of a new equation, the free independent variable with the highest partial correlation coefficient would be selected first for entry. Before entering a variable into the equation, the partial F-statistic that it would have on entry was compared to a preset minimum value (an F-to-enter). The F-statistic was calculated as the square of the partial t-statistic, i.e., the ratio of the coefficient to the estimated error of the coefficient. If the potential value was less than the F-to-enter, no more terms were added to the equation.

After a new term had been added to the equation, other tests were made. If one or more of the terms had a partial F value less than a predetermined F-to-delete, the descriptor with the smallest partial F value was deleted, and

another equation was found, beginning at the top. If the adjusted multiple correlation coefficient did not increase, or if the addition of one or more variable would lower the ratio of observations to terms in the equation to a value less than five, or if all the potential independent variables had been entered, the current equation was reported as final. If none of these conditions existed, a new term was added to the equation and tested.

The test of partial F-statistics for previously entered coefficients allowed mimicking a more sophisticated stepwise procedure in which the calculation would delete the offending descriptor and back up a step [19]. This back-deletion algorithm would be much quicker, but would require substantially more core storage. A low partial F-statistic for a coefficient previously entered into the equation implies that later coefficients also have accounted for the same information. Deletion of the coefficient will lead at least to an equation with fewer terms, and may lead to an equation with a higher multiple correlation coefficient.

In addition to the statistical measures described above, an additional check was made of the data. Stepwise multiple linear regression algorithms break down whenever two or more descriptors are related to a high degree. If one of the descriptors in the data set can be calculated from a linear combination of the other descriptors, then the covariance matrix will be singular. This relationship among variables is called multicollinearity. The data set was investigated for multicollinearities, and was altered when necessary to insure that the covariance matrix was nonsingular.

EVALUATION OF SIMULATIONS

Individual intensities

Seventy equations of the form of Eqn. (1) were developed. These individual equations are not reported here to save space. For each regression analysis the following summary statistics were calculated: multiple correlation coefficient R, the F-statistic, and the standard error of estimate. These quantities were used to determine which individual simulations needed improvement.

The number of terms in the individual equations ranged from 4 terms to 15 terms with a mean of 8.5. These simulations of individual peaks were successful on the whole; the majority of the equations had multiple correlation coefficients greater than 0.8. The distribution of multiple correlation coefficients is shown in Table 5. The overall performance of the system was about the same for even and odd mass peaks. This is interesting because none of the even mass peaks, except the molecular ion, result from a simple fragmentation process. All result from multi-step processes, either rearrangements or multiple fragmentations. Thus, complicated events can be simulated and predicted from calculated structure information.

To simulate the complete mass spectrum of a compound, the intensity of each appropriate peak was calculated using the appropriate simulation equation. When more than one equation was available, the equation with the larger R value was used. For example, given a compound of molecular weight

TABLE 5

Summary of correlation coefficients (r) between simulated and observed intensities

Range	Total	Even m/z	Odd m/z
0.0—0.299	0	—	—
0.300—0.399	2	1	1
0.400—0.499	3	1	2
0.500—0.599	5	3	2
0.600—0.699	10	6	4
0.700—0.799	10	4	6
0.800—0.899	27	12	15
0.900—0.999	13	6	7

114, the intensity at m/z 114 would be calculated as loss of zero rather than m/z 114 because the former equation had a higher correlation coefficient. (For loss of zero the multiple correlation coefficient R was 0.89.)

Intensity of the peak one mass unit greater than the molecular ion (the M + 1 peak) was not simulated directly. The intensity was simply calculated using isotopic abundances given the simulated ion intensity.

An example simulation equation, for m/z 54, is shown in Table 6. This equation has a multiple correlation coefficient of 0.833 (accounts for 69% of the variance of the dependent variable, the observed intensity at m/z 54). Only those coefficients for the four independent variables entered into the equation are shown. For convenience, the relevant descriptor values are repeated for n-decane, methylcyclohexane, and 2-methyl-2-heptene, together with the contribution to intensity (the product of the coefficient and descriptor value). Molecular weight (descriptor 21) and number of unsaturations (descriptor 26) make relatively large positive contributions to the prediction, whereas number of methyl groups (descriptor 1) and cluster three connectivity (descriptor 27) make relatively small negative contributions. All three estimates are close to the observed values, which are shown at the bottom of the table.

TABLE 6

Use of the model equation for the prediction of the intensity of m/z 54 for three example compounds

Descriptor	Coeff.	n-Decane		Methylcyclohexane		2-Methyl-2-heptene	
		Descriptor value	Contribution	Descriptor value	Contribution	Descriptor value	Contribution
1	−1.30	2	−2.61	1	−1.30	3	−3.91
21	0.124	142	17.56	98	12.12	112	13.85
26	8.64	0.0	0.0	1.0	8.64	1.0	8.64
27	−2.37	0.0	0.0	0.289	−0.68	0.289	−0.68
Constant	22.41						
		Predicted value	37.37		41.18		40.31
		Observed value	35		45		38

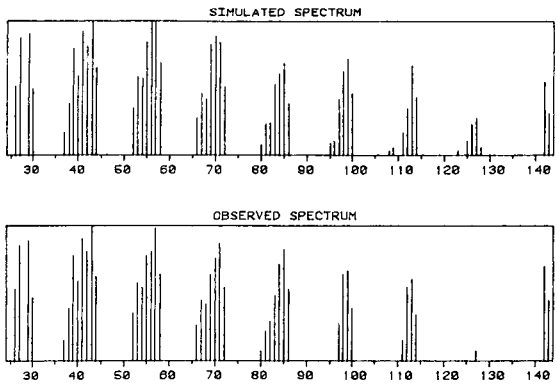

Fig. 1. Simulated and observed mass spectrum of *n*-decane.

Entire spectra

Simulated and observed spectra for three compounds, *n*-decane, methylcyclohexane, and 2-methyl-2-heptene, are shown in Figs. 1—3. These are the compounds for which example descriptors are shown in Table 2; the intensities have been transformed logarithmically. Qualitatively, the pairs of simulated and observed spectra resemble each other strongly. The calculated similarity criteria also show strong agreement.

Two comparison criteria were used to judge quantitatively the similarity of simulated and observed spectra: correlation coefficient and Euclidian distance [20]. For *n*-decane, the correlation coefficient between the observed and simulated spectra is 0.974 and the distance is 42, for methylcyclohexane, 0.973 and 30, for 2-methyl-2-heptene, 0.970 and 38. The range of values for the correlation criterion for the 226 compounds in the model was from 0.829 to 0.988, with median 0.956; for the twenty withheld, range was 0.792 to 0.979, median 0.959. These distributions are shown in Fig. 4. The range of values for the distance criterion was 16 to 115 with median 43 for the compounds in the model; range was 26 to 72 with median 42 for withheld

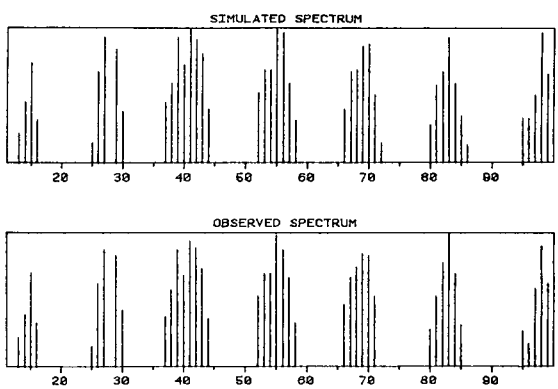

Fig. 2. Simulated and observed mass spectrum of methylcyclohexane.

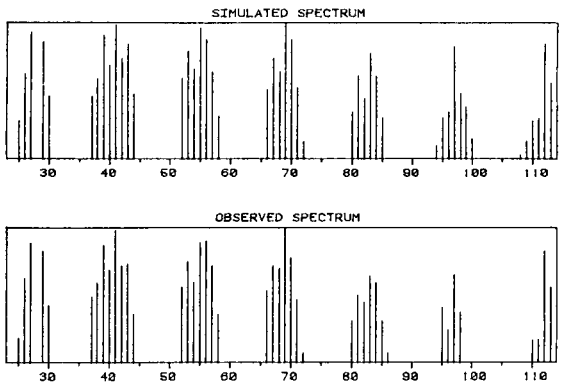

Fig. 3. Simulated and observed mass spectrum of 2-methyl-2-heptene.

compounds. The distributions were generated and plotted for the distance similarity criterion, and the appearances of the plots were similar to those for the correlation coefficient similarity criterion. The fact that the model equations predict spectra of compounds not in the data set with roughly the same distribution of values of similarity criteria as for those compounds used to develop the equations, is strong confirmation, on top of the numerical and statistical tests, of the validity of the model.

To test the quality of the model further, each simulated spectrum was compared to the entire set of 246 observed spectra, as though it were an unknown spectrum. For an ideal model, the experimental spectrum would always be chosen as the most similar to the simulated spectrum. In practice, this performance has not been obtained, and probably cannot be. The correct experimental spectrum is among the top five matches over 60% of the time according to either similarity criterion, whether the spectrum was in the model or not.

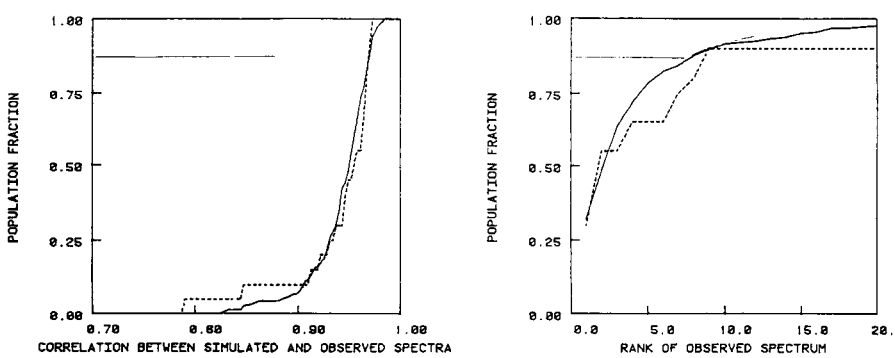

Fig. 4. Cumulative distribution of correlations: (——) training set; (---) prediction set.

Fig. 5. Search results for correlation similarity criterion: (——) training set; (---) prediction set.

The results of the research using the correlation criterion are shown in Fig. 5. This is a cumulation of the rank of the correct observed spectrum according to the criterion. Of the 226 compounds used in the model, 72 or 32% were the best match, 36 were second-best, for a total of first and second rankings of 109 or 48%. A total of 177 (78%) placed among the five best. The results of a search based on the distance criterion were very similar to the search with the correlation criterion. For the 226 compounds in the model, 170 (75%) were among the five most similar; for the twenty withheld compounds, 14 (70%).

The mass spectrum of an organic compound results from many competing reactions. With detailed understanding of the reactions involved, major peaks in the spectrum can be predicted, but not intensities [9]. Using regression analysis of the relationships between the intensities of mass spectral peaks and selected structural characteristics, intensity can be estimated directly, without detailed understanding of the reactions involved. It would be possible, of course, to examine the coefficients of such an equation to attempt to infer general rules about the decomposition mechanisms.

Simulation of mass spectral peak intensities could be of use as a tool in structure elucidation, or as a tool in developing and testing empirical structure fragmentation rules. In both cases, a group of spectra of similar compounds and structural information would be used to develop simulation models for a selected group of peaks.

Simulation can be used to predict true unknowns. Given the observed spectra of a set of similar compounds, either from references or from laboratory work, a model can be developed to predict the spectrum of a hypothetical structure. The spectrum of the unknown can then be compared to the simulated spectrum as well as to the spectra used to form the model, yielding information as to the likelihood that the hypothetical structure was correct. If the simulated spectrum and unknown were more similar than any of the model spectra, this would be evidence confirming the hypothetical structure. In contrast, if the simulated spectrum were grossly dissimilar to the observed spectrum, this would be evidence for rejection of the hypothesis. In intermediate cases, where model spectra and simulated spectrum were all quite similar to the unknown, additional experiments would be indicated.

In routine use, several models could be found, incorporating spectra from structures with features of interest. Separate models could be constructed to predict spectra of compounds with several different functional groups, as well as combinations, if needed. Unknowns could be submitted to appropriate models for comparison.

In developing fragmentation rules, the goal would be to see which structural characteristics enter into the model equations. Presumably, several models would be found for various peaks, using different combinations of structure characteristics. This should be done with some care, for absence of a term from an equation does not necessarily imply that the characteristic does not correlate with the intensity of that peak. It is entirely possible that

a characteristic which correlates highly with a given intensity does not enter the equation. If other characteristics are present which predict observed intensity better than this characteristic, it will not enter the equation.

This research was supported by the National Science Foundation through Grant Number CHE76-83652. The MODCOMP II/25 minicomputer used for this work was purchased with partial financial support of the National Science Foundation.

REFERENCES

1 M. Scholtz, P. Schroder and R. Herzschuh, Int. J. Mass Spectrom. Ion Phys., 21 (1976) 361.
2 H. Budzikiewicz, C. Djerassi and D. H. Williams, Mass Spectrometry of Organic Compounds, Holden—Day, San Francisco, 1967.
3 F. W. McLafferty, Interpretation of Mass Spectra, W. A. Benjamin, New York, 1967.
4 A. B. Delfino and A. Buchs, Helv. Chim. Acta, 55 (1975) 2017.
5 P. C. Jurs and T. L. Isenhour, Chemical Applications of Pattern Recognition, J. Wiley, New York, 1975.
6 G. F. Brissey, R. B. Spencer and C. L. Wilkins, Anal. Chem., 51 (1979) 2295.
7 K. S. Kwok, R. Venkataraghavan and F. W. McLafferty, J. Am. Chem. Soc., 95 (1972) 4185.
8 B. G. Buchanan, D. H. Smith, W. C. White, R. J. Gritter, E. A. Feigenbaum, J. Lederberg and C. Djerassi, J. Am. Chem. Soc., 98 (1975) 6168.
9 N. A. B. Gray, R. E. Carhart, A. Lavanchy, D. H. Smith, T. Jarkony, B. G. Buchanan, W. C. White and L. Creary, Anal. Chem., in press.
10 J. Schechter and P. C. Jurs, Appl. Spectrosc., 27 (1973) 30.
11 J. Schechter and P. C. Jurs, Appl. Spectrosc., 27 (1973) 225.
12 G. S. Zander and P. C. Jurs, Anal. Chem., 47 (1975) 1562.
13 A. J. Stuper and P. C. Jurs, J. Chem. Inf. Comput. Sci., 16 (1976) 99.
14 A. J. Stuper, W. E. Brugger and P. C. Jurs, Computer Assisted Studies of Chemical Structure and Biological Function, Wiley—Interscience, New York, 1979.
15 M. Randić, J. Am. Chem. Soc., 97 (1975) 6609.
16 L. H. Hall, L. B. Kier and W. J. Murray, J. Pharm. Sci., 64 (1975) 1974.
17 W. J. Murray, L. H. Hall and L. B. Kier, J. Pharm. Sci., 64 (1975) 1978.
18 L. B. Kier and L. H. Hall, Molecular Connectivity in Chemical and Drug Research, Academic Press, New York, 1976.
19 N. R. Draper and H. Smith, Applied Regression Analysis, J. Wiley, New York, 1966.
20 G. T. Rasmussen and T. L. Isenhour, J. Chem. Inf. Comput. Sci., 19 (1979) 98.

Analytica Chimica Acta, 132 (1981) 89—97
Elsevier Scientific Publishing Company, Amsterdam — Printed in The Netherlands

ERROR ESTIMATES FOR FACTOR LOADINGS AND SCORES OBTAINED WITH TARGET TRANSFORMATION FACTOR ANALYSIS

BRADLEY A. ROSCOE and PHILIP K. HOPKE*

Institute for Environmental Studies and Nuclear Engineering Program, 1005 W. Western Ave., University of Illinois, Urbana, IL 61801 (U.S.A.)

(Received 11th March 1981)

SUMMARY

Methods of calculating the errors associated with the reproduction of data from the results of target-transformation factor analysis are demonstrated. Errors in the factor loadings and scores are produced by two methods: the jack-knife method, which is time-consuming, and a faster calculation procedure. The agreement shown between the two methods demonstrates the effectiveness of the calculation approach as a quick and simple method of error estimation.

Factor analysis is a multivariate statistical technique [1—3] which attempts to express a data matrix **X** as the product of two cofactor matrices **A** and **F**: **X** = **AF**. The data of the **X** matrix consists of observations of several parameters under different conditions. The columns of the matrix are representative of specific observations for the parameters represented by the rows. It is assumed that the data of **X** are formed by the linear combination of several independent factors. Each factor has its associated set of parameters that distinguish it from other factors. The factors are representative of physically real situations that when put together form the conditions yielding the data of **X**. The **A** matrix is called the loading matrix and contains the parameters representative of the factors contributing to the data matrix **X** while the **F** matrix, called the score matrix, contains the contribution of each factor in **F** to **X**.

The technique can determine the number of causal factors contributing to the data as well as the sources. For this reason, factor analysis has been used in many areas including gas—liquid chromatography [4—6], nuclear magnetic resonances [7—9], source resolution of environmental aerosols [10], and determinations of mineral matter in coal [11—12].

BASIC PRINCIPLES

There is sufficient documentation of the theory and derivation of the factor analysis model in the literature [1—3]; therefore only a brief summary will be presented here. The first step of factor analysis is to determine the

0003—2670/81/0000—0000/$02.50

number of contributing factors to the data. The analysis is begun by forming a matrix **C** which contains the correlation between the observations. After diagonalizing this correlation matrix, eigenvalues and eigenvectors are found which can be used to determine the number of factors present [1, 2, 10]. Abstract factors, **A**, are calculated that reproduce the data; however, the vectors in this matrix will not necessarily have any physical significance. For this reason, target transformation rotations [13, 14] are used to transform the abstract vectors in **A** to vectors in **A'** with physical significance: $\mathbf{A}' = \mathbf{AR}$. As recent studies have shown [15], a minimum of prior knowledge concerning the nature of the **A'** matrix is needed because an iterative approach to the target transformation rotation can yield well defined, physically realistic vectors representing identifiable causal factors in the system being studied. After proper rotations to the **A** matrix, the factor loadings, **F'**, of the physically significant factors can be found and the data can be reproduced: $\mathbf{X} = \mathbf{A}'\mathbf{F}'$.

Error estimates

After the factor analysis solution to a data set is achieved, the error must be calculated. Two methods for the calculation of the uncertainties in the **A** and **F** matrices will be described here: the "jack-knife" method [16, 17], which is time-consuming, and a rapid method described by Clifford [18]. Another method of estimating error has been derived by Malinowski [19]; this yields a root-mean-square error of the factor loadings. The root-mean-square error gives confidence limits in the factor as a whole rather than the individual values in the loading vector. Therefore, no comparisons are made to this method.

The jack-knife method uses multiple determination of **A'** obtained by repeating the complete factor analysis several times with a reduced data set where one observation has been deleted each time. Therefore, to examine all of the possible combinations, the factor analysis must be done one time more than the number of observations in the study. The source profiles of the modified data, A_i', can be determined and used to calculate a better source profile in addition to an error in that profile. This determination is made by first forming a "pseudo value" [17]

$$A_i^* = NA' - (N-1)A_i' \tag{1}$$

where N is the number of observations in the total data set. The mean of the pseudo values will give a better estimate of the source profiles: $\bar{A}_i^* = 1/N \sum A_i^*$. The variance, s^2, of A^* can then be calculated

$$s^2 = [\sum (A_i^*)^2 - (\sum A_i^*)^2/N]/(N(N-1)) \tag{2}$$

The calculation method described by Clifford [18] relies on the error obtained from comparing the reproduced data to the raw data. The derivation is summarized here.

The formulation of the variance-covariance matrix of **X** in the equation $\mathbf{X} = \mathbf{AF}$ is considered. If dx_i is the ith column of **X** and $\bar{x}$ contains the means

of each row, then the variance-covariance matrix of X can be formed by

$$\mathbf{M}_{x,i} = (1/N) \sum d\mathbf{x}_i d\mathbf{x}_i^t \tag{3}$$

where $d\mathbf{x}_i = \mathbf{x}_i - \bar{\mathbf{X}}$. For a least-squares solution to the equation $\mathbf{X} = \mathbf{AF}$, a weight matrix, W, which is inversely proportional to $\mathbf{M}_x$ is used

$$\mathbf{W} = \sigma^2 \mathbf{M}_x^{-1} \tag{4}$$

After the equation $\mathbf{X} = \mathbf{AF}$ has been solved by using the weight matrix W, a variance-covariance matrix for F can be formulated

$$\mathbf{M}_{f,i} = (1/N) \sum d\mathbf{f}_i d\mathbf{f}_i^t \tag{5}$$

where $d\mathbf{f}_i = \mathbf{f}_i - \bar{\mathbf{f}}$ for $\bar{\mathbf{f}}$ containing the means of the rows in F. Because f, and so df, were formed by the principle of least-squares

$$d\mathbf{f}_i = (\mathbf{A}^t\mathbf{W}\mathbf{A})^{-1}\mathbf{A}^t\mathbf{W}d\mathbf{x}_i \tag{6}$$

Substitution of Eqn. (6) into Eqn. (5), and recognition that $(\mathbf{A}^t\mathbf{W}\mathbf{A})$ is symmetric, yields

$$M_f = (1/N)\sum (\mathbf{A}^t\mathbf{W}\mathbf{A})^{-1}\mathbf{A}^t\mathbf{W}d\mathbf{x}_i d\mathbf{x}_i^t\mathbf{W}\mathbf{A}(\mathbf{A}^t\mathbf{W}\mathbf{A})^{-1} = (\mathbf{A}^t\mathbf{W}\mathbf{A})^{-1}\mathbf{A}^t\mathbf{W}M_x\mathbf{W}\mathbf{A}(\mathbf{A}^t\mathbf{W}\mathbf{A})^{-1} \tag{7}$$

Substitution of Eqn. (4) into Eqn. (7) produces a new representation for the variance-covariance matrix of F

$$M_f = \sigma^2(\mathbf{A}^t\mathbf{W}\mathbf{A})^{-1} \tag{8}$$

Therefore, the variance in the f_i terms can be represented by the product of the total variance and the diagonal of $(\mathbf{A}^t\mathbf{W}\mathbf{A})$.

To determine the total variance of the analysis, it is assumed that the original data matrix X has been reproduced to form a matrix X'. An error vector can then be formed from a column of the original and reproduced data, x_i and x_i', respectively

$$\mathbf{e}_i = \mathbf{x}_i - \mathbf{x}_i' = \mathbf{x}_i - \mathbf{A}\mathbf{f}_i = d\mathbf{x}_i - \mathbf{A}d\mathbf{f}_i \tag{9}$$

The weighted sum of the squares of the differences between the original and reproduced data can be represented by $s_i = \mathbf{e}_i^t\mathbf{W}\mathbf{e}_i$, which with Eqn. (9), yields

$$s_i = (d\mathbf{x}_i - \mathbf{A}d\mathbf{f}_i)^t\mathbf{W}d\mathbf{x}_i - (d\mathbf{x}_i - \mathbf{A}d\mathbf{f}_i)^t\mathbf{W}\mathbf{A}d\mathbf{f}_i \tag{10}$$

To determine the nature of the second term of Eqn. (10), both sides of Eqn. (6) are multiplied by $(\mathbf{A}^t\mathbf{W}\mathbf{A})$ to give

$$(\mathbf{A}^t\mathbf{W}\mathbf{A})d\mathbf{f}_i = \mathbf{A}^t\mathbf{W}d\mathbf{x}_i \tag{11}$$

Transposition of this equation, with recognition that the weight matrix W is symmetric, yields $d\mathbf{f}_i^t\mathbf{A}^t\mathbf{W}\mathbf{A} = d\mathbf{x}_i^t\mathbf{W}\mathbf{A}$. Several manipulations of this equation produce $(d\mathbf{x}_i - \mathbf{A}d\mathbf{f}_i)^t\mathbf{W}\mathbf{A} = 0$, which shows that the second term of Eqn. (10) is zero. Thus, Eqn. (6) becomes

$$s_i = (d\mathbf{x}_i - \mathbf{A}d\mathbf{f}_i)^t\mathbf{W}d\mathbf{x}_i = d\mathbf{x}_i^t\mathbf{W}d\mathbf{x}_i - d\mathbf{f}_i^t\mathbf{A}^t\mathbf{W}d\mathbf{x}_i \tag{12}$$

Substituting Eqn. (11) into Eqn. (12) yields

$$s_i = dx_i^t \mathbf{W} dx_i - df_i^t (\mathbf{A}^t \mathbf{W} \mathbf{A}) df_i = Tr(dx_i dx_i^t \mathbf{W}) - Tr(df_i df_i^t (\mathbf{A}^t \mathbf{W} \mathbf{A})) \quad (13)$$

For N observations, i.e., columns of $\mathbf{X}$, a mean value of s_i can be obtained

$$\bar{s} = (1/N) \sum (Tr(dx_i dx_i^t \mathbf{W}) - Tr(df_i df_i^t (\mathbf{A}^t \mathbf{W} \mathbf{A})) \quad (14)$$

Substitution of Eqns. (3) and (5) into Eqn. (14) yields

$$\bar{s} = Tr(\mathbf{M}_x \mathbf{W}) - Tr(\mathbf{M}_f (\mathbf{A}^t \mathbf{W} \mathbf{A})) \quad (15)$$

Multiplying both sides of Eqn. (4) by $\mathbf{M}_x$ and substituting that into Eqn. (15) produces a simplified expression for $\bar{s}$

$$\bar{s} = \sigma^2 Tr(\mathbf{I}_N) - \sigma^2 Tr(\mathbf{I}_p) = \sigma^2 (N - p) \quad (16)$$

where p is the number of rows in $\mathbf{F}$. Thus, an expression for determining the total variance in the reproduction of the data of the equation $\mathbf{X} = \mathbf{AF}$ has been established.

The derivation shows how errors in the $\mathbf{F}$ cofactor matrix may be estimated by comparing the original and reproduced data. This comparison produces the total variance of the data reproduced. The total variance can then be apportioned by multiplying it by the diagonal terms of a simple matrix, $(\mathbf{A}^t \mathbf{W} \mathbf{A})^{-1}$. The errors in the $\mathbf{A}$ cofactor matrix may also be determined by a similar procedure. This is done by initially taking the transpose of the equation $\mathbf{X} = \mathbf{AF}$ and then following the same procedure.

DATA

A comparative study was performed to ascertain the relative merits of each method of error estimation. Two data sets which had been previously source-resolved, were used. The first set consisted of data from a gas—liquid chromatography study done by Weiner et al. [6] and the second set is from a geological study by Bowman et al. [20]. For each data set, comparisons are shown between the results obtained by linear regression analysis and those obtained by factor analysis based on the jack-knife and calculation methods described above.

The data set generated by Weiner et al. [6] is a carefully taken set of solute retention volumes of gas—liquid chromatography on well-characterized columns. Ideally, the solute retention volume is a function of a single mechanism, but for many systems, it is a function of several independent mechanisms. Weiner et al. attempted to distinguish the difference between surface and volume effects on the retention volumes. The effects should add linearly and fit the form of $\mathbf{X} = \mathbf{AF}$.

The other set of data is from a comparative study of samples taken from Borax Lake, California, where a lava flow had occurred. The lava flowed from two different locations and later mixed, yielding a mixture of two previously homogeneous phases. These phases formed a dyke of obsidian and dacite

material. Bowman et al. [20] sampled at various spots and analyzed these samples for 29 elements by neutron activation analysis. They were able to reconstruct the mineralogy of these samples by the use of linear relationships and two assumptions. The first assumption was that there were two mineral phases present in the samples; this made it valid to construct linear functions of elemental concentrations relative to iron concentration by using the least-squares method. The characteristics of these relations made it viable to assume an iron concentration for each mineral phase, so that the elemental concentration profiles of the mineral phases could be calculated [20].

For the factor analysis of these data sets, a computer program called FANTASIA [21] was utilized. FANTASIA was originally developed for source resolution studies on aerosol samples, but can be used for any factor analysis problem. The program uses the correlation about the origin as described by Hopke et al. [1] to form the correlation matrix for the analysis. By use of the proper coding of a control card, the user can select specific options of FANTASIA such as uniqueness tests for elements, source profile iterations, weighting of data, and weighting of the least-squares rotation.

RESULTS

Values obtained by linear regression are compared with those obtained by the jack-knife and calculation methods. Because the linear regression values are based on fitting the data variable by variable rather than all the variables simultaneously, i.e., the covariances of the variables are ignored, the error estimates are lower than by either the jack-knife or the calculation approach. However, the linear regression results are informative by demonstrating trends in the final results by a different approach and are useful for comparisons.

The results obtained with the solute retention study are summarized in Table 1. Values obtained with the jack-knife method and linear regressions by Weiner et al. [6] are reported with the values obtained by factor analysis and the calculated errors as described in this work. In interpretation of these results, it should be noted that there are only three degrees of freedom in this data set of five observations and two factors; thus, the ability of any of the methods to estimate the error properly is limited. However, as can be seen by the results, even with only three degrees of freedom, both the calculation and jack-knife methods produce results that overlap. In addition, these results compare favorably with those obtained by linear regression.

The geological data set was more suited for the study of error estimation techniques since there were 13 degrees of freedom in the data and better agreement in the results was obtained. The results obtained for the elemental profiles of the mineral phases with the jack-knife and calculation methods of error estimation are compared to those obtained from linear regression in Table 2. Again, the results obtained by both the jack-knife and calculation techniques overlap and are in favorable agreement with the results from

TABLE 1

Factor loadings and their associated error for the gas—liquid chromatography solute retention study

Solute	Adsorption constant ($\times 10^{-5}$)		
	Calculation method	Jack-knife method	Linear regression
Carbon tetrachloride	5.18 ± 0.09	5.11 ± 0.11	5.27 ± 0.05
Dichloromethane	4.42 ± 0.15	4.32 ± 0.17	4.50 ± 0.04
Chloroform	12.4 ± 0.6	12.06 ± 0.11	13.56 ± 0.10
Benzene	27.7 ± 0.3	27.48 ± 0.28	27.73 ± 0.19
Toluene	34.2 ± 0.1	34.19 ± 0.10	34.35 ± 0.25
n-Hexane	7.89 ± 0.11	7.83 ± 0.12	7.87 ± 0.07
Cyclohexane	10.6 ± 0.2	10.56 ± 0.22	10.69 ± 0.08
n-Heptane	31.0 ± 0.3	30.94 ± 0.25	30.99 ± 0.15
2-Methylheptane	26.2 ± 0.2	26.06 ± 0.21	26.12 ± 0.13
n-Octane	75.4 ± 1.6	76.90 ± 0.58	76.98 ± 0.34
Solute	Partition constant		
	Calculational method	Jack-knife method	Linear regression
Carbon tetrachloride	0.04 ± 0.55	0.40 ± 0.62	
Dichloromethane	0.12 ± 0.90	0.83 ± 1.33	
Chloroform	3.2 ± 3.9	4.41 ± 4.40	
Benzene	0.0 ± 1.9	1.14 ± 2.43	
Toluene	1.29 ± 0.64	1.23 ± 0.86	
n-Hexane	2.96 ± 0.65	3.40 ± 0.79	3.14 ± 0.47
Cyclohexane	25.2 ± 1.2	25.51 ± 1.67	24.39 ± 0.57
n-Heptane	19.8 ± 1.5	20.37 ± 1.17	20.19 ± 1.05
2-Methylheptane	16.2 ± 1.4	16.80 ± 1.08	16.49 ± 0.90
n-Octane	24.8 ± 9.9	21.44 ± 2.46	21.27 ± 2.40

linear regression. As the calculation method is both quicker and easier to use than the jack-knife method, it has an inherent advantage.

A characteristic of both error techniques is that the error for the entire analysis is assumed to be resident in the parameters for which the errors are calculated. For this reason, both techniques yield over-estimates of the actual error. As a next step, errors for the factor scores were calculated by using the jack-knife and calculation methods. Again, all of the error in the analysis was assumed to be resident in the factor scores. Table 3 contains a summary of these factor scores and their associated error obtained in this study.

When the original data and its errors are reconstructed from the cofactor matrices reported in Tables 2 and 3, the errors are larger than those of the original data. Since the error estimates for the cofactor matrices are over-estimates, this is to be expected.

TABLE 2

Comparison of source mineral profiles and their associated errors for the Borax Lake geological data

	Mineral phase A			Mineral phase B		
	Calculation method	Jack-knife method	Linear[a] regression	Calculation method	Jack-knife method	Linear[a] regression
Th	17.9 ± 0.3	17.9 ± 0.1	17.6 ± 0.1	1.8 ± 0.9	1.4 ± 0.6	2.5 ± 0.3
Sm	5.85 ± 0.06	5.86 ± 0.04	5.85 ± 0.03	4.61 ± 0.18	4.56 ± 0.11	4.60 ± 0.11
U	6.74 ± 0.09	6.75 ± 0.05	6.70 ± 0.04	0.55 ± 0.28	0.37 ± 0.23	0.72 ± 0.14
Na	27700 ± 300	27700 ± 200	27600 ± 200	24600 ± 1000	24400 ± 900	24300 ± 600
Sc	4.48 ± 0.26	4.48 ± 0.04	4.76 ± 0.06	38.9 ± 0.9	39.8 ± 0.9	37.5 ± 0.2
Mn	122 ± 10	122 ± 3	134 ± 3	1410 ± 40	1450 ± 60	1369 ± 10
Cs	16.1 ± 0.2	16.1 ± 0.2	15.9 ± 0.1	0.00 ± 0.66	0.42 ± 0.43	0.5 ± 0.4
La	23.0 ± 0.4	23.0 ± 0.2	22.7 ± 0.3	12.5 ± 1.3	11.9 ± 1.2	12.5 ± 1.0
Fe	6060 ± 550	6050 ± 100	6700	80000 ± 1800	81900 ± 2100	77000
Al	65000 ± 600	65100 ± 600	65000 ± 640	84300 ± 1800	84800 ± 1800	84000 ± 2100
Dy	7.72 ± 0.14	7.73 ± 0.17	7.80 ± 0.20	7.39 ± 0.47	7.30 ± 0.39	7.10 ± 0.65
Hf	3.80 ± 0.05	3.81 ± 0.04	3.80 ± 0.05	3.19 ± 0.16	3.15 ± 0.17	3.20 ± 0.16
Ba	87.2 ± 8.9	87.2 ± 10.0	86 ± 11[b]	130 ± 30	140 ± 30	140 ± 37[b]
Rb	250 ± 7	250 ± 7	245 ± 8	6 ± 22	0 ± 12	27 ± 26
Ce	53.4 ± 0.8	53.5 ± 0.4	52.8 ± 0.5	27.2 ± 2.4	26.2 ± 2.2	27.6 ± 1.6
Lu	0.522 ± 0.008	0.523 ± 0.006	0.52 ± 0.007	0.419 ± 0.024	0.416 ± 0.023	0.43 ± 0.022
Nd	26.9 ± 0.6	26.9 ± 0.4	25.6 ± 0.5	15.3 ± 1.8	15.1 ± 1.6	18.0 ± 1.6
Yb	4.08 ± 0.07	4.09 ± 0.06	4.00 ± 0.06	2.69 ± 0.23	2.65 ± 0.17	2.07 ± 0.20
Tb	1.06 ± 0.01	1.06 ± 0.01	1.05 ± 0.01	0.795 ± 0.031	0.791 ± 0.024	0.810 ± 0.036
Ta	1.18 ± 0.03	1.18 ± 0.03	1.18 ± 0.03	0.49 ± 0.10	0.47 ± 0.08	0.52 ± 0.10
Eu	0.0905 ± 0.0116	0.0900 ± 0.0058	0.100 ± 0.007	1.63 ± 0.04	1.67 ± 0.06	1.60 ± 0.03
K	46400 ± 800	46400 ± 1100	46000 ± 1400	2600 ± 2500	2100 ± 4500	8000 ± 4800
Sb	1.13 ± 0.06	1.13 ± 0.06	1.10 ± 0.08	0.20 ± 0.20	0.16 ± 0.11	0.30 ± 0.25
Zn	42.8 ± 2.0	42.8 ± 1.7	45.0 ± 1.9	118 ± 7	120 ± 9	114 ± 6
Cr	8.0 ± 1.7	7.93 ± 0.78	9.40 ± 0.94	186 ± 6	190 ± 6	178 ± 3
Ti	240 ± 100	236 ± 30	300 ± 55	9360 ± 330	9570 ± 300	9000 ± 180
Co	0.00 ± 0.31	0.0010 ± 0.00358	0.40 ± 0.10	41.6 ± 1.1	42.6 ± 1.1	39.6 ± 0.3
Ca	9510 ± 770	9490 ± 810	10400 ± 1500	78700 ± 2600	80400 ± 4200	75000 ± 4900
V	7.0 ± 5.0	6.4 ± 4.2	9 ± 6	301 ± 17	313 ± 31	300 ± 21

[a]Errors in the linear regression coefficients were not reported in the original work [20]. Errors reported here were produced from the data by the authors. It should be noted that all parameters were found by a regression comparing elemental concentrations to those assumed for iron in the two phases. [b]Values for barium were not reported in the original work, but were constructed here by the authors.

TABLE 3

Mineral phase contributions and their associated errors for the Borax Lake geological data

Sample	Mineral phase A		Mineral phase B		Sum of phases	
	Calculation method	Jack-knife method	Calculation method	Jack-knife method	Calculation method	Jack-knife method
1	81.1 ± 0.9	81.1 ± 0.8	16.8 ± 0.3	16.5 ± 0.6	97.9 ± 1.1	97.6 ± 1.4
2	86.7 ± 1.3	87.1 ± 0.8	15.1 ± 0.4	14.9 ± 0.5	101.8 ± 1.7	102.0 ± 1.3
3	91.5 ± 0.9	91.9 ± 0.8	11.5 ± 0.3	11.2 ± 0.4	103.1 ± 1.2	103.1 ± 1.3
4	91.1 ± 1.2	91.0 ± 0.9	7.02 ± 0.37	6.75 ± 0.42	98.1 ± 1.6	97.8 ± 1.3
5	91.0 ± 1.2	91.0 ± 1.0	9.12 ± 0.35	9.06 ± 0.50	100.1 ± 1.5	100.0 ± 1.5
6	95.4 ± 1.0	95.7 ± 1.0	7.32 ± 0.28	7.22 ± 0.51	102.7 ± 1.2	102.9 ± 1.5
7	96.6 ± 0.9	96.7 ± 1.1	3.62 ± 0.27	3.39 ± 0.50	100.2 ± 1.2	100.1 ± 1.6
8	92.9 ± 0.6	92.7 ± 1.0	4.63 ± 0.17	4.56 ± 0.54	97.5 ± 0.8	97.2 ± 1.6
9	95.2 ± 0.5	94.9 ± 1.0	2.51 ± 0.14	2.51 ± 0.56	97.7 ± 0.6	97.4 ± 1.6
10	102.6 ± 0.8	103.3 ± 1.0	0.0 ± 0.23	0.0 ± 0.52	102.6 ± 1.0	103.3 ± 1.5
11	44.8 ± 1.8	46.6 ± 2.0	56.5 ± 0.5	55.3 ± 1.8	101.4 ± 2.3	101.2 ± 3.8
12	50.0 ± 2.1	49.6 ± 1.2	49.5 ± 0.6	49.4 ± 1.0	99.5 ± 2.8	99.1 ± 2.2
13	61.1 ± 1.4	62.4 ± 1.3	39.4 ± 0.4	38.2 ± 1.1	100.5 ± 1.8	100.5 ± 2.4
14	68.5 ± 1.5	69.3 ± 1.0	30.1 ± 0.4	29.0 ± 0.7	98.6 ± 2.0	98.2 ± 1.7
15	76.4 ± 2.5	76.4 ± 0.7	21.4 ± 0.7	21.2 ± 0.5	97.8 ± 3.2	97.5 ± 1.3

Conclusions

The calculation method of error estimation for the results of factor analysis has been demonstrated to yield error bars consistent with those obtained by the jack-knife method for the two data sets studied. However, two data sets do not provide conclusive results on the ability of either method to estimate errors, but only show that the two methods yield consistent results for the data studied. Both methods will give better estimates of error with more degrees of freedom in the data, but, more degrees of freedom cause the jack-knife method to become more cumbersome while they do not affect the difficulty of the calculation method. The ease and speed of the procedure make it an attractive alternative to the jack-knife method.

This work was supported in part by the Department of Energy, contract number DE-AC02-80EV10403.

REFERENCES

1 P. K. Hopke, R. E. Lamb and D. F. S. Natusch, Environ. Sci. Technol., 14 (1980) 164.
2 E. R. Malinowski and D. G. Howery, Factor Analysis in Chemistry, J. Wiley, New York, 1980.
3 H. H. Harmon, Modern Factor Analysis, University of Chicago Press, Chicago, IL, 1976.
4 R. B. Selzer and D. G. Howery, J. Chromatogr., 115 (1975) 139.
5 S. Wold and K. Anderson, J. Chromatogr., 80 (1973) 43.
6 P. H. Weiner, H. L. Liao and B. L. Karger, Anal. Chem., 46 (1974) 2182.
7 P. H. Weiner, E. R. Malinowski and A. R. Levinston, J. Phys. Chem., 74 (1970) 4537.
8 P. H. Weiner and E. R. Malinowski, J. Phys. Chem., 75 (1971) 1207.
9 P. H. Weiner and E. R. Malinowski, J. Phys. Chem., 75 (1971) 3160.
10 D. J. Alpert and P. K. Hopke, Atmos. Environ., 14 (1980) 1137.

11 B. A. Roscoe and P. K. Hopke, Fourth International Conference on Nuclear Methods in Environmental and Energy Research, Columbia, MO, April 1980.
12 B. A. Roscoe and P. K. Hopke, ANS-ACS Topical Meeting on Atomic and Nuclear Methods in Fossil Energy Research, Mayaguez, Puerto Rico, December 1980.
13 E. R. Malinowski and M. McCue, Anal. Chem., 49 (1977) 284.
14 R. Heindryckx and R. Dams, J. Radioanal. Chem., 19 (1974) 339.
15 B. A. Roscoe and P. K. Hopke, Comput. Chem., 5 (1981) 1.
16 F. Mosteller, Rev. Int. Statist. Inst., 39 (1971) 363.
17 F. Mosteller and J. Tuckey, Data Analysis and Regression, Addison—Wesley, Reading, PA, 1977.
18 A. A. Clifford, Multivariate Error Analysis, Applied Science, London, 1973.
19 E. R. Malinowski, Anal. Chim. Acta, 122 (1980) 327.
20 H. R. Bowman, F. Asaro and I. Perlman, J. Geol., 81 (1973) 312.
21 D. J. Alpert, B. A. Roscoe and P. K. Hopke, FANTASIA: Factor Analysis to Apportion Sources in Aerosols, A Computer Code, IES Staff Paper No. 11, Institute for Environmental Studies, University of Illinois, 1980.

Analytica Chimica Acta, 132 (1981) 99—110
Elsevier Scientific Publishing Company, Amsterdam — Printed in The Netherlands

THE SPECTRAL DETECTABILITY OF FLUORINE IN A HELIUM GLOW DISCHARGE

CYRUS FELDMAN

Analytical Chemistry Division, Oak Ridge National Laboratory, Oak Ridge, TN 37830 (U.S.A.)

(Received 15th May 1981)

SUMMARY

The theoretical basis of the excitation of the fluorine emission spectrum is discussed, and the negative effects of easily excited impurities are demonstrated. Fluorine can be detected by means of its emission spectrum if it is present as a minor impurity in helium. The amount of water vapor and/or organic compounds in the helium must be minimized because these substances produce easily excited fragments in the glow discharge which dissipate the energy needed to excite fluorine atoms. Direct excitation of a diphenyldifluorosilane residue permits detection of about 70 pg of fluorine; if fluorine is volatilized as hydrofluoric acid and injected directly into the glow discharge, a photocurrent peak of 1.8 A g^{-1} of fluorine is obtained.

The aim of this study is to lay the theoretical and experimental groundwork for a spectral method for quantifying inorganic fluoride. A discussion of spectral excitation parameters that affect detection of fluorine is followed by a description of experiments aimed at the detection of inorganic fluoride in a helium glow discharge.

The spectral detection of fluorine has usually been accomplished by observing the spectrum of an isolated diatomic free radical or molecule containing fluorine, such as CaF, SrF, BaF, AlF or AgF. This situation results from the scarcity of spectral alternatives, and from the basic facts of fluorine chemistry. The vapor required for using the fluoride band emission method has usually been generated by evaporating a mineral residue from a crater in a carbon electrode into a d.c. arc. Despite the complicated plasma chemistry involved, and the frequent partial overlapping of the fluoride bands by other bands, detection limits of 100—200 ppm fluorine can be achieved with a relative standard deviation of ±15% [1]. If the fluorine exists in one or more components of a mixture of volatile organic compounds, moderate heat will produce a vapor with an absorption spectrum that is not likely to give any unequivocal evidence of the presence of fluorine, except for cases in which specific fluorocarbons are sought and their absorption spectra are known. Pyrolysis of less volatile fluorine compounds will produce hydrogen fluoride and/or other fluorine-bearing fragments difficult to manipulate and identify.

In view of the above discussion, it would seem logical to look for other pathways for quantifying the total fluorine content of a sample, such as decomposing all fluorine compounds completely and measuring the quantity of neutral or ionized fluorine atoms produced. Such atoms must surely result, for instance, when an arc discharge dissociates CaF_2 vapor into the CaF and Ca^0 that have been observed in such discharges. Yet neither neutral nor ionized fluorine atoms have been observed in such discharges by either emission or absorption. This does not necessarily indicate that fluorine atoms do not exist in these plasmas, but merely that they have not yet been observed by the available emission or absorption techniques. Their "invisibility" is traceable to the very high excitation potentials (e.p.) of both the resonance lines (95.187, 95.483, 95.555 and 95.882 nm; e.p. 12.9—13.0 eV) and the more easily accessible fluorine lines such as 685.602 nm (e.p. 14.4 eV) of the neutral isolated fluorine atom [2, 3].

The resonance lines lie in a wavelength region for which there are no sturdy window materials [4]. To use these lines in either emission or absorption, it would thus be necessary to place the light source, sample and detector (all windowless) within a single enclosure that is evacuated or filled with a non-absorbing gas. This would be inconvenient for practical work.

Non-resonance transitions in the fluorine atom (i.e., transitions between two high-lying, or excited, levels) are less intense than resonance transitions, but are more likely to be observable. To utilize these transitions in absorption, it is necessary to supply the rather intense excitation needed to raise fluorine atoms to the initial $3s\ 4P$ level (12.6 eV) without also completely filling the intended final level (i.e., the $3s\ 4P^0$ or $3s\ 4D^0$ level). The absorption transitions might then be observed by illuminating the excited plasma with a visible-range continuum or an appropriately tuned laser.

Observing the same transitions by emission would be considerably easier; though the excitation required for emission ($\approx$14.4 eV) would be even greater than that required for absorption (12.6 eV), the emission transition would be spontaneous and easy to observe. The high degree of excitation needed for either type of observation cannot be obtained in a flame. The discussion will therefore be restricted to electrical discharges, in which the fluorine-bearing compound is a minor impurity in a carrier gas.

A fluorine compound in the vapor state is partially or completely disintegrated when it enters an electrical discharge. Some of the resulting fluorine-containing fragments then gain or lose electrons to become fluorine atoms. The gas usually chosen to excite the fluorine 685.602 nm (e.p. 14.4 eV) in an electrical discharge is helium, because its lowest excited level is 19.3 eV and it has no intermediate levels to siphon off energy, once the energy has been supplied at this level. However, such siphoning may still occur if easily-excited impurities are present (e.g., molecular gases, free radicals, argon, sample vapors). This may be the reason for the relatively poor efficiency of the inductively coupled plasma (i.c.p.) in exciting this line, since the i.c.p. is an argon discharge (see below).

It is thus necessary to remove the greatest possible number of easily excited species from the discharge to prevent the highly-excited helium atoms from dissipating their energy on species other than fluorine. In practice, this means that the fluorine-bearing species should be isolated before one attempts to excite the fluorine spectrum. Gas chromatography is one way of doing this for organofluorine compounds. For inorganics, it was thought that other pathways might exist.

The conditions existing in the helium effluent from a gas chromatograph are almost ideal for the spectral detection of fluorine. As a result, microwaves [5, 6], inductively-coupled ultra-high frequency (27.12 MHz) energy [7] and the glow discharge [8, 9] have all been used successfully to excite fluorine in such effluents. The detection limits obtained [5, 6] (60 and 8.5 pg F s^{-1}, respectively) are at best comparable to the limit obtained with the glow discharge (11 pg F s^{-1}) [8]. A recent i.c.p. investigation [7] succeeded in detecting fluorine for the first time in such a discharge, but the limit of detection calculated from the data published was about 39,000 pg F s^{-1}.

In the experience of the author, operation of a microwave discharge tends to produce devitrification and coating of the capillary, even when a Beenacker cavity is used in helium at atmospheric pressure [6]. Some authors believe that fluorine species react with the capillary walls of a microwave discharge [5, 10]; in one case [10] this reaction suppressed the fluorine spectrum completely.

Neither the microwave nor the glow discharge has yet been applied to determining inorganic fluorine in solution. The above-mentioned i.c.p. study [7] refers to fluorine added to the gas stream as SF_6; no work with solutions was done in that investigation.

Since the glow discharge offers the advantages, vis-à-vis the microwave discharge, of greater simplicity and freedom from coating, etching and devitrification problems, it was chosen for further study.

EXPERIMENTAL

One glow chamber used in this investigation (the well-type chamber) is shown in Fig. 1. The characteristics of similar chambers have been discussed previously [8, 9]. Removal of the helium inlet tube from this chamber permits the deposition of small quantities of liquid on the bottom of the well. When the inlet tube is replaced and the glow initiated, any vapor arising from the liquid is carried into the discharge. The discharge is viewed through a side-arm, the end-window of which appears in Fig. 1 as a circle. A similar side-arm extends on the side away from the viewer. The cathode assembly in place in the chamber is shown in Fig. 1. The electrode itself is a 3.5 in. (8.9 cm) × 0.060 in. (2.36 mm) diameter tungsten welding rod, the upper end of which fits tightly into a recess in an 0.080 in. (3.15 mm) o.d. × 0.75 in. (29.5 mm) platinum cap. The end surface of the cathode cap is

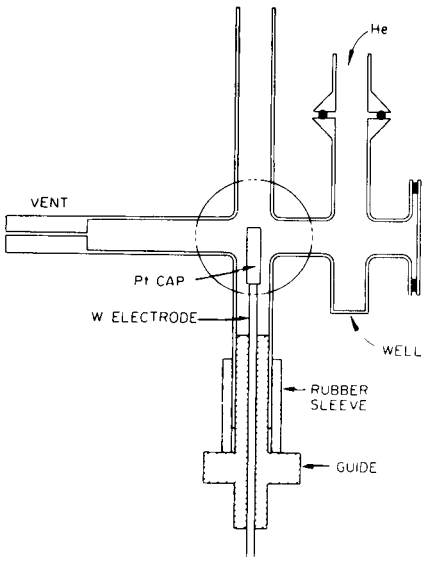

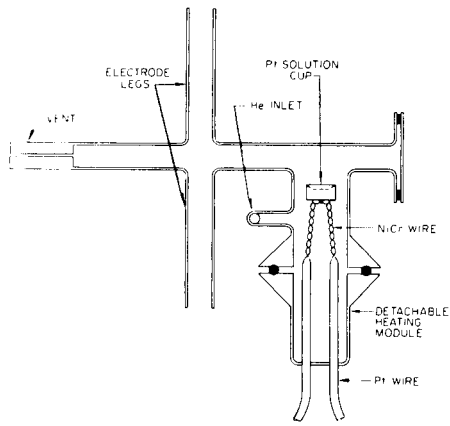

Fig. 1. Well-type glow chamber. Side view (vertical section through optic axis), showing cathode assembly supported in place in lower electrode leg.

Fig. 2. Electrothermal evaporator chamber. Side view (vertical section through optical axis) showing electrothermal evaporation module in place.

flat, as shown; the end surface of the anode is conical. The anode assembly is otherwise similar to the cathode assembly, but has been omitted from Fig. 1 for clarity. Each electrode is held by a stainless-steel guide which centers it in the electrode leg of the chamber. The guide is held in place in this leg by means of a tight-fitting heat-resistant rubber sleeve. In the electrothermal evaporation chamber (Fig. 2), the sample well is replaced by a detachable evaporator module. The sample solution is deposited in a shallow depression in the top surface of a small block of platinum (4 × 6 × 3 mm high). The bottom surface of this block is welded to the center of an inverted U formed by a twisted pair of 0.0253 in. (2.00 mm) diameter nichrome wires. The ends of the U are welded to two 0.080 in. (3.15 mm) diameter platinum wires that project through the bottom of a cup formed from a No. 9 (9 mm i.d.) pyrex O-ring flange. In use, the heater dissipates 86 W (2.15 V, 40 A, 0.05375Ω). The discharge operates very slightly above atmospheric pressure.

The glow discharge electrodes used with the evaporation chamber are the same as those used with the well-type chamber. The electrode gap is 3 mm; its exact value is not critical.

The power supply for the glow discharge and, unless otherwise noted, the optical arrangement of the monochromator and the oscillating refractor plate spectral background correction system are those described earlier [9].

In a few cases, the background correction was made by a static two-detector system [8].

The power supply for the electrochemical evaporator consists of a combination of step-down transformers and an autotransformer capable of driving 50 A through the evaporator at about 2.7 V a.c.

RESULTS AND DISCUSSION

Measurement of the spectroscopic properties of fluorine

The intensity of any fluorine line in an electrical discharge depends on the concentration of the fluorine-bearing species in the gas phase, and on several other factors. In order to study the effects of these other factors, it is necessary to keep the gas phase concentration constant in time and space. This was most conveniently done by using specially prepared mixtures of 0.0013 and 0.0250 mol % difluorodichloromethane in helium. The use of platinum caps on the electrodes prevented chemical attack of the electrodes by the degradation products of the difluorodichloromethane. Except as noted, all observations were made on the fluorine line at 685.602 nm.

Distribution of F 685.602-nm emission intensity in the glow discharge

A 10× magnified image of the discharge was focused on the 50 × 50 mm entrance aperture, so that the signal produced by the detector represented a 5 × 5 mm area in the discharge itself. Moving the discharge vertically with respect to the rest of the system thus made it possible to measure the light emitted by different portions of the discharge.

Experiments of this type showed that most of the F 685.602-nm radiation originated at the cathode and extended 2—4 mm down its side, depending on the current. Imaging this area on the entrance aperture gave a light signal 3.7 times as intense as that obtained from an equal area in the inter-electrode gap. This showed that, as expected, the difficult task of exciting atoms to the 14.4 eV level is performed most efficiently near the cathode, where both the electron density and the potential gradient (i.e., electron-accelerating ability) are highest.

The work described below was therefore done using light only from the cathode glow layer and the adjacent 0.5-mm portion of the electrode gap.

Effect of foreign substances on the intensity of the F 685.602-nm line

As noted above, easily excited impurities would be expected to reduce the intensity of this emission line. Two common impurities were selected for study, namely water vapor and di-isopropyl ether.

The effects of water vapor were studied by observing the intensity of the 685.602-nm line as the concentration of water vapor in the gas stream was gradually reduced. The intensity of the OH band at 306.4 nm was taken as an indication of the relative amount of water vapor present although all of the oxygen and hydrogen atoms that comprise the OH radical in a given

discharge do not necessarily come from H_2O molecules if other H-bearing and/or O-bearing molecules are present. However, because preliminary trials showed that introducing desiccants into the gas stream reduced the intensity of the OH band, it seemed reasonable to infer that the reduction was due to the removal of water vapor.

The experiment was performed by passing a stream of 0.0250% difluorodichloromethane in helium through molecular sieve 5A and anhydrone ($Mg(ClO_4)_2 \cdot 1.48\ H_2O$) traps immediately upstream from the well-type glow chamber (Fig. 1). The intensities of the OH 306.4-nm band and F 685.602-nm line were measured alternately over a period of 4 h (see Fig. 3). The intensity of OH 306.4-nm band decreased steadily over that period, presumably because of the gradual decrease in the concentration of water vapor. The intensity of the F 685.602-nm line rose slowly over most of this period, but when the intensity of the OH band decreased to about 20% of its original value, the intensity of the fluorine line increased sharply. The final vapor pressure of the water was not determined, but could have been no lower than 8×10^{-11} g mol cm^{-3}, which is its steady-state value under these conditions [11]. The implication of this behavior for fluorine detection was clear; water vapor must be eliminated as completely as possible if optimum sensitivity for the spectral detection of fluorine is desired.

The effect of organic vapors on the intensity of the F 685.602-nm line was tested in a different kind of experiment. In this case, again using the well-type chamber (Fig. 1), the normal intensity level of the fluorine line

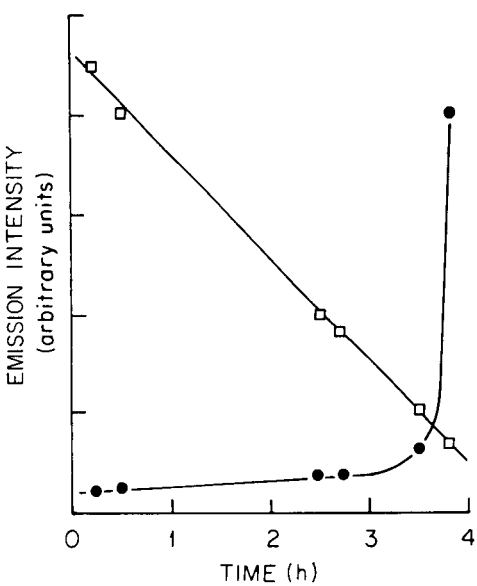

Fig. 3. Intensity of emission for fluorine and OH in the same helium glow discharge as a function of time. (□) OH 306.4-nm band; (•) F 685.602-nm line.

was first established in a 40 cm^3 min^{-1} stream of a 0.0250% CCl_2F_2—He mixture (Fig. 4). The discharge was then turned off, the helium inlet tube was removed, and 1 μl of di-isopropyl ether (b.p. 62°C) was deposited on the floor of the sample well. The sample well was cooled by a water bath kept at 3°C. The helium inlet was then replaced and the glow discharge was ignited (Fig. 4A). For the first 45 s, the intensity of the fluorine line was quite low (about 6% of its normal value); during the same period, the discharge was intensely blue-green, presumably because of the Swan system of C_2 bands. As this color disappeared, the intensity of the fluorine line rose, but to only about 68% of its original value. The experiment was repeated, using a 2-μl sample of di-isopropyl ether (Fig. 4B). As would be expected, this time the initial suppression of the fluorine signal lasted longer, and the signal recovered only about 50% of its original intensity. The randomly spaced decreases in the fluorine intensity to its original level after the bulk of the ether had evaporated were probably caused by the turbulence of the gas stream as it swept the last traces of the ether vapor out of the well and into the gas stream. The failure of the signals in Fig. 4A and B to return to the original level may have been due to the adsorption and gradual desorption of the ether from the walls of the chamber.

If it is assumed that 1 μl of di-isopropyl ether evaporates per minute, the ratio of the concentration of C_2 molecules produced from it (4.53×10^{-7} g mol cm^{-3}) to the concentration of fluorine atoms produced from the CCl_2F_2 (2.04×10^{-8} g atom cm^{-3}) is about 22:1. The results presented in Fig. 4 thus mean that even at these low concentrations, a 22-fold excess of C_2 molecules over fluorine atoms (excitation potentials $\approx$2.44 eV and 14.4 eV, respectively) reduces the intensity of the F 685.602-nm line by a factor of about 17.

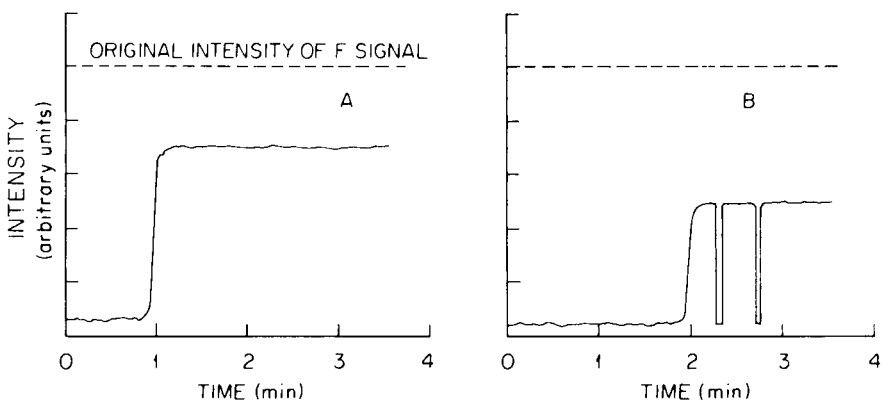

Fig. 4. Effect of di-isopropyl ether vapor on the intensity of the F 685.602-nm line. A, 1 μl of the ether deposited in chamber well (Fig. 1). B, 2 μl of the ether deposited in well after recording the curve shown in Fig. 3.

Effect of current on intensity of F 685.602-nm line

As expected, the intensity of this line increased with discharge current up to currents of about 80 mA. It was desired to explore the effect of still higher currents, but the power supply available could not provide such currents continuously, and the glow chamber could not safely dissipate the power in excess of 30 W which would be liberated by such a discharge.

A relaxation oscillator was therefore built. Used with the existing power supply, it furnished 10 pulses per second with peak currents of more than 11.5 A. Because the spectral background corrector could not be used with a low-repetition-rate pulsed light source, the oscillating refractor plate was removed from the system. The background was instead corrected with a strip chart by scanning the spectrum in the vicinity of the line of interest.

A preliminary scan of the spectrum of 99.996% pure helium with the pulsed discharge in the vicinity of 685.6 nm showed a line of unknown origin less than 0.5 nm away from 685.602 nm; no plausible identification was possible from wavelength tables [12—14]. In order to avoid uncertainties in interpreting results, the experiment was instead done on a different fluorine line of the same multiplet (690.246 nm with an excitation potential of 14.46 eV) which had no such interferences. Figure 5A shows a slow scan of the 690.2-nm region produced by a continuous glow discharge at 40 mA and Fig. 5B shows a similar scan using the pulsed discharge. The pulsed discharge excites a substantial spectral background in this region, but there is no evidence of a peak at 690.246 nm.

To show that the failure of the fluorine line to appear in the pulsed discharge was not due to the high excitation potential of the line, a spectral scan was also made from 777.0 to 778.0 nm. The intense atomic oxygen triplet at 777.194, 777.417 and 777.539 nm showed up clearly, even though the excitation potential is 10.69 eV.

The failure of the pulses to excite the fluorine lines is explained by the

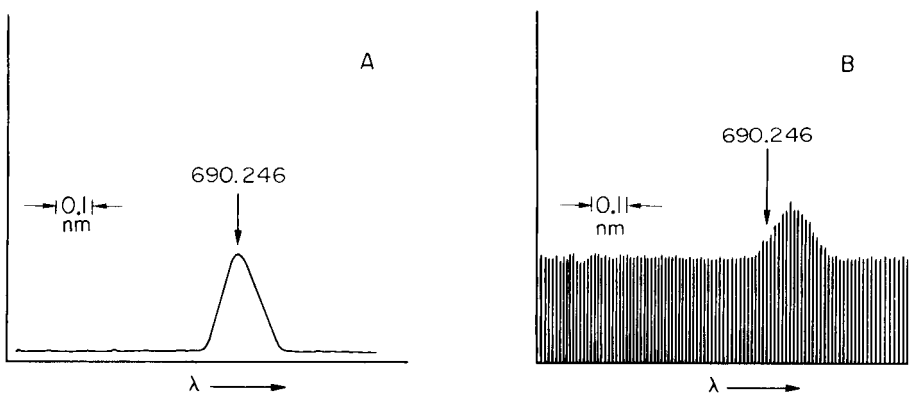

Fig. 5. Spectral scan in the vicinity of the F 690.246-nm line. A, Excitation by continuous glow discharge. B, Excitation by pulsed arc discharge (10 pulses per s).

pulse current measurement. The fact that the peak current is 11.5 A means that the discharge becomes an arc, rather than a glow, destroying the environment that favored the excitation of fluorine lines. The broad, thin and uniform glow layer has been replaced by a very narrow, high-current-density, discharge channel; at the point where this channel emanates from the cathode surface (the "cathode spot"), there was considerable vaporization (not sputtering) of cathode material (in this case, platinum). This metal vapor furnished an abundance of easily excited atoms. Under these circumstances, it is not surprising that the fluorine lines (e.p. 14.4 eV) were not excited; it is in fact somewhat surprising that the oxygen triplet (e.p. 10.69 eV) was excited to some extent.

Application to solid compounds containing fluorine

The previous section showed that certain types of impurities can interfere with the excitation of the emission spectrum of fluorine. The present section will deal with methods for producing fluorine-bearing vapors from solids while minimizing the concomitant vaporization of interfering substances.

In one important area of ecological study (ground water) fluorine occurs in inorganic forms. Attempts were therefore made to detect the fluorine 685.602-nm line in a helium glow discharge when the end face of the cathode (a bare 0.060 in. diameter W/ThO_2 rod) was coated with a residue containing 100—1000 ng F as potassium fluoride. Although emission of the desired line was detected, the cathode layer was very unstable and the line intensity was highly irregular. Attention was therefore turned to organic compounds of fluorine, in particular, diphenyldifluorosilane (DPFS). This compound is formed when diphenyldichlorosilane reacts with fluoride ions in an aqueous medium; it is extractable into organic solvents. This extraction has been used to isolate fluoride from complex mixtures [15]. Because the vapor pressure of DPFS is very low (b.p. 156°C at 50 mm Hg), solutions of this compound in di-isopropyl ether (b.p. 62°C) were used to transfer the fluorine to the electrode.

For each measurement, the end face of the cathode was polished with 400-grit silicon carbide paper. A 1-μl aliquot of the appropriate solution was then deposited on this surface where the solvent evaporated in a few seconds. The electrode assembly was then inserted into the glow chamber (Fig. 1), and the chamber was purged with helium for 45—60 s. The glow discharge was turned on at 80 mA, and kept on for about 60 s. The flow rate of helium was 35 $cm^3\ min^{-1}$. The onset of the glow discharge vaporized the DPFS and excited the vapor. The resultant F 685.602-nm line signal peaks had half-widths of about 1 s. Plots of log peak height vs. log ng F were linear from 2 ng to 40 ng of fluorine, with relative standard deviations of about 5%; however, the slopes of the log—log plots were usually different from unity, suggesting nonlinear response. The efficiency of excitation was calculated in terms of peak photocurrent per gram of fluorine, with 600 V applied to the photomultiplier and all other experimental conditions held constant.

The 4-ng sample of fluorine as DPFS showed an efficiency of 3.1 A g^{-1} of fluorine; the corresponding figure for 40 ng F was 1.1 A g^{-1}. Peaks were detectable at 0.2—0.4 ng F (RSD ≈ 9%); the limit of detection, calculated as 3 times the standard deviation of the background noise, was 70 pg of fluorine.

These experiments showed that under these conditions, the 6:1 ratio of carbon atoms to fluorine atoms did not quench the 685.602-nm signal to a serious degree, although the efficiency of excitation decreased as the size of the sample increased. However, if this technique were applied to the organic phase following extraction of the fluorine from an aqueous medium, conditions would be far less favorable for the excitation of fluoride radiation. In addition to the extracted DPFS, the organic phase would also contain most of the unconverted reagent. It thus seemed advisable to experiment also with much higher carbon-to-fluorine ratios.

If the previously described conditions [15] were followed, 5 ng of fluorine in the organic phase would be accompanied by about 6 μg of diphenyldichlorosilane. A solution of DPFS and the reagent in di-isopropyl ether was prepared at the proper concentration to give the above amounts of the reagents in 1 μl. This residue was excited by the technique described above.

No 685.602-nm peak was obtained, even though 5 ng of fluorine had been detected easily when excess of diphenyldichlorosilane was not present. This indicates that the residue-glow discharge technique cannot be applied to an extract of this type without removing the unused reagent. Future efforts will be devoted to this problem and to evaluating whether the residue-glow technique can be applied to fluorine compounds isolated by the hexamethyldisiloxane vaporization procedure [16].

Separation of volatilization from excitation

In the residue-glow-experiments with DPFS, volatilization and excitation of fluorine were accomplished almost simultaneously by the same process; it was not possible to control the two processes separately.

In order to achieve such control, the electrothermal evaporation chamber shown in Fig. 2 was built. Before each use, the heater assembly was detached from the chamber and the sample cup was polished with powdered silicon carbide (600 grit). The sample solution (up to 5 μl) was deposited in the cup and the solution was evaporated to dryness in a current of air at room temperature. Wherever it was possible to hasten evaporation without risking the loss of fluorine (e.g., as hydrogen fluoride), a low current was passed through the block during the drying process. When the residue was dry, the evaporator was again clamped to the glow chamber.

Apparatus parameters, materials and operating conditions were all chosen with the aim of converting the sample residue to a pulse of fluorine-bearing vapor which would be as brief and intense as possible. It was considered advisable to perform the vaporization as close as possible (upstream) to the glow discharge itself in order to prevent flattening of the concentration peak

by diffusion. If possible, it was desirable to work with a volatile fluorine-containing compound that could travel the 1.6-cm distance from the evaporator to the glow discharge without condensing on the walls of the chamber.

In connection with the analysis of ground-water, it was desired to avoid the liquid extraction/concentration step if possible. The volatile fluorine-containing species most readily found or produced in this medium would be HF, SiF_4 and BF_3. (Tests showed that heating a solution residue that was a simple neutral fluoride such as KF, CaF_2, etc., did not produce a detectable 685.602-nm peak, presumably because no volatile fluoride could be produced.) Heating hydrogen fluorides readily produced a peak ($KHF_2 \rightarrow KF + HF$), although care was needed in drying the KHF_2 residue to avoid volatilizing hydrogen fluoride prematurely. An ammonium hexafluorosilicate residue gave a strong and prompt 685.602-nm response, as might be expected. The peaks obtained by heating complex fluorides such as sodium or potassium hexafluorosilicate were lower and broader than the peak obtained from the ammonium compound, and appeared later.

To be generally useful, a technique would have to be applicable to simple fluorides. It therefore seemed desirable to search for a technique that would produce hydrogen fluoride quickly from such fluorides, but would avoid the danger of its premature loss during the drying of the residue.

Experiments to this end were conducted by depositing 1 μl of potassium fluoride solution containing 100 ng of fluoride in the platinum solution cup, adding a suitable quantity of a test reagent, evaporating the solutions to dryness, and clamping the evaporator onto the glow discharge chamber (Fig. 2). After the chamber had been flushed with helium for 15—30 s, the glow discharge was turned on at 80 mA and a current of 40 A applied to the nichrome heater for about 30 s. The resulting photocurrent peak produced at 685.602 nm by an RCA 4840 photomultiplier tube at 600 V, with entrance and exit slits 50 μm wide on the Ebert 0.5-m monochromator, was calculated in terms of A g^{-1} of fluorine. The test reagents investigated included a variety of buffers and weak organic acids. The most successful reagents found were 1 μl of an 0.05 M pH 3.28 citrate buffer and 1 μl of 1% KH_2PO_4 solution. In each case, the mixed solution was evaporated to dryness in 2 min by passing 7 A (2.6 W) through the nichrome coil while a gentle current of air at room temperature was passed over the evaporator.

The peaks produced by these two reagents are shown in Fig. 6. At this fluorine level, sensitivity with the citrate buffer was 1.2 A g^{-1} and the sensitivity with dihydrogenphosphate solution represented 1.8 A g^{-1}. It should be noted that when the fluorine was present as a residue of DPFS on the cathode, the excitation efficiency was 3.1 A g^{-1} for 4 ng of fluorine and only 1.1 A g^{-1} for 40 ng of fluorine. The sensitivity for 100 ng of fluorine volatilized as hydrogen fluoride upstream from the discharge is thus comparable with the values obtained for smaller amounts of fluorine as DPFS residue. The excitation efficiency in the present case is probably helped by the absence of carbon atoms, but reduced by the presence of water vapor volatilized along with the hydrogen fluoride.

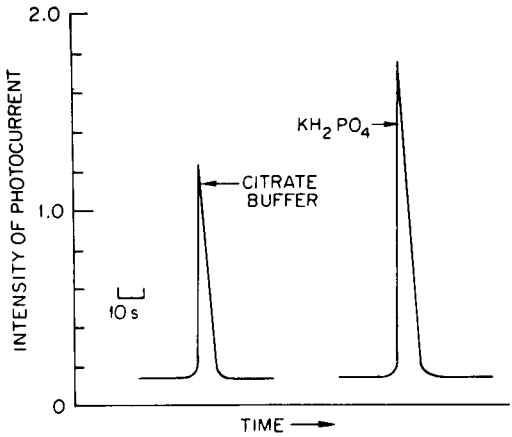

Fig. 6. Fluorine 685.602-nm signals obtained by electrothermal evaporation of hydrogen fluoride from mixed residues of 100 ng F as fluoride and acid buffers.

This research was sponsored by the Office of Energy Research, U.S. Department of Energy, under contract W-7405-eng-26 with the Union Carbide Corporation.

REFERENCES

1 L. H. Ahrens and S. R. Taylor, Spectrochemical Analysis, 2nd edn., Addison—Wesley, Reading, MA, 1961, p. 281.
2 C. E. Moore, An Ultraviolet Multiplet Table, Washington, DC, National Bureau of Standards Circular 488, Section 1, April 28, 1950, p. 22.
3 S. Bashkin and J. O. Stoner, Atomic Energy Levels and Grotrian Diagrams, Vol. I, Elsevier, New York, pp. 212, 216.
4 A. N. Zaidel and E. Ya. Shreider, Vakuumnaya Spektroskopiya i ee Primenenie (Vacuum Spectroscopy and its Application), Moscow, Nauka, 1976.
5 W. R. McLean, D. L. Stanton and G. E. Penketh, Analyst, 98 (1973) 432.
6 B. D. Quimby, P. C. Uden and R. M. Barnes, Anal. Chem., 50 (1978) 2112.
7 R. C. Fry, S. J. Northway, R. M. Brown and S. K. Hughes, Anal. Chem., 52 (1980) 1716.
8 C. Feldman and D. A. Batistoni, Anal. Chem., 49 (1977) 2215.
9 B. A. Tomkins and C. Feldman, Anal. Chim. Acta, 119 (1980) 283.
10 C. A. Bache and D. J. Lisk, Anal. Chem., 39 (1967) 787.
11 F. Trusell and H. Diehl, Anal. Chem., 35 (1963) 674.
12 C. E. Moore, A Multiplet Table of Astrophysical Interest, revised edn., Princeton, NJ, Princeton Observatory, 1945, Part I, pp. 1, 10.
13 G. Harrison, M.I.T. Wavelength Tables, J. Wiley, New York, 1939.
14 A. N. Zaidel, V. K. Profof'ev, S. M. Raiskii, V. A. Slavnyi and E. Ya. Shreider, Tablitsy Spektralnykh Linii (Tables of Spectral Lines), 4th edn., Nauka, Moscow, 1977.
15 R. Bock and H. J. Semmler, Z. Anal. Chem., 230 (1967) 161.
16 D. R. Taves, Talanta, 15 (1968) 969.

Analytica Chimica Acta, 132 (1981) 111—118
Elsevier Scientific Publishing Company, Amsterdam — Printed in The Netherlands

DESORPTION AND FRAGMENTATION STUDIES OF ORGANIC MOLECULES BY LASER-INDUCED MASS SPECTROMETRY

PRABIR K. DUTTA* and Y. TALMI[a]

Analytical and Information Division, EXXON Research and Engineering Co., Linden, NJ 07036 (U.S.A.)

(Received 2nd April 1981)

SUMMARY

Desorption, fragmentation, and cationization of a variety of organic molecules using a laser mass spectrometer are described. At low laser power densities, desorption of organic molecules takes place. With progressively higher laser power densities, fragmentation characteristic of molecular structure occurs and at very high laser power densities, indiscriminate fragmentation occurs. It is also possible to observe parent peaks from mixtures of organic molecules without any fragmentation.

Laser mass spectrometry offers unusual opportunities for studying mass spectra of nonvolatile samples that are difficult to obtain by conventional mass spectrometric methods [1, 2]. In addition, laser mass spectrometry provides a high spatial (as well as depth) resolution capability that allows accurate sampling of regions as small as a few μm. The ultraviolet laser radiation pulse serves both as a source of sample evaporation and ionization. The ionized species are separated and detected by a time-of-flight mass spectrometer. The various mechanisms involved with the laser radiation/solid sample interactions are rather complex and only partially understood and are beyond the scope of this text. In this study, the microprobe feature of the laser mass spectrometer is not utilized; rather, the laser beam is intentionally defocussed to ensure a maximum area of laser-to-sample interaction. In previous studies concerning the feasibility of laser mass spectrometry to organic compounds, emphasis was placed on its "desorption" properties, i.e., its ability to produce sparse spectra, with well-defined parent peaks, of compounds with low vapor pressure. This study, however, attempts to evaluate the molecular fragmentation pattern as well, and to determine whether or not this pattern is influenced by controllable experimental variables.

The few organic compounds selected for discussion here are part of a much larger chemical model system that has been used to determine the feasibility of laser mass spectrometry for various investigations related to

[a]Present address: 20-03 Fox Run, Plainsboro, NJ 08536, U.S.A.

0003—2670/81/0000—0000/$02.50

structure, composition, and environmental fate of different combustible fuels and their derivatives. Another basis for selection is the availability of comparative data obtained by conventional mass spectrometric techniques.

EXPERIMENTAL

The laser mass spectrometer used (LAMMA 500; Leybold-Heraeus GmbH, Köln, W. Germany) has been described comprehensively [3, 4]. This discussion pertains only to those features that apply here. At present, this system is rather limited in respect to sampling procedures. Typically, electron microscope metal grids, of various mesh sizes, are used as sample holders, and the actual practice of affixing the sample to the grid is more or less left to the user's intuition and mechanical aptitude. Accordingly, the various samples examined in this study had matrices with very different physical properties, e.g., coarse microcrystalline, highly pulverized amorphous powders or thin films obtained from evaporated solutions. This variation in matrix properties further complicates the relationship between laser power density and the degree and characteristics of molecular ionic fragmentation, as it affects both the thermal and optical properties of the sample. Nevertheless, a reasonably good correlation is observed between the laser power density and the degree of fragmentation.

The peak laser power at the sample surface is of the order of 1 μJ. The wavelength of the laser energy is 265 nm and the pulse width is 15 ns. On focusing down to 1 μm, the power density is of the order of 10^{11} W cm^{-2}. Attenuation of the laser power density is achieved either by using a set of in-tandem neutral optical density filters (100:1) or by defocusing the laser beam. The latter technique is more convenient and flexible in that it provides a continuous means for power density attenuation. It also gives more reproducible results and allows laser desorption over a wide range of laser power densities.

Typically, laser desorption is performed at a power density range of 10^6—10^7 W cm^{-2}, and the optimum value is chosen based on trial and error variations. Once the conditions for laser desorption have been optimized, the laser power density is progressively increased to obtain different molecular fragmentation patterns. At higher power densities, indiscriminate fragmentation becomes predominant.

RESULTS AND DISCUSSION

Four types of processes resulting from the interaction of laser energy with organic solids are simple desorption, fragmentation, stabilization by association, and ion recombinations, each of which is discussed below.

Laser desorption

Desorption with little or no fragmentation has been reported for various organic solids [5, 6]. A few examples of laser desorption are shown in Fig. 1. The novel feature observed in these desorption experiments is that peaks of parent ions with the attachment and loss of hydrogen atoms are often observed along with parent molecular ion peaks. The intensities of molecular ions with attachment and loss of hydrogen atoms are often higher than the intensity of the parent molecular ion peak. Recently, Mashni and Hess [7] have observed a similar phenomenon for laser mass spectra of solid methanol. They observed the strongest ion signal at m/z 33 for methanol corresponding to the $CH_3OH_2^+$ species.

Peaks were observed at m/z 251—257 for 9-phenylanthracene corresponding to $(P-3H)^+$, $(P-2H)^+$, $(P-H)^+$, P^+, PH^+, PH_2^+ and PH_3^+, where P^+ denotes the parent molecular ion peak at m/z 254. The intensities of $(P-H)^+$, P^+ and $(P+H)^+$ are similar for 9-phenylanthracene. Parent molecular ion peaks of hexaphenylbenzene and tetraphenylporphyrin show a weak signal, whereas $(P+H)^+$ for hexaphenylbenzene and $(P+3H)^+$ and $(P+4H)^+$ for tetraphenylporphyrin show the strongest intensities.

Under proper laser power conditions, mass spectra of various organic compounds with little or no fragmentation were observed, but the highest molecular weight peaks are often associated with gain or loss of hydrogen atoms from the parent molecules.

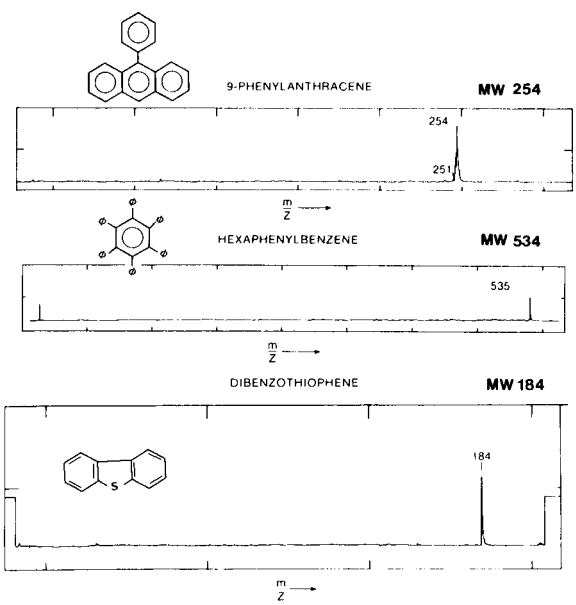

Fig. 1. Laser desorption mass spectra of 9-phenylanthracene, hexaphenylbenzene and dibenzothiophene.

Laser fragmentation

The laser provides a convenient means for controlling the amount of power incident on the sample. The power density can be varied over a few orders of magnitude. At higher laser power densities (compared to levels utilized for laser desorption), characteristic molecular fragmentation patterns were observed. As in electron-impact mass spectrometry, fragmentations via loss of neutral groups such as CO, CN, C_2H_2, C_6H_6, etc., seem highly favorable [8].

Figure 2 shows the fragmentation pattern of 9-phenylanthracene. As mentioned earlier, peaks at $(P + nH)^+$ ($n = -3$ to $+3$) are also observed along with the parent molecular ion peak. The loss of a benzene group from $(P + 2H)^+$ produces a strong peak at m/z 178 corresponding to anthracene.

The mass spectrum of hexaphenylbenzene shows a strong peak at m/z 535 corresponding to $(P + H)^+$. Successive losses of C_6H_6 (m/z 78) from $(P + H)^+$ produces peaks at 457, 379, 301 and 223. Many other peaks are observed at masses of 250—457 which are not readily assignable. Peaks observed at m/z 36—38, 48—51, 60—64 and 72—75 are assignable to species $C_3H_n^+$, $C_4H_n^+$, $C_5H_n^+$, and $C_6H_n^+$, respectively.

The mass spectrum for dibenzothiophene with peaks at m/z 152 and 139, bears a close resemblance to the electron-impact mass spectrum of that compound [9]. These peaks are attributed to the loss of neutral —S and —CHS fragments. A series at m/z 45, 69, 93 and 117 is also characteristic of this and related compounds and has been assigned to C_nHS^+ fragments [8].

Vanadyl tetraphenylporphyrin shows a fragmentation pattern characterized by loss of neutral groups such as oxygen and benzene. The peaks observed are at m/z 681 $(P + 2H)^+$, 680 $(P + H)^+$, 679 $(P)^+$, 664 $(P + H - O)^+$,

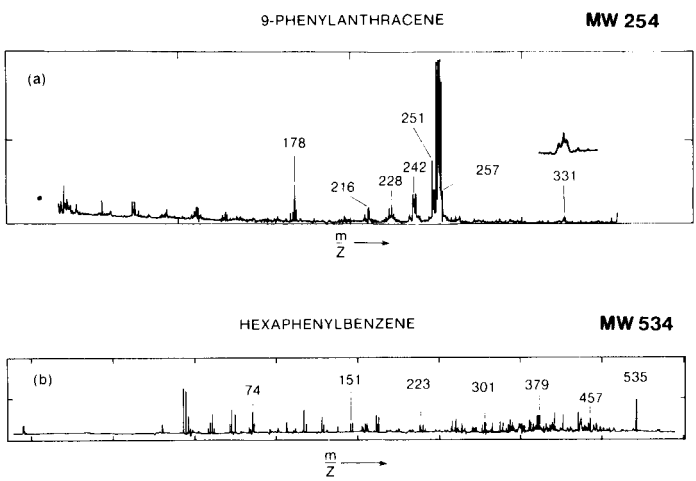

Fig. 2. Fragmentation spectra of 9-phenylanthracene and dibenzothiophene.

600 $(P - H - C_6H_6)^+$, 584 $(P - H - C_6H_6 - O)^+$, 525 $(P + 2H - 2C_6H_6)^+$, 509 $(P + 2H - 2C_6H_6 - O)^+$, 67 $(VO)^+$ and 51 $(V)^+$. The other fragment peaks are at *m/z* 527, 605 and 663.

The mass spectrum of hemin shows a fragmentation pattern that corresponds to losses of the various alkyl side chains, as indicated in Fig. 3. The highest molecular weight peak is observed at *m/z* 617 which corresponds to a loss of chlorine. Groups of peaks are observed at *m/z* 570—575, 558—562, 544—548, 511—514, 496—500, 480—484, 465—468, 451—457, 440—444, 426—428 and 411—416. Figure 3 explains the presence of one of these peaks in each group by the loss of side chains. The presence of some of these peaks at other masses suggests the loss of hydrogen atoms from the parent species.

At still higher power densities, however, all discrimination in fragmentation is lost and carbon (C_n) series are formed. Characteristically, the mass spectrum of triptycene at low power densities (Fig. 4a) shows the parent peaks at *m/z* 251—257 with the remainder of the peaks explained by loss of C_2H_2 and C_6H_6 fragments

$$P(252) \xrightarrow{-C_2H_2} 226 \xrightarrow{-C_2H_2} 200;\ P(256) \xrightarrow{-C_6H_6} 178 \xrightarrow{-C_2H_2} 152;\ P(257) \xrightarrow{-CH_3} 242$$

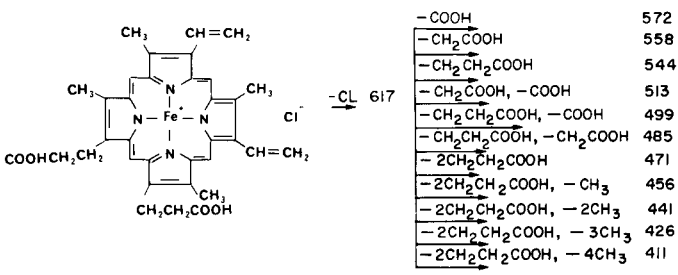

Fig. 3. Fragmentation of hemin.

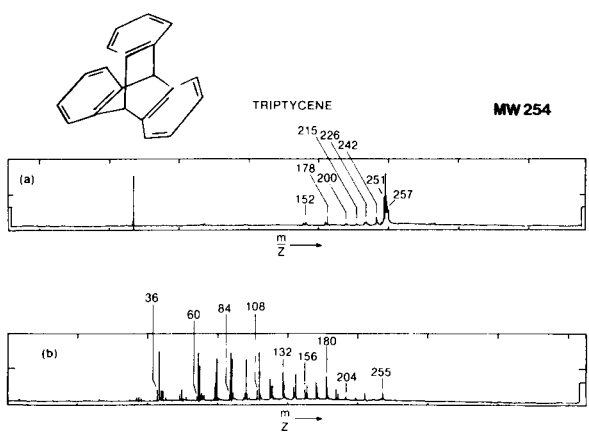

Fig. 4.(a) Laser desorption and (b) indiscriminate fragmentation at higher laser powers for triptycene.

At a higher laser power density, a characteristic C_n series is obtained as illustrated in Fig. 4(b). Thus, through a variation in laser power density, a certain degree of control over the desorption and fragmentation mechanisms can be achieved and consequently also a control over the nature of the structural and molecular information obtainable.

Recombination and cationization

During its 15-ns lifetime, the laser pulse produces ions that are sustained within the microplasma. These ions then travel down the mass spectrometer drift tube which is maintained at a nominal pressure of 10^{-6} torr. Consequently, the possibilities for intermolecular reactions seem slim. However, the ions can rearrange to more stable species by elimination of fragments during migration in the drift tube. The mass spectrum of 9-phenylanthracene (Fig. 2), shows a weak peak at m/z 331 that corresponds to a combination product of the $(P - H)^+$ species with a benzene unit. It is unclear, however, whether this product is formed by intermolecular combination or by intramolecular decomposition of a dimer parent unit.

The attachment of an inorganic cation to an organic molecule is known in connection with phenomena such as laser desorption [5, 10], field desorption [11, 12] and secondary ion mass spectrometry [13]. This phenomenon can actually be considered a special case of the recombination reaction mentioned above. The mechanism of attachment, although often discussed in the literature, is unclear at present [14].

The mass spectrum of hexaphenylbenzene pulverized and mixed with sodium chloride (Fig. 5a) shows a strong peak at m/z 558, corresponding to $[P + H + Na]^+$. The remaining peaks in the spectrum are due to sodium chloride combination ions. With some compounds, parent ions are not detected regardless of how low the laser power density is. In such cases, the deposited energy is either insufficient for laser desorption or high enough to result in fragmentation. Cholesterol provides an example of this pattern. However, on addition of sodium chloride, the more stable $(P + 2H + Na)^+$ molecular ion at m/z 411 is produced with little, if any, associated molecular fragmentation (Fig. 5b, c).

Organic mixtures

For laser desorption to be a practical technique, it must be applicable to complex mixtures. Evaluation of this aspect of the technique was performed with a mixture of the five compounds, carbazole (m.w. 167), dibenzothiophene (m.w. 184), dibenzofuran (m.w. 168), 2,9-dimethyl-4,7-diphenyl-1,10-phenanthroline (m.w. 361), and tetraphenylporphyrin (m.w. 615). A mixture of these compounds was deposited on an electron microscope grid from an acetone solution. The resultant spectrum, obtained at a low laser power density (Fig. 6) consists only of molecular parent ion peaks and parent peaks associated with hydrogen atoms. This illustrates that controlled desorption can be achieved for chemical mixtures. Nevertheless, to

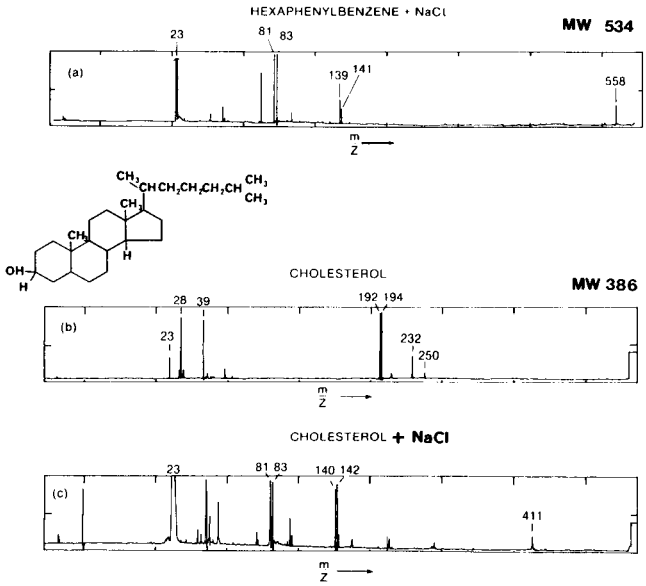

Fig. 5. Laser cationization of hexaphenylbenzene ground with NaCl (a), laser-induced mass spectra of cholesterol (b), and laser-induced mass spectrum of cholesterol with NaCl showing $(P + 2H + Na)^+$ peak (c).

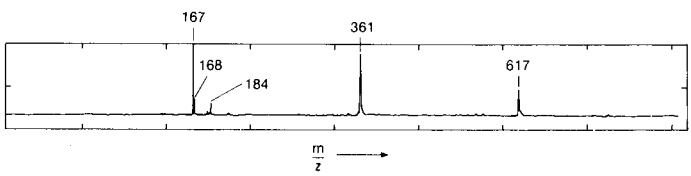

Fig. 6. Laser desorption spectra from a mixture of five compounds.

become a routine mass spectrometric tool, quantitative control over laser power density and better sampling techniques are necessary.

These experiments were performed in the Central Research Laboratory, Leybold-Heraeus, Köln, W. Germany. The authors thank Drs. R. Wechsung and H. J. Heinen for their help and gratefully acknowledge helpful discussions with Dr. F. Hillenkamp, University of Frankfurt, W. Germany.

REFERENCES

1 R. J. Conzemius and J. M. Capellen, Int. J. Mass Spectrom. Ion Phys., 34 (1980) 197.
2 I. D. Kovalev, G. A. Maksiniev, A. I. Suchkov and N. V. Larin, Int. J. Mass Spectrom. Ion Phys., 27 (1978) 101.
3 R. Wechsung, F. Hillenkamp, R. Kaufmann, R. Nitsche, E. Unsold and H. Vogt, Microsc. Acta, 2 (1978) 281.
4 F. Hillenkamp, R. Unsold, R. Kaufmann and R. Nitsche, Appl. Phys., 8 (1975) 341.

5 M. A. Posthumus, P. G. Kistemaker, H. L. C. Meuzelaer and M. C. T. Noever de Brauw, Anal. Chem., 50 (1978) 985.
6 H. J. Heinen, S. Meier, H. Vogt and R. Weschung, 8th Triannual International Mass Spectrometry Conference, Oslo, August 1979.
7 M. Mashni and P. Hess, Chem. Phys. Lett., 77 (1981) 541.
8 M. C. Hamming and N. G. Foster, Interpretation of Mass Spectra of Organic Compounds, Academic Press, New York, 1972, pp. 340—358.
9 J. Heiss, K. P. Zeller and B. Zeeh, Tetrahedron, 24 (1968) 3255.
10 R. O. Mumma and F. J. Vastola, Org. Mass Spectrom., 6 (1972) 1373.
11 G. D. Daves, Acc. Chem. Res., 12 (1979) 359.
12 F. W. Rollgen and H. R. Schulten, Org. Mass Spectrom., 10 (1975) 660.
13 H. Grade and R. G. Cooks, J. Am. Chem. Soc., 100 (1978) 5615.
14 R. Cotter, Anal. Chem., 52 (1980) 1589A.

Analytica Chimica Acta, 132 (1981) 119—126
Elsevier Scientific Publishing Company, Amsterdam — Printed in The Netherlands

A GAS-CONTROL UNIT FOR USE WITH CATHODIC-SPUTTERING CELLS IN ANALYTICAL ATOMIC SPECTROSCOPY

P. L. LARKINS
CSIRO Division of Chemical Physics, P.O. Box 160, Clayton, Vic. 3168 (Australia)
(Received 14th July 1981)

SUMMARY

The design of a gas flow-rate and pressure control unit suitable for use with cathodic-sputtering cells is described. The unit uses semi-automatic control to allow rapid sample exchange and precise reproduction of gas flow rate and pressure. Particular attention is given to the need to minimize contamination of the gas stream by water vapour. With this unit, samples can be changed in less than one minute, pressure in the region of 0.65 kPa (5 torr) can be reproduced to better than 1%, and moisture contamination contributed by the unit can be reduced to less than 5 ppm (v/v).

Cathodic sputtering has been shown by several workers to be a convenient method for direct atomization of solid materials. The atomic vapour produced in this way can be analysed by atomic absorption [1—3], emission [4—8], or fluorescence [9—10] spectrometry. When a single element or simple alloy is used as the cathode, the sputtering cell can be used as the light source for atomic absorption or fluorescence studies [5, 11, 12].

Cathodic sputtering is generally carried out in a stream of flowing gas. Continuous flow is necessary in order to flush residual air from the cell after each sample change and also to remove gaseous impurities generated during the sputtering process. Especially when sputtering is used to atomize samples for chemical analysis, it is important to be able to reproduce accurately the same gas flow-rate and pressure conditions for each sample and to be able to change samples with minimum delay. Most of the work described in the literature and earlier work at this laboratory was carried out with manually-operated gas flow systems. More recent work in this laboratory [2, 8, 10—13] has been done with units of the type described here which employ semi-automatic operation to provide minimum sample replacement time, accurate reproduction of gas flow rate and pressure, and simplicity of operation.

For reproducible sputtering it is important to maintain a low moisture level in the gas supplied to the cell, because water molecules are dissociated by the discharge to produce hydrogen which lowers the sputtering yield. The components used in the present design were carefully selected and tested to ensure minimum contamination of the gas stream with water vapour.

DESCRIPTION

Basic design

The gas-control unit was designed to enable repetition of the following sequence of operations: (a) evacuation of the sputtering cell to a pressure of approximately 0.013 kPa (0.1 torr); (b) establishment of a flow of inert gas at a predetermined cell pressure in the range 0.13—1.3 kPa (1—10 torr) absolute; (c) rapid return of the cell to atmospheric pressure after sputtering; (d) provision of a low flow of inert gas to the cell during sample exchange to minimize the entry of moist air.

The primary control of flow and pressure in this design is effected by the well-known method of pumping against a controlled leak through a fine needle valve. In addition, rapid sample exchange and simplicity of operation are achieved by incorporating a number of solenoid-operated valves connected with the pressure-sensing system and operated as described later. Although not often required, an additional needle valve is incorporated in the vacuum line from the sample cell to the pump to enable variation of the cell pressure at a given flow rate.

A schematic diagram of the gas flow system is given in Fig. 1. In normal operation the unit is supplied with argon or other suitable gas at a pressure of 100—200 kPa (15—30 psi) above atmospheric pressure. The pressure-control valve provides a constant gas pressure of about 10 kPa (1.5 psi) to the fine needle valve V1 which controls the flow rate. The coarse needle valve V2 enables variation of the cell pressure for a given flow rate. The solenoid-operated valves S1 and S4 allow interruption of the gas flow to and from the sputtering cell, respectively. The solenoid-operated valves S2 and S3 provide by-passes around the needle valves to permit rapid sample exchange without

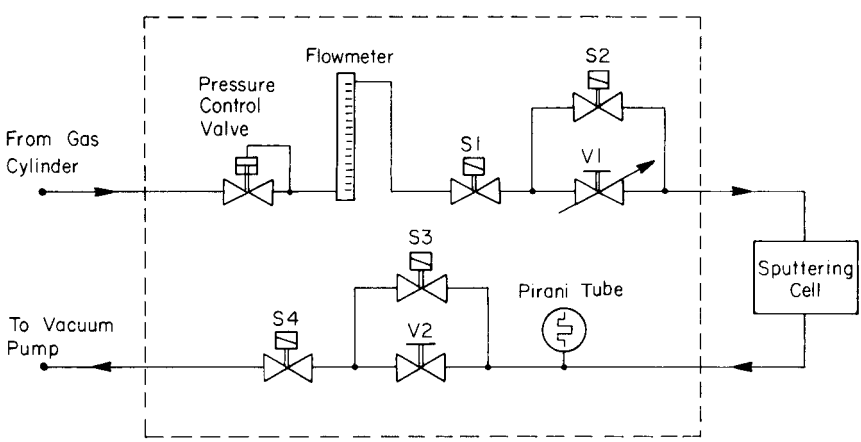

Fig. 1. Schematic diagram of gas flow system. S1—4 are solenoid-operated valves and V1, 2 are needle valves.

alteration of the needle valve settings. Flow rate and cell pressure are indicated by the tapered tube flowmeter and the Pirani-type pressure sensor, respectively. The unit is normally used in conjunction with a rotary-oil pump or a similar pump. Gas-control units based on this design are now made by R & D Instruments Pty. Ltd, Braeside, Victoria, Australia.

Component materials

A good deal of work was done to find the most suitable materials for the various components. The major consideration is the need to avoid contamination of the gas stream by water vapour. Preferred materials from this point of view are metals, especially stainless steel, as most types of rubber and plastics are known to absorb or be permeable to water vapour. However, components such as the diaphragm of the pressure-control valve and the tubing connecting the gas-control unit to the sputtering cell, need to be flexible and this means that the use of metals for these components is difficult.

The diaphragm in most pressure-control valves is a possible major source of moisture contamination. Some manufacturers can provide these valves fitted with flexible stainless-steel diaphragms but where these are not available Viton or butyl rubber are satisfactory alternative materials. For the gas connection to the sputtering cell a high-density polyethylene tubing known as "Dekabon" has been found suitable. This tube has a multilayer construction, including a thin aluminium layer on the inside of the tube, which acts as a moisture barrier.

Connection between the various components is made with brass Swagelok fittings with nylon ferrules and Dekabon or copper tubing. The complete assembly was tested by using a mass-spectrometer helium leak detector and found to be leak-free. A list of components which have been tested and found suitable is given in Table 1. In order to minimize evacuation time and pressure drop through the vacuum system, 9.5 mm o.d. tube is used for the vacuum line from the fine needle valve V1 to the solenoid valve S4 and 19 mm o.d. tube is used to connect the control unit to the pump. Gas connections up to the needle valve V1 are made with 6.4 mm o.d. tubing. The vacuum connections from the gas-control unit to the sputtering cell are normally about 70 cm long.

Even when the materials specified above are used, the system must finally be purged with dry gas for at least 24 h before use to ensure minimum contamination of the gas stream with water vapour, i.e., less than 5 ppm (v/v) of added water at a gas flow rate of the order of 0.1 l min^{-1} (all gas flow rates in this paper refer to volumes at atmospheric pressure). When not in use, the system should be sealed to prevent entry of moist air.

Electronic and electrical system

The electronic circuit associated with the Pirani-type pressure sensor is shown in a simplified form in Fig. 2. The Pirani tube is operated in the constant-temperature (constant-resistance) mode to provide optimum sensitivity

TABLE 1

Components found suitable for use in the gas control unit[a]

Item	Description	Supplier
Pressure control valve	Model 8601B ELF pressure regulator with Viton A diaphragm	Brooks Instrument Division, Emerson Electric Co., Hatfield, PA, U.S.A.
	Model 8300 pressure regulator with stainless-steel diaphragm	Porter Instrument Co., Hatfield, PA, U.S.A.
V1	Very fine metering valve, model SS 4SG	Nupro Co., Willoughby, OH, U.S.A.
	Model 8504 ELF precision needle valve	Brooks Instrument Division, as above
V2	Forged body regulating valve, Model 1RS6	Whitey Co., Cleveland OH, U.S.A.
S1,2	Two-way midget solenoid valve, model 1A3M	Goyen Controls Co. Pty. Ltd., Milperra, N.S.W., Australia.
S3,4	Standard direct-acting stainless-steel solenoid valves model S 301AA04N3BE1	General Controls ITT, Glendale, CA, U.S.A.
Flow meter	Purgemeter type K 10A 3135 N-01A with pyrex float	Fischer & Porter Pty. Ltd., Noble Park, Victoria, Australia.
Pirani tube	Stainless-steel gauge tubes type 3592	LKB Produkter AB, Bromma, Sweden.
	Pirani sensor type WP-01	Ulvac Corporation, Tokyo, Japan.

[a]The above list includes only those items which have been tested. Equivalent components from other suppliers may be suitable but the comments in the text regarding moisture problems should be noted. Most of these components need to be suitable for vacuum service.

in the 0.13—1.3 kPa (1—10 torr) pressure range. In this mode the Pirani tube forms one arm of a resistance bridge circuit. Imbalance in the bridge is detected by the operational amplifier 0A1 which then alters the voltage across the bridge, and hence the current through it, to restore balance. The voltage required to maintain the bridge in balance is a measure of the gas pressure in the gauge tube. Operational amplifier 0A2 enables zero adjustment of the pressure readout meter by compensating for the small current required by the Pirani tube to maintain temperature at zero pressure (<0.01 torr). Amplifier 0A3 is used as a comparator to permit setting of the pressure at which gas flow will automatically recommence after changing samples. This is normally set at about 0.013 kPa (0.1 torr) as a check for leak-free sealing of the sample on the sputtering cell but may be set higher to reduce sample-exchange time.

The Pirani gauge is temperature-sensitive but this is a minor limitation as the operating pressure is only set approximately using the pressure indication. Final adjustment is based on the sputtering voltage in absorption measurements or the light intensity in emission studies. The low-pressure switch setting is also not critical. However the temperature sensitivity of the Pirani gauge precludes its use in a feedback system for sputtering-cell pressure control.

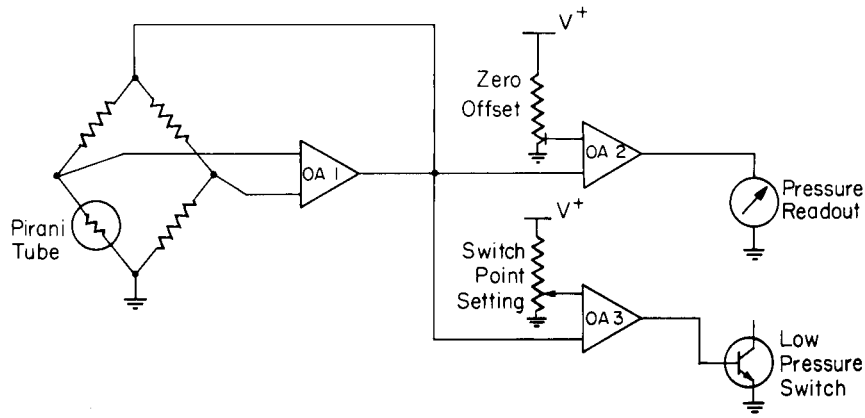

Fig. 2. Simplified diagram of Pirani gauge electronic circuit.

Figure 3 shows a schematic diagram of the switching circuits which provide semi-automatic operation. In a normal operating cycle, the sequence of activation of the solenoid-operated valves is as shown in Table 2.

Pump capacity

In a flowing gas system of this type, the minimum cell pressure achievable is a function of both the pumping rate and the gas flow rate. It is independent

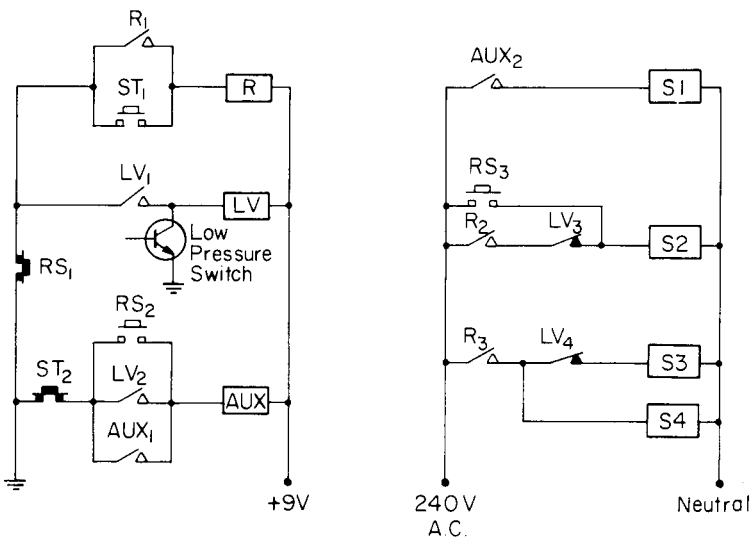

Fig. 3. Schematic diagram of switching circuits. R, LV and AUX are the coils of low-voltage multi-contact relays. Their associated contacts are shown as R_1, R_2, R_3, LV_1, etc.; ST_1 and ST_2 are the two banks of a push-button "momentary on" START switch; RS_1, RS_2 and RS_3 are the three banks of a "push-on push-off" RESET switch. All switches and relay contacts are shown in the de-activated condition. S1—4 are solenoid-operated valves.

TABLE 2

Sequence of activation of valves

Operating state	Condition of solenoid valve				Result
	S1	S2	S3	S4	
START switch activated	Shut	Open	Open	Open	Rapid cell evacuation
Low pressure reached	Open	Shut	Shut	Open	Sputtering conditions established
RESET switch on	Open	Open	Shut	Shut	Rapid return to atmospheric pressure in cell
RESET switch off	Open	Shut	Shut	Shut	Slow gas bleed to sputtering cell

of the ultimate vacuum rating of the pump provided that this is lower than the desired operating pressure. In a sputtering cell used for atomizing a sample for measurement by atomic absorption, a typical cell pressure is about 0.65 kPa (5 torr) at a gas flow rate of about 0.4 l min^{-1}. A glow-discharge lamp or demountable hollow-cathode lamp is typically operated at a pressure of about 0.2 kPa (1—2 torr) and a flow rate of about 0.1 l min^{-1}. Simple calculations provide the data in Fig. 4, which shows the minimum pressure obtainable at the pump inlet as a function of gas flow rate for three pump capacities. The pressure in the sputtering cell or lamp is slightly higher because of the unavoidable pressure drop through the control unit. It can be seen from Fig. 4 that, while a pump with a capacity of 50 l min^{-1} could be used in some circumstances, a pumping speed of 100—200 l min^{-1} is more generally useful.

Gas driers

Earlier versions of this unit incorporated molecular-sieve drying columns together with provision for in situ regeneration by heating under vacuum. Later work established that drying was not necessary when the argon used contained less than 10 ppm water vapour, e.g., special-grade argon (Commonwealth Industrial Gases, Preston, Victoria, Australia). If argon of this quality is not available, a molecular-sieve drying column can easily be fitted in the gas line to the unit. In this case a fine filter should be installed after the drying column to prevent molecular-sieve dust from being carried into the valves.

PERFORMANCE

Sample change time

When a vacuum pump rated at 100 l min^{-1} and a sputtering cell of about 0.2-l volume are used, the time for the system to be evacuated from atmospheric pressure to about 0.013 kPa (0.1 torr) and then to establish the pre-set pressure and flow rate is about 30 s. Return of the cell to atmospheric pressure

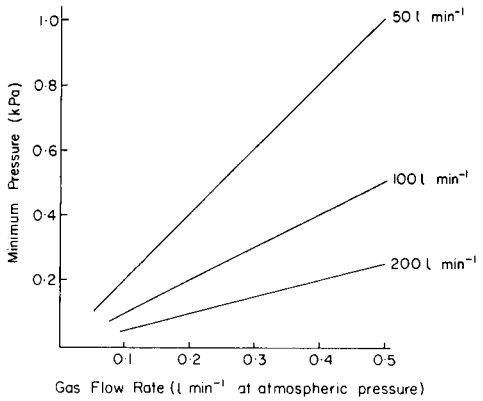

Fig. 4. Dependence of minimum pressure at pump inlet on gas flow rate for various pump capacities.

takes about 5 s. This results in a total sample exchange time, from the finish of sputtering on one sample to the commencement on the next, of less than one minute. The use of a larger sputtering cell or long vacuum-connections from the control unit to the cell will increase this time.

Reproducibility of gas pressure and flow rate

The reproducibility of the pressure after repetitive operation through complete cycles, including sample replacement, was determined by using a Wallace and Tiernan series 300 absolute pressure gauge. When dry argon was used, a cell pressure setting of 0.65 kPa (5 torr) was reproduced to better than 0.005 kPa (0.04 torr) over at least ten complete cycles of operation. The same result was obtained at various argon flow rates in the range 0.1—0.5 l min^{-1}. No direct measurement was made of the reproducibility of the gas flow rate but any significant change in flow rate would be expected to produce some change in pressure.

Indirect evidence of the reproducibility of gas pressure and flow rate is provided by the results of workers who have used this gas-control unit. Gough [2] determined nickel and chromium in an iron-based alloy by atomic absorption measurements on the sputtered vapour of the alloy and obtained a reproducibility of 1% r.s.d. or better. Sullivan [13] determined magnesium at the 0.02% level in an aluminium alloy by measuring its emission at 285.2 nm in a boosted glow discharge [5]. He found that the emission signal reached equilibrium in about 3 min from the initiation of the discharge and showed an r.s.d. of 1.1%. Sullivan's results are noteworthy, as the sputtering of aluminium is particularly sensitive to the presence of water vapour.

The author thanks Mr. D. S. Gough for much helpful discussion on the basic requirements of this unit and Mr. J. R. Meldrum for assistance with the design of the switching circuits.

REFERENCES

1 B. M. Gatehouse and A. Walsh, Spectrochim. Acta, 16 (1960) 602.
2 D. S. Gough, Anal. Chem., 48 (1976) 1926.
3 C. G. Bruhn and W. W. Harrison, Anal. Chem., 50 (1978) 16.
4 W. Grimm, Spectrochim. Acta, 23B (1968) 443.
5 R. M. Lowe, Spectrochim. Acta, 31B (1976) 257.
6 M. E. Waitlevertch and J. K. Hurwitz, Appl. Spectrosc., 30 (1976) 510.
7 H. G. C. Human, N. P. Ferreira, R. A. Kruger and L. R. P. Butler, Analyst, 103 (1978) 469.
8 D. S. Gough and J. V. Sullivan, Analyst, 103 (1978) 887.
9 D. S. Gough, P. Hannaford and A. Walsh, Spectrochim. Acta, 28B (1973) 197.
10 D. S. Gough and J. R. Meldrum, Anal. Chem., 52 (1980) 642.
11 J. V. Sullivan and J. C. Van Loon, Anal. Chim. Acta, 102 (1978) 25.
12 J. V. Sullivan, Anal. Chim. Acta, 105 (1979) 213.
13 J. V. Sullivan, 1981, personal communication.

Analytica Chimica Acta, 132 (1981) 127—137
Elsevier Scientific Publishing Company, Amsterdam — Printed in The Netherlands

CALIBRATION IN QUANTITATIVE ANALYSIS
Part 2. Confidence Regions for the Sample Content in the Case of Linear Calibration Relations

J. AGTERDENBOS

Analytisch Chemisch Laboratorium der Rijksuniversiteit, Croesestraat 77A, 3522 AD Utrecht (The Netherlands)

F. J. M. J. MAESSEN* and J. BALKE

Laboratory for Analytical Chemistry, University of Amsterdam, Nieuwe Achtergracht 166, 1018 WV Amsterdam (The Netherlands)

(Received 3rd July 1981)

SUMMARY

The precision of analytical results determined from linear calibration graphs is discussed. It is assumed that the standard deviation of the analytical procedure has the same value σ_x for all calibration levels and for the sample measurements. The collective and individual influence exerted by the number of both calibration and sample measurements (N and n, respectively) on the precision of the results is calculated on the basis of widths of confidence intervals. In addition, the effects on precision caused by the distribution of the calibration measurements over the calibration range and by the location of the sample in the analytical range are calculated. A quantity, comprising an "eccentricity term", is developed, which contributes to better insight into the problems considered. For the special case that the k calibration levels are equidistant and the same number of replicate measurements m is made at each of these levels ($km = N$), the length of the confidence region is given by $\Delta x = 4s_x (n^{-1} + z/N)^{1/2}$ for $\alpha = 0.05$. The value of z depends on the "eccentricity" of the sample value compared to the centre of gravity of the calibration values, and on the value of k. If the sample value coincides with the centre of gravity of the calibration values, $z = 1$. If the sample value coincides with one of the extreme values of the calibration experiments, the value of z increases to $z = 2.00$ for $k = 2$ and to $z = 3.81$ for $k = 32$.

As was emphasized by Agterdenbos [1] in Part 1 of this series, not much is known about the way the precision of analytical results is affected by the number of calibration measurements on which the calibration graph is based. Other points rarely discussed are the influence of the distribution of calibration measurements over the concentration range, the location of the concentration of the sample within this range, and of the number of replicate sample measurements.

The object of the present study was to consider these points for different cases under defined conditions. Confidence intervals were used as the measure of precision. These were calculated according to the procedure described by Mandel [2], which was considerably simplified. It was assumed that the following conditions are fulfilled:

0003—2670/81/0000—0000/$02.50

(1) the true relationship between concentration and analytical signal is strictly linear for the concentration range considered;
(2) the uncertainties in the concentrations of the standards are negligible compared to the uncertainties affecting the corresponding analytical signals;
(3) the variances of the analytical signals at all calibration levels are statistically homogeneous [3];
(4) the variances of calibration and sample measurements have the same value.

PRINCIPLES OF CALCULATION

Confidence intervals if no calibration is applied

For reasons which will become clear, it is necessary first to recall how the confidence interval for a true value x_s of the content of the analytical sample is calculated from n replicate measurements, if no calibration is considered. In such cases, this interval and its width are given, respectively, by

$$x_m - t_c s n^{-1/2} < x_s < x_m + t_c s n^{-1/2} \text{ and } \Delta x = 2 t_c s n^{-1/2} \quad (1)$$

The symbols used are given in Table 1. The value of t_c depends on the level of significance α and on the number of degrees of freedom Φ that were available for calculation of s. If the only information on σ is obtained from the n replicate measurements applied for calculation of x_m, then $\Phi = n - 1$. It is frequently overlooked, however, that in many practical cases much information on σ is available from other measurements with the same analytical procedure on similar samples (similar samples here are samples such that the same value of σ can be expected). In such cases, all information on σ can be pooled and a better estimate on σ is found because an increase in Φ results in a decrease of t_c. The value of the pooled estimate s_p is found from $\Sigma_i \Phi_i s_p^2 = \Sigma_i \Phi_i s_i^2$, and the Φ value to be applied for calculation of the appropriate t_c value is $\Sigma_i \Phi_i$. It should be noted that σ is a quality parameter for the precision of the analytical procedure applied, and that s is an unbiased estimate of σ; thus both σ and s are independent of n.

The calculation of confidence intervals if calibration is applied

Most of this section summarizes the method applied by Mandel [2] for the calculation of confidence intervals. Figure 1 shows the least-squares fitted calibration graph for a series of standards with concentrations ranging from x_1 and x_N. The corresponding analytical signals are denoted by y_1 to y_N, and y_s is a measurement made on the sample for which the true value, x_s, has to be estimated.

However, the estimate $\hat{x}_s$ instead of the true value x_s is obtained. Algebraically, $\hat{x}_s$ is given by the relation

$$\hat{x}_s = (y_s - \hat{a})/\hat{b} \quad (2)$$

where $\hat{a}$ and $\hat{b}$ are, respectively, the estimated intercept and the estimated slope of the least-squares calibration graph. If more measurements on the

TABLE 1

Symbols used

σ, s	Standard deviation of the analytical procedure (population value and best estimate of this value)
σ_y, s_y	σ and s values expressed in signal units
s_p	Pooled estimate for σ
s_x	$s_y/\hat{b}$
Φ	Number of degrees of freedom available for calculation of s
t_c	Critical value of Student's t
x_s	True value of the content of the analyte in the sample
$\hat{x}_s$	Best estimate of x_s calculated from y_s (see Fig. 1)
x_m	Mean value of replicate measurements on x in the case where no calibration is used
x_i, $\bar{x}$	x value applied in calibration; mean of those x values
x_1, x_N, y_1, y_N	See Fig. 1
x_u, x_l	Upper and lower value of confidence region for x_s
$\bar{\hat{x}}_s$	Mean of n replicate estimates of $\hat{x}_s$
Δx	Width of the confidence region
n	Number of replicate measurements on the sample
N	Number of experiments applied for calibration
α	Level of significance
a, b	True values of intercept and slope of the graph
$\hat{a}$, $\hat{b}$	Best estimates of a, b
y	Signal value
y_s	Signal value for the analytical sample
$\bar{y}_s$	Mean value of signals found for the same sample
y_i, $\bar{y}$	Signal value found in calibration; mean of those values
K	$t_c s_y$
u	$N\Sigma(x_i - \bar{x})^2$
d_i	See Fig. 1 and text
v, v_1, v_2	See Eqn. (3) and text
A	See Eqn. (4)
E, E_N, E_D	Eccentricity term. See Eqn. (7)
f	See Eqn. (8)
L	Length of calibration region $x_N - x_1$
k	Number of calibration levels
m	Number of replicates at each calibration level
ρ	Eccentricity parameter. See Eqn. (9)
B	See Eqn. (11)
z	See Eqn. (13)

sample are made, $\bar{y}_s$ is used in place of y_s and $\bar{\hat{x}}_s$ in place of $\hat{x}_s$. The right side of Eqn. (1) contains three quantities all affected by random error. As these quantities are not statistically independent, the law of propagation of errors does not apply to the standard deviation of $\hat{x}_s$, but it is possible to derive a confidence interval for the true value x_s. To obtain this interval, the following quadratic equation in v has to be solved [2]

$$[\hat{b}^2 - NK^2 u^{-1}]v^2 - [2\hat{b}(\bar{y}_s - \bar{y})]v + [(\bar{y}_s - \bar{y})^2 - (n^{-1} + N^{-1})K^2] = 0 \qquad (3)$$

(For the symbols used, see Table 1.) The value of t_c is discussed below. The value of s_y (see Fig. 1) is calculated from

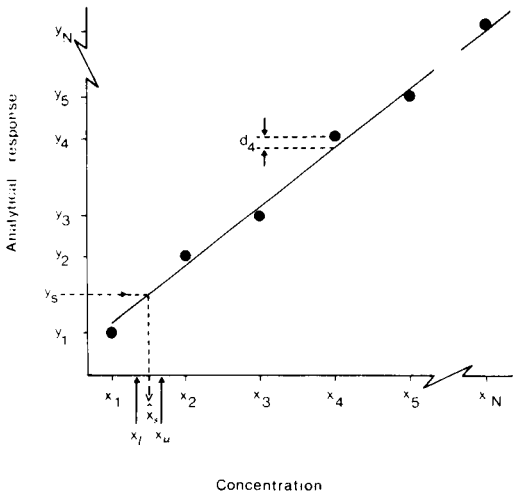

Fig. 1. Least-squares fitted calibration graph based on an evenly spaced distribution of calibration standards with concentrations ranging from x_1 to x_N. x_4y_4 is the 4th pair of associated x and y values, d_4 is the corresponding residual. y_s, analytical signal of the sample; $\hat{x}_s$, estimated concentration of the sample; x_l and x_u, the lower and upper limits respectively of the confidence interval for the true concentration of the sample.

$$s_y^2 = (N-2)^{-1} \sum_i d_i^2$$

If the conditions mentioned above are fulfilled, s_y is the best estimate for σ_y, and σ_y has the same value for calibration measurements at all concentration levels and for measurements of the analytical samples. In practice, analytical chemists are generally more interested in the value of $s_x = s_y\hat{b}^{-1}$, because s_x is an estimate of the quality of the analytical procedure, expressed in the same units as the content of the sample.

Solution of Eqn. (3) yields two values for v, denoted by v_1 and v_2. The lower limit, x_l, and the upper limit, x_u, of the confidence interval of x_s are expressed by $x_l = \bar{x} + v_1$ and $x_u = \bar{x} + v_2$. Consequently the interval for the true value x_s is given by $v_1 + \bar{x} < x_s < v_2 + \bar{x}$; and Δx, its width, by $\Delta x = x_u - x_l = v_2 - v_1$.

A simplified expression for confidence intervals

Equation (3) tends to conceal the factors jointly determining the precision of analytical results, as well as their relative influence on the precision. In this section, a more convenient expression for the width of confidence intervals is presented. Solving Eqn. (3), and writing for the sake of simplicity $(\hat{b}^2 - NK^2u^{-1}) = A$, yields

$$\Delta x = 2KA^{-1}[Nu^{-1}(\bar{y}_s - \bar{y})^2 + AN^{-1} + An^{-1}]^{1/2} \qquad (4)$$

Because in all cases of practical interest $\hat{b}^2$ is much larger than NK^2u^{-1} (see Appendix), further simplifications can be made. Replacement of $(\bar{y}_s - \bar{y})$

by $\hat{b}(\hat{\bar{x}}_s - \bar{x})$, where $\hat{\bar{x}} = n^{-1} \Sigma_1^n \hat{x}_s$, of u by $N\Sigma_1^N(x_i - \bar{x})^2$ and of $s_y\hat{b}^{-1}$ by s_x yields

$$\Delta x = 2t_c s_x \{[(\hat{\bar{x}}_s - \bar{x})^2 / \sum_1^N (x_i - \bar{x})^2] + N^{-1} + n^{-1}\}^{1/2} \quad (5)$$

When it is noted that $\bar{x}$ corresponds to the "centre of gravity" of the calibration graph, it becomes clear that for a given distribution of the calibration measurements the quantity $(\hat{\bar{x}}_s - \bar{x})^2$ depends on the location of the sample value in the concentration range for which calibration has been done, whilst the quantity $\Sigma_1^N(x_i - \bar{x})^2$ is determined by the number and distribution of the calibration measurements over the range. The value of the quotient of the quadratic terms in Eqn. (5) decreases rapidly with decreasing difference between the estimated value of the sample concentration and the centre of gravity of the calibration graph, and becomes zero when $\hat{\bar{x}}_s$ coincides with $\bar{x}$. Therefore the quotient, $(\hat{\bar{x}}_s - \bar{x})^2/\Sigma_1^N(x_i - \bar{x})^2$ is here called the eccentricity term, E. Substitution of E in Eqn. (5) finally yields a comprehensible expression for the uncertainty of results obtained by methods involving the use of calibration curves

$$\Delta x = 2t_c s_x (N^{-1} + n^{-1} + E)^{1/2} \quad (6)$$

A first and notable advantage of Eqn. (6) over Eqn. (3) is that Eqn. (6) expresses the precision of analytical results in terms immediately identifiable to the analytical chemist, viz. in terms taking into account the following aspects: t_c, the statistical level of significance; s_x, the standard deviation of the analytical procedure applied; N, n, the "invested labour", and E, the location of sample measurements in the calibration range.

The next step to be taken is to assess the relative importance of the above factors on the width of confidence intervals. For this purpose, special attention has to be given to the value of E. Its value is easily calculated for any possible distribution of the calibration measurements and for any location of the sample value. In the next section, calculation of E is discussed for one situation which is frequently encountered in analytical practice.

The eccentricity term E

For convenience, the numerator of the quotient constituting the expression for E is denoted by E_N and the denominator by E_D; thus

$$E = (\hat{\bar{x}}_s - \bar{x})^2 / \sum_1^N (x_i - \bar{x})^2 = E_N/E_D \quad (7)$$

In analytical work, the distributions of calibration points employed are usually evenly spaced, and when replicate calibration measurements are made, their number (m) at each of the calibrating concentration levels (k) is often the same. For such situations, which are often encountered in analytical practice, numerical values of E_D can easily be calculated because E_D can be written as

$$E_D = NL^2 f \tag{8}$$

where N is again the total number of calibration measurements and L the concentration range covered by the calibration graph $L = x_N - x_1$; and x_N is the highest calibrating concentration applied (see Fig. 1) or one of the (m) highest concentrations when m replicate measurements are done for each applied calibrating concentration ($N = km$). The quantity f in Eqn. (8) is a factor that depends on the way in which the total number of calibration measurements is distributed over the number of concentration levels used.

Table 2 shows numerical values of the f factor calculated for various k values and valid for evenly spaced distributions of the calibration measurements (including distributions of the "two clouds" type). [In the case of the "two clouds" type of distribution, "evenly spaced" is meaningless of course; obviously, this notation applies only when more than two concentration levels are involved.] For these calculations, equal m values within one particular calibration range are assumed. For calculation of the numerator of the eccentricity term, it should be borne in mind that for the calibration conditions discussed here, the location of the centre of gravity of the calibration graphs is situated halfway between x_1 and x_N and coincides with $\bar{x}$. Consequently, $\bar{x} = \frac{1}{2}(x_1 + x_N)$. The value of $(\hat{\bar{x}}_s - \bar{x})$, cf. eqn. (7), increases with increasing distance between $\hat{\bar{x}}_s$ and the centre of gravity. Considering $(x_N - x_1) = L$ and $(\bar{x} - x_1) = (x_N - \bar{x}) = L/2$, an eccentricity parameter ρ was introduced:

$$\rho = |\hat{\bar{x}}_s - \bar{x}|\, L^{-1} \tag{9}$$

The parameter ρ enables the eccentricity of $\hat{\bar{x}}_s$ to be expressed numerically in terms of its location with respect to $\bar{x}$. In the situations considered, ρ ranges from 0 to 0.5: $\rho = 0$ for $\hat{\bar{x}}_s = \bar{x}$, and $\rho = 0.5$ for $\hat{\bar{x}}_s = x_1$ and for $\hat{\bar{x}}_s = x_N$, showing minimal and maximal eccentricity, respectively. Consequently, the value of E_N ranges between 0 and $(0.5\ L)^2$. Replacement in Eqn. (7) of E_N by $\rho^2 L^2$ and E_D by $NL^2 f$ finally yields

$$E = \rho^2 L^2 (NL^2 f)^{-1} = \rho^2 (Nf)^{-1} \tag{10}$$

This shows that, for evenly spaced calibration points, E depends on ρ and f and is independent of L. Further, E is inversely proportional to N and this allows a further simplification. If B is defined as

$$B = (N^{-1} + n^{-1} + E)^{1/2} \tag{11}$$

TABLE 2

Numerical values of the f factor calculated for various k values and equidistant distributions of the calibration measurements

k	2	3	4	5	6	8	10	12	16	24	32
f	0.250	0.167	0.139	0.125	0.117	0.107	0.102	0.098	0.094	0.091	0.089

then Eqn. (6) simplifies to $\Delta x = 2t_c s_x B$. From Eqns. (10) and (11), it can be seen that

$$B = (n^{-1} + zN^{-1})^{1/2} \tag{12}$$

where

$$z = 1 + \rho^2 f^{-1} \tag{13}$$

The parameter z shows the relative importance of N and n to Δx. It depends on the eccentricity ρ and the number of calibration levels k. Some values are given in Table 3.

For $n \to \infty$

$$B = (zN^{-1})^{1/2} \text{ and } \Delta x = 2t_c s_x (zN^{-1})^{1/2} \tag{14}$$

This represents the contribution to Δx from the error made in the calibration procedure.

For $N \to \infty$, only the sample measurements contribute to Δx, and

$$B = n^{-1/2} \text{ and } \Delta x = 2t_c s_x n^{-1/2}$$

This is the same value as was found when no calibration is applied (see Eqn. 1).

RESULTS AND DISCUSSION

The factor t_c

The value of factor t_c depends on the level of significance (a value $\alpha = 0.05$ is applied here) and on the number of degrees of freedom, Φ, available, for estimating the standard deviation. Contributions to Φ are made by the experiments used for calculation of the calibration graph and by the replicate measurements on the sample under examination. Thus Φ is at least $N - 2 + n - 1 = N + n - 3$, with $N \geqslant 2$ and $n \geqslant 1$. For all or nearly all cases, however, many experiments are necessary to check if the conditions mentioned in the introduction are indeed fulfilled. Considering that (with $\alpha = 0.05$) $t_c = 2.08$ for $\Phi = 20$, $t_c = 2.04$ for $\Phi = 30$ and $t_c = 1.96$ for $\Phi = \infty$, it seems justified to apply a rounded-off value of $t_c = 2$ for most practical cases. (In the very impractical situation that $\Phi = 0$, no confidence region can be calculated.) Results of the calculations are given in Table 4 and in Figs. 2—4. The values of B are presented, and these must be multiplied by

TABLE 3

Values of z for some values of k and ρ

k	$\rho = 0$	$\rho = 0.25$	$\rho = 0.50$
2	1	1.25	2.00
5	1	1.50	3.00
32	1	1.70	3.81

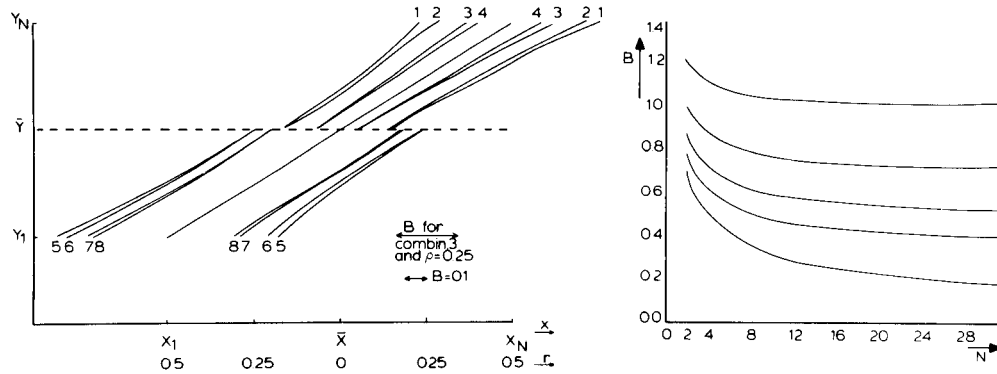

Fig. 2. Variation of the width Δx of the confidence region within the calibration range. B is shown as the distance between the two curved lines (see the example for combination 3 of N, n and k values). The value of Δx is found from $\Delta x = 2t_c s_x B$. Note that the B values are symmetrical with respect to the value $\bar{y} = (y_1 + y_N)/2$ (horizontal dotted line). Therefore, for $n = 3$, lines were drawn only in the lower half of the figure ($y < \bar{y}$) and, for $n = \infty$, only in the upper half ($y > \bar{y}$). Curves: (1) $N = 4$, $k = 4$, $n = \infty$; (2) $N = 4$, $k = 2$, $n = \infty$; (3) $N = 24$, $k = 24$, $n = \infty$; (4) $N = 24$, $k = 2$, $n = \infty$; (5) $N = 4$, $k = 4$, $n = 3$; (6) $N = 4$, $k = 2$, $n = 3$; (7) $N = 24$, $k = 24$, $n = \infty$; (8) $N = 24$, $k = 2$, $n = 3$. Evenly spaced calibration points are assumed, and m has the same value for all calibration levels.

Fig. 3. Variation of B with the values of N and n if the eccentricity $\rho = 0$. Evenly spaced singular calibration points are assumed ($k = N$).

$2t_c s_x$ in order to find Δx. If $\Phi > 20$ or 30 (see above), the value of t_c is the same for all N and n values, and the results given can be used directly for comparison of Δx values. If Φ is smaller and depends on N and n, the variation of t_c with Φ should be taken into account for comparison of Δx values.

An example of the calculation

For calibration, two replicate measurements were made at each of six calibration levels ($m = 2$, $k = 6$, $N = 12$). At x_i values of 1,2.....6, the signals y_i shown in parentheses were found:

$x = 1$ (12.42, 10.13) $x = 2$ (20.69, 22.56) $x = 3$ (31.88, 32.27)
$x = 4$ (40.76, 41.29) $x = 5$ (52.45, 54.20) $x = 6$ (62.27, 61.77)

The usual least-squares calculation gives: $\hat{a} = 1.1133$, $\hat{b} = 10.222$ and $s_y = 1.055$. Therefore $s_y/\hat{b} = s_x = 0.1032$. Measurements on the analytical sample ($n = 3$) gave $y_s = 15.42, 15.91, 14.17$. Thus $\bar{y}_s = 15.167$; $\hat{\bar{x}}_s = (15.167 - 1.113)/10.222 = 1.375$; $\bar{x} = 3.5$; $\rho = (3.5 - 1.375)/5 = 0.425$; $f = 0.117$ (Table 2); $E = 0.425^2/12 \times 0.117 = 0.129$; $z = 2.543$, $B = (1/3 + 2.543/12)^{1/2} = 0.738$.

Earlier experiments resulted in an estimate $s_y = 0.963$ with 20 degrees of freedom; the estimate for s_y from the replicate measurements on the sample is $s_y = 0.897$ with $\Phi = 2$. Thus an overall estimate for s_y from pooling all data gives

TABLE 4

Values of B for different values of N, n, k and ρ

		$\rho = 0$	$\rho = 0.25$				$\rho = 0.50$			
k	→	—[a]	2	4	8	24	2	4	8	24
N	n									
2	1	1.22	1.27				1.41			
2	3	0.91	0.98				1.15			
2	8	0.79	0.87				1.06			
2	∞	0.71	0.79				1.00			
4	1	1.12	1.15	1.17			1.22	1.30		
4	3	0.76	0.80	0.83			0.91	1.02		
4	8	0.61	0.66	0.70			0.79	0.91		
4	∞	0.50	0.56	0.60			0.71	0.84		
8	1	1.06	1.08	1.09	1.09		1.12	1.16	1.19	
8	3	0.68	0.70	0.71	0.73		0.76	0.83	0.87	
8	8	0.50	0.53	0.55	0.57		0.61	0.69	0.74	
8	∞	0.35	0.40	0.43	0.44		0.50	0.59	0.65	
24	1	1.02	1.03	1.03	1.03	1.03	1.04	1.06	1.07	1.08
24	3	0.61	0.62	0.63	0.63	0.64	0.65	0.67	0.69	0.70
24	8	0.41	0.42	0.43	0.44	0.44	0.46	0.49	0.51	0.53
24	∞	0.20	0.23	0.25	0.26	0.27	0.29	0.34	0.37	0.40

[a]For $\rho = 0$, B is independent of k.

$$s_p^2 = [20 \times 0.963^2 + (12 - 2) \times 1.055^2 + (3 - 1) \times 0.897^2]/32 = 0.978$$

and $s_p = 0.989$, thus $s_x = 0.989/10.222 = 0.0968$, for $\Phi = 32$, $t_c = 2$, $B = 0.738$ (see above) and $\Delta x = 4 \times 0.0968 \times 0.738 = 0.286$. For practical purposes, the centre of the confidence region can be considered to coincide with $\hat{\bar{x}}_s$, and so the true value is $1.232 < x_s < 1.518$.

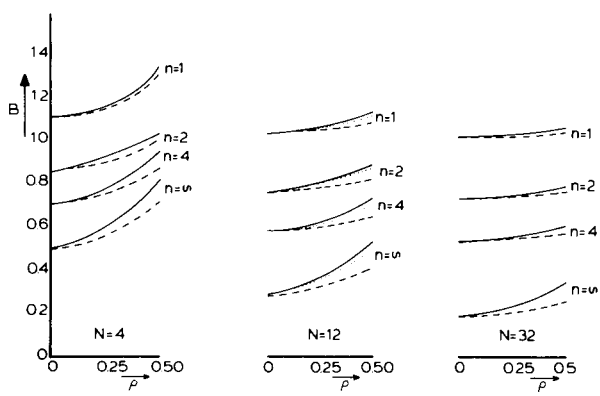

Fig. 4. Variation of B with the eccentricity ρ for $N = 4$, 12 and 32, for $n = 1$, 2, 4 and ∞, and for $k = N$ (—), $k = 2$ (---) and $k = \frac{1}{2}N$(....). For $N = 32$, the values for $k = N$ and $k = \frac{1}{2}N$ practically coincide. Evenly spaced calibration points are assumed, and m has the same value for all calibration levels.

CONCLUSIONS

The above calculations are valid only for cases in which the conditions stated in the introduction are fulfilled. One of these is the homogeneity of the variances over the whole calibration range. However, the variances are not homogeneous in all practical situations, as has been discussed previously [1]. In the example given above, where the condition is fulfilled, the relative standard deviation is about 10% at $x = 1$ and about 1.7% at $x = 6$. Generally, it can be said that the condition is not fulfilled for large values of x_N/x_1, but can be fulfilled for lower values of this ratio.

Though the work of Mandel [2] was published nearly two decades ago, it seems to have been seldom applied in analytical chemistry. Application of the results presented here seems to have some advantages, however: Eqn. (6) is more easily handled than Eqn. (3) and it gives a more direct insight into the relative importance of each of the parameters contributing to Δx. It may be possible to derive Eqn. (6) more directly than as described above from Eqn. (3).

Conclusions that can be drawn from Table 4 and Figs. 2—4 are as follows. First, replicate measurements on the same result in a (sometimes considerable) decrease of the width of the confidence intervals. Secondly, the influence of the eccentricity (ρ) is generally small, but excessive extrapolation should not be used. Thirdly, the influence of k on Δx is small in most cases: at first sight, this means that not much information is gained by using a small number of concentration levels in the calibration procedure. In routine analytical practice, however, many samples are often measured using the same calibration graph, but in such cases this small gain in information is obtained many times. (An objection sometimes made against calibrations with $k = 2$ is that linearity of the graph cannot be checked, but this is not always a realistic objection because in some practical cases non-linearity is not revealed even by procedures with high k values.)

Equations (12) and (13) suggest that for a given value of $(N + n)$, it is possible to optimize each of the values N and n. Unfortunately, two practical difficulties may be encountered: as mentioned above, the measurement of many samples is too often based on only one calibration graph; and the measurement of a sample generally requires more labour than measurement of a calibration standard. For these reasons this type of optimization is not as easy as might be suggested by Eqns. (12) and (13).

APPENDIX

The width of a confidence interval, Δx, can be expressed by Eqn. (5) provided that $NK^2u^{-1} \ll \hat{b}^2$. Substitution of $K = t_c s_y$, $u = N\Sigma_1^N(x_i - \bar{x})^2$, and $s_y = \hat{b}s_x$ into this expression gives $t_c^2 s_x^2 \gg \Sigma_1^N(x_i - \bar{x})^2$. This shows more clearly the analytical significance of the first condition, viz. the width of the analytical range calibrated has to be large compared to the experimental

error. In analytical practice, this condition will generally be fulfilled to a great extent.

REFERENCES

1 J. Agterdenbos, Anal. Chim. Acta, 108 (1979) 315.
2 J. Mandel, The Statistical Analysis of Experimental Data, J. Wiley, New York, 1964, Ch. 12.
3 V. V. Nalimov, The Application of Mathematical Statistics to Chemical Analysis, Pergamon, Oxford, 1963, Ch. 6.

Analytica Chimica Acta, 132 (1981) 139—155
Elsevier Scientific Publishing Company, Amsterdam — Printed in The Netherlands

THE APPLICATION OF pH GRADIENTS IN FLOW-INJECTION ANALYSIS
A Method for Simultaneous Determination of Binary Mixtures of Metal Ions in Solution[a]

D. BETTERIDGE* and BERNARD FIELDS
Department of Chemistry, University College of Swansea, Swansea SA2 8PP (Gt. Britain)
(Received 20th May 1980)

SUMMARY

Under static conditions, pH—absorbance curves are highly characteristic for a given metal ion—ligand combination. If the ligand is an unselective analytical reagent, such as 4-(2-pyridylazo)resorcinol, the pH—absorbance curve obtained by adding the reagent to a mixture of metal ions is similar to a multi-element polarogram. It can be used for the detection of components of the mixture and for their determination. The absence of air segmentation in flow-injection systems means that pH gradients form over the sample/carrier interface when basic solutions are injected into acid carrier streams, or vice versa. Thus there is the possibility of obtaining pH—absorbance curves under the dynamic conditions of flow injection analysis (f.i.a.). Procedures for the creation of known and reproducible pH gradients are given and discussed. The pH-gradient flow-injection method is evaluated by determining with 4-(2-pyridylazo)resorcinol (PAR) binary mixtures of (a) cobalt(II) and manganese(II) and (b) nickel(II) and copper(II) in the presence of similar amounts of cobalt(II) in the ppm range. In the latter example cobalt is kinetically masked by virtue of the relatively slow dissociation of the $Co(HPAR)^+$ complex. Wide or narrow pH changes may be used, the choice being dependent on the critical pH range for complexation. The procedure is simple and accurate, and may be suitable for the rapid determination of a range of mixtures.

The complexation of metal ions with most spectrophotometric reagents, and especially with those ligands which may be protonated, is dependent on the pH of the reaction medium as well as on the nature and concentration of the ligand concerned. Plots of pH vs. absorbance, such as those obtained under static conditions with a number of metals and 4-(2-pyridylazo)resorcinol (PAR) (Fig. 1) are readily established. Such plots are characteristic for any given metal ion—reagent combination and they are additive if the reagent is in large excess. The shape of a curve obtained for a mixture of metal ions takes the form of a series of stepwise increases in absorbance toward higher pH as each metal reaches the pH at which complexation takes place. Provided that the pH regions of increasing absorbance do not overlap, the concentration of each metal may be determined from the absorbance change at each

[a]This paper was presented in part at the Conference on Flow Analysis, Amsterdam, September, 1979.

0003—2670/81/0000—0000/$02.50

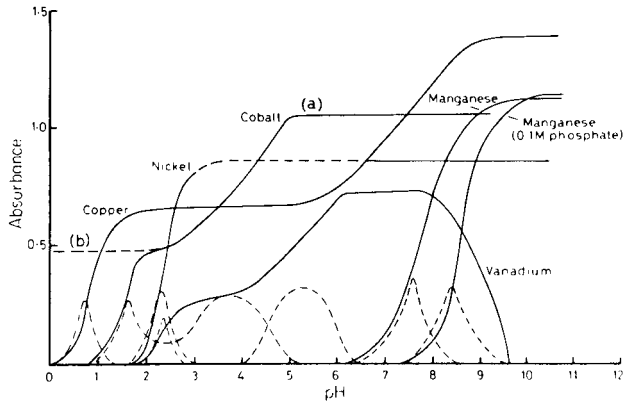

Fig. 1. pH—absorbance curves for the complexes of copper(II), nickel(II), cobalt(II), vanadium(V), and manganese(II) with PAR under static conditions. In the pH range 3—6.5, the nickel(II) complex precipitates slowly. The dashed curves are the first derivatives.

step and each element may be identified by the pH at the point of inflection. These curves are time-consuming to prepare if measurements are made under static conditions. However, the essential information can be obtained in a few seconds by application of flow injection analysis (f.i.a.).

Modifications to the general shape and position of the complexation curve may be brought about as a consequence of side-reactions with hydroxyl ion and/or auxiliary ligands. These do not affect the general conclusions about the value of the information to be obtained from pH—absorbance curves. Indeed, as will be evident from the curves in Fig. 1 for manganese(II), side-reactions can be used to improve the separation of inflection points.

In this paper, theoretical and practical considerations in the construction of known and reproducible pH gradients are discussed, and some examples of analytical application of pH-gradient flow-injection systems to trace metal determination are given. It is shown that pH gradients over a narrow range (ΔpH = 2) and a wider range (ΔpH = 9) can be obtained easily and reproducibly. The importance of the rate of reaction is also demonstrated.

ESTABLISHMENT OF pH GRADIENTS IN THEORY AND PRACTICE

Theory

The pH at any point along the tube when a sample of strong acid has been injected into a carrier stream of weak base will be governed by the extent of chemical reaction which has taken place between the acid and base, and by the physical distribution of the acid and base along the tube. The effect of the chemical reaction follows from elementary acid—base theory. If an acid of concentration C_A and acidity constant K_a with a base of concentration C_B, and the fraction of acid present after reaction, f_A, is defined as $C_A/(C_A + C_B)$, then

$$pH = pK_a - \log[f_A/(1 - f_A)] \quad (1)$$

Within the limits of buffering action, $0.1 < f_A < 0.9$, there is an approximately linear relationship between f_A and pH.

In a flowing system the physical distribution of the injected acid will follow a dispersion pattern, which in its most general form is described by the *C*-curve [1, 2]

$$C_\theta = [2(\pi D/uL)^{1/2}]^{-1} \exp[-(1-\theta)^2(4D/uL)^{-1}] \quad (2)$$

where C is the concentration, $\theta = t/\bar{t}$, t is the time of the measurement, $\bar{t}$ is the mean residence time, D is the diffusion coefficient, u is the flow rate and L the length of tube. Figure 2 outlines such a dispersion. These considerations do not take into account the mode of mixing, which is of course crucial. Taylor, in a seminal paper [3], showed that in narrow tubes at low flow velocities, radial molecular transport plays an important role in bringing about mixing of sample and carrier, and indeed may predominate at very slow flow rates. If the tube were considered as a series of segments, in any one of which the concentration of acid and base were given by the *C*-curve (Fig. 2) and if mixing were by radial diffusion, a pH gradient would be established across the sample plug, the gradient being alkaline at the circumference and acidic at the centre.

Given the arrangement of the apparatus described below, with coils and Y-junctions and given the flow rates employed, this model is a gross oversimplification. Nevertheless, it provides a useful starting point for considering the results below. Whatever the mechanism of mixing, the process is efficient and the net effect of physical dispersion and chemical reaction is that the predicted pH gradient follows the line of the *C*-curve, with the pH at the points of inflection corresponding to pK_a of the weak base if C_A^0 and C_B^0 are equal.

Insofar as the physical dispersion is easy to control and vary, and is reproducible, it is a straightforward matter to alter the pH gradient to suit requirements. The range of pH over the gradient is governed by the choice of weak base. A simple base is used if the pH range is to be narrow but a universal buffer is used if the pH range is to be great. The argument is the same for a

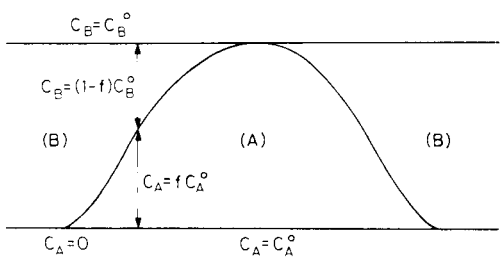

Fig. 2. Schematic radial distribution of a sample of acid in a carrier stream of base. C_A^0 and C_B^0 are the initial concentrations of acid and base, and C_A and C_B the concentrations of acid and base at point x.

strong base injected into a weak acid or series of weak acids as in the following pH gradient for a buffer with a linear pH titration curve including a modified calculation at high acidity.

Flow-injection system for producing pH gradients

Several experimental arrangements were tried, the most convenient being that shown in Fig. 3A. A sample of sodium hydroxide is injected into a carrier stream of distilled water and is allowed to disperse in a wide bore coil. The addition of the dispersed hydroxide peak to the acidic universal buffer produces a pH gradient in the final coil before the detector. The sequence of pH-dependent reactions involving metal complexation takes place as the streams converge.

The advantages of this configuration are that the pH gradient is established independently of the actual sample and can therefore be varied at will, that the sample stream is acidic, and that the sequence of complexing reactions

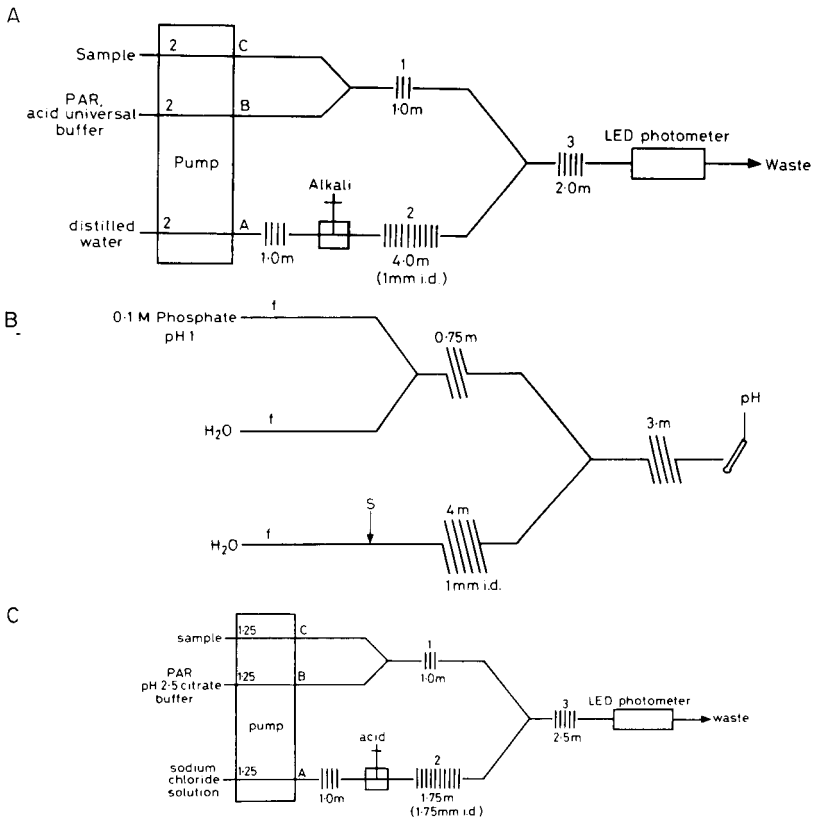

Fig. 3. Flow-injection systems: (A) for the determination of cobalt(II) and manganese(II) simultaneously; (B) for obtaining and measuring pH gradients with phosphate and Britton and Robinson buffer solution; (C) for the simultaneous determination of nickel(II) and copper(II) in the presence of cobalt(II). All coils are of 0.86 mm i.d. tubing unless stated. The numbers on the pump tubings are flow rates in ml min^{-1}.

takes place from low to high pH. Alternative arrangements in which the sample was injected into the carrier required either the sample to be alkaline or for the complexation reactions to take place in a sequence from high to low pH. Both variations would exacerbate problems caused by hydroxy complexes. These are avoided in the proposed configurations. The trade-off is in the use of a large sample volume of the metal ion solution; the sample is pumped continuously through the reaction zone and as much as 5 ml may be required per measurement. However, this is not necessarily disadvantageous because it is well suited for operation in conjunction with an automatic sample changer.

To obtain a pH gradient of wide range, Britton and Robinson universal buffer solution [4] was used.

EXPERIMENTAL

Reagents and apparatus

Analytical reagent-grade chemicals were used unless otherwise stated. Stock metal ion solutions of ca. 10^{-2} M were standardized by titration with EDTA and diluted as required. Solutions of salts for buffers were prepared with distilled water.

Flow-injection system for studies with buffer systems. The arrangement for the study of pH changes in standard buffer systems is shown in Fig. 3B. The detector was a combined glass-calomel electrode assembly.

Flow-injection system for cobalt and manganese determinations. The flow system is outlined in Fig. 3A. The peristaltic tubing and pump speed were chosen to give a flow rate of 2 ml min^{-1} in each of the three streams. Sodium hydroxide solution was injected from a disposable plastic syringe through a septum valve [5]. All coils were of 0.86 mm i.d. polypropylene tubing unless otherwise stated.

The reagent solution (1 l) contained 11.9 ml of 36% hydrochloric acid, 238 ml of Britton and Robinson universal buffer solution, and 200 ml of 5×10^{-3} M PAR solution. Then concentrated hydrochloric acid was added dropwise with rapid stirring until the pH was reduced to 2.24; PAR precipitates at about pH 4 but redissolves at pH 3.

Flow-injection system for copper and nickel determinations. A diagram of the system is presented in Fig. 3C. The flow rate was 1.25 ml min^{-1} in each stream. The wide-bore coil of 1.5 mm i.d. gives increased dispersion.

Sodium chloride solution (112 g l^{-1}) which has the same refractive index as the injected hydrochloric acid solution, was used in stream A (Fig. 3C) to ensure that no refractive index peak was observed when the injected hydrochloric acid passed through the cell. The reagent solution was 10^{-3} M in PAR and 10^{-2} M in sodium citrate, adjusted to pH 2.5 with hydrochloric acid.

Detection system for determinations of cobalt and manganese. A phototransducer was constructed using a gallium phosphide light-emitting diode (LED) (maximum emissivity 565 nm) and a silicon phototransducer acting

as light source and sensor, respectively, as described earlier [6]. A modification was that the light path of 1.5 mm was normal to the direction of flow. The current signal from the phototransistor is converted to voltage by a current-to-voltage converter from which it is directly available for differentiation digitally in a Datalab 4000L microprocessor-based signal analysis system. The Datalab 4000L has a smoothing routine which was used as required. Both the transmittance and differential signal were recorded on a chart recorder.

Detection system for determination of copper and nickel. The detection system was the same as that described above except that a specially-built analog electronic differentiator was used and both transmittances and differentiated signals were output on chart recorders run at the same speed.

In order to determine the absorbance from the transmittance recordings, the initial light intensity I_0 is recorded from the change in signal with the LED on and off with distilled water in the cell. Because the changes in absorbance are generally small, it is convenient to measure the transmittance T and to calculate the absorbance from the relationship $A = \log [I_0/(I_0 - T)]$.

Procedures

Determinations of cobalt(II) and manganese(II). Sample solutions of cobalt(II) and manganese(II) in the ppm range enter the analytical system as stream C and 0.5 ml of 0.575 M sodium hydroxide is injected into the distilled water stream immediately after changeover of samples. Sample changeover is achieved by stopping the pump and moving the pump tubing from one sample to the next. Because of the lengths of coils chosen, the sample solution reaches "steady state" in coil 3 before the hydroxide plug reaches the confluence. In practice, about 5 ml of sample solution is required per determination and each determination takes 2 min.

Determinations of copper(II) and nickel(II). Samples were passed through the system in the same way as for the determination of cobalt(II) and manganese(II), and 0.5 ml of 2.25 M hydrochloric acid was injected into stream A.

RESULTS AND DISCUSSION

Construction of pH gradients

The flow-injection principle provides a simple means of producing pH gradients. The method used previously in which an acidic solution was injected directly into an alkaline buffer system produced very steep gradients because the concentration curve of acid distribution increased at the same time as that of the alkali decreased [7, 8]. The two complexes of interest in that study were produced mutually exclusively at the two pH extremes and so the shape of the pH gradient was of little consequence.

By injecting a solution of alkali into an unbuffered stream and allowing the *C*-curve distribution of alkali to mix at a confluence with a constant concen-

tration of acid buffer, a more gradual pH change is produced. Furthermore, because the alkali distribution may be determined from simple dispersion experiments with indicators, and the acid equivalents of the buffer stream are known and constant, the pH-gradient parameters can be predicted reasonably well.

Britton and Robinson universal buffer solution [4] is such that over the pH range 3.8—8.8 the pH value varies almost linearly with added volume of 0.2 M sodium hydroxide solution. Good pH control can be maintained, however, between pH 2 and 12. In the present application, this buffer is adjusted to an appropriate pH low enough to ensure that no chelates are formed in the coil before the confluence with the alkali. Sodium hydroxide solution injected into stream A (Fig. 3A) passes through a dispersion coil whose dimensions are chosen to ensure large dispersion, according to known principles [1, 2]. For a given acid buffer composition, the volume and concentration of sodium hydroxide injected are such that C_{max}, the concentration of hydroxide at the peak of the concentration curve when passing through the detector, is sufficient when mixed with the sample/reagent/buffer to raise the pH to that required to form both chelates.

The most important experimental variables are the volume of sodium hydroxide injected, the diameter of coil 2 and the relative rates of flow at the point of convergence. The volume and concentration of sodium hydroxide required can be calculated from the known concentration of buffer solution, the dispersion and the relative flow rates of the merging streams. The lateral dispersion of the hydroxide is increased by using for coil 2 a tube of relatively wide bore, 1—1.5 mm i.d. compared to the 0.86 mm i.d. tubing used throughout the rest of the system. The effect of having the ratio of flow between the sample/reagent and hydroxide streams at 2:1 is to increase the dispersion by a factor of 3 but the buffer and hydroxide are still mixed in a 1:1 ratio.

The equations given below predict a pH gradient in the system with a range from 1.3 to 10.7. The actual gradient ranged from approximately pH 1.4 (measured with a glass electrode) to pH $\approx$10.4 as deduced from the complexation reactions.

Calculation of the useful working pH range

The relationship between pH and volume, V, of 0.2 M sodium hydroxide, added to 100 ml of Britton and Robinson buffer solution is

$$pH = 3.91 + 0.0853V \quad (3)$$

within the linear range of buffer [4]. From this equation, expressions for the pH at any point over the sample may be obtained [7] from the concentration of the injected hydroxide $[OH]_0$, the dispersion D which is a measure of [OH] at any point in the sample plug, the concentration of strong acid ([A], or —[A] for strong base) which is added to the buffer in order to achieve the starting or base-line pH, and C_{ST}/C_B which is the concentration

of buffer used relative to the standard concentration C_{ST} for which Eqn. (3) applies. The equations assume that for $2.5 < pH < 11.5$ the effect on pH of dilution of solution is negligible.
The equations are

$$pH = -\log_{10}\left(\frac{[A]}{2} - \frac{[OH]_0}{D} - \frac{(3.91 - 2.5)}{42.7}\frac{C_B}{C_{ST}}\right) \quad \text{(for pH} < 2.5) \quad (4)$$

$$pH = 3.91 + 42.7\,(C_{ST}/C_B)\{([OH]_0/D) - [A]\} \quad \text{(for } 2.5 < pH < 11.5) \quad (5)$$

$$\Delta pH = 42.7\,(C_{ST}/C_B)[OH]_0/D \quad \text{(for } 2.5 < pH < 11.5) \quad (6)$$

where ΔpH is the pH range of the gradient. A working value for the dispersion, D, is calculated from $D = A_0/A_{max}$, where A_0 is the absorbance of the detector cell full of an indicator and A_{max} is the maximum absorbance of an injected sample of the indicator.

It is possible in this way to deduce the amount of hydroxide which must be injected to achieve a particular pH range, and to estimate the pH-gradient shape.

Experimental verification of pH gradients

Figure 4 demonstrates a practical method of predicting the pH gradient obtained from the buffer and hydroxide concentrations and the distribution of hydroxide. Figure 4(1) is the transmittance peak obtained for a sample of 0.5 ml of xylenol orange injected into the system; this corresponds to the distribution of hydroxide when 0.5 ml of hydroxide is injected in an actual determination. The actual hydroxide concentration passing through the detector is given by calculating the absorbance, A, of the indicator for a series of points on the curve. Thus $[OH] = [OH]_0\,A/A_0 = [OH]_0/D$, where A_0 is the absorbance of injected dye and $[OH]_0$ is the initial hydroxide concentration.

Appropriate substitutions in Eqn. (5) for conditions where the concentration of the universal buffer solution was 0.0794 of its standard concentration and an additional hydrochloric acid concentration of 0.0485 M was used to achieve the base-line pH, for each point, gave curve (b) of Fig. 4(2), which is a prediction of the pH gradient over the linear range of the buffer. D_{peak} was found to be 9.4. Clearly at pH less than 2.5, these points are not valid; there the pH is determined predominantly by the excess of acid, and the pH gradient is predicted simply from Eqn. (5). These points are plotted as sections (c) of Fig. 4(2).

When a mixture of cobalt(II) and manganese(II) is examined a pH—transmittance profile is obtained. The actual pH gradient may also be deduced from this curve and from Fig. 1 which shows the pH—absorbance curves for the PAR chelates of cobalt(II) and manganese(II) obtained under static conditions. Thus curve (d) of Fig. 4(3) is the pH gradient given by determining the proportion of each complex formed from curve (c) of Fig. 4, and by matching that with the corresponding degree of complexation shown in Fig. 1, calculating the pH.

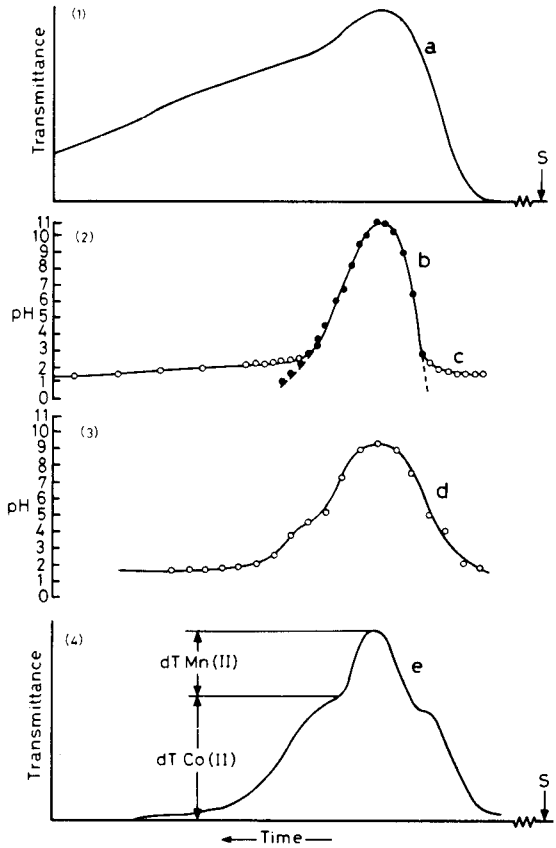

Fig. 4. Experimental and calculated pH—T curves for dye and Co(II)—Mn(II)—PAR mixtures. (1) The distribution of xylenol orange at a fixed pH injected into the stream found experimentally; the same distribution was given by an equal volume of sodium hydroxide solution. (2) Curve b is the calculated pH gradient using the hydroxide concentrations obtained from curve a (see text) and curve c is the calculated pH gradient using Eqns. (4) and (5). (3) The pH gradient calculated from absorbances of cobalt(II) and manganese(II) complexes with PAR. (4) Transmittance—time curves for the cobalt(II) and manganese(II) complexes of PAR over the pH gradient.

The predicted position of the pH gradient from the hydroxide distribution and the pH—absorbance curves match well. Both show that for this particular system extensive changes in pH occur only over a small part of the total hydroxide peak. (The indicator concentration approaches zero after twice the time shown in Fig. 4(1)). The predicted gradient is somewhat sharper than that manifested in the absorbance changes.

Non-linear buffers

For solutions of buffers whose buffer capacity varies with pH, pH gradients may be expected which resemble pH—titration curves of the buffer. A flow-

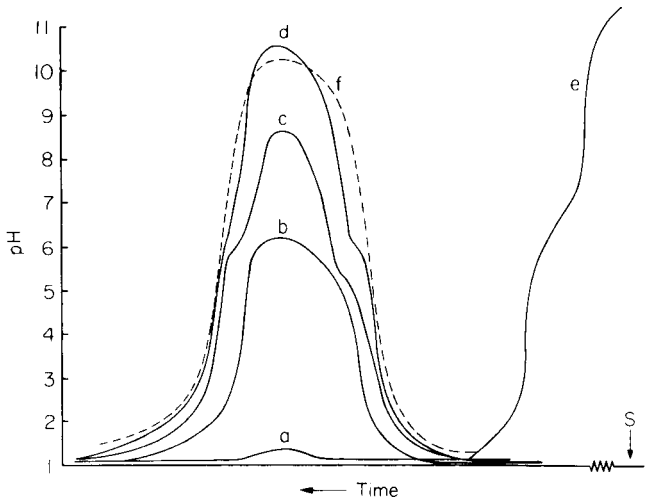

Fig. 5. pH vs. time curves for the addition of hydroxide to buffers compared with static titration. (a—d) 0.5 ml of NaOH injected with 0.1 M H_3PO_4 adjusted to pH 1, for NaOH concentrations of (a) 0.5 M, (b) 0.65 M, (c) 0.75 M, (d) 0.75 M, at a flow rate, F, of (a—c) 1.55 ml min^{-1}, (d) 0.32 ml min^{-1}. (e) Titration curve for phosphate under static conditions. (f) Britton and Robinson buffer solution with 0.5 ml of 0.75 M NaOH injected and a flow rate of 1.55 ml min^{-1}.

injection system for recording these curves is shown in Fig. 3B. Figure 5 shows such curves for a solution of phosphoric acid.

The solution shows high buffer capacity at pH regions corresponding to those on the static curves (Fig. 5, curve e). The peak pH may be controlled by the concentration of alkali injected (compare curves a—c), by the volume injected or by the flow rate (compare curves c and d). The peak pH for curve (d) is greater than for (c) because a slower flow rate decreases dispersion. In contrast, the pH—time curves for the Britton and Robinson buffer solution (Fig. 5, curve f) show no sharp changes in buffer capacity. The shapes and peak heights of the curves were highly reproducible; for example, the standard deviation of the peak pH for curve (c) was 0.12 pH units in a pH change of 7.45 units.

The above study shows that predictable and reproducible pH gradients can be generated under conditions of continuous flow analysis by a simple injection procedure. The proposed system is a great improvement over the direct injection of acid and sample described earlier [8].

The determination of mixtures of cobalt(II) and manganese(II)

pH-gradient flow-injection curves for cobalt(II) and manganese(II) with PAR. Figure 1 shows the pH—absorbance curves for the $Co(PAR)_2$ and $Mn(PAR)_2$ complexes under static conditions and the positions of the derivative peaks expected from the pH—absorbance curves.

Figure 6 shows pH—transmittance curves for $Mn(PAR)_2$ and $Co(PAR)_2$ obtained by pH-gradient flow-injection analysis, and the respective first-

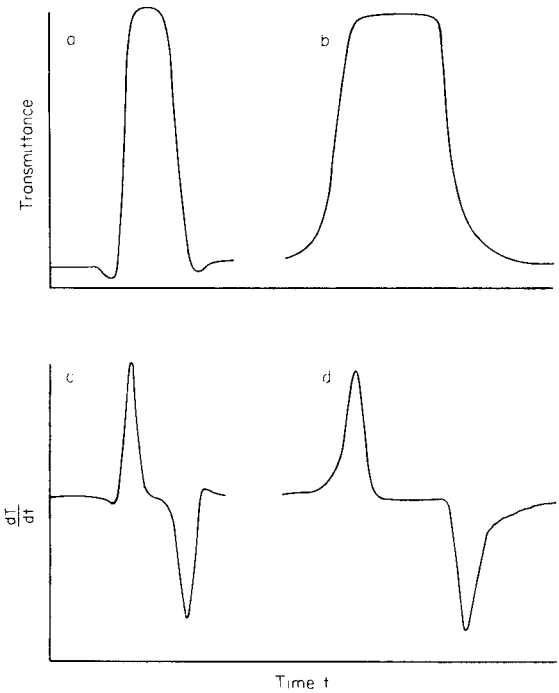

Fig. 6. pH—transmittance curves for (a) manganese(II) and (b) cobalt(II) with PAR, and their respective first-derivative curves (c, d).

derivative curves. These curves show not only the absorbance increase toward higher pH but also the reverse as the pH decreases. Strictly they are transmittance vs. time curves because the pH does not change linearly with time, but it is clear from the different time spans for formation of the $Co(PAR)_2$ and $Mn(PAR)_2$ complexes that the system follows closely that predicted from the static curves. The pH—transmittance curves for the other metals given in Fig. 1, i.e., copper, nickel and vanadium, are presented in Fig. 7 for comparison. It is to be noted that there are considerable qualitative differences between them.

Simultaneous determination of cobalt(II) and manganese(II) with PAR. Figure 8A shows transmittance curves for a series of mixed solutions of cobalt(II) and manganese(II) ions where the manganese(II) concentration was held constant at 1.5 ppm while the cobalt(II) concentration was increased. The absorbance shows a clear stepwise increase from $Co(PAR)_2$ to $Mn(PAR)_2$ formation. Figure 8B shows the absorbances calculated and plotted against concentration. For cobalt(II), the absorbance was measured from the base-line to the absorbance step and for manganese from this step to the peak. Good linear calibration graphs were obtained, showing no mutual interference. At low cobalt concentrations, there are small decreases in absorbance between the increases caused by $Co(PAR)_2$ and $Mn(PAR)_2$; these

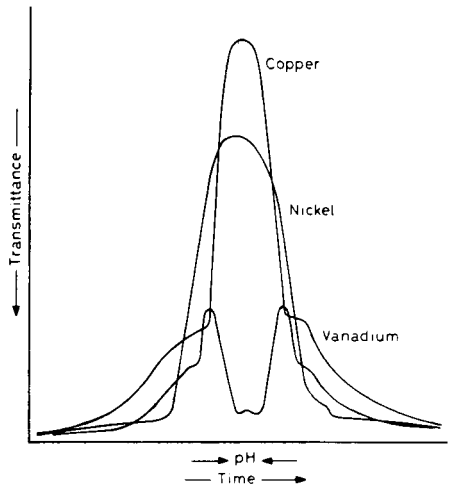

Fig. 7. pH—transmittance curves for copper(II), nickel(II) and vanadium(V) with PAR (cf. Fig. 1).

decreases are due to slight changes in the reagent background absorbance with an acid dissociation of PAR between pH 5 and 7.

A negative injection peak occurs in this and all such systems as a result of the nature of the injection process: injection of the alkali solution forces distilled water in stream A (Fig. 3A) into the weakly coloured reagent stream at the confluence. If the dispersion coil, as in this case, is sufficiently long, the peak passes through the detector before the arrival of the pH gradient.

Figure 9A shows the first derivative of the transmittance curves in Fig. 8A. For both the leading and trailing (positive and negative) pH gradient, two peaks are observed which are almost completely resolved. Figure 9B shows the plots of the peak heights versus concentration. These prove the validity of using derivative plots in flow injection analysis. Tests with a series of concentrations of a single metal ion showed that good linear calibration graphs were obtained provided that the reagent was present in large excess.

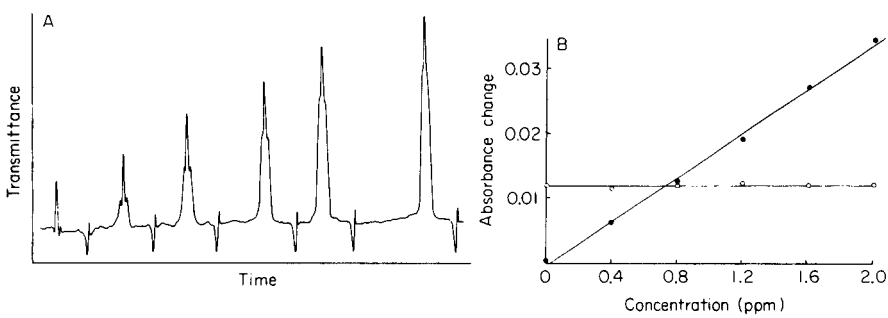

Fig. 8. Determinations on mixtures of cobalt(II) and manganese(II) solutions. (A) Transmittance vs. time; (B) calibration graph of absorbance vs. concentration. Cobalt concentration (•) varies; manganese concentration (○) is 1.5 ppm.

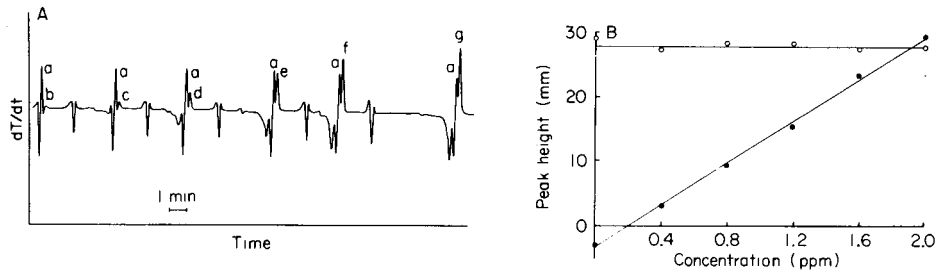

Fig. 9. (A) Derivative of the transmittance curve given in Fig. 8A. (B) Calibration graphs of peak heights. The manganese peaks are indicated by (a) and the cobalt peaks by (b—g).

The theoretical parameters which govern the nature of the pH—absorbance curve are complex and a theoretical curve can be arrived at only if side-reactions with other ligands and the possibility of the formation of complexes of more than one stoichiometry are taken into account. Any changes in slope will be emphasised by the derivative of the curve. Figure 10A shows the transmittance traces obtained when increasing amounts of manganese were determined in the presence of 1.5 ppm cobalt; the derivative curve is shown in Fig. 10B. The calibration graphs corresponding to these traces are shown in Figs. 11A and B.

Simultaneous determination of copper and nickel with PAR with kinetic masking of cobalt

The system described above reaches equilibrium rapidly so the static pH—absorbance curves can be used as a guide to the dynamic conditions of f.i.a.

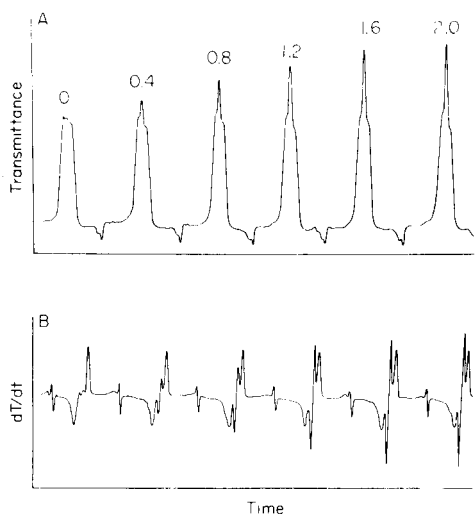

Fig. 10. Determination on mixtures of cobalt(II) and manganese(II) solutions with the cobalt(II) concentration constant at 1.5 ppm. The manganese(II) concentrations (ppm) are indicated on the peaks. (A) Transmittance vs. time; (B) first derivative.

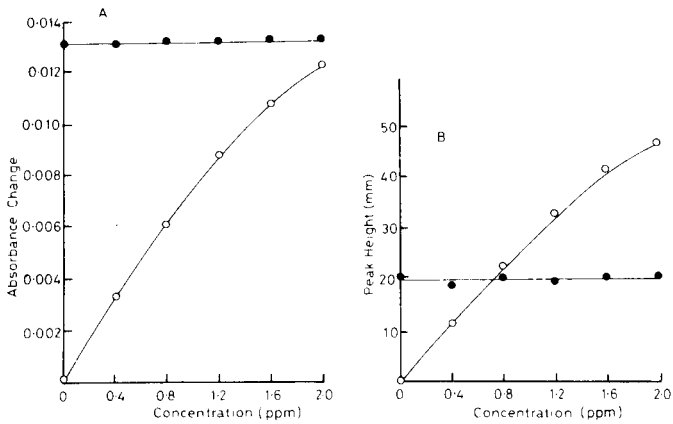

Fig. 11. Calibration graphs for manganese(II) obtained from Fig. 10A and B, respectively. A scale adjustment (1/2) has been made for the cobalt readings.

The effect of using a system in which the rate of reaction is slow compared with the rate of dispersion will now be considered. It was decided to test the method in relation to the possible analysis of an effluent from a local industrial plant. The effluent contained 1—5 ppm nickel(II), about 1 ppm copper(II) and less than 0.5 ppm cobalt(II). All three ions form PAR complexes in the pH range 0.5—3 (Fig. 1) so that the pH gradient must be narrow if the metals are to be resolved. Preliminary experiments showed that copper and nickel ($\Delta pH_{1/2} \approx 1$) could be readily resolved but it proved impossible to differentiate cobalt from either ($\Delta pH_{1/2} \approx 0.5$). However, the cobalt may be kinetically masked. The technique utilizes the slow kinetic rate of the reaction $Co(HPAR)^+ + H^+ \rightarrow Co^{2+} + H_2PAR$ at high acidity [7] to stabilize the absorbance caused by cobalt(II) while changes in absorbance of the copper and nickel complexes with pH are measured. Thus the complexes of all three metal ions are formed and the pH gradient goes from high to low pH.

When the complexes are formed in a neutral solution which is then acidified, the complexes of Cu(PAR) and $Ni(PAR)_2$ dissociate rapidly and the absorbance follows pH as indicated in Fig. 1 (curve a). However, although $Co(PAR)_2$ dissociates to $Co(HPAR)^+$ and PAR rapidly down to pH 2.5, the dissociation of $Co(HPAR)^+$ is very slow and the absorbance does not change down to pH 0, so that the curve follows curve (b) in Fig. 1. Under such circumstances, the absorbance of $Co(HPAR)^+$ remains effectively constant over the pH range 0—2.5 in a flow system.

The experimental procedure for f.i.a. is to arrange that the complexes form in coil 1 (see Fig. 3C) in the citrate buffer at pH 2.5. An acid injection of 2.25 M hydrochloric acid then establishes the required pH gradient (pH 2.5—0). Owing to the narrow range of pH gradient required, a simpler buffer system may be used rather than a complex mixture with uncertain masking effects. Citrate provides an almost linear titration curve with hydrogen ions

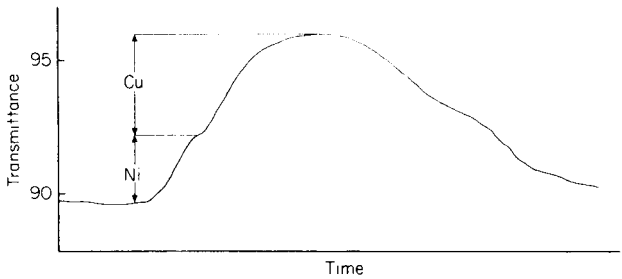

Fig. 12. pH—transmittance curve for a mixture of copper(II) and nickel(II) obtained with PAR, illustrating the positions of absorbance determinations.

over the pH range 4—1.5, and the hydrochloric acid concentration controls the pH over the remainder of the range.

Figure 12 shows the form of the transmittance curve obtained. As expected from the direction of the pH gradient, the nickel complex dissociates first, followed by the copper complex. The pH ranges over which the two complexes dissociate are very close and are separated only by an inflection. In order to determine the precise position at which the absorbance should be measured, the derivative of the curve is recorded simultaneously, the minimum giving the position of the inflection; the light intensity is then recorded on the transmittance curve and the absorbance is calculated. The absorbance is also calculated at the peak and at the base-line, allowing the change in absorbance for each complex to be determined. All measurements are made on the leading interface. Figure 13 shows calibration curves for nickel(II) in the presence of a constant copper(II) concentration of 1.5 ppm, and for copper(II) with a constant nickel(II) concentration of 2 ppm. The graphs are good and little mutual interference is observed. If the derivative peak heights are plotted against concentration, good calibration curves are again obtained.

The solution containing 2 ppm copper(II) and 2 ppm nickel(II) was measured again after it had been made 0.5 ppm with respect to cobalt(II); there was no effect on the final results. The complex $Co(HPAR)^+$ is formed in the system and results in a shift in the base-line but this absorbance remains constant over the pH gradient. Other transition metal ions expected in the effluent, within the limits indicated, were tested as potential interferences. No interference was caused by 10 ppm levels of manganese(II), lead(II), zinc(II) or chromium(III) but iron(II) interfered at the ppm level.

The pH limits for this system were chosen for a number of reasons. First, at pH values between 2.5 and 6 the nickel complex forms a precipitate a few minutes after preparation. The pH and time for formation of this precipitate is buffer-dependent and the presence of citrate allows the use of a pH somewhat in excess of 2.5. Secondly, the formation of $Co(PAR)_2$ ($pH > 2.5$) will result in changes in the absorbance of cobalt itself which may interfere with the determination. Thirdly, the pH extremes are chosen according to the relative proportions of the two analytes in the samples.

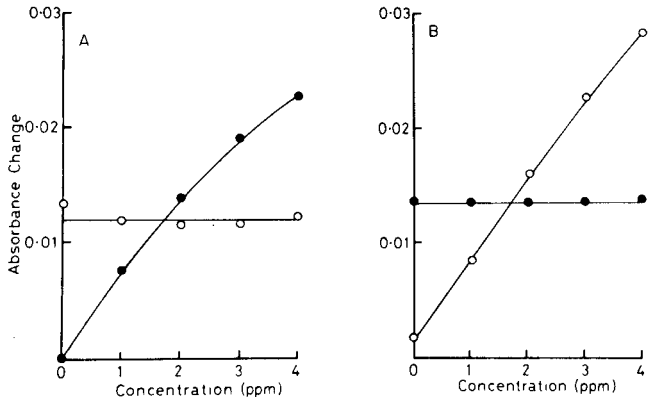

Fig. 13. Calibration curves for nickel and copper. (A) [Ni^{2+}] varied, [Cu^{2+}] constant at 1.5 ppm. (B) [Cu^{2+}] varied, [Ni^{2+}] constant at 2.0 ppm.

The absorbance measurements are limited by the width of the chart paper in the present system, so that best accuracy for both analytes is achieved if the absorbance changes are of the same order. The pH limits are used to restrict the proportion of nickel in the sample that forms the complex, thereby altering the slope of the calibration curve. If the nickel concentration is high, the upper limit should be reduced. Similar ideas may be applied to controlled dissociation of the copper complex. If the copper(II) concentration is relatively high, the amount of acid injected should be reduced. Within a series, however, consistency must be maintained.

In all such systems, pH changes occur continuously at all points in the stream and generally, although not always, it is desirable for the thermodynamically predicted equilibria to follow closely, in terms of time, the pH changes, in order that predicted pH—absorbance curves occur. It is important therefore that the complex formation and dissociation reactions are rapid.

Buffer effects

Manganese(II) precipitates in alkaline solutions as a hydroxide or with buffer components such as phosphate or borates. Similar precipitations occur with nickel, copper and cobalt at varying pH but mainly under conditions of pH > 8. In order that the $Mn(PAR)_2$ chelate may be formed at pH 9 it is necessary to mask the manganese initially, and this may be done with ascorbic acid [9]. In the Britton and Robinson buffer system, precipitation of insoluble metal complexes was found not to occur below pH 10 provided that the citrate concentration remained above that of the metal ions; here, citrate appears to be the effective masking agent. In the presence of the amounts of these constituents in coil 3 (Fig. 3C), i.e., ca. 10^{-5} M metal ion and 3.3×10^{-3} M citrate, the pH at which precipitation of the metal hydroxides occurs from pM—pH plots [10] is 12.5 for manganese(II) and cobalt(II). Hydrolysis of the metal—citrate complex occurs for nickel(II) at pH 11.5 and copper(II) at pH 12 under the same conditions [7].

The dissociation of complexes formed between metal ions and buffer components may become the rate-determining step in the PAR complex formation. Such a case is presented by the reaction: Ni(cit) + 2 PAR → $Ni(PAR)_2$ + cit (where cit = citrate), the dissociation of the nickel citrate being the rate-determining step [7]. In such systems coil lengths must be sufficient to allow equilibrium to be attained where necessary. In the determination of nickel and copper, the total length of coils 1 and 3 ensures that the $Ni(PAR)_2$ formation reaches equilibrium.

Conclusions

It has been demonstrated that the existence of an interfacial region in flow-injection systems can be exploited to analytical advantage. Specifically, it has been shown that pH gradients can be created and used over both a wide range $\Delta pH = 9$, and a narrow range $\Delta pH = 2$. It was known earlier that a steep gradient over a wide pH range can be used [8, 11]. The underlying considerations for developing a pH gradient approach were based on thermodynamics, but it was accepted that kinetic factors had to be taken into account. With the example of kinetic masking provided by the determination of nickel and copper in the presence of cobalt, kinetic effects have been shown to be important and potentially useful.

It can be concluded that a variety of determinations of mixtures may be carried out rapidly and reliably by application of pH-gradient f.i.a. Current work is concentrating on means of obtaining programmable pH gradients and of achieving efficient extraction and processing of the analytical information in the pH-gradient flow-injection peaks.

We are grateful to the Science Research Council for a Studentship for B.F. and to NATO for the award of research grant No. 1492.

REFERENCES

1 O. Levenspiel, Chemical Reaction Engineering, 2nd edn., J. Wiley, New York, 1972, Ch. 9.
2 J. Růžička and E. H. Hansen, Anal. Chim. Acta, 99 (1978) 37.
3 G. Taylor, Proc. R. Soc. London, Ser. A, 219 (1953) 186.
4 H. T. S. Britton and R. A. Robinson, J. Chem. Soc., (1931) 1456.
5 D. Betteridge, Anal. Chem., 50 (1978) 832A.
6 D. Betteridge, E. L. Dagless, B. Fields and N. F. Graves, Analyst, 103 (1978) 897.
7 B. Fields, Ph.D. Thesis, University College of Swansea, 1981.
8 D. Betteridge and B. Fields, Anal. Chem., 50 (1978) 654.
9 M. Langora-Hulickova and L. Sommer, The Coordination and Analytical Chemistry of N-Heterocyclic Azo Dyes, J. E. Purkyne-University, Brno, Czechoslovakia.
10 J. Kragten, Atlas of Metal—Ligand Equilibria in Aqueous Solution, Horwood, Chichester, 1978.
11 S. Baban, D. Betteridge, D. Beetlestone and P. Sweet, Anal. Chim. Acta, 114 (1980) 319.

Analytica Chimica Acta, 132 (1981) 157—164
Elsevier Scientific Publishing Company, Amsterdam — Printed in The Netherlands

KINETIC DETERMINATION OF TRACES OF COPPER(II) BY ITS CATALYTIC EFFECT ON THE OXIDATION OF 4,4′-DIHYDROXY-BENZOPHENONE THIOSEMICARBAZONE BY HYDROGEN PEROXIDE

J. L. FERRER-HERRANZ and D. PÉREZ-BENDITO*
Department of Analytical Chemistry, Faculty of Sciences, University of Córdoba (Spain)
(Received 5th May 1981)

SUMMARY

The kinetic method is based on the catalytic effect of copper(II) on the oxidation of 4,4′-dihydroxybenzophenone thiosemicarbazone by hydrogen peroxide. The reaction is followed spectrophotometrically at 415 nm. The kinetic parameters of the reaction are reported and a rate equation is suggested. Three methods of rate measurement are compared. The calibration graphs are linear in the range 10—90 ng Cu ml^{-1}. There are few interferences. The method is applied to the determination of copper in waters.

Many methods for the kinetic determination of copper(II), based on its catalytic effect on oxidation reactions, including both oxidation by hydrogen peroxide and aerial oxidation of organic compounds, have been reported. This paper is part of an investigation on the use of thiosemicarbazones containing hydroxyl groups in kinetic—catalytic methods of analysis [1—3]. The synthesis and properties of 4,4′-dihydroxybenzophenone thiosemicarbazone (4,4′-DBPT) have been described by Toribio [4]. The present paper describes the kinetics of the oxidation of this reagent when catalyzed by copper(II) and the utilization of the reaction for the determination of as little as 10 ng Cu ml^{-1}. The procedure is applied to the determination of copper in waters. This is useful because there are only a few kinetic procedures suitable for the determination of copper in waters [5—9]. Among the thiosemicarbazones, only the oxidation of 1,2-naphthoquinone-4-sulphonate-2-thiosemicarbazone by hydrogen peroxide, which is also catalyzed by copper(II) and enhanced by ascorbic acid, has previously been described [10]. This method is more sensitive but less precise than the one proposed here.

EXPERIMENTAL

Reagents and apparatus

4,4′-Dihydroxybenzophenone thiosemicarbazone (4,4′-DBPT) was synthesized by the condensation of 4,4′-dihydroxybenzophenone with thiosemicarbazide [4]. A 0.1% (w/v) solution of the reagent in ethanol was used.

0003—2670/81/0000—0000/$02.50

A copper(II) solution (20.6 μg ml^{-1}) was prepared by dilution of a copper sulphate solution that had been standardized iodimetrically. All solvents and reagents were of analytical-reagent grade.

A Perkin-Elmer 575 spectrophotometer with 1.0-cm glass cells and equipped with an electronic thermostat was used for the kinetic measurements. A Radiometer PHM 62 pH meter with a combined glass-calomel electrode was also used.

Procedures

Determination of copper. To a solution containing up to 0.7 μg of copper(II) in a 10-ml volumetric flask, add 2 ml of 0.1% reagent solution, 2 ml of 0.3% hydrogen peroxide and 2 ml of ammonia—ammonium chloride buffer (pH 10.2). Dilute to 10 ml with distilled water. Immediately transfer a portion of the reaction mixture to a thermostatted 1.0-cm cell at 35 ± 0.01°C, and record the change of absorbance at 415 nm with time, against a similar solution containing no copper. Begin the measurements exactly 3 min after mixing the solutions. Calculate the reaction rate from the absorbance—time curve, using one of the standard procedures indicated later.

Determination of copper in waters. Into a series of 10-ml volumetric flasks pipette aliquots of the sample (as supplied) containing $\leqslant$0.3 μg of copper. Add known amounts of the standard copper solution to the sample aliquots (ensuring that the total concentration is in the range of the calibration graph) and 100 μg of sodium fluoride, and follow the procedure above. Use the fixed-time method for rate measurement (see below). Evaluate the copper content by extrapolation of the graph, or by direct calibration.

RESULTS

Catalytic action of copper(II)

In alkaline solution the reagent showed only one absorption band at 350 nm. The oxidation of 4,4′-DBPT by hydrogen peroxide in alkaline medium was very slow. In the presence of traces of copper(II), the oxidation rate increased and new, unresolved absorption bands at 415 and 445 nm appeared rapidly (Fig. 1), giving a yellow solution. The 415-nm band increased with time, coinciding with the decrease of the band at 445 nm. The absorbance at 415 nm is a measure of the copper concentration. Other metal ions tested did not catalyze this reaction. When other oxidants such as periodate or peroxodisulphate were used, the reagent was rapidly oxidized; copper had no effect on oxidation by the former, and very little on the latter. Aerial oxidation of the reagent was not enhanced by the presence of copper(II). Furthermore, when periodate was used, another new absorption band appeared at 550 nm.

Effects of reaction variables

The oxidation rate depended on the relative concentration of reagent and copper(II), the pH, the hydrogen peroxide concentration and the temperature.

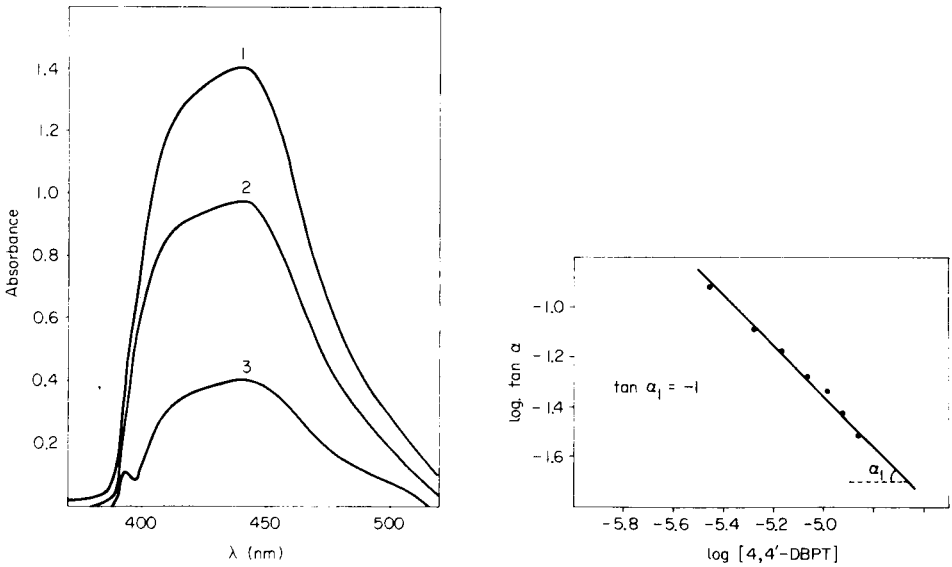

Fig. 1. Effect of copper(II) on the absorption spectra resulting from oxidation of 4,4'-DBPT: (1) 30.5 ng Cu ml^{-1} present; (2) no copper present (both against a distilled water reference); (3) difference between (1) and (2). 2 ml of 0.1% reagent, 2 ml of 0.3% H_2O_2, pH 10, 20°C; curves recorded after 5 min.

Fig. 2. Determination of order of reaction with respect to 4,4'-DBPT.

The reaction conditions were chosen so that the rate of the uncatalyzed reaction was very small compared with that of the catalyzed reaction.

The differential variant of the tangent method [11] was used for processing the kinetic data, because there is a linear relation between absorbance and time during the first 3—8 min.

The influence of temperature on the rate was studied in the range 25—40°C. The absorbance—time curves at different temperatures showed that the absorbance increases linearly during the first 15 min and does not change after 35 min. The slopes of these curves become steeper when the temperature is increased. A temperature of 35°C was selected for further study. From the slopes of these curves and the Arrhenius equation the activation energy for the catalyzed reaction was calculated to be 16.23 kcal mol^{-1}.

The effect of the reagent concentration on the rate was studied in the range 3×10^{-6}—1.5×10^{-5} M. The rate decreases linearly as the 4,4'-DBPT concentration increases; 9.3×10^{-6} M reagent (2 ml of 0.1% solution) was selected for further study. A logarithmic plot (Fig. 2) shows that the reaction rate is inversely proportional to the 4,4'-DBPT concentration.

The effect of hydrogen peroxide concentration was studied in the range 5×10^{-3}—5×10^{-2} M for both the catalyzed and uncatalyzed reactions. The reaction rate depends linearly (first order) on the concentration at least up to 5×10^{-2} M for the uncatalyzed reaction and up to 2.5×10^{-2} M for the

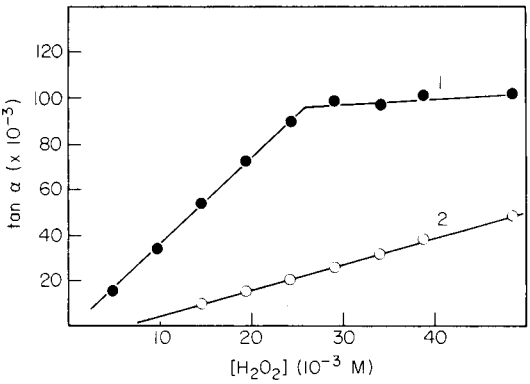

Fig. 3. Dependence of the reaction rate on hydrogen peroxide concentration. (1) Catalyzed; (2) uncatalyzed reaction. Conditions as in the procedure.

catalyzed reaction (Fig. 3); 1.7×10^{-2} M hydrogen peroxide (2 ml of 0.3% solution) was selected for further study.

The reaction rate also depends linearly on the ammonia concentration in the range 0.052—0.282 M and decreases exponentially as the ammonium and hydrogen ion concentrations increase. The dependence on pH is shown in Fig. 4. An ammonia—ammonium chloride buffer solution of pH 10.2 was therefore used in subsequent work. The copper-catalyzed oxidation is first order with respect to ammonia and is −1/3 with respect to the ammonium ion.

The absorbance—time curves for solutions containing different amounts of copper(II) were recorded against a similar solution containing no copper (Fig. 5). The initial slopes indicate a first-order reaction with respect to copper.

The various kinetic dependences are summarized in Table 1. On the basis of the kinetic investigation, the following equation is suggested for the copper(II)-catalyzed oxidation of the reagent by hydrogen peroxide in alkaline medium at pH 10.2

$$d[4,4'\text{-DBPT}]_{ox}/dt = k[4,4'\text{-DBPT}]^{-1}[H_2O_2][Cu^{2+}][H^+]^{-1}[NH_4^+]^{-1/3}[NH_3]$$

where $[4,4'\text{-DBPT}]_{ox}$ is the concentration of the oxidized reagent and k is the conditional rate constant. This equation does not include the effect of the uncatalyzed reaction.

Calibration

The tangent method was used to calculate the rate of the catalyzed reaction, which was plotted as a function of the copper concentration. The fixed-time and the fixed-absorbance (variable-time) methods [11] were also used. For the fixed-time method, measurements were made after 5 min. For the fixed-absorbance method, the inverse of the time necessary to obtain an absorbance of 0.400 was plotted against the copper concentration. In all

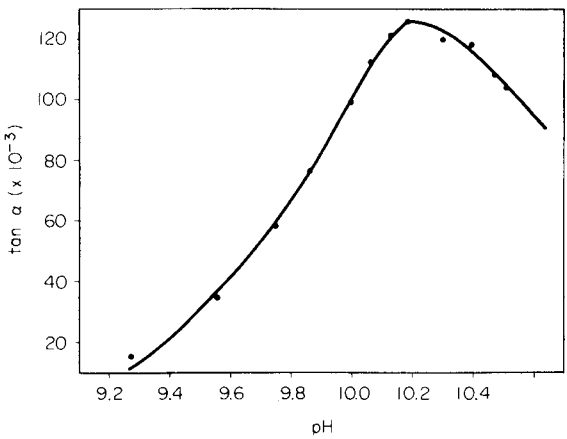

Fig. 4. Dependence of the reaction rate on pH. Conditions as in the procedure.

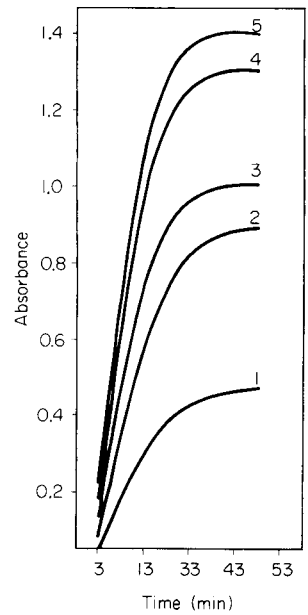

Fig. 5. Effect of copper concentration. Curves 1—5 correspond to 10, 20, 30, 40 and 50 ng Cu ml^{-1}, respectively. Conditions as in the procedure.

cases, the calibration graph is linear in the concentration range indicated in Table 2. The accuracy and precision of the three methods applied for 30.6 ng Cu ml^{-1} is included in Table 2, from which it is concluded that the fixed-absorbance method has a positive systematic error ($t'_{exp} > t$) whereas the fixed-time method is more precise. Although the tangent method is accurate and precise, the permissible concentration range is slightly narrower than when the fixed-time method is used. Therefore the fixed-time method is recommended.

Interferences

In order to assess possible analytical applications of the kinetic reaction, the influence of other ions on the reaction rate in the presence of copper(II)

TABLE 1

Summary of kinetic data: V_0 is the initial rate

Dependence of V_0 on	Concentration range	Dependence of V_0 on	Concentration range
$[4,4'\text{-DBPT}]^{-1}$	3.5×10^{-6}—1.4×10^{-5} M	$[NH_3]$	0.052—0.28 M
$[H_2O_2]$	5.0×10^{-3}—2.5×10^{-2} M	$[NH_3]^{-1/3}$	0.28—0.70 M
$[H_2O_2]^0$	2.5×10^{-2}—5.0×10^{-2} M	$[NH_4^+]^{-1/3}$	0.022—0.16 M
$[H^+]^{-1}$	pH 9.5—10.2	$[Cu^{2+}]$	10—90 ng ml^{-1}

TABLE 2

Linear concentration range, accuracy and precision of the kinetic methods for determination of copper(II)

Method	Concentration range (ng Cu ml^{-1})	Relative standard deviation (%)	t'_{exp}
Tangent	10—70	1.13 (n = 9)	1.69 (t = 2.23)
Fixed-time	15—90	0.82 (n = 10)	0.84 (t = 2.26)
Fixed-absorbance	15—90	1.09 (n = 10)	3.32 (t = 2.26)

was examined. The tangent method was used to detect activating or inhibiting effects, because a change in slope was considered to be more clearly measured than the change in a single data point.

The results are summarized in Table 3. The alkaline and alkaline earth metals, in a ratio to copper of at least 100-fold by weight, do not interfere, in common with most other ions. Cd, Ag, Ce(IV) $S_2O_3^{2-}$ and SCN^- interfere at above 50-fold amounts; Mo(VI), Fe(III), Ni and Co interfere above 2-fold amounts, because these ions form complexes with the reagent, but if the fixed-time method is applied, they interfere at above 5-fold amounts. The positive interferences of indium and gallium are due to the activating role of both ions in the catalyzed reaction. Cyanide and EDTA, above 2-fold amounts, are strong inhibitors, so that only the uncatalyzed reaction takes place.

TABLE 3

Influence of other ions in the kinetic determination of 30.6 ng Cu ml^{-1} by the tangent method

Other ion[a]	Tan α ($\times 10^{-3}$)	Cu found (ng ml^{-1})	Other ion	[ion]/[Cu(II)]	Tan α ($\times 10^{-3}$)	Cu found (ng ml^{-1})
—	67.8	30.5	SO_3^{2-}	100	67.2	30.1
Al(III)	69.3	31.3	Oxalate	100	68.0	30.6
Ti(IV)	67.5	30.3	Tartrate	100	70.2	31.8
Cr(VI)	67.2	30.1	Citrate	100	70.2	31.8
V(V)	70.2	31.8	Cd(II)	50	68.6	30.9
Zn(II)	69.0	31.1	Ag(I)	50	68.6	30.9
Hg(II)	68.6	30.9	Ce(IV)	50	68.8	31.0
Sn(II)	69.4	31.3	$S_2O_3^{2-}$	50	68.6	30.9
Sb(III)	68.4	30.8	SCN^-	50	68.8	31.0
Bi(III)	68.0	30.6	Mn(II)	5	66.6	29.8
Pb(II)	69.2	31.2	Mo(VI)	1	69.6	31.4
ClO_4^-	69.8	31.5	Fe(III)	1	70.2	31.8
BrO_3^-	67.2	30.1	Ni(II)	1	68.7	30.9
IO_3^-	66.6	29.8	Co(II)	1	68.0	30.6
IO_4^-	66.0	29.5	Ga(III)	1	73.8	33.7
$S_2O_8^{2-}$	69.6	31.4	In(III)	1	76.8	35.4

[a]Wt. ratio: Cu = 100.

TABLE 4

Kinetic determination of copper(II) in waters

Water sample	Cu found (ng ml^{-1})		
	Kinetic method		Atomic absorption method[c]
	A[a]	B[b]	
Untreated, natural	35	37	40
Commercial, natural	3	4	4
Sea	52	53	50
Industrial waste[d]	130	130	130

[a]Standard addition. [b]Direct calibration. [c]At 324.8 nm. [d]From a fertilizer factory (200 μg NaF added).

Determination of copper in waters

The technique described above was applied to the determination of traces of copper in water samples. Linear plots were obtained for standard additions of 20, 30 and 40 ng Cu ml^{-1} to each sample examined. In order to remove interferences, sodium fluoride was added. The results obtained are compared with those obtained by atomic absorption spectrometry in Table 4. When the atomic absorption method was used, the sample had to be preconcentrated. However, with the method proposed here, volumes of 0.5—3 ml were used without pretreatment.

DISCUSSION

The mechanism of this catalytic reaction has not been completely elucidated, but it seems that copper(II) serves as a mediator in the electron transfer. When 3.5×10^{-3} M reagent was titrated photometrically at 415 nm with 3.5×10^{-3} M potassium periodate, without copper, the end-point corresponded to a 2:1 molar ratio of reagent to periodate. Thus oxidation of the reagent involves the loss of one electron. The reaction steps in the catalyzed reaction, therefore, could be [12]

$$4,4'\text{-DBPT}_{red} + \text{Cu(II)} \rightarrow 4,4'\text{-DBPT}_{ox} + \text{Cu(I)}$$

$$2\text{Cu(I)} + H_2O_2 \rightarrow 2\text{Cu(II)} + 2OH^-$$

It can be assumed that the second reaction proceeds much more quickly than the first. The direct interaction of the reagent with hydrogen peroxide is kinetically hindered. It is also probable that a transient complex between copper(I) and 4,4′-DBPT is formed and that regeneration of copper(II) takes place from this complex. Probably for this reason, a large excess of hydrogen peroxide with respect to the reagent is needed.

The oxidation product was not identified. However, 4,4′-DBPT could be oxidized by a one-electron mechanism [13] to produce a resonance-stabilized phenoxy radical (I)

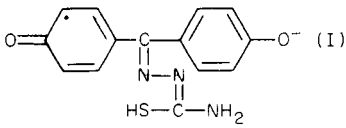

(I)

The probable existence of this radical is supported by the u.v.—visible absorption spectrum. Also the semiquinone radical is known to be reasonably stable in alkaline solution [14].

REFERENCES

1 D. Pérez-Bendito, M. Valcárcel, M. Ternero and F. Pino, Anal. Chim. Acta, 94 (1977) 405.
2 D. Pérez-Bendito, M. Valcárcel, M. Ternero and F. Pino, Anal. Chim. Acta, 109 (1979) 401.
3 D. Pérez-Bendito, M. Valcárcel, M. Ternero and F. Pino, Microchem. J., 25 (1980) 102.
4 F. Toribio, Doctoral Thesis, University of Córdoba, Spain, 1979.
5 V. I. Richkova, I. F. Dolmanova and V. M. Peshkova, Teploenergetika, (1972) 66.
6 V. I. Richkova and I. F. Dolmanova, Zh. Anal. Khim., 29 (1974) 1222.
7 I. F. Dolmanova, V. P. Poddubienko and V. M. Peshkova, Zh. Anal. Khim., 28 (1973) 592.
8 K. Hirayama, Nippon Kagaku Kaishi, (1976) 768.
9 N. Shigeroni, K. Kazuhiro and K. Takuji, Chem. Lett., 7 (1980) 849.
10 R. P. Igor, M. D. Jaredic and T. G. Pecev, Talanta, 27 (1980) 361.
11 K. B. Yatsimirskii and L. P. Tikhonova, in E. Wänniren (Ed.), Essays on Analytical Chemistry, Pergamon, Oxford, 1977, p. 529.
12 R. Bontchev, Talanta, 17 (1970) 499.
13 W. V. Kaeding, J. Org. Chem., 28 (1963) 1063.
14 S. Patai, The Chemistry of the Hydroxyl Group, Part I, Interscience, New York, 1971.

Analytica Chimica Acta, 132 (1981) 165—173
Elsevier Scientific Publishing Company, Amsterdam — Printed in The Netherlands

SOLVENT EXTRACTION OF MICROGRAM AMOUNTS OF MAGNESIUM WITH 8-QUINOLINOL AND TETRABUTYLAMMONIUM IODIDE FOLLOWED BY SPECTROPHOTOMETRY WITH CHLOROPHOSPHONAZO-III

KEN KANEKO[a], MINORU YOSHIDA* and TAKEJIRO OZAWA[b]

Department of Chemistry, Faculty of Science, Tokyo Institute of Technology, Meguro-ku, Tokyo (Japan)

(Received 23rd June 1981)

SUMMARY

A rapid and sensitive solvent-extraction procedure for the separation of magnesium is reported. Microgram (0.1—10) amounts of magnesium are extracted with a chloroform solution of 8-quinolinol and tetrabutylammonium iodide in the presence of tartrate and phosphate. Magnesium is then back-extracted into an aqueous buffer solution (pH 7.3; tetrabutylammonium hydroxide—boric acid) and determined spectrophotometrically using chlorophosphonazo-III. Up to 500 mg of sulphate, phosphate or cyanide, 200 mg of chloride, 20 mg of aluminum, barium or silicate, and 2 mg of calcium can be tolerated.

Many photometric methods have been reported for the determination of microgram amounts of magnesium. The chlorophosphonazo-III [2,7-bis(4-chloro-2-phosphonobenzeneazo)-1,8-dihydroxynaphthalene-3,6-disulphonic acid] method reported by Ferguson et al. [1] is one of the most sensitive (molar absorptivity 48000 l mol^{-1} cm^{-1}). Many common ions, however, interfere seriously with the determination of magnesium by this reagent. Even sub-milligram amounts of sodium, potassium or ammonium ion interfere, and the method cannot be applied in the analysis of actual samples.

Jankowski and Freiser [2] reported the extraction of a magnesium 8-quinolinolate—tetrabutylammonium ternary complex into chloroform. They determined up to 140 μg of magnesium by measuring the absorbance of the complex in the organic phase at 388 nm. Disadvantages of this method are that the molar absorptivity of the complex is low (7280 l mol^{-1} cm^{-1}), and that the pH range for maximum extraction of the complex is narrow (11.20—11.88). Cations such as aluminum interfere, being co-extracted as the 8-quinolinolate.

The present work was designed to establish a sensitive and practical method by combining the two methods mentioned above. Magnesium is

[a]Present address: Kawamura Institute of Chemical Research, Kami-Kizaki, Urawa-shi, Saitama Prefecture, Japan.
[b]Present address: Department of Environmental Chemistry, Faculty of Engineering, Saitama University, Shimo-Okubo, Urawa-shi, Saitama Prefecture, Japan.

first extracted into chloroform as the ternary complex, back-extracted into an aqueous buffer solution (pH 7.3), and finally determined with chlorophosphonazo-III. Conditions for the extraction of the ternary complex at lower levels of magnesium (below 10 μg) than those examined by Jankowski and Freiser are described in detail. The extraction—back-extraction procedure is effective not only for the elimination of interfering ions but also for the concentration of magnesium.

EXPERIMENTAL

Apparatus and reagents

A Hirama Model 6 spectrophotometer with 10-mm glass cells, an Iwaki Model KM shaker and a TOA-Denpa Model HM-5A pH meter were used.

Redistilled water was used for all experiments. All the chemicals were of analytical grade and were used without further purification.

Standard magnesium solution (1000 ppm). Dissolve 1.00 g of magnesium metal (99.99%) in 30 ml of 6 M HCl, and dilute to 1 l. Standardize by titration with EDTA. Prepare working standards by appropriate dilution.

Extracting reagent solution A. Dissolve 0.74 g (2×10^{-3} mol) of tetrabutylammonium iodide (Bu_4NI) and 2.9 g (2×10^{-2} mol) of 8-quinolinol (oxine) in 1 l of chloroform. This solution is used for the recommended analytical procedure.

Extracting reagent solution B. Dissolve 3.7 g (10^{-2} mol) of Bu_4NI and 2.9 g of oxine in 1 l of chloroform. This solution is used for the examination of the extracting conditions.

Potassium phosphate solution (1 M). Dissolve 174 g of dipotassium hydrogenphosphate and 56 g of potassium hydroxide in 1 l of water.

Tetrabutylammonium hydroxide (Bu_4NOH) solution (5.4×10^{-2} M). Add 10 g of Bu_4NI and 6.3 g of powdered silver oxide to about 400 ml of water. After stirring for 1 h, filter off the silver iodide, and dilute the filtrate to 500 ml [1].

Buffer solution for back-extraction (pH 7.3). Add 5 g of boric acid to 25 ml of the Bu_4NOH solution and dilute to 1 l.

Chlorophosphonazo-III (CP-III) solution (2×10^{-4} M). Dissolve 82.9 mg of CP-III (Dojindo Laboratories, Kumamoto-shi) in a small volume of water containing 9 ml of the Bu_4NOH solution and dilute to 500 ml; the pH of this solution becomes 7.3.

Recommended procedure

Transfer up to 40 ml of a sample solution containing 0.1—10 μg of magnesium to a 100-ml separatory funnel. Add 2 ml of 0.2 M potassium sodium tartrate solution, 2 ml of 1 M sodium citrate solution and a few drops of a 0.1% tropaeolin O solution. Add 1 M sodium hydroxide solution dropwise until the color of the indicator changes to orange. Add 2 ml of the potassium phosphate solution and dilute to 50 ml if necessary. Shake this solution with

20 ml of the extracting reagent solution A for 2 min. When the two layers have separated, transfer the organic layer to another 100-ml separatory funnel. Add 20 ml of the buffer solution (pH 7.3) to the organic phase and shake the mixture vigorously by hand. After the phase separation, transfer the aqueous layer to a 25-ml glass-stoppered test tube. Add 5 ml of the CP-III solution and mix well. Measure the absorbance of the solution at 669 nm against a reagent blank solution prepared by mixing 20 ml of the buffer solution and 5 ml of the CP-III solution.

RESULTS AND DISCUSSION

Determination of magnesium with chlorophosphonazo-III

The conditions for the spectrophotometric determination of magnesium with CP-III established by Ferguson et al. [1] were adopted in this study with slight modifications. A buffer solution of pH 7.3 instead of 7.0 was used because the maximum coloration was obtained at pH 7.3. The reproducibility was improved when the pH of the CP-III solution was previously adjusted to 7.3 by adding Bu_4NOH.

In order to examine the effect of the extraction—back-extraction procedure on the coloration of CP-III—Mg complex, 20 ml of the buffer solution was shaken with 20 ml of the extracting reagent solution B. The aqueous layer was separated and mixed with 5 ml of the CP-III solution with or without the addition of known amounts of magnesium. The absorbances measured were not affected by this treatment.

It was shown that magnesium extracted into chloroform as the Mg—oxine—Bu_4N^+ ternary complex is quantitatively back-extracted into aqueous solutions of pH below 9, as will also be indicated from the results of the following section. The Bu_4NOH–boric acid buffer solution of pH 7.3 is used for back-extraction, and magnesium in the back-extract can then be directly measured by spectrophotometry with CP-III. Aluminum remains in the organic phase as its oxinate at this pH.

Extraction of the ternary complex into chloroform

Effect of pH. A solution (50 ml) containing 6 μg of magnesium, whose pH was controlled by Sørensen's buffer solutions was shaken for 2 min with 20 ml of extracting reagent solution B. After phase separation, magnesium was back-extracted into the pH 7.3 buffer solution and determined with CP-III as described above. Curve A in Fig. 1 shows the relation between the absorbance and pH of the aqueous phase measured after the extraction. The pH range of constant extraction for magnesium was very narrow (10.4—10.7) and the extractability decreased remarkably between pH 10.7 and 12. This optimal pH range was lower and narrower than that reported by Jankowski and Freiser [2]. The difference must, however, be ascribed to the low amount of magnesium examined, because almost the same pH—extractability curve as that of Jankowski and Freiser was obtained at their higher magnesium

concentration. Jankowski and Freiser [2] reported that the use of tartrate extended the pH range of 100% extraction, preventing hydrolysis of magnesium at higher pH. This was confirmed for low amounts of magnesium in the presence of 8 mM tartrate (curve B, Fig. 1), yet there remained a small depression between pH 10.7 and 11.2. Various salts were tested in attempts to obtain constant extraction over a wider pH range. The addition of phosphate (40 mM) was found to give satisfactory results. Constant maximum extraction was obtained above pH 10.8 (curve C, Fig. 1). Phosphate buffers can be used to adjust the pH of the aqueous phase in this system.

In the recommended procedure, the pH of the aqueous solution is adjusted by adding 1 M sodium hydroxide solution using tropaeolin O as indicator (transition interval, pH 11—13) in the presence of tartrate and citrate (see below). The final addition of the potassium phosphate solution brings the pH value to slightly above 12. Tropaeolin O is not extracted into chloroform and has no effect on the final measurements.

Extracted species. The composition of the ternary complex in the organic phase was determined by a continuous variations plot for the three-component system. The extraction was carried out at pH 12.3 for 63 solutions containing different amounts of magnesium, oxine (Q) and Bu_4NI; their total amount was maintained at 2.06×10^{-5} mol. The maximum absorbance was obtained in the region corresponding to a composition: Mg^{2+} Q_3^- Bu_4N^+ (Fig. 2). This agrees with the composition obtained by Jankowski and Freiser [2] at pH 11.5 by the mole ratio method.

Extraction of oxine and Bu_4N^+. To examine the extraction behavior of the complex further, the variation of the distribution of oxine and Bu_4N^+ with pH in the absence of magnesium was investigated. The amount of oxine distributed in chloroform was determined as follows. A mixture of

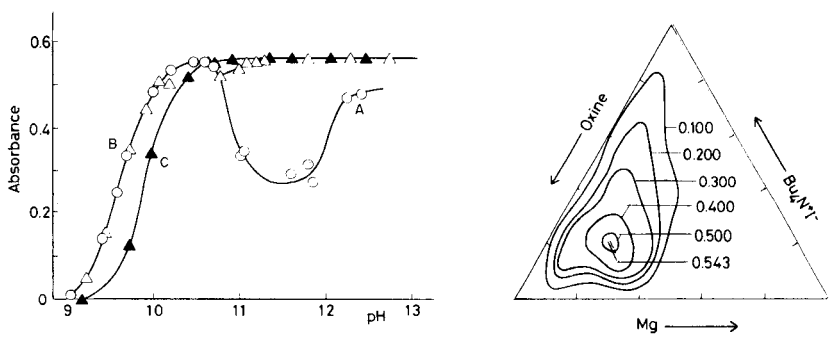

Fig. 1. Effect of pH on the extraction of magnesium. Extracting reagent solution B; Mg 6 μg; V_{org} = 20 ml; V_{aq} = 50 ml. Curve A (○) without tartrate or phosphate; curve B (△) $[tartrate]_{aq}$ = 8 mM; curve C (▲) $[PO_4^{3-}]_{aq}$ = 40 mM.

Fig. 2. Continuous variations diagram for the Mg^{2+}—oxine—Bu_4N^+ three-component system. V_{org} = 20 ml; V_{aq} = 20 ml; Mg^{2+} + HOx + Bu_4NI = 2.06×10^{-5} mol; pH 12.3. Numerical values on the contour lines show the absorbances obtained by the final measurements with CP-III.

20 ml of an oxine—Bu_4NI—$CHCl_3$ solution and 50 ml of a buffered aqueous solution was shaken for 2 min. After phase separation, a 5-ml aliquot of the organic layer was diluted to 50 ml with chloroform and 5 ml of this solution was shaken with 20 ml of 1 M hydrochloric acid. Oxine in the chloroform solution was measured photometrically by means of its absorbance in the aqueous layer at 390 nm, being back-extracted as the quinolinolium ion.

Curves A, B and C in Fig. 3 show the variation of the distribution of oxine to the organic phase with pH at different concentrations of Bu_4NI. Curve A (without Bu_4NI) agrees well with the percentage extraction calculated from the reported values of the dissociation constant and the partition coefficient of 8-quinolinol [3]. The distribution curve shifts to higher pH as the Bu_4NI concentration increases, indicating that oxinate forms an extractable species with Bu_4N^+ in the higher pH range.

The distribution of Bu_4N^+ between the aqueous and the organic phase was also examined under the extraction conditions used for curve B. Another 5-ml aliquot of the chloroform solution prepared for the determination of oxine was shaken for 2 min with 15 ml of a 2.67×10^{-2} M oxine solution in chloroform and 50 ml of an aqueous solution containing 10 μg of magnesium, 0.4 mmol of tartrate and 2 mmol of sodium hydroxide. A linear relationship was obtained between the amount of Bu_4N^+ and the amount of magnesium in the chloroform layer which was determined by CP-III photometry after back-extraction. The amount of Bu_4N^+ distributed in the organic phase was determined on the basis of this relation.

The percentage extraction of Bu_4N^+ in chloroform at various pH values is shown by curve D in Fig. 3. Curve D coincides with curve B in the pH range 9—12.6; this seems to confirm the existence of an extractable oxine—Bu_4N^+ complex. In the higher pH region, the extraction of Bu_4N^+ increases up to pH 13.1 and then decreases again. The general trend of curve D resembles that of curve A in Fig. 1. The partition of Bu_4N^+ was also examined in the presence of phosphate or tartrate at pH 12.0 (Fig. 3). Tartrate has no effect on the distribution of Bu_4N^+, but almost all Bu_4N^+ is extracted into the organic phase even at pH 12 when phosphate is present.

All these results suggest that the extractability of magnesium in the higher pH region is controlled not only by its hydrolysis but also by the partition of Bu_4N^+ between the two phases, and that the role of phosphate in this system is quite different from that of tartrate.

Effect of sulfate. Sulfuric acid is frequently used to dissolve solid samples with or without hydrofluoric acid, and a large amount of sulfate remains in the sample solutions. Curves A and B in Fig. 4 show the effect of the sulfate concentration on the extraction of magnesium with extracting reagent B. Although an 8 mM concentration of sodium sulfate in the sample solution did not affect the result (curve A), a 0.1 M concentration gave higher absorbances (curve B). The chloroform layer became greenish-blue in the interference of sulfate. An increase of the absorbance was also observed without magnesium above pH 11.4, but never in the absence of either oxine or Bu_4N^+.

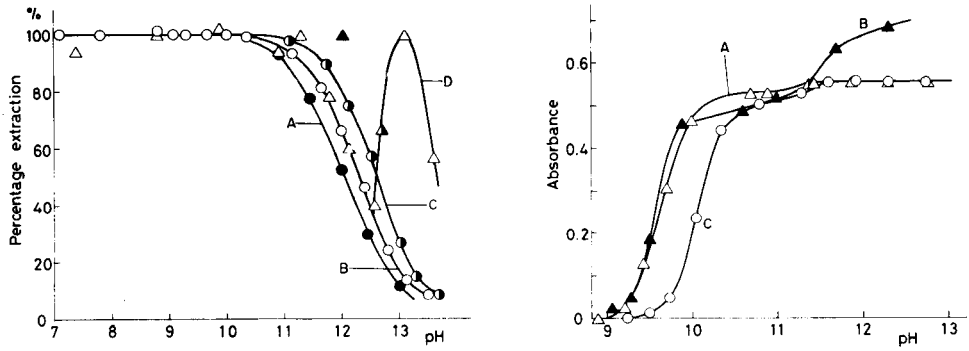

Fig. 3. The distribution of oxine and Bu_4N^+ as a function of pH. Curves A (•), B (○) and C (⊙) show the distribution of oxine; curve D (△) and points (▲) and (▲) show the distribution of Bu_4N^+. For curve A, oxine (2×10^{-2} M) solution in $CHCl_3$ was used; for curves B and D and points (▲) and (▲), extracting reagent solution A was used; for curve C, extracting reagent solution B was used; (▲) in the presence of 8 mM tartrate; (▲) in the presence of 40 mM phosphate.

Fig. 4. Effect of sulfate on the extraction of 6 μg of magnesium. V_{org} = 20 ml; V_{aq} = 50 ml; $[\text{tartrate}]_{aq}$ = 8 mM. Curve A (△), $[SO_4^{2-}]_{aq}$ = 8 mM; curves B (▲) and C (○), $[SO_4^{2-}]_{aq}$ = 0.1 M. For curves A and B, extracting reagent solution B was used; for curve C, extracting reagent solution A was used.

As the amount of oxine or Bu_4N^+ increased, the absorbance increased. When a chloroform solution containing 1×10^{-1} M of oxine and 5×10^{-2} M of Bu_4N^+ was shaken with a pH 13.2 aqueous solution without sulfate, the solution again became greenish-blue.

All these results indicate that the extraction of large amounts of Bu_4N^+ is responsible for the interference of sulfate. An ion-pair between Bu_4N^+ and oxine is formed when large amounts of sulfate are present, and is extracted into chloroform at higher pH. The Bu_4N^+ in the ion-pair is transferred to the aqueous phase in the back-extraction, while oxine remains in the chloroform. The pH of the aqueous layer rises, because the buffer capacity of the Bu_4N^+—boric acid solution is relatively small, and the absorbance of excess of CP-III at 669 nm increases accordingly.

In order to avoid the interference of sulfate, the concentration of Bu_4N^+ or oxine must be lowered. When the Bu_4N^+ concentration in chloroform is decreased to 2×10^{-3} M, as in extracting reagent A, there is no interference even from 0.1 M sulfate (curve C, Fig. 4).

Effect of shaking time and temperature. Shaking for 20 s to 5 min gave constant extraction at 17°C, but at 30°C, the extraction reached a maximum on shaking for 20—40 s and then gradually decreased on further shaking up to 70 sec, finally reaching a constant value for shaking times exceeding 70 s. A shaking time of 2 min was therefore adopted. At the 6 μg Mg level, the absorbance obtained by the recommended procedure at 30°C was about 2% lower than that obtained at 17°C.

Percentage extraction and effect of volume ratio. The mean value of the absorbance obtained by the recommended procedure for 6 μg Mg was 0.549 (35 determinations, relative standard deviation ±0.8%). Direct determination of 6 μg of magnesium by the CP-III method gave a mean absorbance of 0.590 (±0.8%). As already stated, recovery of magnesium in the back-extraction may be regarded as 100%. Therefore, the percentage extraction for magnesium as the ternary complex into chloroform and the distribution ratio of magnesium between the organic and aqueous phase can be calculated to be 93% and 33.7, respectively. The extraction of magnesium decreased as the volume of the aqueous phase increased from 50 to 150 ml, but better sensitivity was obtained when extraction is done from 150 ml of sample solution. The absorbances calculated from the distribution ratio obtained above agree well with the observed values (Table 1).

Effect of aluminium and calcium

Aluminum forms a complex with oxine, and is extracted quantitatively into chloroform at pH 4.4—11.0. A moderate amount of aluminum does not affect the final spectrophotometry in the above procedure, because aluminum oxinate remains in chloroform during the back-extraction. But, the extraction of magnesium as the ternary complex into chloroform is suppressed by large amounts of aluminum. Curve A in Fig. 5 shows the effect of 12.5 mg of aluminum on the extraction of magnesium in the presence of 40 mM phosphate. A different extraction curve (B) was obtained when phosphate was replaced by 8 mM tartrate. When both phosphate and tartrate were added (curve C), magnesium was quantitatively extracted at pH 11.5—12.8; up to 20 mg of aluminum can then be tolerated.

Without phosphate, 10 μg of calcium causes a positive error in the determination of magnesium. Up to 1 mg of calcium can be masked by addition of 2 ml of the 1 M potassium phosphate solution, forming a precipitate of calcium phosphate. The extraction of magnesium is, however, suppressed by 2 mg of calcium because of coprecipitation of magnesium. When 2 ml of 1 M sodium citrate solution is added before the addition of phosphate, coprecipitation is reduced and 2 mg of calcium can be tolerated.

TABLE 1

Effect of volume of the aqueous phase (V_{aq}) on the extraction of 6.00 μg of magnesium (Volume of the organic phase, 20 ml)

V_{aq} (ml)	50	75	100	125	150
Absorbance					
observed[a]	0.550	0.532	0.517	0.492	0.474
calculated	0.549	0.531	0.514	0.498	0.482

[a]Obtained by CP-III spectrophotometry after back-extraction.

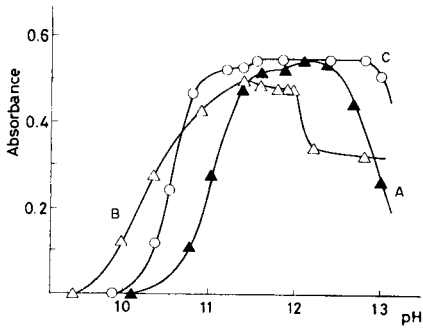

Fig. 5. The extraction of Mg (6 μg) in the presence of large amounts of Al (12.5 mg) as a function of pH. V_{org} = 20 ml; V_{aq} = 50 ml; extracting reagent solution A was used. Curve A(▲), $[PO_4^{3-}]_{aq}$ = 40 mM; curve B (△), [tartrate]$_{aq}$ = 8 mM; curve C (○), [tartrate]$_{aq}$ = 8 mM and $[PO_4^{3-}]_{aq}$ = 40 mM.

Effect of diverse ions

The effects of diverse ions were investigated for 6 μg of magnesium under the conditions of the recommended procedure (Table 2). Many transition metals caused significant interferences because of the formation of complexes with oxine. The addition of cyanide before the extraction eliminated the interference of nickel and copper. The other transition metals must be

TABLE 2

Effect of diverse ions on the determination of 6.00 μg of magnesium

Ion	Added as	Amount (mg)	Mg found (μg)	Ion	Added as	Amount (mg)	Mg found (μg)
Cl^-	NaCl	35.5	6.00	Cr(VI)	$K_2Cr_2O_7$	0.25	6.02
		213	5.92			2.5	4.99
NO_3^-	KNO_3	62	6.03	Mn^{2+}	$MnCl_2 \cdot 4H_2O$	0.01	6.06
		372	5.99			0.1	6.90
SO_4^{2-}	Na_2SO_4	576	6.04	Fe^{3+}	$Fe(NO_3)_3 \cdot 9H_2O$	0.25	6.00
PO_4^{3-}	—[a]	570	5.94			2.0	5.23
CN^-	KCN	600	5.99	Co^{2+}	$Co(NO_3)_2 \cdot 6H_2O$	0.3	5.56
F^-	NaF	1.5	5.98			3.0[c]	5.23
		7.6	7.45	Ni^{2+}	$Ni(NO_3)_2 \cdot 6H_2O$	0.4	5.99
SiO_2	—[b]	20	5.95			4.0[c]	5.99
		100	3.99	Cu^{2+}	$Cu(NO_3)_2 \cdot 3H_2O$	0.4	6.22
Be^{2+}	$BeCl_2$	0.2	5.96			4.0[c]	5.99
		0.5	4.90	Zn^{2+}	$Zn(NO_3)_2 \cdot 6H_2O$	0.27	6.00
Sr^{2+}	$SrCl_2 \cdot 6H_2O$	0.25	6.03	Cd^{2+}	$Cd(NO_3)_2 \cdot 4H_2O$	0.02	6.10
		2.5	8.42			0.1	8.05
Ba^{2+}	$BaCl_2 \cdot 2H_2O$	5.0	6.00	Hg^{2+}	$Hg(NO_3)_2 \cdot xH_2O$	0.1	6.10
		20	6.18	Pb^{2+}	$Pb(NO_3)_2$	0.1	6.59
Ti(IV)	$Ti(SO_4)_2 \cdot xH_2O$	0.05	5.98	Sn(IV)	$SnCl_4 \cdot xH_2O$	0.1	6.00
		1.0	2.06				

[a]Potassium phosphate solution prepared as stated in Experimental. [b]SiO_2 was dissolved after fusion with 8 times its weight of NaOH; the weights are given in terms of SiO_2. [c]2 ml of 2% KCN solution was added.

TABLE 3

Determination of magnesium in anorthite (Phenocrysts in the 1940 lava of the Miyake-jima volcano)[a]

Volume of sample soln.[b] (ml)	Mg added (μg)	Mg found (μg)	Content (MgO %)
2.00	0	0.99_4	0.071_0
4.00	0	2.01	0.071_8
4.00	3.00	4.99	0.071_0
6.00	0	2.99	0.071_1
6.00	3.00	5.97	0.070_7
		Mean	0.0711
		Std. dev.	0.00041

[a]Previous data 0.08% [4], 0.35% [5]. [b]1.161 mg of sample per ml.

pre-extracted by oxine in chloroform (without Bu_4N^+) at pH 7 before the extraction of magnesium.

APPLICATION

Anorthite, a calcium-rich end-member of the plagioclase solid-solution, contains only a little magnesium with the main composition of $CaAl_2Si_2O_8$, and the accurate determination of magnesium in it by conventional methods is difficult. The proposed method for magnesium was therefore tested. The anorthite sample used was obtained from the 1940 lava of the Miyake-jima volcano as very large phenocrysts [4, 5].

The powdered sample (290.3 mg) was decomposed by a $HF—H_2SO_4$ mixture and evaporated to fumes of sulfur trioxide. After cooling, the decomposition product was dissolved in water and the solution diluted to 250 ml. Aliquots (2—6 ml) of the solution were used for determinations by the proposed method. The results show good agreement in spite of changing the sample amounts (Table 3). The method was also checked by adding known amounts of magnesium to 4-ml and 6-ml aliquots of the solution; again the results show satisfactory recoveries.

REFERENCES

1 J. W. Ferguson, J. J. Richard, J. W. O'Laughlin and C. V. Banks, Anal. Chem., 36 (1964) 796.
2 S. J. Jankowski and H. Freiser, Anal. Chem., 33 (1961) 776.
3 R. G. W. Hollingshead, Oxine and Its Derivatives, Vol. 1, Butterworth, London, 1954, pp. 32, 50.
4 S. Kôzu and I. Katô, J. Japn. Assoc. Mineral. Petr. Econ. Geol., 26 (1941) 127.
5 H. Tsuya, Bull. Earthquake Res. Inst., Tokyo Imp. Univ., 33 (1955) 371.

Analytica Chimica Acta, 132 (1981) 175—185
Elsevier Scientific Publishing Company, Amsterdam — Printed in The Netherlands

DESCRIPTION OF LIQUID—LIQUID EXTRACTION EQUILIBRIA IN EXCHANGE EXTRACTIONS OF CHELATES

Part 3. Calculation of pH—pA Diagrams and Enrichment Factors in pH—pA Coordinates

F. MACÁŠEK*

Department of Nuclear Chemistry, Comenius University, CS-816 31 Bratislava (Czechoslovakia)

D. VANČO

Institute of Preventive Medicine, 809 58 Bratislava (Czechoslovakia)

(Received 25th June 1981)

SUMMARY

Equilibrium values of free ligand concentration (pA) in extraction systems which contain comparable amounts of metal and extraction agents, particularly exchange extraction systems, can readily be calculated with a desk computer. The technique is applied in the treatment of extraction systems where step-wise complexation, hydrolysis, masking and polynuclear complex formation of the metal take place in the aqueous phase. Data of normalized coordinates are tabulated and proved to be useful in finding pA in extraction systems of chelates $MA \ldots MA_4$, of various compositions. The same mathematical approach is used to calculate enrichment factors for two-element separations as a function of pA and pH. Model systems of the Zn, Pb, Co(II), Co(III) and Fe(II) diethyldithiocarbamates and Fe(III) and Sc 8-quinolinolates serve as examples.

The description of metal complex extraction equilibria in terms of equilibrium free ligand concentration, introduced by Rydberg [1], is widely used [2]. Some mathematical complications arise when the number of equilibria which must be considered is large and when the amounts of interacting components (mainly the central atom and extraction agent) are similar and therefore their material balance must be solved simultaneously. This is the case in exchange extraction systems [3, 4] and also in substoichiometric separations, concentration-dependent distribution and extraction titrations. To achieve an exact mathematical treatment, large universal programs, such as HALTAFALL [5, 6], have been written. Their correct use presupposes that an adequate set of equilibrium constants is available. Hence, in cases when the constants are unknown or unreliable, or they cannot be used because of thermodynamic non-ideality [2], other approaches may be suitable, such as the use of empirical side-reaction (Ringbom) coefficients [7], simplification of material balances [8] based upon average stoichiometric coefficients [9], the empirical concept of corresponding (isodistribution) extraction systems [10] or a semiempirical approach [4].

Progress in computational techniques has enabled calculations to be made which had been considered uneconomical until quite recently. Though there still exists the barrier of availability of reliable input data, the computations themselves are now readily achieved. It also appears that no substantial deviations from thermodynamic ideality occur at least in a number of chelate extraction systems which are used in exchange extractions [4, 11]. This paper provides some examples of mathematical modelling of such systems which could serve a more general purpose. The symbols used in this paper are as given previously [4] or are given in Table 1.

FREE LIGAND CONCENTRATION AND ENRICHMENT FACTORS

In the previous paper [11], the material balance of components was given in the initial form $c_A r' = \alpha[A]v + \bar{n}_t c_M$, where $\bar{n}_t$ was the mean total ligand number for the system containing complexes MA_n [4] or $[MA_{n-1}HA]$ [11] and MB_j, but neither lower complexes with ligand A nor polynuclear complexes M_mB_j were taken into account. When the last species are considered and volume changes are negligible ($r' = r$, $v = 1$), the equation obtained is

$$\sum_{i=1}^{n+1} \{\alpha a_{i-1} + a_i [ic_M/(1 + \bar{m}_t) - rc_A]\}[A]^i - \alpha[A]X_{MB} - rc_A X_{MB} = 0 \quad (1)$$

where α is the ratio of the amount of all forms of free extraction agent to the amount of A^- in the aqueous phase, and $a_i = \beta_i[r(K_D)_{MA\,i} + 1]$ are weighted stability constants for the two-phase systems with volume ratio

TABLE 1

Symbols used

a_i	$\beta_i[(K_D)_{MAi} + 1]$, weighted stability constants in the two-phase system
a	$(1/n)\log \beta_n$, mean consecutive constant
a_t	$(1/n)\log a_n$, parameter of stability constant normalization in the two-phase system
K_i	$[MA_i]/[MA_{i-1}]\,[A]$, consecutive stability constants
$\bar{m}$	$\Sigma_{m=1}\,\Sigma_{j=0}\,(m-1)\,\beta_{mj}\,[M]^{m-1}\,[B]^j/(X_{MA} + X_{MB})$, the mean excess of central atom number (above $m = 1$) in a mixture of complexes M_mB_j
$\bar{m}_t$	As $\bar{m}$, in the two-phase system
M, N	Central atoms
$\bar{n}_t$	Mean total ligand (A) number in the two-phase system
q	nc_M/rc_A, stoichiometric quotient
$S_{M,N}$	Enrichment factor in separation of M from N
x	$rc_A\,10^{at}/\alpha$, normalized acidity function
x_i	ith approximation of root of a polynomial
X_{MB}	$\Sigma_{j=0}\,\Sigma_{m=1}\,\beta_m\,[M]^{m-1}\,[B]^j$, complexation function of M_mB_j formation (likewise X_{MA}, X_{NA} and X_{NB})
y	$[A]10^{at}$, normalized free ligand concentration
β_i	$[MA_i]/[M][A]^i$, stability constant for adduct formation
β_{mj}	$[M_mB_j]/[M]^m[B]^j$, stability constant with competing ligand B ($\beta_{10} = 1$)

$V_0/V = r$ (a_i is zero when $i < 0$ or $i > n$). If the complex MA_i is not extracted, then a_i is identical with β_i; when its distribution constant is very large, a_i equals its two-phase stability constant. Basically, a_n can easily be extended to the case of extraction of adduct complexes ($MA_{n-s} \cdot sHA$), when $a_n = \beta_{ns}\{r(K_D)_{MA_{n-s}\cdot sHA} + 1\}\{[H]\ (K_D)_{HA}\}^s$.

Normalization of Eqn. (1) can be achieved if, as was proposed by Dyrssen and Sillén [12], a mean stability constant parameter, $a = (1/n)\log \beta_n$, and its analogue for a two-phase system, $a_t = (1/n)\log a_n$, are used, as was done by Skytte-Jensen [13]. By introducing the product $[A]\ 10^{a_t} = y$ instead of [A], it is possible to obtain a "full" normalization of Eqn. (1), as was done in systems with excess of extractive ligand [12]. If only the highest complex formation ($a_i = 0$ if $i \neq n$) is considered and if $X_{MB} = 1$, the normalized version of Eqn. (1) is obtained in the form

$$y^{n+1} + y^n(q-1)x + y - x = 0 \tag{2}$$

where $x = rc_A\ 10^{a_t}/\alpha$ and $q = nc_M/rc_A$. In general, the last two terms of this equation should be multiplied by X_{MB}. Besides the molar composition coefficient q, x becomes a new normalized parameter, which can be used together with y to describe the exchange extraction system ($q = 1$), and other systems containing a metal and a chelating agent in similar amounts ($q > 0$), in coordinates identical to those for qualitatively different systems (see below). For $q = 0$, the solution $y = x$ is valid. For $q = 2$ (substoichiometric extraction), a limit value $y = a_t$ is obtained when $x \gg 1$.

When [A] is calculated the distribution ratio of element M is given by

$$D_M = \beta_n(K_D)_{MA_n}[A]^n/(X_{MA} + X_{MB})\ (1 + \bar{m}) \tag{3}$$

as that of another element (N) present in the system in minor concentration compared with M (its polymerization can always be neglected) is given by

$$D_N = \beta_p(K_D)_{NA_p}\ [A]^p/(X_{NA} + X_{NB}) \tag{4}$$

Thus, regarding the separation efficiency during an exchange extraction, the enrichment factor is $S_{M,N} = S = D_M(1 + rD_N)/(D_N(1 + rD_M)$. Thus neglecting $\bar{m}$ and if $p \geqslant n$,

$$[A]^p r(S-1) - [A]^{p-n}(X_{NA} + X_{NB})/\beta_p(K_D)_{NA_p}$$

$$+ S(X_{MA} + X_{MB})/\beta_n(K_D)_{MA_n} = 0 \tag{5}$$

The functions X_{NA} and X_{MA}, if included, are themselves polynomials of the order p and n, respectively. From this equation, [A] can be evaluated at a certain pH value (which influences complexation functions X_{MB} and X_{NB}) and at a given value of S. If complexation in the aqueous phase is negligible and the extraction of M strongly prevails ($D_M \gg 1$ and $D_N \ll 1$), a trivial dependence of S on pA is obtained, viz., $\log S = -\log\{r\beta_p(K_D)_{NA_p}\} - p\log[A]$. In general, however, enrichment factors are more complicated functions of both pA and pH values and their optimization is necessary.

Solving Eqns. (1) or (2) and (5) presents the same problem: finding the roots of a polynomial expression. The highest degree which can be encountered in practice is probably n or $p = 4$. Therefore, an iteration procedure is desirable for finding real positive roots.

As is known, the iteration procedure usually ensues from a Newton-Raphson formula such as $x_{i+1} = x_i - f(x_i)/f'(x_i)$, where x_i is identical with A from Eqns. (1) and (5), or with y from Eqn. (2), and f represents the left side of these equations and f' their first derivative. For the present purpose Laguerre's version of iteration [14] was used

$$x_{i+1} = x_i - uf(x_i)/\{f'(x_i) \pm [H(x_i)]^{1/2}\} \quad (6)$$

where u is the degree of the polynomial, $H(x_i) = (u-1)\{(u-1)[f'(x_i)]^2 - uf(x_i)f''(x_i)\}$, and the sign of its square root in Eqn. (6) is the same as the sign of $f'(x_i)$. The convergence of iterations was found to be very good; even when the first approximation (x_1) differed by five orders from a true root of a polynomial of the 4th order, 6 iterations led to a value which deviated only by 0.3%. The calculation of the first and second derivatives of the solved equations, after their analytical expression, does not present any serious complications. Some problems arose with the polynomials of higher degree when $x \approx y$ (see Eqn. 2). In these conditions, however, Moore's method of iteration [15], which is in the library of standard programs for the Hewlett-Packard 9825A desktop computer which was used, also located two positive roots with a negligible imaginary part, and the root of higher value was of no physical significance. Therefore, x appeared to be convenient as the first approximation of y in order to avoid inconvenience in solving Eqn. (2) by the Laguerre algorithm.

For the calculation of free ligand concentration from Eqn. (1) at different pH values, a program EPAD was written for the Hewlett-Packard 9825A desktop computer. The following algorithm was used in the program.

1. Put $\bar{m}_t = 0$.
2. Calculate complexation function X_{MB} (hydrolysis and masking).
3. Calculate [A] by Laguerre's iteration procedure from Eqn. (1) until $[A]_{i+1}$ does not differ by more than 0.1% from $[A]_i$.
4. Calculate D_M from Eqn. (3).
5. Calculate the concentration of free metal ion from a separate mass balance in the aqueous phase.
6. End the calculation if the mass balance in the aqueous phase fits to within 1%, otherwise repeat the procedure from item 2 onwards.

The evaluation of [A] from Eqn. (5) by Laguerre's method presented no difficulty. Further, a program SEFAC written here for the HP 9825A located the positive roots [A] for a given set of $S_{M,N}$ (usually from 10^{-4} to 10^4) together with the recovery fraction R_M (or R_N) at different pH values and at different volume ratios r.

TYPICAL pH—pA DIAGRAMS

The equilibrium constants used in these calculations were the same as in previous papers [4, 11] or were taken from critical tables [16]. When the lower complexes were taken into account, the statistically probable spread factor of the stability constants was considered. Thus consecutive constants were related by $K_{i+1}/K_i = (n - i + 1)\,(i + 1)/(n - i)i$ [12]. The aim of these calculations is illustrative and their comparison with experimental data requires further critical screening of equilibrium data.

In Fig. 1, pA values are plotted as a function of acidity at different molar compositions of the extraction system indicated by values of q given. The curves belonging to stoichiometric chelates ($q = 1$) have been drawn in a thicker line. A different abscissa was chosen in these illustrations; pH is not generally used. It must be borne in mind that if the extraction agent is a simple acid (HA), a proportionality $\log(\alpha - 1) = \log[r(K_D)_{HA} + 1] + pK_{HA} - pH$ holds; it is demonstrated by the parallel pH abscissae in Fig. 1C and D.

Thus, for the zinc diethyldithiocarbamate (Fig. 1A) and iron(III) 8-quinolinol chelates (Fig. 1B) the abscissa is $\log(rc_A/\alpha)$. These systems may serve as typical models for chelates of M^{2+} and M^{3+} widely encountered in practice [3]. It should be remarked that there is only a small difference in these diagrams when they are plotted in normalized coordinates, $\log y = a_t - pA$ vs. $\log x = \log(rc_A/\alpha) + a_t$, as was expected.

The reason why chelate exchange extraction systems are used in analytical practice is sometimes expressed only vaguely. What is clear, however, is that if a distribution of some element depends on the pA value only, it should make no difference which analytical composition is chosen to reach a certain pA value. For example, it can be calculated that pA = 6.0 is to be found in the absence of hydrolysis, in the zinc diethyldithiocarbamate—carbon tetrachloride system (Fig. 1A) under the following conditions:

q	= 0.0	0.98	1.0
$\log(rc_A/\alpha)$	= −6.00	−4.30	−2.98

Because the same rc_A/α value can also be obtained in systems of various analytical composition and phase ratios (e.g., $\log rc_A/\alpha = -2.98$ at $rc_A = 2 \times 10^{-3}$ mol dm^{-3} and pH 5.8 or at $rc_A = 2 \times 10^{-2}$ mol dm^{-3} and pH 4.5) there are several ways of reaching pA = 6.0 and the subsequent extractive recovery of an element.

There are other reasons in favour of exchange extraction systems, viz. an increased stability of extraction agent when present as a chelate, higher extraction capacity of an organic phase at higher pA and pH values, kinetic inertness and the spectral (optical) properties of chelate solutions. Another reason which deserves more attention is the ligand-buffering effect of the excess of metal [3]. It can be observed in Fig. 1A and B that there is only a

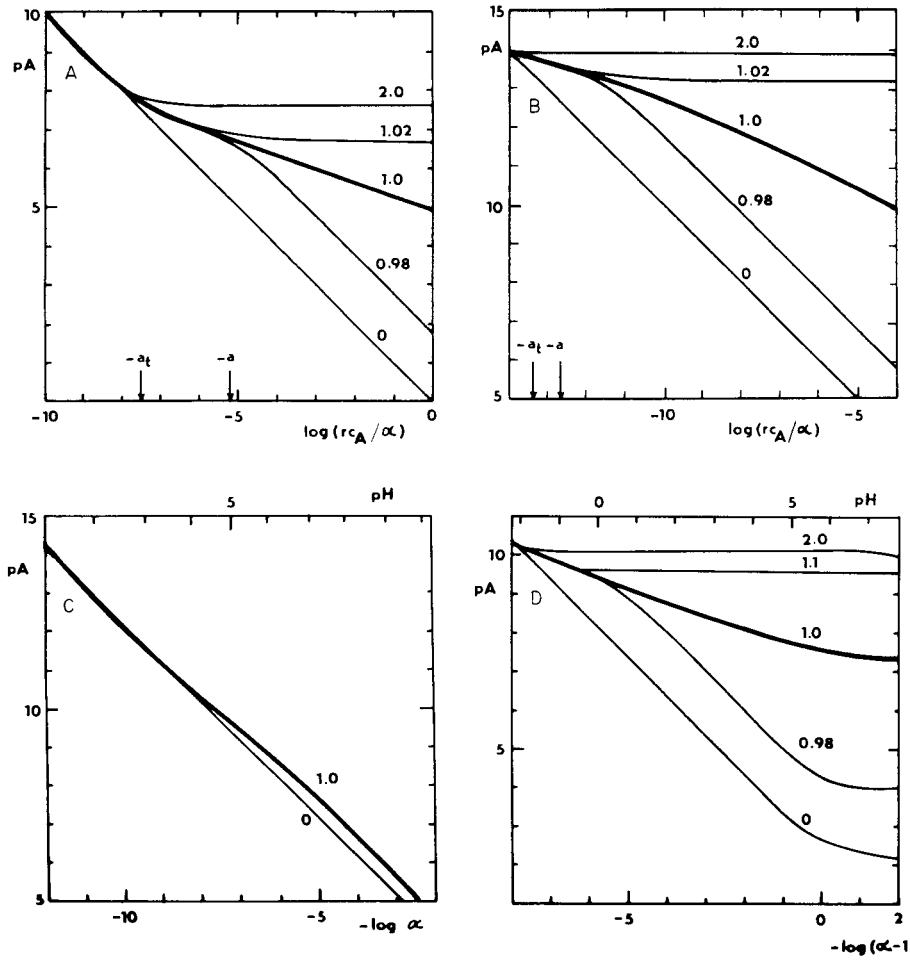

Fig. 1. pA as a function of acidity function (α), extraction agent concentration (c_A) and phase ratio (r) at different values of q (indicated by the numbers on the graphs). (A) For zinc diethyldithiocarbamate in CCl_4; pK_{HA} = 3.40, log K_D = 2.39; β_1 = 5.48, β_2 = 10.37, $(K_D)_{MA_2}$ = 4.81. (B) For iron(III) 8-quinolinolate in $CHCl_3$; pK_{HA} = 9.66, pK_{H_2A} = 5.0, log K_D = 2.66; β_1 = 13.18, β_2 = 26.35, β_3 = 38.10, $(K_D)_{MA_3}$ = 3.60. (C) For scandium 8-quinolinolate in $CHCl_3$ (formation of $ScOx_3 \cdot HOx$); $c_A = 5 \times 10^{-3}$ mol dm^{-3}; β_{41} = 39.83, $(K_D)_{MA_3 \cdot HA}$ = 2.99; for hydroxo complexes, β_{11} = 9.10, β_{12} = 17.3, β_{22} = 22.0, β_{13} = 24.7, β_{14} = 29.4. (D) For lead diethyldithiocarbamate in $CHCl_3$–citrate (0.1 mol dm^{-3}), $rc_A = 5 \times 10^{-3}$ mol dm^{-3}; diethyldithiocarbamate log stability constants, β_1 = 7.90, β_2 = 15.19, $(K_D)_{MA_2}$ = 5.0; for hydroxo complexes, β_{11} = 6.14, β_{21} = 7.84, β_{12} = 10.7, β_{13} = 14.0; for $[Pb(HCit)]^-$, β_1 = 5.7.

2% excess of metal above the stoichiometric ratio (q = 1.02), which is sufficient to keep the pA value constant over a wide interval of acidity.

Systems insensitive to pH offer well-known advantages. Moreover, they are almost inevitably used to achieve reproducibility in exchange extraction

systems. Stoichiometric chelate systems ($q = 1$) are characterized by a strong influence of phase composition on pA, which is much greater than the influence of pH in "common" systems, i.e., those with an excess of chelating agent. The ratio $q = 1$ can be relatively easily shifted to lower values in practice, e.g., by purification of the metal chelate or washing with aqueous phase. For instance, in the zinc diethyldithiocarbamate system (Fig. 1A) under the conditions where $\log(rc_A/\alpha) = -3$, if the ratio $nc_M/c_A r$ is changed from 1.02 to 0.98, pA decreases drastically by 3.2, equivalent to the same increase of pH in a system with pure diethyldithiocarbamate. The last difference can hardly be ignored during experimental work, but the first would easily remain forgotten. For this reason, if it appears possible, the effect of the presence of a small excess of free metal in the aqueous phase is appreciable. It can be proved that another metal present at high concentration may function as a buffering component.

Adducts of the scandium 8-quinolinolate ($ScOx_3 \cdot HOx$) type do not possess buffering properties and behave as systems with excess of chelating agent even at $q > 1$ (Fig. 1C). It can be noted that this effect can be used in connection with another trace exchange extraction, because if its distribution in the system with metal chelate depends on pH in the same manner as with the free chelating agent, it gives evidence of adduct formation in the organic phase, and vice versa. Formation of the polynuclear species, $Sc_2(OH)_2^{4+}$, was included in the calculation used to produce Fig. 1C. Nevertheless, in comparison with the results when only mononuclear complexes were taken into account, the pA values in the system with $c_A = 5 \times 10^{-3}$ mol dm^{-3} differed insignificantly. For instance, in the system with a stoichiometric chelate ($q = 1$) at pH 5.0, where $\bar{m}_t$ should reach the value 0.45, the calculated pA was 9.636, but in the systems where $\bar{m}_t$ was postulated to be zero, pA was found to be 9.651. The evaluated distribution ratios were 3.05×10^{-2} and 6.67×10^{-2}, thus polymerization in the aqueous phase may have only a small effect on pA in other similar cases.

As a final example (Fig. 1D) calculations for the system lead diethyldithiocarbamate ($c_A = 5 \times 10^{-3}$ mol dm^{-3})—chloroform with 0.1 mol dm^{-3} citrate buffer are presented; this system is widely used in exchange extractions and spectrophotometric determinations [3]. To illustrate better the character of limit values of pA at higher pH values, the abscissa of the diagram is $\log(\alpha - 1)$. Considering the stability constant for $[Pb(HCit)]^-$ formation, complexation with citrate becomes of importance only in systems with excess of metal and at higher pH; it prevents the formation of polynuclear species such as $Pb_2(OH)^{3+}$, so that they need not be considered in the calculations.

Because in real chelate systems the dominating equilibrium consists of the heterogeneous reaction of chelate dissociation, $(MA_n)_{org} \rightleftharpoons M^{n+} + nA^-$, the normalized form of Eqn. (1) does not differ too much from the "full" models in Fig. 1, C and D. Listing of real roots of polynomial (2) as the function of normalized parameter x and the ratios q which could often be

encountered in practice, is reasonable. Results obtained by solving Eqn. (2) for systems of various compositions containing different chelates MA . . . MA_4 are presented in Table 2.

It is of particular interest that in stoichiometric chelate systems a reduced form of Eqn. (2) is sufficient at $y^n \gg X_{MB}$, namely $y^{n+1} - x = 0$; by considering the side complexation, a simple equation is obtained for use in connection with exchange extraction systems

$$(n + 1)\text{pA} = -\log x - \log X_{MB} \tag{7}$$

An example is the calculation of pA in the stoichiometric lead diethyldithiocarbamate system (2.5×10^{-3} mol dm^{-3}) in chloroform (Fig. 1D), at pH 3.0, when $\log \alpha = -2.80$. The parameter $a_t = 0.5 \log a_2 = 0.5 \log [\beta_2 r(K_D)_{MA_2} + 1] = 10.10$, and the normalized $\log x = \log(rc_A/\alpha) + a_t = 5.0$. Table 2 gives the corresponding value $\log y = 1.667$ and $\text{pA} = a_t - \log y = 8.43$. This is the same value as that obtained from Eqn. (7), because X_{MB} was practically unity under these conditions, or from a "full" balance of the species listed in the legend to Fig. 1D.

The data in Table 2 may be used to describe a great variety of real extraction systems with macro amounts of metal, exchange extraction systems in particular, with sufficient precision. For exchange extraction systems, Eqn. (7) is also useful in this respect.

ENRICHMENT FACTORS

Because, as discussed above (see also [10]), the problem of separation of two elements is not a matter of analytical composition of thermodynamically ideal systems, but of equilibrium concentrations which can be achieved in a different way, separation by exchange extraction can be described with the help of the same equilibrium parameters as in extraction with excess of chelating agent. As shown above, finding appropriate values of those parameters is no more difficult than in other systems. A brief illustration of enrichment factors may be given in the same systems, as a function of pA and pH, based on solving Eqn. (5).

The first example concerns the possibility of separation of iron and cobalt with diethyldithiocarbamate. As reported before [4], there is substantial difference in exchange extraction with zinc diethyldithiocarbamate in carbon tetrachloride and in chloroform solutions. The enrichment factors $S = 10$ and 100 were located in the considered region of pA and pH (Fig. 2). In the carbon tetrachloride system, where cobalt(II) is separated from iron(II), the calculated value of $S_{Co,Fe}$ remains constant over a wide range of pH (curves 2 and 3, Fig. 2), but the value changes in chloroform, where cobalt(III) diethyldithiocarbamate is formed [4]. However, recovery of cobalt(II) in the former system would be efficient only at $\text{pA} \simeq 7.6$, when $S_{Co,Fe} = 10$ (curve 2, Fig. 2). In the extraction of diethyldithiocarbamates with chloroform, iron(II) extraction prevails over cobalt(III) and $S_{Fe,Co}$

Normalized coordinates of pA as a function of rc_A/α ($\log x = a_t + \log rc_A/\alpha$, $\log y = a_t - pA$) for chelate formation (MA, MA_2, MA_3, MA_4) at different $q = nc_M/rc_A$ values

$\log x$	$\log y$ for MA chelate				$\log y$ for MA_2 chelate			
	$q = 0.98$	$q = 1.00$	$q = 1.02$	$q = 2.00$	$q = 0.98$	$q = 1.00$	$q = 1.02$	$q = 2.00$
−1.000	−1.037	−1.038	−1.039	−1.074	−1.004	−1.004	−1.004	−1.008
−0.500	−0.596	−0.598	−0.600	−0.683	−0.535	−0.535	−0.536	−0.565
0.000	−0.205	−0.209	−0.213	−0.383	−0.164	−0.166	−0.168	−0.265
0.500	0.137	0.129	0.122	−0.183	0.101	0.094	0.088	−0.109
1.000	0.445	0.432	0.418	−0.074	0.315	0.301	0.288	−0.040
1.500	0.736	0.711	0.687	−0.026	0.515	0.485	0.457	−0.013
2.000	1.022	0.978	0.935	−0.009	0.727	0.660	0.602	−0.004
2.500	1.315	1.238	1.161	−0.003	0.984	0.830	0.716	−0.001
3.000	1.629	1.493	1.358	−0.001	1.343	0.999	0.790	−0.000
3.500	1.980	1.746	1.514	−0.000	1.806	1.166	0.827	−0.000
4.000	2.381	1.998	1.616	−0.000	2.302	1.333	0.842	−0.000
4.500	2.831	2.249	1.668	−0.000	2.801	1.500	0.847	−0.000
5.000	3.311	2.499	1.688	−0.000	3.301	1.667	0.849	0.000
5.500	3.804	2.750	1.696	−0.000	3.801	1.833	0.849	0.000
6.000	4.302	3.000	1.698	0.000	4.301	2.000	0.849	0.000
	$\log y$ for MA_3 chelate				$\log y$ for MA_4 chelate			
−1.000	−1.000	−1.000	−1.000	−1.001	−1.000	−1.000	−1.000	−1.000
−0.500	−0.512	−0.512	−0.513	−0.523	−0.504	−0.504	−0.504	−0.508
0.000	−0.138	−0.140	−0.142	−0.209	−0.121	−0.122	−0.124	−0.175
0.500	0.079	0.074	0.069	−0.078	0.065	0.061	0.056	−0.061
1.000	0.242	0.230	0.218	−0.027	0.197	0.186	0.175	−0.021
1.500	0.398	0.367	0.340	−0.009	0.325	0.294	0.269	−0.007
2.000	0.577	0.497	0.437	−0.003	0.488	0.398	0.342	−0.002
2.500	0.855	0.624	0.506	−0.001	0.813	0.499	0.388	−0.001
3.000	1.304	0.749	0.543	−0.000	1.301	0.600	0.411	−0.000
3.500	1.801	0.874	0.558	−0.000	1.801	0.700	0.420	−0.000
4.000	2.301	1.000	0.564	−0.000	2.301	0.800	0.423	−0.000
4.500	2.801	1.105	0.565	−0.000	2.801	0.900	0.424	−0.000
5.000	3.301	1.250	0.565	0.000	3.301	1.000	0.425	−0.000
5.500	3.801	1.375	0.566	0.000	3.801	1.100	0.425	−0.000
6.000	4.301	1.500	0.566	0.000	4.301	1.200	0.425	−0.000

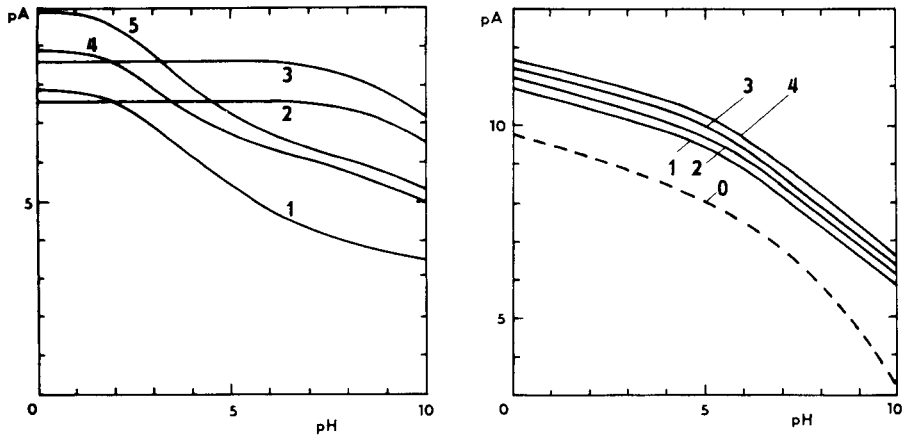

Fig. 2. pA—pH dependences at various enrichment factors for Co(II)/Fe(II) separation in diethyldithiocarbamate—CCl_4 (curves 2, 3) and Fe(II)/Co(III) separation in diethyldithiocarbamate—$CHCl_3$ (curves 1, 4, 5) at $r = 1$. S values (1) 1; (2, 4) 10; (3, 5) 100. For Co(II) (log values), $\beta_1 = 5.69$, $\beta_2 = 10.77$, $(K_D)_{MA_2} = 5.38$ (CCl_4); Co(III), $\beta_1 = 6.28$, $\beta_2 = 12.09$, $\beta_3 = 17.43$, $(K_D)_{MA_3} = 5.0$ ($CHCl_3$); Fe(II), $\beta_1 = 5.58$, $\beta_2 = 10.56$. $(K_D)_{MA_2} = 5.0$ (CCl_4), 4.0 ($CHCl_3$). For hydroxo complexes, Co(II) (log values), $\beta_1 = 5.10$, $\beta_2 = 9.20$, $\beta_3 = 10.50$; Co(III), $\beta_1 = 12.0$; Fe(II), $\beta_1 = 5.70$, $\beta_2 = 9.00$.

Fig. 3. pA—pH dependences at various enrichment factors for Fe(III)/Sc(III) separation in 8-quinolinol—$CHCl_3$. Numbers on the graphs indicate the log $S_{Fe,Sc}$ values. The constants used are as in Fig. 1B and C, and for Fe(III) hydroxo complexes (log values), $\beta_1 = 11.0$, $\beta_2 = 21.7$, $\beta_3 = 25.1$.

depends also on pH (curves 4 and 5, Fig. 2). Again, $S = 100$ and 1000 at low pH are of theoretical interest only, because recovery of >95% of iron would be observed only in the region of pA <6.5 and pH 7—8. This can be the case when exchange extraction at high pH is preferred to extraction with excess of reagent at lower pH and the same pA, because at low pH $S_{Fe,Co}$ can drop to 1 (curve 1, Fig. 2).

Similarly, the best conditions for iron(III) separation from scandium(III) were sought in systems with 8-quinolinol (Fig.3). If the constants used in calculation were valid in real systems, curve 4, corresponding to $S_{Fe,Sc} = 10^4$, would indicate the proper value of pA and pH for such a separation. The multiple roots of Eqn. (5) at $S = 1$, where the separation would not be at all effective, were scattered along the dotted line. The choice whether an exchange or common extraction system should be applied, depends on their availability. An optimal system for separation of macro amounts of iron from micro amounts of scandium may be considered as that given by curve 3 in Fig. 3, i.e. $S_{Fe,Sc} = 10^3$, and the point with coordinates pA = 10.0 and pH = 6.0 is selected. As ensues from Fig. 1B, the value pA 10.0 can be achieved in systems up to equivalent amounts of iron at log $(rc_A/\alpha) < -4$, i.e., at $rc_A < 20$ at pH 7 (log $\alpha = 5.32$). For reason of solubility of iron 8-quinolinolate, however, the optimal conditions would

be achievable only by the presence of an excess of 8-quinolinol; a 2% excess (q = 0.98) would give pA = 10.0 if $rc_A = 2 \times 10^{-3}$ mol dm^{-3}, and the removal of macro amounts of iron from traces of scandium (which remain in the aqueous phase) would be ensured. Polymerization of iron in the aqueous phase, however, will probably diminish the distribution ratio according to Eqn. (3), so that the actual enrichment factor will be lower.

In conclusion, it can be said that the choice of composition of an extraction system should be based on the approach to optimal conditions of separation given by equilibrium pA and pH values. It can be done by superposition of pA–pH diagrams, at different stoichiometric ratios (q) in respect of major elements, and at various enrichment factors (S) of separated elements.

REFERENCES

1 J. Rydberg, Acta Chem. Scand., 4 (1950) 1503.
2 Y. Marcus and A. S. Kertes, Ion Exchange and Solvent Extraction of Metal Complexes, Wiley—Interscience, London, 1967.
3 Yu. A. Zolotov and B. Ya. Spivakov, Zh. Anal. Khim., 25 (1970) 616.
4 D. Vančo and F. Macášek, Anal. Chim. Acta, 121 (1980) 249.
5 N. Ingri, W. Kakolowicz, L.G. Sillén and B. Warnquist, Talanta, 14 (1967) 1261.
6 F. Gaizer, Coord. Chem. Rev., 27 (1979) 195.
7 A. Ringbom, Complexation in Analytical Chemistry, Wiley—Interscience, New York, 1963.
8 F. Macášek, Chem. Zvesti, 28 (1974) 3.
9 H. Irving, F. J. C. Rossotti and R. J. Williams, J. Chem. Soc., (1955) 1906.
10 F. Macášek, Zh. Anal. Khim., 35 (1980) 427.
11 D. Vančo and F. Macášek, Anal. Chim. Acta, 131 (1981) 323.
12 D. Dyrssen and L. G. Sillén, Acta Chem. Scand., 7 (1953) 663.
13 B. Skytte-Jensen, Acta Chem. Scand., 13 (1959) 1347.
14 A. Ralston, A First Course in Numerical Analysis, McGraw-Hill, New York, 1965.
15 J. B. Moore, J. Assoc. Comput. Mach., 14 (1967) 311.
16 J. Kragten, Atlas of Metal—Ligand Equilibria in Aqueous Solution, Horwood, Chichester, 1978.

Analytica Chimica Acta, 132 (1981) 187—193
Elsevier Scientific Publishing Company, Amsterdam — Printed in The Netherlands

PREPARATION AND ANALYTICAL PROPERTIES OF A CHELATING RESIN CONTAINING CYSTEINE GROUPS

CHUEN-YING LIU and PENG-JOUNG SUN*

Department of Chemistry, National Taiwan University, Taipei, Taiwan (Republic of China)

(Received 21st May 1981)

SUMMARY

A macroporous, cross-linked polyacrylonitrile copolymer was synthesized, the nitrile groups were converted to carboxylic acid by hydrolysis, and these carboxylic acid groups were treated with L-cysteine and 1,6-hexanediol (binding agent). Studies of the basic characteristics of this resin showed that it was highly selective for silver(I), mercury(II), gold(III) and platinum(IV) in aqueous acidic solution, the maximum capacities being 0.97, 0.65, 1.22 and 0.39 mmol g^{-1} of dry resin, respectively. These four metal ions can be separated from each other, or concentrated from very dilute solutions, on a short column of the resin. The effects of different acids and of various common metal ions are reported.

The chemical behavior of an ion-exchange resin is determined by the nature of the functional groups attached to the hydrocarbon skeleton. Highly selective chelating resins can be synthesized by attaching appropriate ligand groups to the resin matrix. Cysteine, with three coordination sites, is an interesting ligand: at low pH values, only the sulfhydryl group is used in complex formation [1]. Studies have shown that sulfur-containing ligands exhibit better selectivity for the noble and heavy metals than their oxygen and nitrogen analogs [2]. Although many complexes of cysteine and its alkyl esters, both in solution and in the solid state with a variety of metals have been described [3—10], less information is available about the complexes of noble metals with cysteine [11, 12]. No information on resins containing cysteine groups seems to have been reported. This paper describes the synthesis and basic characteristics of a resin with cysteine ligands and its analytical application in the chromatography of silver and some noble metals.

EXPERIMENTAL

Instrumentation and reagents

A Radiometer pH meter was used with saturated calomel (Type K401) and glass (Type G202B) electrodes, which were calibrated against Beckman standard buffer solutions of pH 4.00 and 7.00. A Hitachi model 624 digital spectrophotometer connected to a Hitachi model QD_{15} recorder and 10-mm

quartz cells was used for all absorbance measurements. Infrared spectra were recorded on a Perkin-Elmer model 580 spectrophotometer.

Analytical-grade chemicals were used throughout. Stock solutions of silver and platinum ions were standardized by classical titrimetric and gravimetric method. The stock solutions of all other metal ions were standardized by EDTA titration.

Synthesis of the chelating cysteine-containing resin

A macroporous, cross-linked copolymer was prepared by the reaction of acrylonitrile and divinylbenzene as described by Vernon and Eccles [13]. The copolymer was air-dried, ground and sieved. The 60—100 mesh fraction was used for the further synthesis after being washed with 12 M HCl, water and acetone. The copolymer (200 g) was stirred at 80°C with 1 l of 37% (w/v) sodium hydroxide solution until ammonia evolution ceased. The hydrolyzed polymer was cooled to room temperature, collected by filtration under suction and washed with 12 M HCl, water and acetone.

For the first esterification, the carboxylic acid resin (200 g) was mixed with 600 g of molten 1,6-hexanediol (m.p. 41°C) containing 50 ml of 18 M sulfuric acid as catalyst. The mixture was kept at 70°C for 30 h for esterification. The product was collected from the hot solution by filtration under suction, and washed with boiling methanol. For the second esterification, a mixture of 55 g of this product and 300 g of L-cysteine was added to 500 ml of dioxane containing 20 ml of 18 M sulfuric acid. The mixture was heated at 90°C for 30 h. The final product was collected by filtration under suction and washed sequentially with water, 12 M HCl, water and acetone.

Characterization of resin

In order to verify the presence of cysteine groups in the synthesized resin, the infrared spectrum of the resin was obtained with KBr pellets after each step in the synthesis. The i.r. spectrum of the polyacrylonitrile—divinylbenzene copolymer showed bands at 2260—2240 cm^{-1} (—C≡N), whereas the spectrum of the hydrolyzed product exhibited bands at 3500—2500, 1720, and 920 cm^{-1} (—COOH). The spectrum of the diol ester intermediate (Fig. 1a) exhibited bands at 3450 (—OH), 1735, 1163, and 1064 cm^{-1} (—COOR). The spectrum of the final product (Fig. 1b) showed bands at 2545 (—SH), 2960, 1610, and 1513 ($—NH_3^+$), and 1735, 1163 and 1064 cm^{-1} (—COOR).

The nitrogen and sulfur contents, the hydrogen ion capacity, the capacities for Ag(I), Hg(II), Au(III) and Pt(IV) at pH 1, and the acid ionization constants, were determined with the results shown in Table 1.

The distribution coefficients of the metal ions, defined by the equation D = (mmol of metal/g of dry resin)/(mmol of metal/ml of solution), were determined by using the batch equilibrium method. For each equilibrium experiment, 25 ml of a mixture consisting of various amounts of acid and 0.3 mmol of the metal ion in question was treated with 0.2 g of fresh resin and the solution was stirred for 8 h at room temperature (25°C). The solution

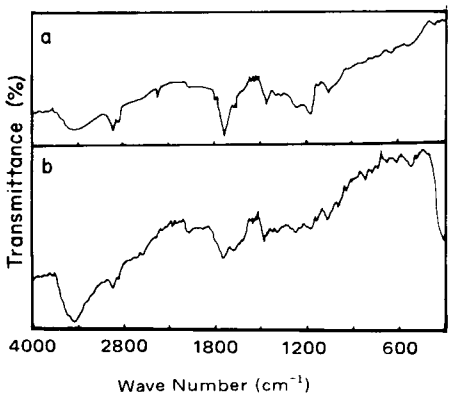

Fig. 1. Infrared spectra: (a) $RCOO(CH_2)_6OH$ intermediate; (b) resin with cysteine group.

was filtered to remove the resin and the metal ion content of the filtrate was determined by conventional spectrophotometric procedures. The results are shown in Tables 2 and 3.

On the basis of these experiments, the order of selectivity of the resin was Au > Ag > Hg > Pt > Mo. The results also show that the resin readily retains Au(III), Ag(I), Hg(II) and Pt(IV) from either 0.1 M $HClO_4$ or 0.1 M HCl. Molybdenum is also retained by the resin from 0.1 M HCl. Negligible adsorption was shown by the alkali metals, alkaline earths, iron(III), cobalt(II), nickel(II), zinc(II), cadmium(II), and lead(II) in 0.1 M acid. This suggested that column chromatographic separation and concentration of metal ions (Pt(IV), Hg(II), Ag(I), Au(III)) should be possible with this resin.

Chromatographic application

The resin column (6 mm i.d., 55 mm long) was conditioned with 30 ml of 0.1 M HCl at 0.5 ml min^{-1}. A sample that contained 0.4—1.5 μmol each of Ag(I), Hg(II), Au(III) and Pt(IV) in 0.1 M acid was added to the column and the liquid level was allowed to drop to the top of the resin bed. The wall of the reservoir was rinsed with 0.1 M hydrochloric acid and then 10 ml of 0.1 M hydrochloric acid was used to elute any other metal ions from the column while the above metals were retained. The retained

TABLE 1

Physical and chemical characterization of the cysteine-containing resin (60—100 mesh)

Percent cross-linking	5.8%	Gold capacity[b]	1.22 mmol g^{-1}
Nitrogen content[a]	1.16 mmol g^{-1}	Mercury capacity[b]	0.65 mmol g^{-1}
Sulfur content	1.15 mmol g^{-1}	Silver capacity[b]	0.97 mmol g^{-1}
Hydrogen ion capacity	2.85 mmol g^{-1}	Platinum capacity[b]	0.39 mmol g^{-1}
pK_a (—COOH, $—NH_3^+$, —SH)	5.65, 6.59, 7.16	Molybdenum capacity[b]	0.22 mmol g^{-1}

[a]The nitrogen content of the original copolymer was 25.0% (17.9 mmol g^{-1}). All weights refer to dry resin. [b]At pH 1.0.

TABLE 2

Distribution coefficients in perchloric, hydrochloric or hydrobromic acid of varied molarity

Ion	Final acidity (M) 0.1	0.5	1.0	2.0	3.0	5.0	6.0	7.0	8.0
Perchloric acid									
Ag	95	102	104	104	117	96	—	—	—
Au	1360	2430	13300	18000	24300	28300	20600	2800	1150
Hg	54	43	40	38	22	21	21	17	13
Pt	39	46	55	75	68	50	34	34	—
Hydrochloric acid									
Au	220	315	337	442	473	473	537	—	—
Hg	58	22	20	16	0	0	—	—	—
Pt	17	6	9	14	9	4	—	—	—
Mo	16	28	1	3	27	12	16	26	—
Hydrobromic acid									
Au	112	195	165	282	374	326	195	—	—

Pt(IV), Hg(II), and Ag(I) were eluted sequentially with 0.5 M HCl, and with a 6 M HCl—2 M $HClO_4$ solution. The metals were determined spectrophotometrically as their chloride complexes at 262, 229 and 213 nm, respectively. The gold(III) retained by the resin was eluted with 0.1% thiourea in 0.1 M HCl and determined spectrophotometrically at 269 nm as the thiourea complex. A separation curve for the 4-component mixture is shown in Fig. 2.

The effects of other metal ions on the recoveries of Pt, Hg, Ag and Au are listed in Table 4. Samples containing gold and various other metal ions were separated on the column by elution with 6 M HCl; good recoveries of gold were obtained in all cases (Table 5).

TABLE 3

Distribution coefficients in mixtures of hydrochloric acid and perchloric acid

Ion	Final concentration (M)						
	$HClO_4$	1.5	2.0	2.5	3.0	3.5	4.0
	HCl	7.0	6.0	5.0	4.0	3.0	2.0
Au		498	548	577	578	578	676
Hg		10	0	12	12	12	12
Pt		25	26	25	25	19	19

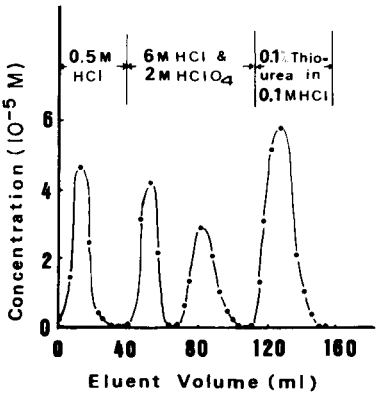

Fig. 2. Separation of Pt(IV), Hg(II), Ag(I) and Au(III) with the resin column. Column 55 × 6 mm i.d.; flow rate 0.5 ml min^{-1}; 0.45 μmol each of Ag, Hg and Pt; 1.50 μmol of Au.

Concentration procedure

The resin column (6 mm i.d., 25 mm long) was conditioned with 0.1 M HCl; then 500 ml of a very dilute solution of the metal ion tested was passed through the column at a flow rate of 0.5 ml min^{-1}. The sorbed metal ions were eluted and determined spectrophotometrically. The results are shown in Table 6.

DISCUSSION

The infrared frequencies for the cysteine-containing resin are in good agreement with those for the cysteine monomer [5]. A potentiometric titration curve obtained when the synthesized resin in the acid form was titrated with 0.1 M KOH at ionic strength 0.1 showed three breaks, only the first of which was quite distinct, corresponding to pK values of 5.65, 6.59 and 7.16 which are assignable to the residual carboxylic acid, amino and the sulfhydryl

TABLE 4

Effect of 5.0 μmol of various metal ions on the recovery of 0.45 μmol of Pt(IV), Hg(II) and Ag(I) and 1.50 μmol of Au(III)

Metal ion	Recovery (%)			
	Pt	Hg	Ag	Au
Cu	97	100	100	100
Fe	99	101	101	100
Pb	97	99	99	100
Zn	100	101	100	100
Ni	100	100	100	100

TABLE 5

Separation of 1.50 μmol of gold from 15 μmol of another metal ion

Metal ion	Ca(II)	Cd(II)	Co(II)	Cu(II)	Hg(II)	Mg(II)	Mn(II)	Ni(II)	Fe(III)	Pb(II)
Au found (μmol)	1.48	1.40	1.45	1.47	1.40	1.51	1.46	1.45	1.58	1.64
Error (μmol)	−0.02	−0.10	−0.05	−0.03	−0.10	+0.01	−0.04	−0.05	+0.08	+0.14

group, respectively. Accordingly, the resin capacities were measured at pH 1.0, which was sufficiently acidic to avoid any interaction of the metal ions with other coordinated groups in the synthesized resin, and ensured that only the sulfhydryl group was involved in complexation.

The maximum capacity of the resin, determined by the batch method in perchloric acid medium, was 1.10 mmol g^{-1} for silver, 0.65 mmol g^{-1} for mercury, 1.34 mmol g^{-1} for gold and 0.59 mmol g^{-1} for platinum (Fig. 3A). The sulfur content of this resin is 1.15 mmol g^{-1}, so that 1:1 complexes are indicated for the resin functional group with silver and gold while 2:1 complexes are indicated for mercury and platinum. Several workers have similarly reported that cysteine binds silver and gold at a 1:1 ligand-to-metal ratio [14, 15], but mercury and platinum at a 2:1 ratio [12, 16]. The formation of the 1:1 complex with gold suggests that gold(III) was reduced to gold(I) by the resin [15]. The higher than theoretical capacity for gold on the basis of 1:1 complex formation in perchloric acid medium may be due to some reduction of gold to the metal. In hydrochloric acid medium, the maximum capacity was 1.16 mmol g^{-1} for gold, 0.48 mmol g^{-1} for mercury and 0.14 mmol g^{-1} for platinum (Fig. 3B). The formation of a 1:1 complex of gold with the resin functional group is indicated. The reduction potential of the metal ions is clearly decreased by the formation of stable chloro complexes in the hydrochloric acid medium compared with in perchloric acid medium.

TABLE 6

Collection of metal ions from dilute solutions

Metal ion	Amount added[a] (μmol)	Eluent	Recovery (%)
Ag	0.45	6 M HCl—2 M $HClO_4$	100.2
	0.23	6 M HCl—2 M $HClO_4$	98.1
Au	1.50	0.1% thiourea in 0.1 M HCl	99.5
	1.50	10^{-3} M thiourea in 10^{-3} M HCl	90.3
	0.45	0.1% thiourea in 0.1 M HCl	78.4
Hg	0.45	6 M HCl—2 M $HClO_4$	101.2
	0.23	6 M HCl—2 M $HClO_4$	91.1
Pt	0.45	0.5 M HCl	99.6
	0.23	0.5 M HCl	65.7

[a]In 500 ml of 0.1 M HCl.

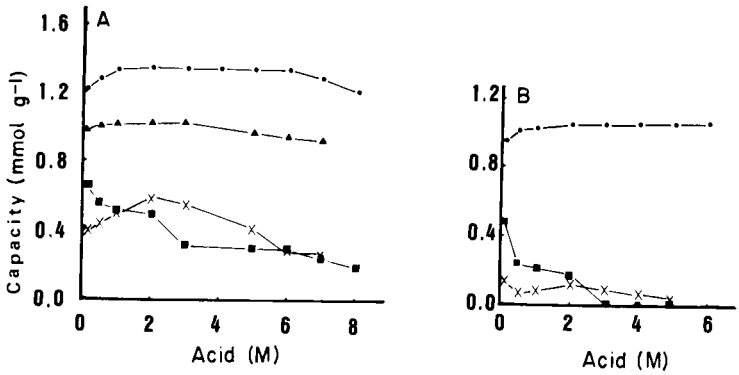

Fig. 3. Total capacity of the cysteine-containing resin for metal ions versus molarity of (A) perchloric acid and (B) hydrochloric acid: (•) Au(III); (▲) Ag(I); (■) Hg(II); (×) Pt(IV).

The lower capacities for mercury and platinum in hydrochloric acid than in perchloric acid at the same hydrogen concentration can be ascribed to competition of the chloride ion with the resin ligand.

REFERENCES

1 P. Dhar and G. N. Mukherjee, J. Indian Chem. Soc., 56 (1979) 1258.
2 F. E. Beamish, Talanta, 14 (1967) 991.
3 C. A. McAuliffe and S. G. Murray, Inorg. Chim. Acta Rev., 6 (1972) 103.
4 H. Shindo and T. L. Brown, J. Am. Chem. Soc., 87 (1965) 1904.
5 Y. K. Sze, A. R. Davis and G. A. Neville, Inorg. Chem., 14 (1975) 1969.
6 C. P. Sloan and J. H. Krueger, Inorg. Chem., 14 (1975) 1481.
7 P. de Meester, D. J. Hodgson, H. C. Freeman and C. J. Moore, Inorg. Chem., 16 (1977) 1494.
8 Y. N. Kothari and D. H. Busch, Inorg. Chem., 8 (1969) 2276.
9 A. Kay and P. C. H. Mitchell, J. Chem. Soc. (A), (1970) 2421.
10 V. R. Ott, D. S. Swieter and F. A. Schultz, Inorg. Chem., 16 (1977) 2539.
11 M. Chandrasenkharan, M. R. Udupa and G. Aravamudan, Inorg. Chim. Acta, 7 (1973) 88; J. Inorg. Nucl. Chem., 36 (1974) 1417.
12 G. Pneumatikakis and N. Hadjiliadis, J. Inorg. Nucl. Chem., 41 (1979) 429.
13 F. Vernon and H. Eccles, Anal. Chim. Acta, 82 (1976) 369.
14 G. D. Zegzhda, S. I. Neikovskii, T. V. Zegzhda, F. M. Tulyupa and N. A. Dorofeeva, Chem. Abstr., 90 (1979) 77249d.
15 T. D. Zucconi, G. E. Janauers, S. Donahe and C. Lewkowicz, J. Pharm. Sci., 68 (1979) 426.
16 W. Stricks and I. M. Kolthoff, J. Am. Chem. Soc., 75 (1953) 5673.

Analytica Chimica Acta, 132 (1981) 195—199
Elsevier Scientific Publishing Company, Amsterdam — Printed in The Netherlands

Short Communication

DETERMINATION OF NITROPHENOL DERIVATIVES IN VARIOUS CROPS BY REVERSED-PHASE ION-PAIR HIGH-PERFORMANCE LIQUID CHROMATOGRAPHY

H. ROSEBOOM*, J. I. J. WAMMES and R. C. C. WEGMAN

Unit for Residue Analysis, National Institute of Public Health, P.O. Box 1, 3720 BA Bilthoven (The Netherlands)

(Received 13th July 1981)

Summary. A method for the determination of nitrophenol derivatives in various crops and soil is described. The sample is extracted with dichloromethane; the extract is evaporated to dryness and the residue is dissolved in an alkaline methanol/water mixture. After filtration this solution is injected. The eluent contains methanol, water, a phosphate buffer and hexadecyltrimethylammonium as the pairing ion. Blank chromatograms for various crops do not show interfering peaks with detection at 365 or 405 nm. The limit of detection is usually around 0.01 mg kg^{-1}; recoveries generally exceed 80% (coefficient of variation, 5—10%). For 2,4-dinitrophenylthiocyanate and dinocap, recoveries are somewhat lower.

Nitrophenol derivatives like 4,6-dinitro-2-cresol (DNOC), 2-*sec*-butyl-4,6-dinitrophenol (dinoseb) and 2-*tert*-butyl-4,6-dinitrophenol (dinoterb) are widely used as herbicides on a variety of crops and can give rise to residues in various foods. For the determination of these compounds, various methods have been described; gas chromatography is used for the final measurement, which makes it necessary to derivatize the phenols in order to increase their volatility. The derivatization procedures used include methylation with diazomethane [1, 2], acetylation with acetic anhydride [3], and the formation of heptafluorobutyryl derivatives after reduction of the nitro group [4].

Recently, the high-performance liquid chromatographic (h.p.l.c.) separation of several nitrophenols has been reported [5, 6]. In both methods the ion-pair technique is used, either with tetrabutylammonium [5] or hexadecyltrimethylammonium [6] as the pairing ion. The latter system seems to give better chromatographic efficiency.

In this communication, a method for the determination of a number of nitrophenol derivatives in various crops and soil samples, based on h.p.l.c. with hexadecyltrimethylammonium as the pairing ion, is described. The method is fast and simple and its sensitivity is quite adequate.

Experimental

Reagents. The nitrophenol derivatives were obtained as analytical standards from the manufacturers and were used without purification.

Dichloromethane (Brocacef, Maarssen, The Netherlands) was distilled prior to use. Sodium sulphate (Analar; B.D.H.) was dried for 5 h at 400°C. Potassium carbonate (zur Analyse, Merck) was dissolved in water to a concentration of 0.1 M.

Hexadecyltrimethylammonium bromide (cetrimide; Baker) was dissolved in methanol (zur Analyse, Merck) to a concentration of 10 g l^{-1}. K_2HPO_4 and NaH_2PO_4 (reagent grade, Baker) were used as aqueous 0.25 M solutions. Appropriate volumes of these cetrimide and phosphate solutions were mixed with methanol and water to give an eluent of the desired composition. After mixing, the eluent was passed through a 0.45-μm filter.

High-performance liquid chromatography. A model 6000 A solvent delivery system, U 6K injector and a model 440 absorbance detector (all from Waters Assoc., Milford, MA, U.S.A.) were used. The stainless steel column (15 cm × 4.6 mm i.d.), packed with LiChrosorb 5 RP 18, was obtained from Chrompak. The eluent was 75% (v/v) methanol in water, containing 0.18% (w/v) cetrimide and 0.006 M phosphate. The flow rate was 1 ml min^{-1} and the detector was operated at 365 or 405 nm.

Procedure. Samples of various crops were chopped into small pieces using a food cutter and a sub-sample of 50 g was put into the beaker of a macerator with 100 ml of dichloromethane. After macerating for 2 min and, if necessary, centrifugation, an aliquot of 50 ml was dried over sodium sulphate and evaporated to a few milliliters in a rotary evaporator at 40°C. This solution was transferred to a calibrated centrifuge tube and evaporated to dryness under a stream of nitrogen at 40°C. The residue was dissolved in 1 ml of a mixture of 0.1 M K_2CO_3 solution and methanol (1:1). This solution was filtered through a 0.45-μm filter by means of a 10-ml glass syringe with Luer end-fitting and a portion (10 or 20 μl) of the filtrate was injected onto the h.p.l.c. column.

For cereals, the procedure was modified. Samples were homogenized by grinding and a sub-sample of 25 g was extracted with 100 ml of dichloromethane by shaking mechanically for 30 min. An aliquot (50 ml) was then filtered over a Büchner funnel and the clear filtrate treated as described above.

Results and discussion

In Fig. 1A is shown the chromatogram of a blank potato extract, for which the equivalent of 250 mg of potato was injected. A clean chromatogram without interfering peaks was obtained with detection at 365 nm, as was pointed out previously [6]. Figure 1B shows the chromatogram of the extract of a blank potato sample, spiked with DNOC, dinoseb and dinoterb at concentrations of 0.1 mg kg^{-1}. These chromatograms prove that under the recommended conditions, these nitrophenols give well-separated, symmetrical peaks and that clean chromatograms are obtained.

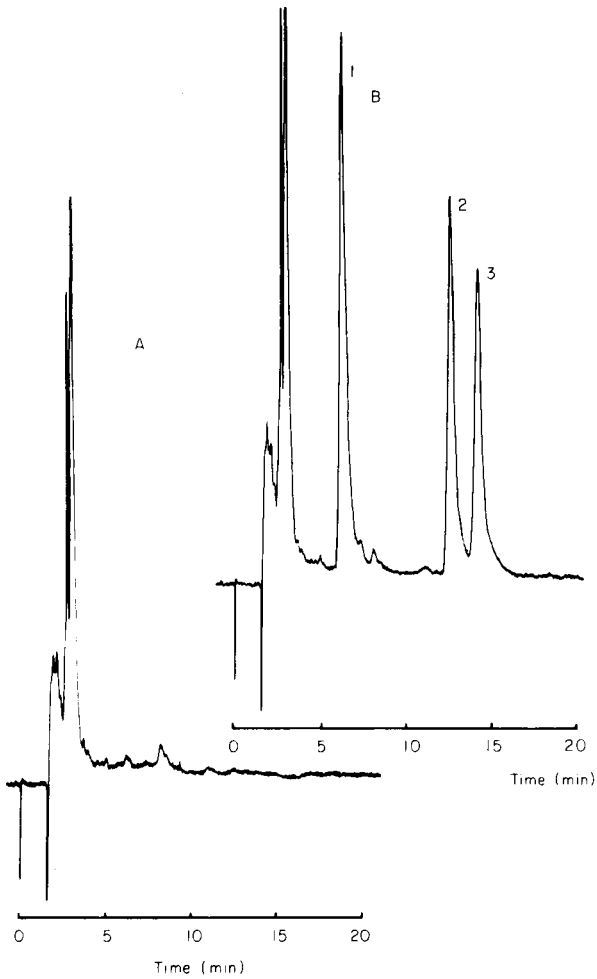

Fig. 1. Chromatograms of potato extracts. For conditions, see Experimental. (A) Blank; (B) spiked to a concentration of 0.1 mg kg^{-1} with DNOC (1), dinoseb (2) and dinoterb (3).

From the signal-to-noise ratio in the chromatogram of Fig. 1B, a detection limit of 0.005–0.01 mg kg^{-1} can be calculated, which is well below the tolerance limit of 0.05 mg kg^{-1}.

In some samples, the determination of DNOC may be difficult because of a large, tailing peak at the solvent front. Accuracy can then be improved by using an eluent containing 0.24% cetrimide, which provides better separation between the tail and DNOC because the retention times of the nitrophenols are increased.

Instead of dissolving the residue in a mixture of methanol and the potassium carbonate solution, it was also dissolved in 3 ml of light petroleum or toluene, after which the phenols were extracted into 1 ml of the alkaline methanol/

water mixture. There were no significant differences between the chromatograms obtained in the two different ways so that, for reasons of simplicity, dissolution in the methanol/water mixture was chosen. Filtration of the final solution before injection proved to be necessary and effective in preventing plugging of the column.

The results of recovery studies of the nitrophenols added to various crops and soil samples are given in Table 1. As can be seen, the recovery is generally very good and the reproducibility is also satisfactory at this rather low level.

Apart from the three most widely used herbicides mentioned in Table 1, the method was also used for the determination of the nitrophenol derivatives dinoseb-acetate, 2,4-dinitrophenyl thiocyanate, 2,4-dinitro-3-methyl-6-*tert*-butylphenyl acetate (medinoterb-acetate) and 2-(1-methylheptyl)-4,6-dinitrophenol crotonate (dinocap). These compounds are not free phenols, but esters, with the exception of 2,4-dinitrophenyl thiocyanate, but in the final alkaline solution the esters are hydrolyzed to the free phenols. Dinocap is a mixture of 4—6 isomers, but after hydrolysis in alkaline medium two main peaks were obtained on injection onto the liquid chromatograph. Under the chromatographic conditions used for the determination of the other compounds, the retention times of these two peaks were very long. Therefore, the recovery of dinocap was determined with an eluent that contained only 0.011% of cetrimide; under such conditions the retention times were 10 and 12 min. The sensitivity for dinocap is not as good as that for the other compounds; the limit of detection is about 0.1 mg kg^{-1}, which is still well below the tolerance limit of 1 mg kg^{-1}. The limits of detection for dinoseb-acetate, 2,4-dinitrophenyl thiocyanate and medinoterb-acetate are in the same range as those for the free phenols.

The recoveries for some nitrophenol derivatives are given in Table 2. It can be concluded that for these compounds also, the recovery and reproducibility are satisfactory, although the results are not as good as for the free

TABLE 1

Recoveries and coefficient of variation of nitrophenols from various crops and soil samples. Unless stated otherwise, the spiking level is 0.05 mg kg^{-1}. Each value is the mean of 4 determinations.

Crop/Soil	Recovery (%) ± c.v. (%)			Crop/Soil	Recovery (%) ± c.v. (%)		
	DNOC	Dinoseb	Dinoterb		DNOC	Dinoseb	Dinoterb
Potato	86 ± 9	90 ± 14	86 ± 15	Sprout	82 ± 7	95 ± 6	97 ± 9
Potato[a]	91 ± 4	87 ± 3	83 ± 2	Cauliflower	84 ± 6	94 ± 9	94 ± 10
Wheat	95 ± 8	65 ± 3	65 ± 2	Carrot	88 ± 11	101 ± 4	100 ± 2
Bean	93 ± 6	99 ± 12	94 ± 9	Apple	93 ± 13	68 ± 7	72 ± 8
Spinach	89 ± 9	87 ± 8	93 ± 2	Sand	85 ± 6	93 ± 8	91 ± 9
Leek	105 ± 9	92 ± 6	81 ± 6	Peat	105 ± 7	100 ± 6	98 ± 5

[a]0.2 mg kg^{-1}.

TABLE 2

Recoveries of nitrophenol derivatives from some crops

Crop	Conc. (mg kg^{-1})	Recovery (%) and c.v. (%)			
		Medinoterb-acetate	2,4-Dinitrophenyl thiocyanate	Dinoseb-acetate	Dinocap
Bean	0.5	85 ± 8	74 ± 5	83 ± 7	—
Leek	0.5	84 ± 3	54 ± 5	82 ± 4	—
Wheat	1.0	76 ± 8	100 ± 4	103 ± 4	66 ± 10
Apple	1.0	—	—	—	91 ± 5

phenols. Recoveries of 2,4-dinitrophenyl thiocyanate and dinocap are rather low. It was shown that 2,4-dinitrophenyl thiocyanate degrades on standing in the final alkaline solution, which probably accounts for the low recovery and large variation. It is, however, necessary to leave the alkaline solution standing for about 1 h to achieve complete hydrolysis of the esters.

For dinocap, the recoveries were calculated from the height of the first of the two peaks. When the second peak was used, the results were essentially the same. It should be kept in mind, however, that dinocap is a mixture of isomers and that the ratio of these isomers in the mixture is not necessarily always the same. Therefore, it is rather difficult to determine an exact concentration of dinocap.

For the most widely used nitrophenol derivatives, the method gives good results with respect to recovery, reproducibility and sensitivity. The speed and ease of operation of the method make it attractive for routine use in monitoring programs.

REFERENCES

1 T. R. Edgerton and R. F. Moseman, J. Agric. Food Chem., 26 (1978) 425.
2 A. J. Cessna, J. Agric. Food Chem., 27 (1979) 191.
3 R. T. Coutts, E. E. Hargesheimer and F. M. Pasutto, J. Chromatogr., 195 (1980) 105.
4 K. W. Kirby, J. E. Keiser, J. Groene and E. F. Slach, J. Agric. Food Chem., 27 (1979) 757.
5 J. C. Hoffsommer, D. J. Glover and C. Y. Hazzard, J. Chromatogr., 195 (1980) 435.
6 H. Roseboom, C. J. Berkhoff, J. I. J. Wammes and R. C. C. Wegman, J. Chromatogr., 208 (1981) 331.

Analytica Chimica Acta, 132 (1981) 201—204
Elsevier Scientific Publishing Company, Amsterdam — Printed in The Netherlands

Short Communication

DOSAGE DE SEPT AGENTS CONSERVATEURS DANS LES DENRÉES ALIMENTAIRES PAR CHROMATOGRAPHIE LIQUIDE A HAUTE PERFORMANCE

A. COLLINGE et A. NOIRFALISE*

Laboratoire de Toxicologie et Bromatologie, Université de Liège, 151, Boulevard de la Constitution, B-4020 Liège (Belgique)

(Reçu le 18 juin 1981)

Summary. (Determination of seven food preservatives by high-performance liquid chromatography.) Solvent-programmed h.p.l.c. is applied for the determination of sorbic, benzoic and salicylic acids and *p*-hydroxybenzoic acid as well as three of its esters, singly or in mixture; quantitative separation takes less than 20 min. Recoveries varied from 90.9 to 99.4% for the concentration range 200—1000 ppm when the method was applied to mayonnaise.

Résumé. Une technique h.p.l.c. en programmation de solvants est proposée pour la séparation et le dosage de sept agents conservateurs seuls ou en mélange. L'application aux mayonnaises est proposée; les taux de récupération varient de 90,90 à 99,36% selon les composés envisagés pour des concentrations de l'ordre de 200—1000 ppm.

L'utilisation intensive d'agents conservateurs dans les denrées alimentaires en particulier pose nécessairement le problème de la recherche et du dosage de ces agents. L'avènement de la chromatographie liquide à haute performance (h.p.l.c.) a permis de réduire pratiquement à une seule manipulation les quatre ou cinq étapes des techniques antérieures de dosage. Malheureusement, la plupart des méthodes proposées [1—13] soit n'envisagent pas le dosage de l'ensemble des agents conservateurs les plus couramment utilisés, soit requièrent un temps de réalisation toujours supérieur à 30 min. Poursuivant nos investigations dans ce domaine [1], nous avons tenté de réduire ce temps de réalisation, tout en améliorant qualitativement le pouvoir de résolution, en travaillant en programmation de solvants. Ceci ne s'est pas fait au détriment de la précision des dosages.

Partie expérimentale

Matériel et équipement. Le chromatographe liquide à haute performance utilisé est un Pye-Unicam type LC-XPD avec pompe haute pression à double piston réciproque type XPD700 BAR (programmeur de gradient type LCXP), vanne Rhéodyne Model 7120 de 20 μl, détecteur Pye-Unicam u.v. à longueur d'onde variable (190—380 nm) couplé à un enregistreur Philips PM8251/02. La colonne est une colonne métallique HIBAR remplie de LiChrosorb RP18 (10 μm; Merck 50334).

Les conditions instrumentales sont les suivantes: débit sur la colonne 1,0 ml min^{-1}; température ambiante 22—26°C; longueur d'onde 240 nm; déroulement du papier, 5 mm min^{-1}.

Solutions standards. Les solutions stock sont des solutions à 500 mg l^{-1} dans le méthanol (Merck 6012). Les solutions de travail sont obtenues par une dilution hydro-alcoolique à 10—200 mg l^{-1} des solutions stock.

Phases mobiles. Solution A est une solution aqueuse d'acide perchlorique (Merck) à 1% (v/v). Solution B est un mélange 50:50 de solution A et d'isopropanol (Merck) dégazifié par barbottage à l'hélium. Pour le programmation, le mélange de départ est fait de 35% de solution B et 65% de solution A. La programmation linéaire atteint en 10 min 100% de solution B et le maintien pendant 10 min.

Préparation des échantillons. Une aliquote exactement pesée (ca. 3 g) de mayonnaise est additionnée de 1 ml d'acide sulfurique à 10% (p/v) et 20 ml d'éthanol. Le tout est agité mécaniquement durant 5 min, centrifugé, puis laissé au repos durant 2 h en chambre froide. Le surnageant est ensuite filtré sur membrane Fluoropore 0,45 μm.

Les dosages sont effectués par mesure de la hauteur de pic par comparaison à un étalonnage externe.

Résultats et discussion

Ainsi que le montre le Tableau 1, la séparation des sept agents conservateurs testés suivant la technique décrite ci-dessus est très valable et nettement supérieure à celle que permettait d'obtenir la technique mise au point antérieurement (isocratique 82% acid perchlorique á 1%, 18% isopropanol et lecture à 225 nm), qui n'était prévue que pour la mise en évidence et le dosage de l'acide benzoïque et de l'acide sorbique [1]. Le temps nécessaire pour une séparation quantitative des sept agents est inférieur à 20 min.

TABLEAU 1

Facteurs de capacité (k') et limites de dosage pour les sept agents conservateurs séparés par h.p.l.c. en programmation de solvants, et comparaison avec les résultats obtenus par technique isocratique [1]

Agents conservateurs	H.p.l.c. programmation solvants		H.p.l.c. isocratique [1]	
	k'	Limites de dosage (ppm)	k'	Limites de dosage (ppm)
Acide *p*-hydroxybenzoïque (PHB)	1.38	0.03	1.60	0.11
Ester méthylique PHB	4.41	0.06	5.70	0.33
Acide sorbique	4.69	0.02	6.20	0.10
Acide benzoïque	5.10	0.06	7.80	0.04
Ester éthylique PHB	5.70	0.30	13.00	0.50
Acide salicylique	5.94	0.37	14.40	0.62
Ester propylique PHB	6.64	1.17	41.60	3.12

La précision des dosages est par ailleurs satisfaisante ainsi que le montre les taux de récupération obtenus tant pour des solutions aqueuses (concentration 30—50 ppm) que pour des mélanges dans la mayonnaise (concentration 200—1000 ppm) (Tableau 2).

Les résultats supérieurs obtenus pour l'acide *p*-hydroxybenzoïque peuvent s'expliquer par le fait qu'au moment de son élution, la composition du solvant sur la colonne n'a pas encore été modifiée et que pratiquement dès lors le dosage se fait dans des conditions isocratiques. Pris isolément, l'acide benzoïque et l'acide salicylique seraient dosés avec précision en opérant à 225 nm (isocratique), et l'acide sorbique, l'acide *p*-hydroxybenzoïque ainsi que ses esters le seraient plus précisément à 254 nm (programmation). Lorsqu'ils sont en mélange toutefois et que dès lors il convient de recourir au système de programmation de solvants préconisé dans cet travail, seul le choix de la longueur d'onde de 240 nm se révèle possible. Nous avons vérifié expérimentalement que le gain obtenu globalement tant en précision qu'en durée de réalisation l'emporte dans ce cas sur les pertes de précision individuelle éventuelles. Il reste cependant que, lorsque l'on dispose d'un détecteur u.v. à longueur d'onde variable, une seconde chromatographie à la longueur d'onde spécifique est toujours un contrôle valable.

Conclusion

Les conditions opératoires que nous proposons permettent de réaliser, avec une bonne précision, en moins de 20 min, non compris le temps de préparation que varie en fonction de la nature de l'échantillon, une identification et un dosage différentiel des sept principaux agents conservateurs utilisés dans l'industrie des denrées alimentaires. Nous avons appliqué cette mode opératoire à l'analyse des mayonnaises; suivant les agents envisagés, les taux de récupération varient de 90,90 à 99,36% avec des écarts-type variant de 2,48 à 6,31.

TABLEAU 2

Taux de récupération en solution aqueuse et dans les mayonnaises

Agents conservateurs	Solutions aqueuses (30—50 ppm)		Solutions "mayonnaises" (200—1000 ppm)	
	N essais	Récupération (%)	*N* essais	Récupération (%)
Acide *p*-hydroxybenzoïque (PHB)	7	100.07 ± 1.29	11	99.39 ± 2.68
Ester méthylique PHB	5	97.97 ± 2.55	8	96.16 ± 2.48
Acide sorbique	8	99.47 ± 1.97	7	94.21 ± 3.34
Acide benzoïque	8	98.30 ± 2.17	8	94.16 ± 6.31
Ester éthylique PHB	8	101.75 ± 2.73	7	94.18 ± 2.80
Acide salicylique	8	99.26 ± 3.04	8	90.90 ± 4.54
Ester propylique PHB	6	99.47 ± 2.14	7	93.79 ± 4.03

BIBLIOGRAPHIE

1 A. Collinge et A. Noirfalise, Anal. Chim. Acta, 121 (1980) 337.
2 J. J. Nelson, J. Chromatogr. Sci., 11 (1973) 28.
3 F. A. Fitzpatrick, A. F. Summa et A. D. Cooper, J. Soc. Cosmet. Chem., 26 (1975) 377.
4 D. S. Smyly, B. B. Woodward et E. C. Conrard, J. Assoc. Off. Anal. Chem., 59 (1976) 14.
5 M. C. Bennet et D. R. Petrus, J. Food Sci., 42 (1977) 1220.
6 L. Ciraolo, R. Calapaj et M. T. Clasadonte, Rass. Chim., 29 (1977) 181.
7 G. Clarke et I. A. Rashid, Analyst, 102 (1977) 685.
8 V. Das Gupta, J. Pharm. Sci., 66 (1977) 110.
9 F. Eisenbeiss, M. Weber et S. Ehlerding, Chromatographia, 10 (1977) 262.
10 M. A. McCalla, F. G. Marck et W. H. Kipp, J. Assoc. Off. Anal. Chem., 60 (1977) 71.
11 N. D. Brown, L. L. Hall et H. K. Sleeman, J. Chromatogr., 166 (1978) 316.
12 A. W. Archer, Analyst, 105 (1980) 407.
13 C. Gertz et J. Hild, Z. Lebensm. Unters. Forsch., 170 (1980) 103, 110.

Analytica Chimica Acta, 132 (1981) 205—208
Elsevier Scientific Publishing Company, Amsterdam — Printed in The Netherlands

Short Communication

COMPUTER CONTROL OF THE PERKIN-ELMER MODEL 580B INFRARED SPECTROPHOTOMETER

J. R. CHIPPERFIELD*

Department of Chemistry, University of Hull, Hull HU6 7RX (Gt. Britain)

G. H. KIRBY

Department of Computer Studies, University of Hull, Hull HU6 7RX (Gt. Britain)

(Received 22 July 1981)

Summary. Control is achieved via the spectrophotometer communications interface by a Digico M16V minicomputer. Programs for control and data handling have been developed in BASIC with assembly language subroutines to deal with communications between computer and spectrophotometer. The advantages of this system compared to a special data station are discussed.

The Perkin-Elmer model 580B infrared spectrophotometer (PE 580B) is fitted with a microprocessor, and can be controlled either manually or by an external controller. The usual controller is a Perkin-Elmer Infrared Data Station which contains a microprocessor, visual display unit, and a twin 7-in. floppy disc unit. With this data acquisition unit, the spectrophotometer can be completely controlled by programs, and spectra can be stored, re-plotted, compared, and processed. The programs supplied by the manufacturer are written in machine code, although there is a simple high-level language instruction set to enable the user to program certain functions; such software is sometimes unsuitable for research applications, and cannot easily be changed by the user.

It seemed valuable to use a more powerful, general-purpose computer as controller, in order to achieve the following: (a) ability to write programs in a high-level language such as BASIC, PASCAL or FORTRAN; (b) hard-disc storage with much greater capacity than floppy discs; (c) addition of special graphics units and printers not available on the Perkin-Elmer Data Station; (d) faster processing resulting from more advanced computer architecture; (e) use of an available laboratory minicomputer rather than purchase of a special-purpose data station; (f) transfer of results to a larger computer system.

In this communication, connection of the spectrophotometer to a Digico M16V minicomputer is described and the problems associated with this are discussed.

Communicating with the PE 580B

The PE 580B can be fitted with a communications interface to permit external control as indicated in the manufacturer's guide. This interface can

0003—2670/81/0000—0000/$02.50

be accessed by a serial link connected to a RS232C port on the accessory panel of the PE 580B. Data are received and transmitted by the interface as 8-bit ASCII characters with one start and one stop bit, a variety of baud rates from 300 to 9600 being available. The PE 580B is controlled via the communications interface by commands, each of which consists of a record starting with a $ character immediately followed by a 2-letter mnemonic code. Some commands require a single parameter, either numeric or a string, which is separated by one space from the code. Commands are terminated by either carriage return (CR) or line feed (LF).

All records transmitted by the interface are preceded by one delete character (DEL) and are terminated by CR LF. The PE 580B responds to each record of input by a 4-digit error code, which is all zeros if the record was acted upon successfully. Further output depends on which command is being processed and may be terminated with a further error code. For each command the format of the next output record can always be predicted from the current one. Table 1 illustrates the sequence of communications following the sending of a status command, $ST.

By default the interface operates in respond mode 1 whereby output records are queued until the interface receives a prompt character (ASCII DC1, i.e. X-ON or control-and-Q) from the controller. The record at the head of the queue is then transmitted. This simple method allows the rate at which records are transmitted to be controlled by the user. The respond command is available to change to mode 0 for transmission as soon as information is available, should that be preferred.

Control of the PE 580B by a Digico computer

A Digico M16V minicomputer (Digico Ltd., Wedgewood Way, Stevenage, England) has been used for a variety of laboratory computing applications with software written in Digico assembly language with a BASIC program to provide a simple user interface to the assembly language software [1]. This present application illustrates different, simpler techniques for instrument control by a separate computer. The microprocessor-controlled PE 580B functions as an intelligent terminal when connected to the Digico

TABLE 1

Sequence of data transfers between computer and PE 580B when the status of the instrument is determined by means of a $ST command

Controlling computer	Data direction	Spectrophotometer interface	Comments
$ST CR LF	→		Request for status of instrument.
X-ON	→		Prompt to send a record.
	←	DEL 0000 CR LF	Error code sent.
X-ON	→		Prompt to send a record.
	←	DEL 580.02—0.0 CR LF	Status information record (62 chrs).
X-ON	→		Prompt to send a record.
	←	DEL 0000 CR LF	Error code to show end of operation.

computer via the communications interface, the PE 580B having the necessary intelligence to interpret and act upon data received and to transmit data back.

An asynchronous line operated at 1200 baud connects the PE 580B to a generalised communication interface card (GCIC) in the Digico computer. The GCIC enables this computer to be interfaced to a variety of transmission equipment by using serial links terminating in V24/RS232 ports. Writing to and reading from terminals attached to the GCIC is accomplished by a Digico executive subroutine %MCD (available from the manufacturer) which must be called from an assembly language program. The program written here occupies less than 1K of 16-bit words and has subroutines to assign, connect, write to, read from, disconnect and release the PE 580B via the GCIC. A convenient user interface to this program is provided by a BASIC program which interacts with a user at a VDU adjacent to the PE 580B and remote from the computer. Digico BASIC has a character function, SLOT£, which enables a subroutine written in assembly language to be executed by means of the call LET A£ = SLOT£(B£,*N*). The two parameters to SLOT£ indicate the subroutine required, by means of an integer number *N*, and any data for it, in the form of the character string B£. Any result to be returned from the subroutine is also in the form of a character string and is left in A£.

The BASIC program requests the user to indicate the tasks to be performed by the PE 580B in the form of the commands understood by its communications interface. The program adds the necessary terminator and passes the complete record to the appropriate assembly language subroutine using the SLOT£ function. Obviously, it would be possible for the user to input the tasks required in a fuller form, for example STATUS, in which case the BASIC program would have to translate this to the appropriate mnemonic code $ST and add the terminator.

One immediate advantage of using a separate computer to control the PE 580B is that the prompt character necessary in the default respond mode can be sent automatically. A prompt character is therefore appended to every command record sent to the PE 580B so that the user sees the error code displayed on his terminal as soon as it is sent back. If a further record is expected, e.g., a status record as in Table 1, the writing of another prompt character by the Digico computer occurs immediately after display of the error code.

The principal advantage of computer control is the large capacity for storage of spectra offered by a file storage system based on hard discs, such as that available to BASIC users on minicomputers. It is computationally convenient to operate the PE 580B in its default respond mode when a wavenumber range is scanned. Every record of transmittance data has the format, expressed in Fortran conventions, 9(I5,','), I5 with the final record having the value −9999 in its last field. A record of transmittance data is read by the Digico executive function into a buffer of 62 characters (including the DEL, CR and LF) and is inspected by code in the BASIC program to determine whether another similar record is expected or whether only the error code remains to be transmitted. Following storage of the fields of transmit-

tance data, a prompt is sent to the PE 580B for transmission of the next record. No temporary stop in scanning, resulting from filling of the PE 580B communications interface buffer, has been noticed.

Loss of data during communications has not been experienced. The PE 580B communications interface does not receive and transmit data at the same time, and the Digico executive function controlling the GCIC is used in half-duplex standby mode with a request to read being issued immediately after a write and before testing for completion of the write, as described in the Executive Manual.

It was found more acceptable to test each character received for a LF, rather than to use a count of characters to determine the end of a record read by the Digico executive function, because this copes with situations where an unexpected number of characters is received. An additional precaution found to be useful, particularly during software development and testing, is a time-out on reading. The Digico executive function allows specification of the maximum permitted elapsed time before receipt of the next character. If no data transmission occurs from the PE 580B interface within this time (e.g., because of a hardware failure) then execution ultimately reverts to the BASIC program and an appropriate reply is communicated to the user.

The transmittance data need no processing before being stored in a random access file during or after data acquisition. It is available afterwards for processing and/or display in any way desired by the user. In order to make use of the facility on the PE 580B for replotting a stored spectrum on the recorder of the instrument by means of the $PB command, the interface requires the packing of each transmittance into a 12-bit signed integer by transmission as a character pair. A separate BASIC program has been written to do this.

Conclusion

The control of the PE 580B by a separate computer allows the user to write programs for data acquisition and for subsequent handling of the spectra in a high-level programming language. Whilst assembly language subroutines may be necessary in order to achieve the speed desirable to avoid loss of characters in communication, these can be called from high-level language programs on most computing systems. Much of the programming can therefore be done by the user rather than an experienced programmer. Any high-level language which can handle input and output of character strings on a specified channel could be used. The use of character strings by Digico for communication between BASIC and assembly language subroutines, whilst not always convenient in laboratory computing [1], makes the programming for this application relatively straightforward.

The authors are grateful to Mr. G. Collier for his assistance with the spectrophotometer and to Mr. P. F. Martin for his contribution to the programming.

REFERENCE

1 G. H. Kirby, J. R. Chipperfield and D. E. Webster, Comput. Chem., 3 (1979) 135.

Analytica Chimica Acta, 132 (1981) 209—213
Elsevier Scientific Publishing Company, Amsterdam — Printed in The Netherlands

Short Communication

REDUCTION OF OXIDE IONS OF URANIUM IN SINGLE-FILAMENT SURFACE-IONIZATION MASS SPECTROMETRY WITH APPLICATION TO ROCK SAMPLES

M. H. KAKAZU, N. M. P. MORAES, S. S. IYER* and C. RODRIGUES

Área de Processos Especiais, Instituto de Pesquisas Energéticas e Nucleares, Caixa Postal 11049, Pinheiros, São Paulo (Brazil)

(Received 20th July 1981)

Summary. Ion-emission characteristics of a single-filament surface-ionization source for uranium are described. It is shown that a graphite coating over uranium samples enhances reduction of oxides to U^+ and improves quantitative performance. Results obtained for uranium in several rock samples are in reasonable agreement with results reported by others.

In surface-ionization mass spectrometry, the use of oxide ions for isotope abundance measurements causes errors because of the polyisotopic nature of oxygen and the possible isobaric interference from isotopes of other elements. In ion-emission studies of uranium atoms, Studier et al. [1] observed that a single-filament surface-ionization source suffers from the low emission of U^+ ions in the absence of deliberately introduced reducing agents. With the use of a V-shaped single filament, Dietz and Hendrickson [2], NBS group [3] and Baldock [4] obtained a stable beam of U^+ ions without any reducing agents. The V-shaped filament appears to be as efficient as a triple filament and it has been suggested that this is because it is equivalent to a triple filament closed up [5]. Fenner [6] observed that the metal ion emission of uranium in a V-type filament was enhanced by various types of treatment of the filament loaded with uranyl nitrate. This was explained as being due to the reduction of uranyl nitrate to a chemical form in which metal ions are easily produced as well as to the increased work function of the filament surface. Arden and Gale [7] described a single-filament (V-type) surface-ionization source in which a small quantity of colloidal suspension of graphite in distilled water (prepared from Aquadag) loaded on top of a deposit of uranyl nitrate in phosphoric acid, yielded a steady beam of U^+ ions.

Recently, Schuhmann et al. [8] described a technique for the suppression of monoxide ions of rare-earth elements in surface-ionization mass spectrometry. They discussed the effect of monoxide interference in the quantitation of Gd, Dy, Yb, and Lu abundances by the isotope dilution technique. They produced monoxide-free spectra of rare-earth elements by a controlled leakage of propane or hydrogen to the source chamber for a steady-state ion gauge pressure of 10^{-4} torr during the measurement process.

0003—2670/81/0000—0000/$02.50

This communication describes an investigation of the ion-emission characteristics of uranium using a single-filament (flat type) ionization source and different types of sample loading including treatment with phosphoric acid and graphite. Intensities of oxide and metal ions of uranium were measured for different values of filament currents and for different types of sample loading. The technique finally chosen involves addition of a colloidal suspension of graphite on top of uranyl nitrate sample deposited on a single filament. It was employed in the quantitation of uranium abundances in rock samples by a mass spectrometric isotope dilution method.

Experimental

Uranium solutions. The uranium solution was prepared from National Bureau of Standards uranium isotopic standard U500.

Samples examined after loading on a zone-refined rhenium single filament (flat type) were uranyl nitrate, and uranyl nitrate in phosphoric acid, with and without colloidal suspension of graphite (Aquadag) in distilled water placed on top of each deposit.

Preparation and calibration of tracer solution. National Bureau of Standards uranium isotopic standard NBS U970 was used in the preparation of the tracer solution. The tracer solution was calibrated by mass spectrometric isotope dilution using NBS uranium isotopic standard U950a. The tracer solution was stored in a cool dry place and was calibrated periodically. Calibration measurements for two measurements at six-month intervals for different amounts of standard and tracer gave values of (10.36 ± 0.1) and 10.37 ± 0.1 μg of uranium per gram of tracer solution, confirming the stability of the tracer solution.

Treatment of rock samples. Depending on the concentration of uranium in the rock sample, a known amount of tracer was added so as to obtain a U^{235}/U^{238} ratio near unity. The sample was dissolved in a teflon pressure bomb using 15 ml of 40% hydrofluoric acid and 0.5 ml of 72% perchloric acid. Dissolution was complete in 2 h at 120°C.

The uranium was separated by a two-stage ion-exchange method. First, uranium was separated from thorium [9] on Dowex 1-X8 resin, 200—400 mesh, in the chloride form and then separated from other elements, mainly iron and alkaline earth metals [9, 10], on the same resin in the ascorbate form.

Mass spectrometric procedure. The isotopic measurements were done with a Varian TH-5 solid-source single-focussing mass spectrometer equipped with faraday cup and secondary electron multiplier as detectors. Sample containing less than microgram amounts of uranium was loaded on the flat rhenium filament; the filament current was increased slowly and the ion currents were measured with a secondary electron multiplier. For the determination of uranium by the isotope dilution method, the isotopic ratios were calculated from peak heights on a strip-chart recorder.

Results and discussion

Parameter dependencies. The measured ion currents for different conditions are plotted in Fig. 1. It is observed that the ion-emission characteristics of U^+, UO^+ and UO_2^+ are quite similar for uranyl nitrate with and without phosphate in the absence of graphite. The UO_2^+ and UO^+ ion emissions start at a lower temperature than the U^+ ion emission. The addition of graphite enhances the emission of U^+ at a lower temperature and it also reduces the field of stability of emission of UO_2^+ and UO^+ ions with and without phosphate.

Arden and Gale [7] observed that the addition of graphite to a V-shaped filament loaded with uranyl nitrate did not produce U^+ ions of sufficient stability compared to a filament loaded with uranyl nitrate in phosphoric acid. However, this study shows that the emission characteristics are similar with or without the addition of phosphoric acid. It is clear that the technique of Arden and Gale [7] can easily be adapted for flat-type single filaments,

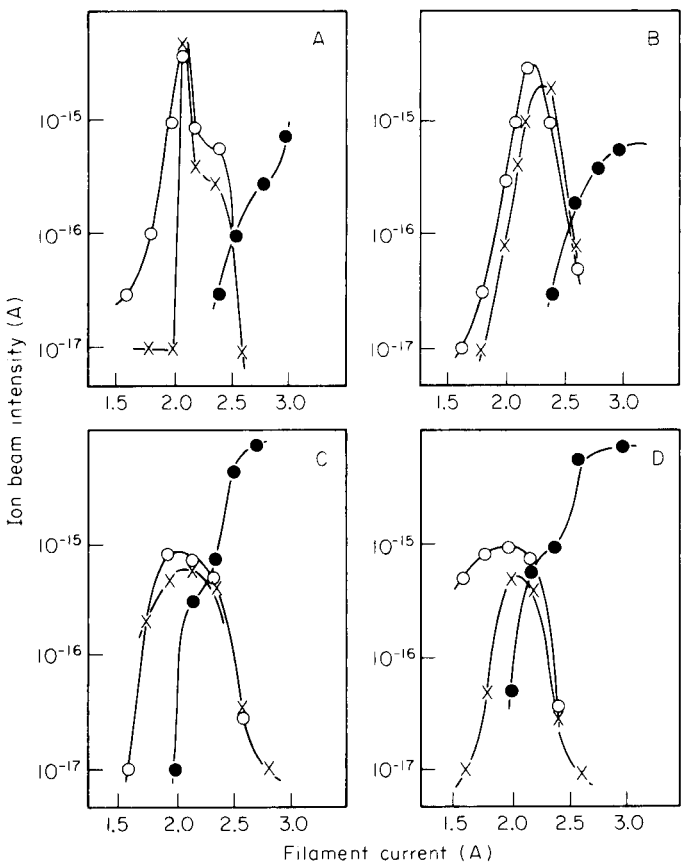

Fig. 1. Thermionic emission characteristics of U^+, UO^+ and UO_2^+ in single-filament deposits from (A) uranyl nitrate; (B) uranyl nitrate in phosphoric acid; (C) colloidal suspension of graphite on deposit of uranyl nitrate; (D) colloidal suspension of graphite on deposit of uranyl nitrate in phosphoric acid. (○) UO_2^+; (×) UO^+; (•) U^+.

but it was observed that the reduction of uranium oxide to uranium ion depended on the quantity of graphite deposited on the filament. For microgram amounts of uranium on the filament, a graphite/uranium ratio of about 100 yielded the highest U^+/UO_2^+ and U^+/UO^+ ratios. Higher concentration of graphite (graphite/uranium >200) impeded the emission of UO_2^+, UO^+ and U^+ ions, whereas a graphite/uranium ratio of less than 50 provided no reduction of oxide ions. Studier et al. [1] observed that the degree of carbonization had a marked effect on the temperature of the metal-ion emission. They observed that the filament temperature during carbonization seemed more critical than the duration of the process.

Quantitative results. The proposed method was employed to quantify uranium isotopes. The precision obtained was of the order of ±0.4%. The isotopic ratios were corrected for mass discrimination by using the measured isotopic ratio for the NBS isotopic standard U500. The value obtained for the mass discrimination was 0.996 ± 0.003.

Uranium abundances in two USGS rock standards and six granite samples from Wyoming [11] were determined. The uranium values obtained are listed in Table 1 along with values obtained by other workers. The uranium values for AGV-1 and GSP-1 are within the range of values listed by Flanagan [12]. The values obtained for the granite samples agree well except for MS-1 and GM-1 (20.43). The uranium values given by Stuckless and Ferreira [11] for two different lots of the same rock samples also show a large variation. This is due to the non-uniform distribution of uranium in the rock samples because the uranium is concentrated in accessory minerals such as zircon, apatite and monazite [13]. The rock samples used here were taken from the original coarse fraction [14], hence the deviation in the uranium values may be attributed to the variation in the distribution of these minerals.

TABLE 1

Comparative values of uranium in granite rocks

Concentration (ppm)			
Rock sample	Present work[a]	Stuckless and Ferreira [11]	Flanagan [12]
AGV-1	2.03 ± 0.4		1.88 (1.4—2.1)
GSP-1	1.78 ± 0.3		1.96 (1.7—2.15)
DDH-7	3.62 ± 0.04	3.69	
MS-1	16.7 ± 0.2	15.15	
GM-1 (20.43)[b]	15.1 ± 0.3	13.08	
GM-1 (78.58)[b]	28.0 ± 0.3	27.32, 25.71[c]	
GM-1 (87.17)[b]	59.0 ± 0.7	56.21, 58.18[c]	
GM-1 (230.95)[b]	11.3 ± 0.1	11.13	

[a]Mean and standard deviation for 4–5 measurements on each sample. [b]Numbers in parentheses indicate the different depths. [c]Values obtained for different portion of the gross sample.

A study [15] on the effect of laboratory sampling methods on the error has shown that high inaccuracy can result from sampling problems.

In conclusion, the present study provides a simple method for the quantitation of uranium isotope ratios using a single-filament surface-ionization source, which can be applied with sufficient accuracy and precision to rock samples.

The granite samples were supplied by J. S. Stuckless of U.S. Geological Survey. Helena M. Shigematsu is thanked for her technical assistance.

REFERENCES

1 M. H. Studier, E. N. Sloth and L. P. Moore, J. Phys. Chem., 66 (1962) 133.
2 L. A. Dietz and H. C. Hendrickson, in R. J. Jones (Ed.), Selected Measurements Methods for Plutonium and Uranium in Nuclear Fuel Cycle, U.S. Atom. Energy Comm., Oak Ridge, TN, 1963.
3 U.S. Natl. Bur. Standards. Tech. Note, 546 (1970) 58.
4 R. Baldock, in W. L. Mead (Ed.), Advances in Mass Spectrometry, Vol. 3, Inst. Petroleum, London, 1966.
5 M. H. Wilson and R. J. Daly, J. Sci. Instrum., 40 (1963) 273.
6 N. C. Fenner, J. Sci. Instrum., 41 (1964) 48.
7 J. W. Arden and N. H. Gale, Anal. Chem., 46 (1974) 687.
8 S. Schuhmann, J. A. Phillipotts and P. Fryer, Anal. Chem., 52 (1980) 214.
9 J. Kritl, K. Mencl and A. Moravec, Radiochem. Radioanal. Lett., 21 (1975) 115.
10 M. Chakravorty and S. M. Khopkar, Chromatographia, 10 (1977) 372.
11 J. S. Stuckless and C. P. Ferreira, I.A.E.A. Symp. on Exploration of Uranium Ore Deposits, Vienna, 1976, p. 717.
12 F. J. Flanagan, Geochim. Cosmochim. Acta, 33 (1969) 81.
13 J. S. Stuckless, H. T. Millard, Jr., C. M. Bunker, I. T. Nkmo, J. N. Rosholt, C. A. Bush, C. Huffman, Jr., R. L. Keil, J. Res. U.S. Geol. Survey, 5 (1977) 83.
14 J. S. Stuckless, U.S. Geol. Survey, Denver, CO, personal communication, 1980.
15 C. O. Ingamels, J. C. Engels and P. Switzer, Geochemistry, 24th International Geol. Congr., Montreal, 1972, p. 405.

Analytica Chimica Acta, 132 (1981) 215—218
Elsevier Scientific Publishing Company, Amsterdam — Printed in The Netherlands

Short Communication

MINIMIZATION OF INTERFERENCE EFFECTS FROM IODINE-CONSUMING SAMPLES IN THE DETERMINATION OF WATER WITH THE KARL FISCHER REAGENT IN A FLOW-INJECTION SYSTEM

INGRID KÅGEVALL*, OVE ÅSTRÖM and ANDERS CEDERGREN
Department of Analytical Chemistry, University of Umeå, S-901 87 Umeå (Sweden)
(Received 24th April 1981)

Summary. A principal feature of the flow-injection approach for determination of water with the Karl Fischer reagent is the small influence of side reactions. This is confirmed by the determination of water in an iodine-consuming sample, penicillin (fugacillin).

The determination of water by flow-injection analysis (f.i.a.) with the Karl Fischer reagent was reported recently [1]. The method described was shown to be capable of 120 determinations per hour and the concentration range 0.01—5% (v/v) of water could be covered by using a single Karl Fischer reagent solution. The results obtained with a specially constructed potentiometric detector showed relative standard deviations of about 0.5% which was somewhat better than those obtained with a spectrophotometric detector. The latter detector, however, was found to be simpler to operate and gave a linear response. The closed f.i.a. system is attractive for safety reasons because contact with the toxic reagent is avoided. Furthermore, the cost per determination is low; about 2000 determinations can be made per litre of reagent.

A principal feature of the f.i.a. approach, when compared with the conventional Karl Fischer batch titration method, is the expected small influence of side reactions. The reason for this is that, in a flow-injection system, effects from such reactions are minimized by the short reaction time. This is exemplified in this communication by the determination of water in a penicillin preparation, fugacillin. This type of substance reacts with iodine at a rate sufficiently high to give a significant positive error in the standard titration procedure.

Experimental

Instrumentation and measurement technique. The reagent was driven by a four-channel peristaltic pump (Minipuls 2, Gilson, France); silicone rubber tubing was chosen in order to withstand the very reactive Karl Fischer reagent [1]. The spectrophotometric detector [1] consisted of a small grating monochromator, a halogen lamp, an u.v.-enhanced photodiode and a home-made flow-through cuvette in teflon (volume 20 μl, light path 10 mm).

0003—2670/81/0000—0000/$02.50

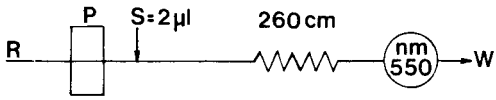

Fig. 1. Flow diagram used for determination of water in fugacillin: R = 7 mM reagent; P = pump; S = point of sample injection. The reagent flow rate was 1.7 ml min^{-1}. The coil length is taken as the distance between sample injection and detector.

A schematic diagram of the experimental arrangement is shown in Fig. 1. The tubings were made from teflon (0.5 mm i.d.) and the end-connectors were ordinary chromatographic connectors (Altex). Samples (2 µl) were injected with a standard liquid chromatography inlet slide valve for low pressure into the carrier and reagent stream of the Karl Fischer solution which was pumped at a flow rate of 1.7 ml min^{-1}. The change in concentration was then measured spectrophotometrically at 550 nm.

Reagents, samples, standards and standardization. All organic liquids were of analytical grade. Solvents were dried before use with molecular sieves (3 or 4 Å). The Karl Fischer stock solution contained 25.4 g of iodine, 38.4 g of sulfur dioxide and 80 ml of pyridine, diluted to 1 l with methanol. The fugacillin samples were prepared by dissolving 0.5062 g or 1.00 g of fugacillin in dry methanol (<0.005% v/v H_2O) and diluting to 10.0 ml or 50.0 ml, respectively. All sample solutions were standardized coulometrically with the Fischer reagent.

Results and discussion

Determination of water in fugacillin. The determination of water in an iodine-consuming substance, fugacillin, with the manual Karl Fischer titra-

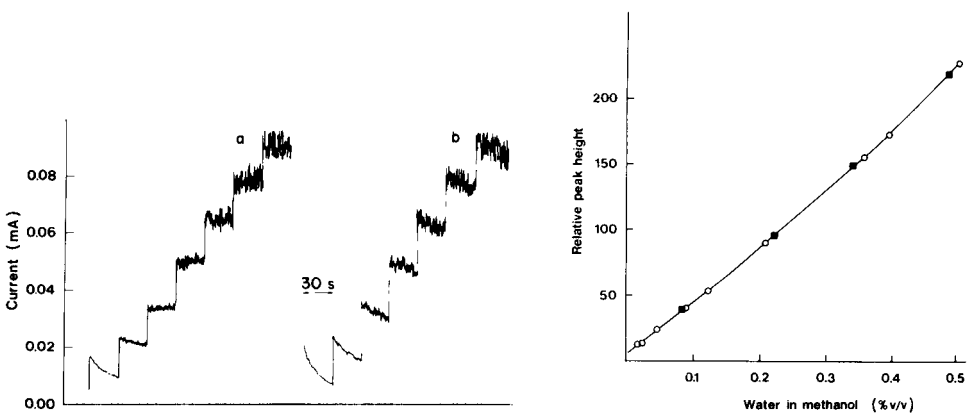

Fig. 2. Manual biamperometric titration of water in (a) a methanol sample; (b) a fugacillin sample. The Karl Fischer reagent (0.62 mg ml^{-1}) was added in steps of 0.02 ml and 0.04 ml, respectively, at 30 s intervals. The titration volumes were: (a) 20 ml and (b) 30 ml.

Fig. 3. Calibration curve for methanol obtained for 2-µl sample with the flow-injection arrangement given in Fig. 1. (○) methanol; (■) 2.5% w/w of fugacillin in methanol.

tion is illustrated in Fig. 2, curve b. Compared with Fig. 2, curve a, which represents the titration of a pure water-in-methanol sample, a stable current value is never obtained in this titration because of the occurrence of side reactions. This means that the end-point of the titration of the fugacillin sample is not sufficiently well-defined to permit an accurate determination of the water content. It should be mentioned that the drift is much larger when the official procedure in the Pharmacopeia Nordica [2] is followed. This is because the stronger reagent used will give rise to a larger excess of iodine at the end-point of the titration.

As has been shown by Verhoef [3], the reaction rate of the main Karl Fischer reaction is, apart from being proportional to the concentration of sulphur dioxide and water, dependent on the concentration of iodine as well as triiodide. The rate constant with respect to the iodine reaction is about four orders of magnitude larger than that for the triiodide. Thus, the greater the iodide concentration, the greater the conversion of iodine to triiodide and the lower the effective rate constant. This means that the main Karl Fischer reaction is favoured at the beginning of a titration when the concentration of iodide is low and the concentration of water is relatively high. At the end of a titration, the reaction rate of the main reaction is low because the iodide concentration is high and the concentration of water is low. Therefore, during the final stages of titration, side reactions are favoured in comparison with the main reaction.

One principal advantage of the flow-injection technique, compared with a standard batch titration, is the short time of reaction. In Table 1 the flow-injection results are compared with those obtained coulometrically. The latter values are considered to be correct because the sample was diluted about 400 times. This means that the extent of side reaction should be insignificant. This was also indicated by the fact that no shift in the base-line (corresponding to a certain iodine level) was noted for the fugacillin samples. As can be seen in Table 1, no significant differences between the coulometric and the flow-injection results were obtained when the maximum concentration of fugacillin in the methanol solution was 2.5% (v/v).

TABLE 1

A comparison between results obtained by coulometric titration and f.i.a. for two different concentrations of fugacillin in the methanol solution. The titre of the Karl Fischer reagent used was 0.007 M

Fugacillin in methanol (% w/w)	Water found in the methanol (% v/v)	
	Coulometry	F.i.a.[a]
6.0	0.214 0.215	0.227 ± 0.006[b] (n = 3)
2.5	0.085_0 0.084_6	0.086 ± 0.003 (n = 5)

[a]The time of reaction for these results was about 20 s. [b]95% confidence interval; the uncertainty in the calibration curve has been taken into account.

It should be pointed out that, for interfering substances which react with iodine more rapidly, a weaker reagent and/or a shorter reaction time should be chosen. However, for small excesses of iodine, the rate of the main Karl Fischer reaction will be too low to allow kinetic discrimination between the main and the side reactions. This problem might be circumvented by means of the rapidly reacting reagents discussed by Verhoef [3] and by Cedergren [4]. The need for using such reagents is obvious from the following example in which the iodine concentration of the Fischer reagent is assumed to be as low as 0.25 mM and the concentration of sulphur dioxide is 0.5 M; if 2 μl of a sample containing 0.1% of water is introduced and mixed instantaneously with 500 μl of the reagent and if no further dilution occurs during transport to the detector, then the time for 99% reaction will be about 3 min.

The relevance of using a calibration curve obtained for water in methanol solutions for the evaluation of the water content of the fugacillin samples was studied in some separate experiments, the results of which are given in Fig. 3. In these experiments, various amounts of water were added to a sample solution containing 2.5% (w/w) of fugacillin in methanol (this corresponds to a water concentration in the methanol sample of 0.085%). The concentration of water in these samples was determined by coulometric titration. The flow-injection results (equal to the mean of several peak height values) for each sample were then plotted as a calibration curve for methanol as shown in Fig. 3. As can be seen, the points representing the fugacillin samples fit very well to the methanol standard curve. This means that the flow-injection method is expected to give accurate results even for large variations in the water content of the fugacillin preparations.

Work is in progress in order to study whether the design of the f.i.a. system can be chosen in such a way as to eliminate the calibration problem arising from solvent effects, as was discussed earlier [1]. The possibilities offered by the f.i.a. method with respect to trace water determination will be reported in a later paper.

REFERENCES

1 I. Kågevall, O. Åström and A. Cedergren, Anal. Chim. Acta, 114 (1980) 199.
2 Pharmacopeia Nordica, Editio Svecica (Swedish edn.), 1 (1964) 75.
3 J. C. Verhoef, Mechanism and Reaction Rate of the Karl Fischer Titration Reaction, Dissertation, Amsterdam, 1977.
4 A. Cedergren, Talanta, 25 (1978) 229.

Analytica Chimica Acta, 132 (1981) 219—221
Elsevier Scientific Publishing Company, Amsterdam — Printed in The Netherlands

Short Communication

POTENTIOMETRIC TITRATION OF PERMANGANATE WITH RESACETOPHENONE OXIME

G. ABDUL HUQ and S. BRAHMAJI RAO*

Department of Chemistry, SVU Autonomous Post-Graduate Centre, Anantapur 515 003 (India)

(Received 15th May 1981)

SUMMARY

Milligram amounts of permanganate can be titrated with resacetophenone oxime (4-acetylresorcinol oxime) as a reducing titrant in the presence of phosphoric acid (0.5 M). The stoichiometry between permanganate and the oxime is 3:1 (MnO_4^-:oxime). The titration is successful in the presence of large amounts of dichromate or vanadate or moderate amounts of cerium(IV).

Permanganate reacts vigorously in neutral, acidic and basic conditions with many organic and inorganic substances [1] but it is normally titrated with solutions of inorganic reducing agents because of the greater simplicity and reversibility of such reactions compared to the reactions with organic compounds. However, many of the inorganic reductants used also react with other oxidizing anions such as dichromate, vanadate and cerium(IV). These anions are generally less reactive than permanganate towards organic reductants. Thus organic reductants may prove more useful in determining permanganate selectively provided that there are no induced reactions [2].

During studies on the analytical reactivity of 4-acetylresorcinol oxime (resacetophenone oxime) with permanganate, dichromate, vanadate and cerium(IV), it was observed that permanganate alone is decolorized in acidic solutions. The possibility of utilizing this reaction for a selective potentiometric titration of permanganate was therefore investigated.

Experimental

Potassium permanganate (0.05 M) solution was standardized against arsenic trioxide [1]. A standard solution of the oxime (0.1 M) was prepared in a 100-ml volumetric flask by dissolving 1.6708 g of the compound in aqueous 50% ethanol. Further dilutions were made with conductivity water. A Toshniwal potentiometer (model PL-51) was employed for potential measurements with a platinum indicator electrode and a saturated calomel reference electrode.

0003—2670/81/0000—0000/$02.50

TABLE 1

Effect of phosphoric acid concentration on the potentiometric titration of 5 ml of 0.05 M permanganate solution

$[H_3PO_4]$ (M)	0.125	0.250	0.500	1.000	1.500
Oxime consumed (ml)	8.30	8.35	8.30	7.40	6.0[a]

[a]Turbidity.

Results and discussion

Reaction conditions. Permanganate is decolorized by the oxime in both sulfuric acid and phosphoric acid solutions. However, potentiometric titrations in ca. 0.5 M sulfuric acid solutions showed slow potential changes near the end-point, which suggests that the reaction is slow. This problem did not arise with phosphoric acid solutions. Tests with different concentrations of phosphoric acid (Table 1) proved that concordant values were obtained in the acid range 0.125—0.500 M, and an acid concentration of 0.500 M was chosen for further studies.

To establish the stoichiometry of the reaction, 5-ml aliquots of 0.05 M permanganate solution were mixed with 10 ml of 2 M phosphoric acid solution and diluted with enough conductivity water to give a total volume of 40 ml. These mixtures were titrated with a 0.01 M solution of the oxime. A typical titration curve (Fig. 1) showed a potential jump of 150—200 mV for 0.1 ml of the oxime solution. These titrations showed that the reaction stoichiometry is 1:3 (oxime:MnO_4^-), i.e., 1 ml of 0.01 M oxime corresponds to 3.6 mg of permanganate. The probable course of the reaction is

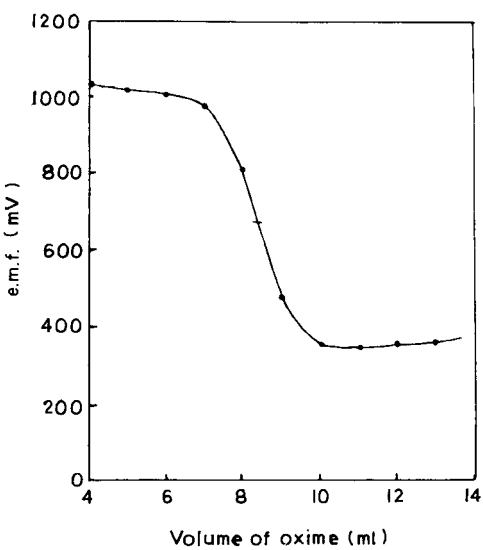

Fig. 1. Potentiometric titration curve: $[MnO_4^-] = 6.25 \times 10^{-3}$ M; $[H_3PO_4] = 0.50$ M; [oxime] = 0.01 M.

TABLE 2

Determination of permanganate with 0.01 M oxime solution

Taken (mg)	6.0	14.9	29.6	44.6	59.4	89.2
Found (mg)	6.1	15.0	29.7	43.9	56.7[a]	82.7[a]
Error (%)	+1.7	+0.7	+0.3	−1.6	−4.8	−8.6

[a]Turbidity.

$$C_6H_3(OH)_2C(CH_3)=NOH + 5\ H^+ \xrightarrow{7.5\ (O)} C_6H_3O_2(OH) + CH_3COOH + HNO_3 + \tfrac{5}{2}H_2O$$

Determination of permanganate. Solutions containing known amounts of permanganate were titrated with the standard 0.01 M oxime solution with the results presented in Table 2. Turbidity was observed when more than about 50 mg of permanganate was titrated. In such cases, better results were achieved by increasing the acidity so that it was around 0.4 M at the end-point, but the method is not recommended for large amounts of permanganate.

The potentiometric titration of permanganate (14.9 mg) was examined in the presence of dichromate, vanadate, or cerium(IV). No interference (error $\leqslant 2\%$) was caused by 11—108 mg of dichromate, 10—198 mg of vanadate, or 0.7—14 mg of cerium(IV). With the larger amounts of cerium(IV), there was some turbidity but this did not affect the end-points. Tests with these oxidizing ions in the absence of permanganate showed no significant redox reaction with the oxime.

The authors thank the Council of Scientific and Industrial Research, New Delhi, India, for the award of a reseach fellowship to G.A.H.

REFERENCES

1 I. M. Kolthoff and R. Belcher, Volumetric Analysis, Vol. III, Interscience, New York, 1957, p. 61.
2 G. G. Rao and U. Muralikrishna, Anal. Chim. Acta, 13 (1955) 8.

Analytica Chimica Acta, 132 (1981) 223—228
Elsevier Scientific Publishing Company, Amsterdam — Printed in The Netherlands

Short Communication

POTENTIOMETRIC TITRATION OF CHLORINE AND ITS OXY COMPOUNDS IN WATER

E. BARBOLANI, G. PICCARDI* and F. PANTANI

Institute of Analytical Chemistry, University of Florence, Via Gino Capponi 9, 50121 Florence (Italy)

(Received 26th June 1981)

Summary. Potentiometric titrations at constant current with identical platinum electrodes are applied to mixtures of chlorine, chlorine dioxide and chlorite. The procedure is compared with the common amperometric method. Chlorine can be titrated with phenylarsine oxide at pH 7 even in mixtures with chlorine dioxide and chlorite, and three-component mixtures can be resolved by titrations at pH 2 and 7 with and without iodide addition. The behavior of chlorine and chlorite mixtures can be characterized by appropriate titrations.

Determinations of chlorine and oxychlorine species in the presence of each other are usually based on titrating several samples under different conditions (various reducing agents and media), the individual components or their total being determined on separate samples. Control titrations on solutions of Cl_2, ClO_2, ClO_2^-, and their mixtures are usually done iodometrically. The method described by Haller and Listek [1] involves four titrations with sodium arsenite, from which the concentration of each constituent may be obtained. Chlorine dioxide is removed by hydrolysis at high pH

$$2\ ClO_2 + 2\ OH^- \rightarrow ClO_2^- + ClO_3^- + H_2O \qquad (1)$$

and the solution is then neutralized to pH 7 for the titration of free chlorine. This procedure is also cited in the Standard Methods [2] with phenylarsine oxide as titrant. However, chlorine dioxide is converted very slowly in reaction (1), the rate of reaction being strongly dependent on the alkalinity of the medium [3, 4]; and accurate results are obtained only under controlled conditions for neutralizing the excess of alkali.

Electrometric methods are employed to determine the equivalence point. The amperometric method was proposed as early as 1942 by Marks and Glass [5]; this method has been used subsequently with one indicator electrode and a reference electrode [1, 6, 7, 8] or with dual indicator electrodes [9]. Potentiometric methods have also been studied [10] for determining chlorine and chlorine dioxide through successive titrations of known amounts of potassium iodide and hydrogen peroxide with the test solution, but there are several drawbacks and completely wrong results can be obtained because of reactions of the peroxide in the alkaline medium used. In the

0003—2670/81/0000—0000/$02.50

potentiometric titrations reported by Norkus and co-workers [3, 11], hydrogen peroxide was avoided; chlorine and chlorine dioxide were determined by two successive titrations of sodium arsenite at two pH values followed by titration of the chlorite formed using osmium tetroxide as catalyst. A residual chlorine electrode [12] cannot distinguish between different oxychlorine compounds; it gives a Nernstian response with any oxidizing agent that liberates iodine stoichiometrically from iodide solution.

Potentiometric titration at constant current has not previously been proposed for the determination of chlorine and oxychlorine compounds. Polarized indicator electrodes have the virtue of reaching a steady potential quickly, because they are forced to, and their use is often worthwhile in cases where unpolarized electrodes behave sluggishly.

Experimental

Reagents. Chlorine solutions were prepared by absorbing chlorine into deionized water. Chlorine dioxide was prepared from potassium chlorate and oxalic acid in 2.5 M sulfuric acid. All chemicals were of analytical-reagent grade. Diluted solutions were standardized daily by titration with phenylarsine oxide in iodide solution [2] to a constant-current potentiometric end-point.

Apparatus. The recording instrumentation comprised the following parts. A metronome transmitted a pulse to an automatic burette (Metrohm E535) thus transferring a pre-set volume of the phenylarsine oxide titrant to the magnetically stirred titration cell. The increment in the analog signal produced by the burette moved the pen of the recorder (Hewlett-Packard 7044A) along the x-axis. The potential or current was measured on a Metrohm E520 potentiometer or a Keithley 602 microammeter, the signal being transferred to the y-axis of the recorder. The covered titration cell had inlets for the electrodes and the titrant.

For amperometric titrations, platinum and silver electrodes were used. Potentiometric titrations were done at zero current or at a constant current of 1 μA, with two identical platinum electrodes (each of 0.96 cm^2 surface area). The electrodes were pretreated as recommended by Kolthoff and Tanaka [13]. In the chronopotentiometric measurements, the constant cathodic current was generated by an AMEL 549 amperostat.

Results

In the amperometric titrations usually employed in the determination of chlorine and its oxy compounds, the current of a short-circuited cell, consisting of a platinum electrode immersed in the oxidant solution and a silver electrode immersed in a concentrated solution of potassium chloride, is measured. The titrant is phenylarsine oxide, and the oxidant is either chlorine or the triiodide produced on addition of iodide to the mixture. The current passing through the system causes some loss of electroactive species; the error introduced by reduction of triiodide on the platinum electrode depends

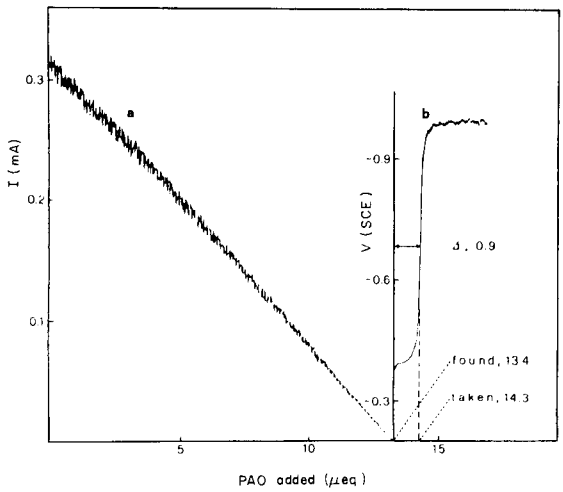

Fig. 1. (a) Amperometric titration of triiodide with phenylarsine oxide (PAO) as titrant. (b) Chronopotentiometric determination of the silver halide formed on the silver electrode during the same amperometric titration.

on the current and the titration time, and increases as the triiodide concentration increases. When a constant-flow titrator is used, as in the present work, the titration curve is like that shown in Fig. 1 (curve a). At the end-point, less than the theoretical amount of reagent has been added, and the difference corresponds to the coulombs obtained by integrating the current vs. time curve. A silver halide film forms on the silver electrode during the flow of current, and this was shown by the chronopotentiometric method (Fig. 1, curve b) to correspond to the iodine reduced at the platinum electrode. The error to be expected on samples containing 0.5—1 mg of chlorine is 5—10%. In the direct titration without iodide, the current observed is lower and so the resulting error is less, but such titrations are useful only for chlorine in the absence of chlorine dioxide. To avoid errors from the flow of current during titrations, a back-titration procedure can be employed, in which the excess of reducing agent is titrated with an oxidizing agent and the end-point is marked by the current appearing with the first excess of the oxidant. Thus the direct titration and back-titration cannot be considered equivalent, as is generally reported. The inconvenience of back-titration led to a study of other possible techniques.

In potentiometric titrations at constant current [14, 15], the errors outlined above are absent or greatly reduced, and the technique proved to be useful for determining chlorine or oxychlorine compounds in the presence of iodide. In the absence of iodide, the electrolysis error is not significant because of the low value of the imposed current. It was observed that for incompletely reversible couples the shapes of the titration curves varied considerably, depending on the pretreatment of the electrodes (see Fig. 2). Even in the presence of chlorine dioxide, clear equivalence points are obtained in

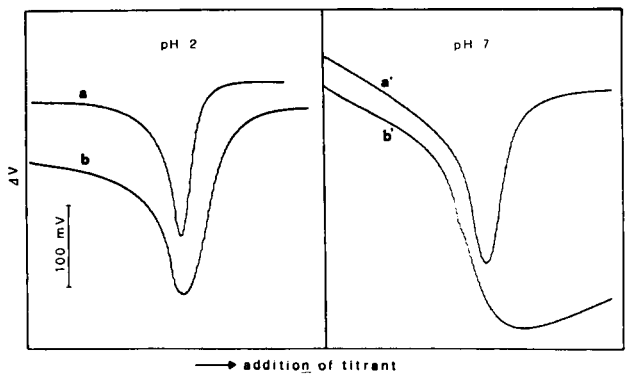

Fig. 2. Potentiometric titration curves at constant current (1 μA) for chlorine with no iodide present at pH 2 and at pH 7 with (a, a') and without (b, b') pretreatment of the electrodes.

the titration of chlorine at both pH 2 and 7, unlike the amperometric technique. Electrode pretreatment does not affect the curve shape when iodide is added because the titration is then based on the reversible I_3^-/I^- couple; this system is necessary when oxychlorine compounds, e.g., chlorine dioxide and chlorite, are to be determined. This titration at constant current is advantageous because chlorine can be determined even in mixtures with chlorine dioxide and/or chlorite, so that chlorine dioxide need not be removed [2].

Chlorine, chlorine dioxide and chlorite mixtures can be resolved through three titrations: (a) at pH 2 in the presence of iodide, all three species are determined (5 eq mol^{-1} for ClO_2 and 4 eq mol^{-1} for ClO_2^-); (b) at pH 7 in the presence of iodide, only chlorine and chlorine dioxide (1 eq mol^{-1}) are determined; (c) at pH 7 without iodide, only chlorine is determined. Particular attention must be paid to chlorine and chlorite mixtures. The reaction between chlorine and chlorite at pH <7 proceeds rapidly: $\frac{1}{2}Cl_2 + ClO_2^- \rightarrow Cl^- + ClO_2$. Accordingly, the results of successive titrations will differ from the original composition of the mixture at such pH values. The possibility that chlorine dioxide is formed at certain pH values was investigated. Figure 3 shows the microequivalents of oxidants found by titration with phenylarsine oxide of mixtures containing a fixed amount of chlorine and variable amounts of chlorite, plotted against the ClO_2^-/Cl mole ratios in the solutions titrated. The mixtures were left for some minutes at pH 3.7—4.0 before titration at pH 2 or 7. The titrations without iodide at pH 7 (line c) show a decrease of free chlorine down to a 1:1 ClO_2^-/Cl mole ratio corresponding to the formation of chlorine dioxide, which is not titrated under such conditions. The values found in the titrations at pH 7 with iodide present (line b) are constant because both chlorine and chlorine dioxide yield one equivalent of iodine.

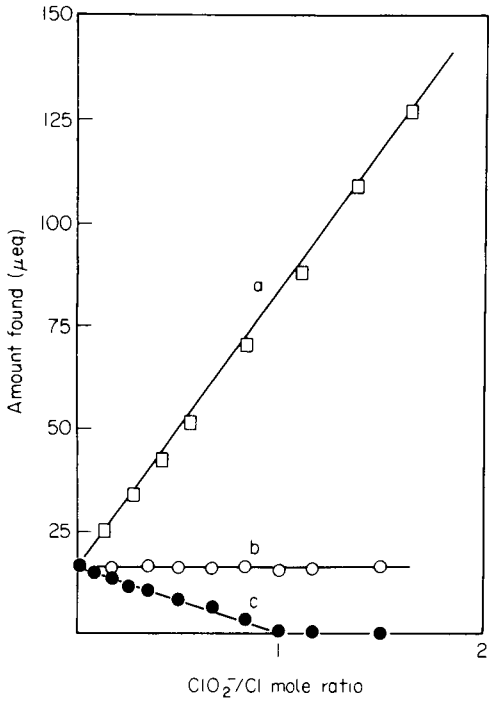

Fig. 3. Titration of mixtures of chlorine (16.7 μeq) and chlorite with (a, b) and without (c) addition of iodide. Mixtures were kept for a few minutes at pH 3.7—4.0 before titration at pH 2 (a) or at pH 7 (b, c).

The problem of the determination of these compounds simultaneously present in water is of interest because both chlorine and chlorine dioxide appear in water coming from purification plants.

A financial contribution from the Municipality of Florence is gratefully acknowledged.

REFERENCES

1 J. F. Haller and S. S. Listek, Anal. Chem., 20 (1948) 639.
2 APHA, Standard Methods for the Examination of Water and Waste Water, 14 edn., 1975, New York.
3 P. K. Norkus and S. P. Stul'gene, Zh. Anal. Khim., 24 (1969) 1077.
4 G. Piccardi, E. Barbolani and F. Pantani, Water, Air, Soil Pollut., 13 (1980) 197.
5 H. C. Marks and J. R. Glass, J. Am. Water Works Assoc., 34 (1942) 1227.
6 H. P. Kramer, W. Allan Moore and D. W. Ballinger, Anal. Chem., 24 (1952) 1892.
7 H. C. Marks and N. S. Chamberlain, Anal. Chem., 24 (1952) 1885.
8 ASTM, Manual on Industrial Water and Waste Water, 1977, Philadelphia.
9 J. J. Morrow, J. Am. Water Works Assoc., 58 (1966) 363.
10 K. D. Dobryshin, I. E. Flis, I. M. Vorob'ev and V. A. Kokushkina, Zh. Anal. Khim., 21 (1966) 752.
11 Yu. Yu. Yankauskas and P. K. Norkus, Zh. Anal. Khim., 28 (1973) 2257.

12 L. P. Rigdon, G. J. Moody and J. W. Frazer, Anal. Chem., 50 (1978) 465.
13 I. M. Kolthoff and N. Tanaka, Anal. Chem., 26 (1954) 632.
14 E. Bishop, Analyst, 83 (1958) 212.
15 R. Gauguin, Anal. Chim. Acta, 18 (1958) 29.

Analytic Chimica Acta, 132 (1981) 229—233
Elsevier Scientific Publishing Company, Amsterdam — Printed in The Netherlands

Short Communication

POTENTIOMETRIC TITRATIONS IN NON-CONDUCTING SOLUTIONS WITH AN INTERFACIAL ANTIMONY ELECTRODE

BOLESŁAW WALIGÓRA* and MARIA PALUCH

Department of Physical Chemistry and Electrochemistry of the Institute of Chemistry, Jagellonian University, 3 Karasia Street, 30-060 Kracow (Poland)

(Received 27th April 1981)

Summary. The micro interfacial device described is based on an antimony/antimony scratch/0.1 M KCl/Hg_2Cl_2/Pt cell. Acid—base reactions occurring in solvents such as dry ligroin, benzene, cyclohexane, dichloroethane, chloroform and pentyl acetate are readily monitored.

Potentiometric titration in non-aqueous media normally affords positive results only in conducting solvents. In the case of solvents which do not exhibit electric conductance (e.g., hydrocarbons), conventional methods fail because the indicator electrode does not show the characteristic potential changes necessary for quantitative interpretation. However, the interfacial voltaic cell described previously [1] enables acid—base reactions to be monitored in non-conducting media. The interfacial voltaic cell discussed here is a development of the microadsorption electrode of Kamieński et al. [2] which was used initially as a potentiometric detector in chromatography and for atmospheric contaminants [3]. The special construction of that device made it possible to monitor the course of chemical reactions at the phase boundary of two immiscible liquids. The form of the interfacial cell described in the present communication can be immersed in the solutions.

Experimental

Measuring system. The cell used is shown schematically in Fig. 1. It consists of a calomel (CE) and an antimony (AME) electrode with a salt bridge (SB) filled with saturated or 0.1 M potassium chloride connecting the two electrodes. After the electrodes have been inserted into ground-glass joints I and II of the bridge, a compact micro cell is obtained (Fig. 1, MC). The ground-glass joints facilitate disconnection of the set and cleaning of the electrodes, an operation necessary in serial measurements.

The essential part of the interfacial cell is a metallic scratch on the disc of porous corundum (Fig. 1, III) which closes the outlet of the salt bridge. The corundum disc (5-mm diameter and 3-mm thick) is connected to the broadened end of the bridge (SB). The pointed end of the antimony electrode (0.5-mm diameter) contacts the external surface of the porous corundum at point IV and is connected with the reference electrode through the salt bridge.

0003—2670/81/0000—0000/$02.50

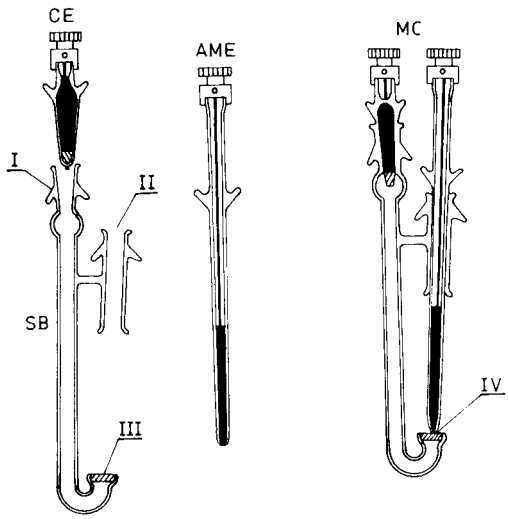

Fig. 1. The interfacial micro cell (immersible form): CE, calomel electrode; AME, antimony microelectrode; SB, salt bridge; I and II, ground-glass joints for inserting the electrodes; III, corundum disc; MC, assembled cell; IV, working surface of the cell.

Direct contact of the two electrodes is obviously unnecessary in conducting solutions, but when non-conducting media are used (e.g., gases or pure hydrocarbons), electric conductance must be ensured somehow. The metallic scratch formed on the porous corundum disc wetted by the potassium chloride solution acts as the conductor in non-conducting systems. Before each titration, the cell is disconnected and cleaned, and the surface of the corundum disc is scratched with chemically pure antimony.

Construction and preparation of the indicator antimony microelectrode. The microelectrodes used were constructed by fusing antimony into Supremax glass capillary tubes under vacuum. Figure 2 shows the furnace arrangement (B) and the capillary tube construction (A). Powdered antimony metal is poured into a capillary tube (A, ca. 0.5 mm i.d.) fused at its lower end, and then air is evacuated in order to obtain a vacuum of 10^{-2}—10^{-4} mm Hg. The capillary tube is closed at the narrow part (Fig. 2, I). The closed capillary tube is placed in the electric furnace (Fig. 2, B) and heated to the melting point of antimony (630° C); the closed end (Fig. 2, II) of the tube is then broken off. Air coming into the tube forces the fused antimony into the elongated part of the capillary tube (Fig. 2, III). The needle-shaped microelectrode thus formed is cooled rapidly after the furnace has been removed. Subsequently the lower end of the capillary (Fig. 2, C-IV) is ground off in order to expose the surface of the antimony and a lead (V) is soldered on. In order to fit the electrode to the salt bridge (Fig. 1, II), the outer wall of the tube (Fig. 2, VI) is ground in a steel sleeve. This procedure is based on the preparation of bismuth, tin, cadmium and lead microelectrodes [4].

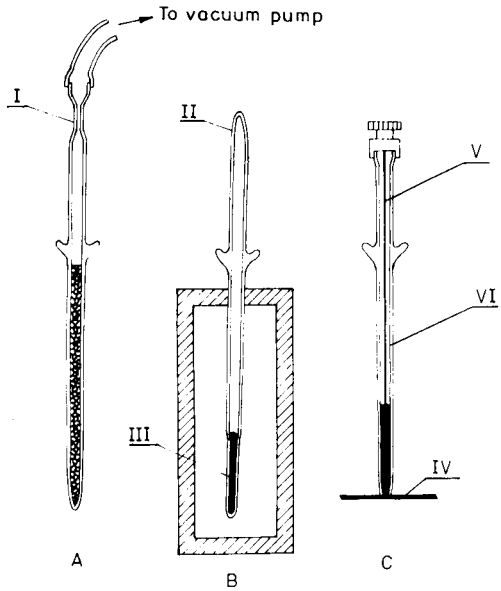

Fig. 2. The furnace and construction of the antimony interface electrode. See text for explanation.

Procedure. A vibron electrometer or simple valve pH meter, depending on the type of solvent, was used for measuring the changes in the e.m.f. of the interfacial cell. The titrants were added from a microburette in 0.05—0.1-ml portions. After each addition of the acid, the titrated solution was mixed for about 15 s with a magnetic stirrer. The e.m.f. of the cell was measured 30 s after each addition.

Samples and reagents. Strychnine, homatropine, hyoscyamine, aconitine, hydroquinidine, *n*-dodecylamine, trimethylamine, α-picoline and α,α'-lutidine were used as test materials. The solvents tested were dry cyclohexane, benzene, chloroform, ligroin, pentyl acetate and dichloroethane. Trichloracetic acid and picric acid were used as the titrants and were dissolved in the same solvent as the base titrated.

Results and discussion

In all experiments 3—10 ml of dilute solutions of an organic base were titrated. However, the volume of the sample may be reduced by further miniaturization of the immersed interfacial cell. The titration curves obtained are shown in Figs. 3—6. The shapes of these curves in dry organic solvents prove that the interfacial voltaic cell is useful for the determination of organic bases in non-conducting media, for they exhibit sharp changes at the inflection points. During the titration of alkaloid solutions with picric acid in benzene and ligroin, some insoluble salts were formed; they did not interfere, how-

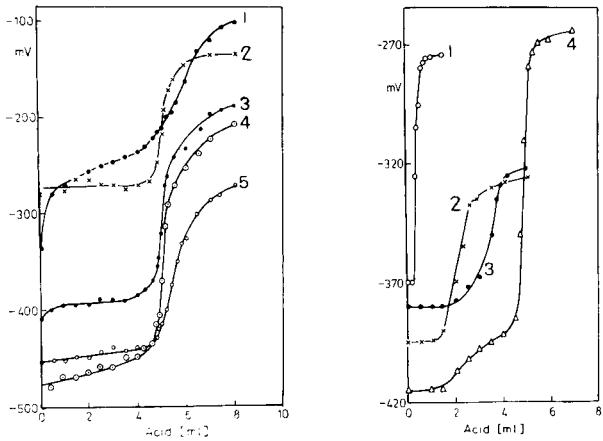

Fig. 3. Potentiometric titration curves of strychnine (0.005 M) with picric acid (0.01 M) in: (1) cyclohexane; (2) pentyl acetate; (3) dichloroethane; (4) chloroform; (5) benzene.

Fig. 4. Potentiometric titration curves of: (1) hydrochinidine (0.01 M); (2) trimethylamine (0.005 M); (3) aconitine (0.01 M) and (4) *n*-dodecylamine with trichloroacetic acid (0.01 M) in benzene.

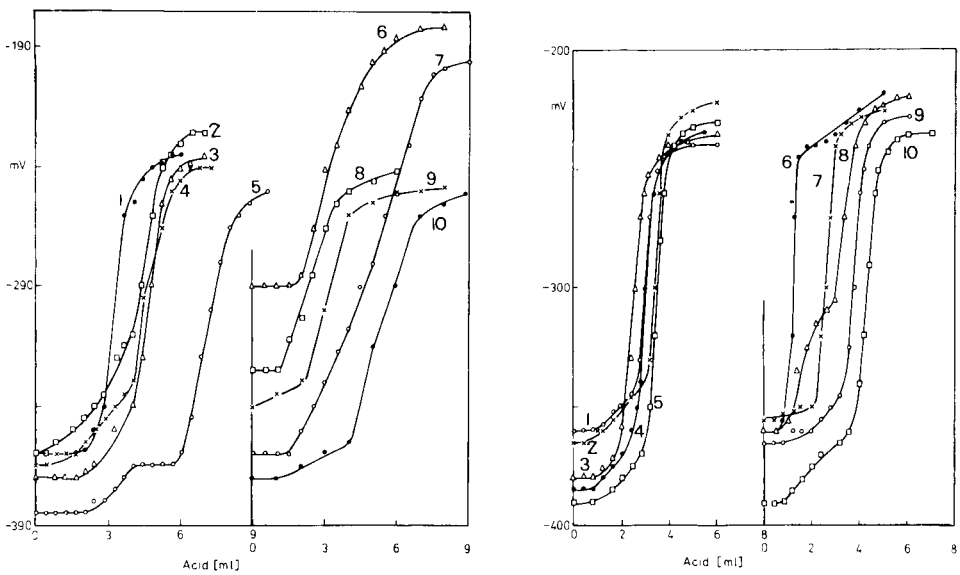

Fig. 5. Potentiometric titration curves of: (1) α-picoline (0.001 M); (2) hyoscyamine (0.001 M); (3) *n*-dodecylamine (0.001 M); (4) α,α′-lutidine (0.001 M); (5) homatropine (0.001 M) with picric acid (0.002 M); and (6) *n*-dodecylamine (0.001 M); (7) homatropine (0.001 M); (8) hyoscyamine (0.001 M); (9) α,α′-lutidine (0.001 M); (10) α-picoline with trichloroacetic acid (0.002 M) in benzene.

Fig. 6. Potentiometric titration curves of: (1) homatropine (0.001 M); (2) α,α′-lutidine (0.001 M); (3) *n*-dodecylamine (0.001 M); (4) α-picoline (0.001 M); (5) hyoscyamine (0.001 M) with picric acid (0.002 M); and (6) α-picoline (0.001 M); (7) α,α,-lutidine (0.001 M); (8) *n*-dodecylamine (0.001 M); (9) homatropine (0.001 M); (10) hyoscyamine (0.001 M) with trichloroacetic acid (0.002 M) in chloroform.

ever, with the determination of the bases. Obviously, careful standardization is necessary in the titration of any compound.

The trends of the titration curves in different solvents change only slightly. The distinct potential changes of the interfacial electrode observed during the titration are due to the fact that the chemical reaction is monitored not in the bulk of the solution but at the boundary of two phases with markedly different dielectric constants. In such a case the reacting substances are concentrated at the interface, i.e., at the working surface of the interface cell.

REFERENCES

1 B. Waligóra and M. Paluch, Anal. Chim. Acta, 119 (1980) 375.
2 B. Kamieński, Z. Było and B. Waligóra, Bull. Acad. Pol. Sci. Lett. Ser. A, (1951) 199.
3 B. Kamieński and J. Kulawik, Bull. Acad. Pol. Sci. Cl. 3, 3 (1955) 401; 4 (1956) 529.
4 B. Waligóra and M. Paluch, Chem. Anal., 10 (1965) 693.

ANALYTICA CHIMICA ACTA, Vol. 132

AUTHOR INDEX

ANALYTICA CHIMICA ACTA
(including COMPUTER TECHNIQUES AND OPTIMIZATION)

INFORMATION FOR AUTHORS

Analytica Chimica Acta publishes original papers, short communications, preliminary communications, and reviews dealing with every aspect of modern chemical analysis, both fundamental and applied.

Reviews are written by invitation of the editors, who welcome suggestions for subjects. Short communications are usually complete descriptions of limited investigations, and should generally not exceed four printed pages. Preliminary communications of important urgent work can be printed within 4 months of submission, if the authors are prepared to forego proofs.

Submission of papers

Authors should submit three copies of the manuscript in double-spaced typing on one side of the paper only, with a margin of 4 cm, on pages of uniform size. If any variety of machine copying is used (e.g., xerox), authors should ensure that all copies are easily legible and that the paper used can be written on with both ink and pencil. Authors are advised to retain at least one copy of the manuscript. Manuscripts should be preceded by a sheet of paper carrying (a) the title of the paper, (b) the name and full postal address of the person to whom proofs are to be sent, (c) the number of pages, tables and figures.

Manuscripts should be sent to the editorial addresses given on the covers of current issues; submission to the publisher leads to delays. Submission of a manuscript implies that the work described has not been, and will not be, published elsewhere (except as an abstract, or as part of a lecture, review or academic thesis). Upon acceptance of the manuscript, the author(s) resident in the U.S.A. will be asked to transfer the copyright of the article to the publisher. This transfer will ensure the widest possible dissemination of information under the U.S. Copyright Law. For articles by authors not resident in the U.S.A., the copyright passes to the publisher upon acceptance of the manuscript, if it has not been previously reserved by a government institution or company.

The preferred language of the journal is English, but French and German manuscripts are also acceptable. For authors whose first language is not English, French or German, linguistic improvement is provided as part of the normal editorial processing.

Notes on the preparation of manuscripts

Authors are given every latitude, consistent with clarity and brevity, in the style and form of their papers. Very useful advice is provided in the Handbook for Authors issued by the Chemical Society and American Chemical Society.

Title and initial layout. All manuscripts should be headed by a concise but informative title. This is followed by the names of the authors, and the address of the laboratory where the work was carried out. The author to whom correspondence should be addressed must be indicated by an asterisk (without a footnote). If the present address of an author is different from that mentioned, it should be given in a footnote. Acknowledgements of financial support should not be made in footnotes, but at the end of the paper.

Summary. Research papers and reviews begin with a Summary (50—250 words) which should comprise a brief factual account of the contents of the paper, with emphasis on new information. Short communications and preliminary communications require summaries, which should not exceed 50 words. Uncommon abbreviations, jargon and reference numbers must not be used. The Summary should be suitable for use by abstracting services without rewriting. Papers in French or German require a Résumé or Zusammenfassung preceded by a Title and Summary in English; authors are encouraged to provide translations where necessary.

Introduction. The first paragraphs of the paper should contain an account of the reasons for the work, any essential historical background (as briefly as possible and with key references only) and preliminary experimental work.

Experimental. The experimental methods may be described after the introductory material, or after the discussion of results, depending on the nature of the paper. Detailed experimental descriptions should, however, be restricted to one section of the paper, and not scattered throughout the text. Working procedures should be given in the imperative mood; sufficient detail should be given to allow any reasonably experienced worker to carry out the procedure. Detailed descriptions of well-known techniques and equipment are unnecessary, as are simple preparations of reagents or solutions, and lists of common chemicals. Manufacturers should be named only if the product differs essentially from that of other manufacturers. Local suppliers for multi-national concerns should not be named. In writing, complete sentences should be used, and procedural steps should not be numbered.

Results and discussion. These may be treated together or separately. In discussing results, unnecessary repetition of experimental detail, unsupported elaboration of hypotheses, and verbose exposition of ideas should be avoided. Chemical formulae should not be used in the text unless confusion is likely to arise from the use of names. Formulae should, however, be used for brevity in tables and figures. Calculations well known to specialists are unnecessary. Conclusions should be added only if needed for interpretation; they should not be used as extended summaries nor should they duplicate the summary.

Acknowledgements. These should be kept as short as possible, and placed, without a heading, at the conclusion of the text.

References

The references should be collected at the end of the paper, numbered in the order of their appearance in the text (*not* arranged alphabetically), and typed on a separate sheet. If the paper forms part of a series, the reference to the previous part should appear as the first reference, the number being cited at the title of the paper. References given in tables should be numbered according to the position of the table in the text. Every reference listed must be cited in the text. Reference numbers in the text are set in square brackets on the line. Numerals referring to equations are placed in parentheses, e.g., Eqn. (1).

In the list of references, the following forms should be adopted.

Journals

1 W. Lund and M. Salberg, Anal. Chim. Acta, 76 (1975) 131.

2 M. McDaniel, A. D. Shendrikar, K. D. Reizneir and P. W. West, Anal. Chem., 48 (1976) 2240.

The title of the journal must be abbreviated as in the Bibliographic Guide for Editors and Authors.

Books

1 D. D. Perrin, Masking and Demasking of Chemical Reactions, Interscience—Wiley, New York, 1970, p. 188.

2 S. Hofmann, in G. Svehla (Ed.), Wilson and Wilson's Comprehensive Analytical Chemistry, Vol. 9, Elsevier, Amsterdam, 1979, p. 89.

Titles of papers are unnecessary. Citations of reports which are not widely available (e.g., reports from government research centres) should be avoided if possible. Authors' initials should not be used in the text, unless real confusion could be caused by their omission. If the reference cited contains three or more names, only the first author's name followed by et al. (e.g., McDaniel et al.) should be used in the text; but the reference list must contain the initials and names of *all* authors.

Tables, computer programs, and figures

Tables and figures must be essential for the clear and concise presentation of the material. The same information should not be given in tables and figures, and material from the published literature should not be reproduced.

Tables. All tables should be numbered with Arabic numerals, and have brief descriptive headings; they should be typed on separate pages. The layout should be given serious thought, so that the significance of the results can be grasped quickly. Column headings should be brief.

Tables with only two or three headings are best printed horizontally, e.g.,

Hg^{2+} added (μg)	1.0	2.0	3.0	5.0
Extraction (%)	95.0	99.8	99.5	89.0

Experimental information which is relevant to all the results in the table is best given in parentheses immediately after the heading. No column should contain the same number or unit throughout its length. Footnotes to tables are denoted by superscript a, b, c... The units used should be clearly stated. Confusion can arise from the use of powers in column headings. The following usage is recommended: e.g., if molar absorptivities are listed, the heading should be $\epsilon(10^4\ l\ mol^{-1}\ cm^{-1})$ so that a number 2.32 in the column signifies 23 200.

Alphanumeric computer output is usually unsuitable for reproduction and should therefore be retyped and presented as tables; capitals can be used to simulate computer output if such simulation is essential for illustration.

Computer programs. Algorithms should be described clearly and concisely by means of a suitable algorithmic notation, although a standard high-level programming language may also be used. Complete program listings are not normally admissible. Flow charts should be avoided in favour of a textual or tabulated description of the program or data flow. Statements on the portability of the software described to other computer systems, as well as on its availability to interested readers, should be given.

Figures. Figures should be prepared in black waterproof drawing ink on drawing or tracing paper of the same size as that on which the manuscript is typed. One original (or sharp glossy print) and two photostat (or other) copies are required. Attention should be given to line thickness, lettering (which should be kept to a minimum) and spacing on axes of graphs, to ensure suitability for reduction during printing. Axes of a graph should be clearly labelled, along the axes, and outside the graph itself.

The following standard symbols should be used in graphs:

▼ ▽ ■ □ + × ● ○ ▲ △

Simple straight-line graphs are not acceptable, because they can readily be described in the text by means of an equation or a sentence. Claims of linearity should be supported by regression data that include slope, intercept, standard deviations of the slope and intercept, standard error, and the number of data points; correlation coefficients are optional. Explanatory information should be placed not in the figure, but in the legend, which should be typed on a separate sheet of paper. All figures should be numbered with Arabic numerals, and require descriptive legends.

Photographs should be glossy prints and be as rich in contrast as possible; colour photographs cannot be accepted. In general, line diagrams are more informative and less liable to dating than photographs of equipment, which are therefore not usually acceptable.

Computer outputs for reproduction as figures must be good quality on blank paper, and should preferably be submitted as glossy prints.

Nomenclature, abbreviations and symbols

In general, the recommendations of the International Union of Pure and Applied Chemistry (IUPAC) should be followed, and attention should be given to the recommendations of the Analytical Chemistry Division in the journal *Pure and Applied Chemistry* (see also *IUPAC Compendium of Analytical Nomenclature*, 1978).

Basic SI and other accepted metric nomenclature are given in the Appendix. In accordance with IUPAC rules, the mass number, atomic number, number of atoms and ionic charge should be designated by a left upper index, a left lower index, a right lower index and a right upper index, respectively, placed round the atomic symbol. For example, the phosphate ion should be designated as PO_4^{3-} (*not* PO_4^{-3} or PO_4^{---}), and phosphorus-32 as ^{32}P (*not* P^{32} or P-32).

The Stock notation for the indication of stoichiometric valency states (and indirectly the proportion of the constituents) should be used. Examples are iron(III) chloride rather than ferric chloride, and potassium hexacyanoferrate(II) rather than potassium ferrocyanide. These rules are valid for French and German as well as English usage.

The use of nanometre (nm) and micrometre (μm) for the expression of analytical wavelengths has long superseded mμ or Å or μ, all of which should be avoided, although Å is sensibly retained in crystallographic work.

Natural or Naperian logarithms should be denoted by ln and decadic logarithms by log.

Molarity (mol l^{-1} or M) is the preferred concentration unit, but normality (N) can be used for convenience if it does not introduce ambiguity.

Unusual abbreviations require definition when first used. Abbreviations for long chemical names (e.g., EDTA, HEDTA, TBAH, en, pn, Tris) are useful, especially in equations, tables or figures. For ease of distinction, well-known techniques may be abbreviated by using lower-case letters and full stops, such as, g.c.-m.s., u.v., i.r., a.a.s., ^{13}C-n.m.r., a.s.v., d.p.p., etc. In the interests of clarity, however, excessive use of abbreviations is not encouraged.

Ambiguity in expressing dilution can be avoided by the use of, e.g., (1 + 2) rather than 1:2 which could mean either one part diluted with two parts or one part diluted to twice its volume.

Symbols, formulae and equations should be written with great care, capitals and lower-case letters being distinguished where necessary. Greek letters and unusual symbols should be defined by name in the left-hand margin beside their first appearance in the paper. Wherever possible, mathematical expressions should be typed on one line, by using brackets, e.g. $\{[()]\}$, and the solidus, e.g., $A/b = x^{1/2}/(u + v)^{5/6}$; this is valuable in conserving vertical space. Particular attention should be given to the correct sequence of brackets and to the correct placing of superscripts and subscripts in complicated equations; careful proof-reading of such equations is essential. Short equations should not be numbered unless required for subsequent reference.

Decimal points should be indicated by full stops in papers written in English and by commas in French and German papers. All decimal numbers smaller than unity should include a leading zero (e.g., 0.11).

Appendix

Basic SI units

metre	m	candela	cd
kilogram	kg	mole	mol
second	s	(an Avogadro number of	
ampere	A	particles such as atoms,	
degree Kelvin	K	molecules, ions, electrons.)	

Derived SI units

joule	J	kg m^2 s^{-2}	farad	F	A s V^{-1}
newton	N	J m^{-1}	weber	Wb	V s
watt	W	J s^{-1}	henry	H	V s A^{-1}
coulomb	C	A s	tesla	T	V s m^{-2}
volt	V	J A^{-1} s^{-1}	hertz	Hz	s^{-1}
ohm	Ω	V A^{-1}	degree Celsius	°C	K − 273.15

Other units

litre	l	10^{-3} m^3	hour	h	3.6 × 10^3 s
gram	g	10^{-3} kg	dyne	dyn	10^{-5} N
poise	P	10^{-3} m^{-1} s^{-1}	atmosphere	atm	101.325 kN m^{-2}
electron volt	eV	1.6021 × 10^{-19} J	molar	M	mol l^{-1}
calorie	cal	4.184 J	molal	*m*	mol kg^{-1}
minute	min	60 s	curie	Ci	3.7 × 10^{10} s^{-1}

Prefixes to abbreviations for the names of units indicating

Multiples		Sub-multiples			
tera (×10^{12})	T	milli (×10^{-3})	m	pico (×10^{-12})	p
giga (×10^9)	G	micro (×10^{-6})	μ	femto (×10^{-15})	f
mega (×10^6)	M	nano (×10^{-9})	n	atto (×10^{-18})	a
kilo (×10^3)	k				

Vol. 132

ACA announcements

ANNOUNCEMENTS OF MEETINGS

FLOW ANALYSIS II

The 2nd International Conference on Flow Analysis will be arranged at Lund in southern Sweden from June 18–21, 1982, by the Analytical section of the Swedish Chemical Society. The scope and aims of the conference will be the same as for the FA – Amsterdam 1979 Conference, and the programme is intended to reflect the rapid development and increasing importance of continuous flow analysis during recent years.

The scientific programme will include invited plenary lectures and submitted research papers, which will be presented as lectures or as poster papers at the discretion of the Scientific Committee. The time available for presentation of contributed papers given in lecture session will be 25 minutes followed by 5 minutes of discussion. The Scientific Committee expects the programme to cover a wide and representative selection of current research on all aspects of continuous flow analysis. The main topics will be: theory of flow analysis; instrumentation design for continuous segmented and unsegmented flow analysis and flow injection analysis; new detector systems; possibilities for complete automation; and applications in industrial, environmental and clinical analysis. Plenary lectures will be given by Dr. H. Poppe (Amsterdam, The Netherlands), Professor J. Růžička (Lyngby, Denmark), Dr. L.R. Snyder (New York, USA), and Dr. R. Tijssen (Amsterdam, The Netherlands).

Abstracts of papers and posters submitted for presentation must be sent to the Swedish Chemical Society before February 15th, 1982. Authors will be informed by April 15th whether or not the paper has been accepted for presentation. The papers presented will be reviewed for publication in a special issue of *Analytica Chimica Acta*.

Further information from: "Flow Analysis II", c/o The Swedish Chemical Society, Upplandsgatan 6 A, 1 tr. S-111 23 Stockholm, Sweden.

"CAC-HOLLAND" INTERNATIONAL CONFERENCE ON CHEMOMETRICS IN ANALYTICAL CHEMISTRY

An international conference on chemometrics in analytical chemistry will be held at the Energy Research Center of the Netherlands (ECN), in Petten, The Netherlands, on September 15–17, 1982. The conference is being organized under the auspices of the Analytical Division of the Royal Netherlands Chemical Society (KNCV) and the Chemometrics Society.

Topics will include: application and development of formal techniques for design, optimization and evaluation of analytical procedures and results; application of systems theory, operations research, information theory, statistics and other chemometrical techniques in analytical chemistry; data retrieval, pattern recognition, artificial intelligence, etc.; computerized signal- and data-processing, optimum filtering techniques, noise reduction methods; and education in chemometrics.

The program will include invited plenary lectures, and invited and submitted research papers. The papers presented at the conference are to be refereed for publication in a special issue of *Analytical Chimica Acta*.

For further information contact: The Secretariat, CAC-Holland, Laboratory for Analytical Chemistry, University of Amsterdam, Nieuwe Achtergracht 166, 1018 WV Amsterdam, The Netherlands. (Telephone: 020-522-3541.)

SAC 83, INTERNATIONAL CONFERENCE AND EXHIBITION ON ANALYTICAL CHEMISTRY

SAC 83, organised by the Analytical Division of the Royal Society of Chemistry, will be held on July 17–23, 1983, at the University of Edinburgh in Scotland. As in past SAC conferences, the scientific programme will be organised around plenary, invited and contributed papers and posters covering the whole field of analytical chemistry. In addition, there will be 1-day Symposia on particular analytical themes organised by RSC groups and other associated bodies. The programme will include a series of workshops, where research workers can demonstrate new apparatus and techniques,

as well as informal evening discussion meetings. Abstracts of contributed papers will be required in November, 1982.

A new and exciting feature of SAC 83 will be a group of one-day UPDATE courses, convened by international authorities on the following topical subjects: flow injection analysis (Prof. J. Růžička), narrow column HPLC (Prof. J. Knox), microcomputers in analytical chemistry (Prof. D. Betteridge), new techniques in fluorescence (Prof. J.N. Miller), and inductively-coupled plasma emission spectroscopy (Dr. L. Ebdon). Each UPDATE will provide an all-day tutorial and practical demonstration session in which exhibitors and other manufacturers will be invited to participate. They will be held on the Wednesday, as an alternative to a scientific or cultural visit.

An extensive exhibition of commercial apparatus, equipment and books will be a major feature of the conference. Most of the exhibits will be immediately adjacent to the Lecture Theatres and poster area, and lecture-free times will be organised to facilitate attendance at the exhibition.

Delegates may register for the whole conference or, if they are members of the Royal Society of Chemistry, for individual days. Registration for the UPDATES is separate. Students, accompanying and retired persons may attend the whole conference at a reduced fee. For further information, contact The Secretary, Analytical Division, The Royal Society of Chemistry, Burlington House, London W1V 0BN, Great Britain.

CALENDAR OF FORTHCOMING MEETINGS

Jan. 4–9, 1982 Orlando, FL, U.S.A.	**1982 Winter Conference on Plasma Spectrochemistry** Contact: 1982 Winter Conference, c/o ICP Information Newsletter, Chemistry GRC Towers, University of Massachusetts, Amherst, MA 01003, U.S.A. Tel. (413) 545-2294. (Further details published in Vol. 130, No. 1 and Vol. 133, No. 3)
Jan. 19–20, 1982 Amsterdam, The Netherlands	**Symposium on "Detection in High-Performance Liquid Chromatography"** Contact: Mrs. Peschier, Hewlett-Packard Nederland B.V., Analytical Department, van Heuven Goedhartlaan 121, 1181 KK Amstelveen, The Netherlands. (Tel.: 020–472021).
Feb. 16–17, 1982 Edinburgh, Scotland	**Advances in Chromatography: Industrial and Petrochemical Applications** Contact: The Royal Society of Chemistry, Analytical Division (Scottish Region), Burlington House, London W1V 0BN, Great Britain.
March 8–12, 1982 Atlantic City, NJ, U.S.A.	**1982 Pittsburgh Conference and Exhibition on Analytical Chemistry and Applied Spectroscopy** Contact: Mrs. Linda Briggs, Program Secretary, Pittsburgh Conference, Department J-057, 437 Donald Road, Pittsburgh, PA 15235, U.S.A.
March 22–26, 1982 Nottingham, Great Britain	**International Conference on ESR of Organic and Bioorganic Radicals** Contact: Dr. J.B. Raynor, Chemistry Department, The University, Leicester LE1 7RH, Great Britain.
March 23–25, 1982 Brighton, Great Britain	**Electro-Optics/Laser International '82** Contact: Dr. H.G. Gerrard, Kiver Communications SA, 161–185 Ewell Road, Surbiton, Surrey KT6 6AX, Great Britain.
March 28–April 2, 1982 Las Vegas, NV, U.S.A.	**183rd American Chemical Society National Meeting** Contact: A.T. Winstead, American Chemical Society, 1155 Sixteenth Street, NW, Washington, DC 20036, U.S.A.
March 30–April 1, 1982 Birmingham, Great Britain	**Royal Society of Chemistry Annual Chemical Congress** Contact: Royal Society of Chemistry, Burlington House, London W1V 0BN, Great Britain.
April 5–8, 1982 Las Vegas, NV, U.S.A.	**International Symposium "Advances in Chromatography"** Contact: Prof. A. Zlatkis, Chemistry Department, University of Houston, Central Campus, 4800 Calhoun, Houston, TX 77004, U.S.A. Tel.: (713) 749-2623.

April 14–16, 1982 Amsterdam, The Netherlands	**12th Annual Symposium on the Analytical Chemistry of Pollutants** Contact: Prof. Dr. Roland W. Frei, The Free University, De Boelelaan 1083, 1081 HV Amsterdam, The Netherlands.
April 15–17, 1982 Tokyo, Japan	**International Symposium "Advances in Chromatography"** Contact: Prof. A. Zlatkis, Chemistry Department, University of Houston, Central Campus, 4800 Calhoun, Houston, TX 77004, U.S.A. Tel.: (713) 749-2623.
April 21–23, 1982 Neuherberg near Munich, G.F.R.	**Second International Workshop on Trace Element Analytical Chemistry in Medicine and Biology** Contact: Dr. P. Schramel, Gesellschaft fuer Strahlen- und Umweltforschung, Institut fuer Angewandte Physik, Physikalisch–Technische Abteilung, Ingolstaedter Landstrasse 1, D–8042 Neuherberg, G.F.R. (Further details published in Vol. 124, No. 2)
April 27–30, 1982 Munich, G.F.R.	**Biochemische Analytic Conference** Contact: Prof. I. Trautschold, Medizinische Hochschule Hannover, Karl-Wiechert-Allee 9, 3000 Hannover 61, G.F.R. (Further details published in Vol. 124, No. 2)
May 2–6, 1982 Interlaken, Switzerland	**2nd International Symposium on Instrumental TLC (HPTLC)** Contact: Dr. R.E. Kaiser, Institute for Chromatography, P.O. Box 1141, D-6702 Bad Dürkheim, G.F.R.
May 11–14, 1982 Ghent, Belgium	**4th International Symposium on Quantitative Mass Spectrometry in Life Sciences** Contact: Prof. A. De Leenheer, Symposium Chairman, Laboratoria voor Medische Biochemie en voor Klinische Analyse, De Pintelaan 135, B-9000 Ghent, Belgium.
June 5–12, 1982 Honolulu, HI, U.S.A.	**American Society for Mass Spectrometry Annual Meeting** Contact: Dr. H.M. Fales, National Institute of Health, Building 10 7N322, Bethesda, MD 20205, U.S.A.
June 6–12, 1982 Frankfurt, G.F.R.	**European Meeting on Chemical Engineering and ACHEMA Exhibition Congress 1982** Contact: DECHEMA P.O. Box 970146, D-6000 Frankfurt/M 97, G.F.R.
June 7–11, 1982 Philadelphia, PA, U.S.A.	**VI International Symposium on Column Liquid Chromatography** Contact: R.A. Barford, ERRC – SEA, U.S. Department of Agriculture, 600 E. Mermaid Lane, Philadelphia, PA 19118, U.S.A.
June 18–21, 1982 Lund, Sweden	**Flow Analysis II** Contact: Flow Analysis II, c/o The Swedish Chemical Society, Upplandsgatan 6A, 1 tr., S-111 23 Stockholm, Sweden.
June 28–30, 1982 East Lansing, MI, U.S.A.	**35th American Chemical Society Annual Summer Symposium** Contact: A.I. Popov, Chemistry Department, Michigan State University, East Lansing, MI 48824, U.S.A.
July 11–16, 1982 Washington, DC, U.S.A.	**6th International Conference on Computers in Chemical Research and Education (ICCCRE)** Contact: Dr. Stephen R. Heller, Chairman, 6th ICCCRE, EPA, MIDSD, PM–218, 401 M Street, S.W., Washington, DC 20460, U.S.A. Tel. (202) 755–4938, Telex: 89–27–58. (Further details published in Vol. 126 and Vol. 133, No. 2)
July 11–16, 1982 Louvain-la-Neuve, Belgium	**6th IUPAC Conference on Physical Organic Chemistry** Contact: Professor A. Bruylants, Université Catholique de Louvain, Laboratoire de Chimie General et Organique, Bâtiment Lavoisier 1 Place Louis Pasteur, 1348 Louvain-la-Neuve, Belgium.
July 13–15, 1982 Sheffield, Great Britain	**First Biennial National Atomic Spectroscopy Symposium** Contact: Dr. E.B.M. Steers, Physics Department, Polytechnic of North London, Holloway, London N7 8DB, Great Britain.

July 19–23, 1982 Nantes, France	**8th International Conference on Non-aqueous Solutions** Contact: Prof. M. Chabanel, UER de Chimie, Université de Nantes, 2 rue de la Houssinière, F-44072 Nantes Cédex, France
Aug. 2–7, 1982 Pretoria, South Africa	**13th International Symposium on the Chemistry of Natural Products** Contact: The Symposium Secretariat – S.219, CSIR, P.O. Box 395, Pretoria, 0001 Republic of South Africa.
Aug. 11–13, 1982 Hameenlinna, Finland	**6th European Symposium on Polymer Spectroscopy (ESOPS 6)** Contact: Professor Johan Lindberg, Department of Wood and Polymer Chemistry, University of Helsinki, Meritullinkatu 1 A, SF 00170 Helsinki 17, Finland.
Aug. 15–21, 1982 Perth, Australia	**The 12th International Congress of Biochemistry** Contact: Brian Thorpe, Department of Biochemistry, Faculty of Science Australian National University, Canberra A.C.T. 2600, Australia.
Aug. 22–27, 1982 Tokyo, Japan	**Fourth International Conference on Organic Synthesis (IUPAC)** Contact: Professor Teruaki Mukaiyama, Chairman of the Fourth ICOS (IUPAC), c/o The Chemical Society of Japan, 1-5 Kanda-Surugadai, Chiyoda-ku, Tokyo, Japan.
Aug. 29–Sept. 4, 1982 Kyoto, Japan	**5th International Congress of Pesticide Chemistry** Contact: Rikagaku Kenyusho (The Institute of Physical and Chemical Research), 2–1 Hirosawa Wako-shi Saitama Pref. 351, Japan.
Aug. 30–Sept.3, 1982 Vienna, Austria	**9th International Mass Spectrometry Conference** Contact: Interconvention, P.O. Box 105, A - 1014 Vienna, Austria. (Further details published in Vol. 120)
Sept. 6–10, 1982 Bordeaux, France	**VIII International Conference on Raman Spectroscopy** Contact: Professor J. Lascombe, Laboratoire de Spectroscopie Infrarouge et Raman, Université de Bordeaux I, F-33405 Talence, France
Sept. 12–17, 1982 Kansas City, MO, U.S.A.	**184th American Chemical Society National Meeting** Contact: A.T. Winstead, American Chemical Society, 1155 Sixteenth Street, NW, Washington DC 20036, U.S.A.
Sept. 13–17, 1982 London, Great Britain	**14th International Symposium on Chromatography** Contact: The Executive Secretary, Chromatography Discussion Group, Trent Polytechnic, Burton Street, Nottingham, NG1 4BU, Great Britain.
Sept. 15–17, 1982 Petten, The Netherlands	**"CAC-Holland" International Conference on Chemometrics in Analytical Chemistry** Contact: Dr. H.C. Smit, Laboratory for Analytical Chemistry, University of Amsterdam, Nieuwe Achtergracht 166, 1018 WV Amsterdam, The Netherlands.
Sept. 19–24, 1982 Philadelphia, PA, U.S.A.	**9th National Meeting of the Federation of Analytical Chemistry and Spectroscopy Societies (FACSS)** Contact: Division of Analytical Chemistry, American Chemical Society, Department of Chemistry, Notre Dame, IN 46556, U.S.A.
Sept. 20–23, 1982 Oslo, Norway	**Food Research and Data Analysis** Contact: B. Eidstuen, P.O. Box 50, N-1432 Aas-NLH, Norway. Tel.: 47-2-94 08 60. (Further details published in Vol. 130, No. 1 and Vol. 133, No. 3)
July 17–23, 1983 Edinburgh, Scotland, Great Britain	**SAC '83, International Conference and Exhibition on Analytical Chemistry** Contact: The Royal Society of Chemistry, Analytical Division, Burlington House, London W1V 0BN, Great Britain. Tel.: 01-734-9971.
Aug. 28–Sept. 2, 1983 Amsterdam, The Netherlands	**9th International Symposium on Microchemical Techniques** Contact: Symposium Secretariat, c/o Municipal Congress Bureau, Oudezijds Achterburgwal 199, 1012 DK Amsterdam, The Netherlands. Tel: (020) 552 3459.

(continued from back cover)

Short Communications

Printed in The Netherlands.

CONTENTS

(continued on inside page of cover)